Phase transitions in adsorbed layers formed on crystals of square and rectangular surface lattice

A. Patrykiejew[a], S. Sokołowski[a], K. Binder[b]

[a]*Faculty of Chemistry, MCS University, 20031 Lublin, Poland*
[b]*Institut für Physik, Johannes-Gutenberg-Universität Mainz, 55099 Mainz, Germany*

ELSEVIER

Amsterdam–Lausanne–New York–Oxford–Shannon–Tokyo

Contents

1. Introduction 209
2. Preliminaries 212
   2.1. The gas–solid corrugation potential 212
   2.2. Basic theoretical models 215
      2.2.1. Lattice models of localized adsorption 217
      2.2.2. Early theories of adsorption on corrugated surfaces 219
      2.2.3. Continuous space models 223
3. Theories of surface phase transitions 226
   3.1. Ordered states and order–disorder transitions 226
   3.2. Critical phenomena in surface systems 233
   3.3. Commensurate and incommensurate phases 241
   3.4. Melting phenomena 254
   3.5. Multilayer adsorption, wetting and interfacial phenomena 264
4. Lattice gas models 271
   4.1. Monolayers 271
   4.2. Multilayer adsorption 281
5. Films on surfaces with finite corrugation 291
   5.1. Adsorption on a noncorrugated substrate 292
   5.2. Films on square and rectangular lattices: experimental background 295
   5.3. Two-dimensional films on lattices with square and rectangular symmetry 299
   5.4. Dense monolayer and bilayer films on a square lattice 311
   5.5. Orientational effects in molecular films 323
6. Final remarks 332
Acknowledgements 335
References 335

ELSEVIER

Surface Science Reports 37 (2000) 207–344

surface science reports

www.elsevier.nl/locate/surfrep

Phase transitions in adsorbed layers formed on crystals of square and rectangular surface lattice

A. Patrykiejew[a,*], S. Sokołowski[a], K. Binder[b]

[a]*Faculty of Chemistry, MCS University, 20031 Lublin, Poland*
[b]*Institut für Physik, Johannes-Gutenberg-Universität Mainz, 55099 Mainz, Germany*

Manuscript received in final form 2 September 1999

Abstract

This article gives a survey of phase transitions in adsorbed films on well defined surfaces of square and rectangular symmetry of the lattice. The discussion concentrates on the effects of periodic changes of the adsorbate–substrate potential on the structure and thermodynamic properties of adsorbed films. Different theoretical approaches are briefly reviewed, with an emphasis on those which explicitly take into account final corrugation of the surface potential. Several aspects of statistical mechanical description of phase transitions in surface layers, such as order–disorder, melting, commensurate–incommensurate transitions in monolayer films as well as transitions connected with the formation of multilayer films (layering and wetting) are presented. Theoretical discussion is followed by the presentation of numerous experimental and computer simulation studies for various systems. Then the properties of monolayer films of molecular adsorbates on different substrates of a square and rectangular symmetry is discussed. It is pointed out that computer simulation methods provide a very powerful tool which allows to probe the inner structure of such systems and provides direct information concerning both orientational and positional ordering.

Keywords: Computer simulations; Equilibrium thermodynamics and statistical mechanics; Surface thermodynamics

1. Introduction

Phase transitions and ordering phenomena in adsorbed films formed on well defined crystal surfaces have been attracting a great deal of interest for many years [1–5] and the activity in this field is still growing. The literature which presents the results of both experimental and theoretical studies is overwhelmingly abundant and the achievements are outstanding. The progress in this field has gained a particular impetus due to introduction of several powerful experimental techniques (e.g., neutron

* Corresponding author. Tel.: +48815375687; fax: +48815333348.
E-mail address: andrzej@miki.umcs.lublin.pl (A. Patrykiejew).

0167-5729/00/$ – see front matter
PII: S0167-5729(99)00011-4

scattering [6–10], various forms of electron spectroscopy [11–20], light particle, e.g. helium, scattering [21–23], and many others [24–28]), the extensive use of computer simulation methods (Monte Carlo and molecular dynamics) [5,29–36] and, last but surely not the least, owing to very intensive theoretical studies [1–3,37–46], for which the discovery of rich two-dimensional world of phase transitions and substrate induced forms of order in adsorbed layers has become a challenge, but also has created a unique opportunity to verify various ideas and predictions stemming out of theoretical work.

The systematic investigation of surface phases and surface phase transitions in adsorbed layers began in the late 1960s [1,47–49] just after the development of the technology for the production of the graphite substrate with highly uniform surface [50]. Already very early experiments of Thomy and Duval [47–49], who measured adsorption isotherms of simple gases (krypton, xenon, methane) on graphite at low temperatures, revealed that monolayer films exhibit remarkably similar phase behavior to what is so well known from everyday observations of three-dimensional bulk matter. In particular, it was clearly demonstrated that the two-dimensional counterparts of gas, liquid and solid phases do exist. However, this simple picture stemming from those experiments did not last long. Over the years, hundreds of papers reporting the new findings were published and particularly extensive studies were carried out for the films formed on graphite [51–56]. It soon became clear that several phenomena observed in adsorbed films do not have simple counterparts in the three-dimensional bulk matter. The misfit between the lattice spacing of the substrate surface and the preferred lattice spacing of the adsorbate (determined by the interactions between the adsorbed particles) leads to the formation of incommensurate phases, axially ordered phases and other forms of ordering specific to surface systems.

Experimental achievements strongly stimulated theoretical studies and, without doubt, greatly contributed to the development of theories for two-dimensional melting [37–39,57–60], commensurate–incommensurate transitions [33,42,61–63], finite size scaling theory [5,64–66], theory of wetting and roughening phenomena [44,45,67–71] and the theory of critical phenomena in systems of low dimensionality [72,73]. All those experimental and theoretical efforts were also vastly supported by computer simulation studies [29–36,74–84] that greatly contributed to our present understanding of processes and phenomena occurring at surfaces and in the adsorption systems. At present, our knowledge and understanding of the phase behavior in many experimental systems seem to be quite deep. Phase diagrams for noble gases and simple molecules adsorbed on graphite are now well established [53,55] and the inner structure of many phases as well as the mechanism of phase transitions are presently already known.

A natural structure of a two-dimensional dense phase on a ''flat'', noncorrugated surface is a hexagonal packing of molecules which results from the obvious tendency of the system to assume the most favorable structure, which minimizes the free energy. At low temperatures the entropy contribution to the free energy is rather small, and it is the potential energy contribution that dominates the system free energy. In the case of hexagonal lattices, the intrinsic lattice constant for the film, however usually is different from the distance between the adjacent minima of the potential wells at different surface cells, but nevertheless, at least the symmetry of the substrate potential and the symmetry of the adsorbate preferential structure are the same. Thus, for a small misfit, even a slight corrugation of the substrate potential may considerably stabilize the commensurate phase [1,53]. For a large misfit, incommensurate phases are formed and these are usually described within the domain wall formalism [61,85–90].

One should also note that the surface corrugation of the graphite basal plane, as well as of the dense (111) planes of various metals, is quite small. It has been even argued [91,92] that the films on some

metals, e.g., argon, krypton and xenon adsorbed on Ag(111), behave practically in the same way as the adsorbed layers formed on a flat, noncorrugated surface.

The above picture changes completely when one considers crystal planes of lower density with the surfacial lattice of other than hexagonal symmetry. In particular, for the surfaces characterized by square or rectangular symmetry, e.g. the (100) and (110) planes of f.c.c. crystals, one expects to find many new phenomena due to specific interplay between the adsorbate–adsorbate and adsorbate–solid interactions. Although the activity in this field is also very high on both the experimental [13,14,18,20,93–111] as well as theoretical [15,42,112–133] sides, our understanding of the properties and behavior of films adsorbed on such surfaces is considerably less advanced. The reason for such a situation is that these systems exhibit much higher complexity of interactions, which in case of metallic materials are still not quite well understood. The variety of possible ordered phases, as well as — in many cases — unclear nature of the phase transitions between them, makes the study very exciting but also difficult and tedious.

In the cases of square and rectangular lattices, the surface corrugation potentials exhibit usually much higher periodic variations [1] and there is a natural difference in the symmetries of such lattices and the preferred symmetry of the adlayers. Thus, the competition between the adsorbate–adsorbate and the adsorbate–adsorbent interactions must be much stronger and may lead to the formation of the new types of ordering in the film. Indeed, several experimental studies have revealed the existence of the higher order commensurate phases [110,134] and axially ordered phases [15,20,18,97] in addition to the registered and incommensurate (floating solid) phases. The mechanisms of phase transitions between all those different types of surface phases are quite complex and are not so well described and understood as in the case of hexagonal surfaces.

In this review, we tackle several questions concerning general aspects of the formation and properties of the adsorbed films deposited on square and rectangular surfaces. Our discussion is primarily directed towards the presentation of recent studies performed for such systems with the help of computer simulation methods. In particular, we shall concentrate on the investigation of various phase transitions occurring in adsorbed layers. It seems appropriate, however, to include also in the discussion a general overview of surface phase transitions, emphasizing their specificity, as compared to the behavior of three-dimensional bulk uniform systems, and the role of the substrate surface structure on the behavior of adsorbed films. The abundance of various phenomena occurring in surfacial layers and evidenced by numerous experimental and computer simulation studies, renders it necessary to exclude several important problems from the discussion. Thus, we shall not consider here adsorption on reconstructed surfaces as well as the adsorbate induced surface reconstruction processes. Also, the kinetics of domain growth and dynamical aspects of adsorption phenomena will not be covered here. Instead, we will concentrate on the influence of the surface corrugation potential on the equilibrium properties of monolayer as well as multilayer films.

In Section 2 we will introduce some basic definitions and notation and briefly discuss some fundamental problems of the interactions between the adsorbate and the solid substrate, as well as between the adsorbed species. The appropriate description of the molecular interaction potentials is essential for computer simulations, but it is also of great general importance. In the same section we will recall some early mean-field type theories developed to describe adsorption on crystalline surfaces exhibiting finite periodic variations of the gas–solid potential. Those attempts must be now considered as naive but we think that the presentation of the advance of our knowledge requires the mention of those early attempts. Finally, after this historical introduction, we will present the basic models that will

be discussed in the following parts of this article. Section 3 is devoted to the general discussion of theoretical ideas developed in order to describe various surface phases and surface phase transitions. Then in Section 4, we will concentrate on the computer simulation studies performed within the general framework of lattice gas models for both monolayer and multilayer adsorbed films. It will be demonstrated that even such idealized models provide very valuable information and in many cases lead to the results which are in very good agreement with the experimental data, as well as produce new insights.

In Section 5, we will discuss the problems of adsorbed films formed on crystalline surfaces exhibiting finite corrugation of the surface potential. Here, we shall first briefly survey the experimental situation, emphasizing the studies pointing to a direct correlation between the structure of surface phases and the corrugation potential. Then, we will concentrate on the results of the computer simulation studies performed for model as well as real systems. The use of computer simulations for investigation of the interplay between the surface corrugation and different forms of ordering in adsorbed layers is particularly attractive. In contrast to real systems, in computer simulation one can arbitrarily change the interaction potentials and the effects of surface corrugation in order to examine various regimes in which different forms of ordering are stable. One particularly interesting problem is the mechanism of the melting transition in adsorbed films. Experiments and theory show that it is still a very controversial question. We shall briefly consider this topic and discuss recent progress achieved due to the application of computer simulation methods. Although our interest in this section is mainly directed towards the problems of monolayer adsorption, we shall consider also some aspects of the effects connected with the formation of thicker films and the influence of higher adsorbed layers on the structure of the first adsorbed layer, adjacent to the solid surface. Finally, we will also discuss the properties and structure of films formed by nonspherical molecules adsorbed on crystalline surfaces of square and rectangular symmetry.

In the concluding Section 6, we will briefly summarize and discuss the material presented in this article and point to some still open questions that require further studies.

2. Preliminaries

2.1. The gas–solid corrugation potential

In the most general situation, the surface of a solid material may have quite complex and irregular structure, which in adsorption literature is usually termed as heterogeneous [135]. In such cases, also the adsorbed films exhibit a high degree of nonuniformity and do not possess well defined structures. Thus, the surface heterogeneity can completely destroy any form of order, as well as any phase transitions in the adsorbed film [136]. This is the fundamental reason why the attempts to observe experimentally phase equilibria in adsorbed layers were not successful until the methods of preparation of materials with highly homogeneous surfaces were developed [50,51,137,138]. Even so, the experimental study meets several problems due to the always present residual heterogeneities resulting from the limited size of crystallites, the defects of the crystal lattices, the presence of steps, etc. All these imperfections are known to influence the internal structure of the film and to affect particularly the surface phase transitions, leading to rounding and shifting of the transition region [46]. Among the well understood problems are the finite size effects [65] and the adsorption at stepped surfaces

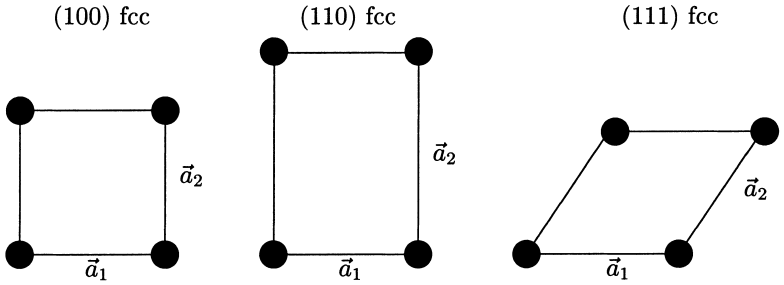

Fig. 1. Top view of the f.c.c. (100), (110) and (111) surface unit cells showing the unit cell vectors $\boldsymbol{a}_1$ and $\boldsymbol{a}_2$. The lengths of the unit cell vectors for (110) and (111) surfaces are expressed in units of $\boldsymbol{a}_1$ for the (100) surface.

[139–141], so characteristic to vicinal planes of metal crystals [142]. Some aspects of the finite size effects will be discussed later in the following section.

Here, we assume that the surface exposed to the gas phase is a perfect single plane of a crystal. In such a simple situation we can fully characterize the surface lattice by its unit lattice vectors $\boldsymbol{a}_1$ and $\boldsymbol{a}_2$ Fig. 1. The interaction of the gas atom with the crystal can be represented by the potential $v(\boldsymbol{\tau}, z)$, where $\boldsymbol{\tau} = (x, y)$ is the two-dimensional vector specifying the location of the adatom in the plane parallel to the surface and z is the distance from the surface, located at $z = 0$ and assumed to run through the centers of the uppermost layer of the crystal atoms. The periodic structure of the crystal surface causes the potential $v(\boldsymbol{\tau}, z)$ also to be a periodic function, such that

$$v(\boldsymbol{\tau}, z) = v(\boldsymbol{\tau} + k_1\boldsymbol{a}_1 + k_2\boldsymbol{a}_2, z), \tag{2.1}$$

where k_1 and k_2 are integers. This periodicity property of the potential $v(\boldsymbol{\tau}, z)$ has prompted Steele [143] to represent $v(\boldsymbol{\tau}, z)$ in the form of the Fourier series

$$v(\boldsymbol{\tau}, z) = v_0(z) + \sum_{\boldsymbol{q}\neq 0} v_{\boldsymbol{q}}(z)\exp[\mathrm{i}\boldsymbol{q}\cdot\boldsymbol{\tau}], \tag{2.2}$$

where $v_0(z)$ is the interaction potential averaged over the entire surface and the sum runs over the nonzero two-dimensional reciprocal lattice vectors $\boldsymbol{q}$:

$$\boldsymbol{q} = n_1\boldsymbol{b}_1 + n_2\boldsymbol{b}_2, \tag{2.3}$$

where $\boldsymbol{b}_1$ and $\boldsymbol{b}_2$ are the basic reciprocal lattice vectors and n_1 and n_2 are integers.

The magnitudes and the functional dependence upon z of the Fourier coefficients $v_{\boldsymbol{q}}(z)$ are primarily determined by the nature of interactions in the system. Steele [143] has assumed the gas–solid interaction to be a sum of interactions between the adsorbate atom and all the individual atoms forming the crystal, with the pair potential given by the (12,6) Lennard-Jones function

$$u(r) = 4\varepsilon_{\mathrm{gs}}\left[\left(\frac{\sigma_{\mathrm{gs}}}{r}\right)^{12} - \left(\frac{\sigma_{\mathrm{gs}}}{r}\right)^{6}\right], \tag{2.4}$$

where σ_{gs} and $\varepsilon_{\mathrm{gs}}$ have been determined using the standard mixing rules [144]

$$\sigma_{\mathrm{gs}} = \tfrac{1}{2}(\sigma_{\mathrm{gg}} + \sigma_{\mathrm{ss}}) \quad \text{and} \quad \varepsilon_{\mathrm{gs}} = \sqrt{\varepsilon_{\mathrm{gg}}\varepsilon_{\mathrm{ss}}} \tag{2.5}$$

and $\sigma_{\mathrm{gg}}(\sigma_{\mathrm{ss}})$ and $\varepsilon_{\mathrm{gg}}(\varepsilon_{\mathrm{ss}})$ are the Lennard-Jones potential parameters for the gas (solid). Using the above assumptions Steele has derived analytic expressions for $v_0(z)$ and $v_{\boldsymbol{q}}(z)$ that apply to surfaces of different symmetry.

The usefulness of the expansion (2.2) depends primarily on how fast it converges. It turns out that the convergence of the series is quite fast for the graphite basal plane and for (100) and (111) faces of the f.c.c. crystal [131,143]. On the other hand, for the (110) plane of the f.c.c. crystal it is necessary to include significantly more terms in order to obtain reliable results [133].

The expressions for the Fourier coefficients derived by Steele have rather limited application to real systems, since the Lennard-Jones potential is not the best choice for the representation of two body interactions in adsorption on ionic crystals, e.g., NaCl and MgO, or on metals.

An important ingredient of the potential field above the surface of an ionic crystal is the electric field which polarizes the adsorbate [145]. Thus, the effective interaction between the adsorbate atom, or molecule, and the substrate may be considerably different from that resulting solely from the van der Waals-like forces. In some cases the presence of an electric field causes that for different adsorbates the potential minima (adsorption sites) correspond to different positions over the surface lattice unit cell, as it was found for simple atomic (rare) gases adsorbed on NaCl and KCl [146]. The situation becomes much more complex for molecular adsorbates. In such cases, the dipole, quadrupole as well as higher multipole moments are often a primary source of interactions determining the arrangement of admolecules over the surface, as well as their orientations [23,55,147,148].

In the case of metallic substrates, the problem of the evaluation of the depth, as well as the shape (i.e., corrugation) of the holding potential is particularly difficult, and in this case a simple model based on the van der Waals atom–atom interaction is completely inadequate. Actually, we usually do not have at our disposal any simple analytic expression for the gas–metal interaction potentials. Therefore, one must rely on experimental estimations [149–151] and available ab initio calculations for some systems [152,153]. Among the experimental methods allowing to probe the depth as well as the corrugation of the surface potential we just mention here the atomic helium scattering [22,150,151] and the inelastic neutron scattering [154]. The problem with the atomic helium scattering is, as observed by Kern and Comsa [22], that the helium atoms experience the corrugation of the repulsive part of the interaction potential, while the adsorbate atoms feel the corrugation of the attractive potential, and the resulting potential wells. Besides, one cannot assume that the corrugation felt by small and light helium atoms is the same as observed for heavier and larger adsorbate atoms. The potential barriers between adjacent minima are, even for the van der Waals forces, determined by the relative size of the adsorbate and the surface lattice cell and by the strength of the gas–solid potential given by the parameter ε_{gs}.

However, the use of inelastic neutron scattering experiments to determine the properties of the binding potential has been shown [154] to give quite reliable results.

Coming back to the problem of the gas–metal interaction potential, we should note that recent experimental [155] and theoretical [152,153] studies have demonstrated that even the closed packed faces of metal crystals, e.g. Pt(111), show quite strong periodicity of the surface potential, against a wide-spread belief [91,92] that such surfaces can be considered as essentially noncorrugated. The self-consistent Hartree–Fock [152] and ab initio [153] calculations pointed out that the hybridization between occupied rare gas orbital and empty d-orbitals of transition metals considerably enhances the surface corrugation effects. On metals, similarly to ionic crystals, the most favorable sites are not always located over the centers of the surface unit lattice cell, but may correspond to positions directly over the surface atoms, as found for Xe/Pt(111) system [22], as well as to other positions.

In fact, there are not so many direct and reliable estimations of the surface corrugation potential, apart from rather well known examples of simple gases on graphite [156], lamellar dihalides [138], and on some close packed metal surfaces [22]. It should be noted that even in the case of simple gases

adsorbed on graphite, for which the interaction potentials are believed to be known quite well, it turns out that the corrugation effects are probably higher than obtained from theoretical calculations. It has been demonstrated by computer simulations [157–162] that in order to obtain a good agreement with experimental data the periodic variations of the surface potential need to be higher. To take this effect into account, the expression (2.2) has been modified [157] by introducing the adjustable "corrugation parameter" V_b, so that Eq. (2.2) takes the following form:

$$v(\boldsymbol{\tau}, z) = v_0(z) + V_b \sum_{\boldsymbol{q}\neq 0} v_{\boldsymbol{q}}(z)\exp[i\boldsymbol{q}\cdot\boldsymbol{\tau}]. \tag{2.6}$$

For the values of $V_b > 1$, the effects due to the corrugation are enhanced with respect to those predicted by Eq. (2.2), while for $V_b < 1$ they are weakened.

In many cases, to study the basic effects of surface potential corrugation and surface lattice symmetry it suffices to retain only very few leading terms in the expansion (2.2) (or (2.6)) and consider the Fourier amplitudes as adjustable parameters. A good example of such an approach is the study performed by Bruch and Venables [112], who considered the conditions that must be satisfied by the system geometry and the binding potential in order to stabilize uniaxially ordered structures in monolayer films. The above assumption is justified by the known property of the Fourier coefficients $v_{\boldsymbol{q}}(z)$, which usually decay rapidly with $|\boldsymbol{q}|$ and z. In many cases this decay is exponential [143], i.e.,

$$v_{\boldsymbol{q}}(z) \propto \exp[-|\boldsymbol{q}|z]. \tag{2.7}$$

From the above property of the corrugation potential, we immediately conclude that its direct effect on the admolecules located beyond the first layer is bound to be very weak, if any at all. It does not mean, of course, that the structure of the second and higher layers is unaffected by the properties of the surface potential. The attraction between admolecules and the surface is responsible for the formation of subsequent adsorbed layers and its strength is a chief factor determining the film growth mode [43], as well as internal structure of particular layers. The effects due to the surface corrugation are transmitted to the higher layers through the interaction with the admolecules from the first layer, which are under a strong influence of the surface corrugation potential. These effects have been demonstrated by the molecular dynamics simulation of Phillips and Shrimpton [162], as well as by the Monte Carlo study of Patrykiejew et al. [63,163].

The most pronounced effect of the corrugation potential is the often observed formation of ordered structures of the symmetry determined by the geometry of the surface lattice, as will be discussed in the following parts of this article, in which we wish to elucidate the effects of the corrugated potential in some model systems, emphasizing that ambiguities hampering the interpretation of experimental systems — such as the possible effects of the aforementioned surface steps — are absent and the substrate surface is strictly ideally periodic without any defects. Of course, we shall also invoke several examples of experimental studies and try to show that both theory and computer simulations lead to new insights and allow for better understanding of experimental observations.

2.2. Basic theoretical models

The properties and structure of adsorbed films are controlled by the combined effects due to admolecule–admolecule and admolecule–substrate interactions as well as by the imposed thermodynamic constraints (specified temperature, film density, bulk gas pressure). Of course, in real

situations, as well as in computer simulations, the effects due to finite size of the surface may considerably affect the structure of adlayers [63], but we shall not discuss such problems here.

In general, at low temperatures the adsorbate–adsorbate interaction tends to enforce the formation of hexagonal close-packed (h.c.p.) solid phase in monolayer films, while the corrugated admolecule–substrate potential favors the formation of registered structures. A simple criterion enabling to classify the adsorbed films with respect to their structure has been developed by Park and Madden [164]. Assuming that the substrate surface lattice unit cell vectors are $\boldsymbol{a}_1$ and $\boldsymbol{a}_2$ and the overlayer unit cell is characterized by the unit vectors $\boldsymbol{e}_1$ and $\boldsymbol{e}_2$, the relation between these two sets can be written as

$$\begin{bmatrix} \boldsymbol{e}_1 \\ \boldsymbol{e}_2 \end{bmatrix} = \begin{bmatrix} \alpha_{11} & \alpha_{21} \\ \alpha_{21} & \alpha_{22} \end{bmatrix} \begin{bmatrix} \boldsymbol{a}_1 \\ \boldsymbol{a}_2 \end{bmatrix}. \tag{2.8}$$

Park and Madden have classified the adsorbed layers with respect to the behavior of $\det[\alpha_{ij}]$ and singled out three cases. The first case groups all systems for which $\det[\alpha_{ij}]$ is an integer. This situation corresponds to the registered or commensurate adsorbed films. The second case involves the situations in which $\det[\alpha_{ij}]$ is a rational number. When this condition is satisfied the adsorbed film forms the so-called ''high-order'' commensurate phase, with only a certain fraction of adatoms located directly over the adsorption sites. Finally, when $\det[\alpha_{ij}]$ is an irrational number (case three) the adsorbed layer is incommensurate with the substrate surface lattice. The above classification parametrizes the adsorbed layer structure with respect to the relative sizes of the surface and adlayer unit cells. The area of the surface unit lattice cell is given by $\boldsymbol{a}_1 \times \boldsymbol{a}_2$, and the area of the adsorbed layer unit cell is equal to $\boldsymbol{e}_1 \times \boldsymbol{e}_2$, so that $\det[\alpha_{i,j}]$ is equal to the ratio of these two areas. A more detailed discussion of all the above cases is presented in Section 3.

The criterion of Park and Madden vastly oversimplifies the reality. The distinction between the incommensurate and the high-order commensurate phases may cause problems, as it is usually possible to approximate an irrational number by a suitably chosen rational number that falls into the region of experimental resolution. Aubry [165] has even proposed to consider any incommensurate adsorbed layer as a sufficiently high-order commensurate phase. When the conditions change and the density of the film increases or decreases, it is supposed that the resulting changes in the film structure are due to a series of first-order transitions between different high-order commensurate phases. This leads to the so-called ''devil's staircase'' of phase transitions.

Another weakness of the above criterion is that it does not include incommensurate phases exhibiting domain wall networks [61,62]. In such cases the incommensurate phase is composed of large commensurate domains separated by walls which can have different structure, thickness and orientation (Section 3).

A useful measure of the relative size of the adsorbate and the surface lattice unit cell is the so-called dimensional incompatibility parameter [166], defined as

$$I = (a - r_1)/r_1, \tag{2.9}$$

where a is the surface lattice constant and r_1 is the distance between adsorbate atoms in the surface phase. Of course, in the case of a rectangular symmetry of the surface lattice, one can define two different dimensional incompatibility parameters I_1 and I_2, by taking $a = |\boldsymbol{a}_1|$ and $a = |\boldsymbol{a}_2|$. As will be discussed in Section 5, the behavior of films formed on corrugated surfaces is closely related to the magnitude of the parameter I.

2.2.1. Lattice models of localized adsorption

Assuming that the potential barriers between adjacent minima of the surface potential are high, as compared to the admolecule–admolecule and thermal energies, one can treat the adsorbed atoms as bound to those adsorption sites and unable to take different positions over the surface. The locations of the surface potential minima form a regular lattice of the same geometry as that of the substrate's surfacial layer. The resulting model of localized adsorption can be represented in the general framework of the lattice gas model [5,127,167–173].

In the simplest version of such a model, every site i is characterized by a single degree of freedom, the occupation variable, n_i, which equals 1 when the site is occupied by the adsorbate atom, and equals 0 when the site is empty. In this way, the model mimics the exclusion of multiple occupation of the same surface element. Assuming that the interaction energy between the adsorbate particles and the substrate is the same for all sites and equal to V_0 (V_0 is negative for attractive interaction) and that the interaction between adsorbed atoms is pairwise additive and represented by the potential $u(r_{ij})$, with r_{ij} being the distance between the sites i and j, the Hamiltonian for the above model reads

$$\mathscr{H} = V_0 \sum_i n_i + \frac{1}{2} \sum_{i \neq j} u(r_{ij}) n_i n_j. \tag{2.10}$$

To meet the usual experimental conditions of equilibrium between the adsorbed film and the bulk uniform gas, it is convenient to work in the grand canonical ensemble. Now the chemical potential of the adsorbate μ is the independent thermodynamic parameter, and the Hamiltonian for this case is obtained by subtracting the term $\mu N = \mu \sum n_i$ from Eq. (2.10), i.e., we have

$$\mathscr{H}' = \mathscr{H} - \mu N = (V_0 - \mu) \sum_i n_i + \sum_{i \neq j} u(r_{ij}) n_i n_j. \tag{2.11}$$

The surface coverage θ is a conjugate variable to μ and can be calculated from the following relation:

$$\theta = -\left(\frac{\partial (F/kT)}{\partial \mu} \right)_T, \tag{2.12}$$

where F is the system free energy given by

$$F = -kT \ln \mathrm{Tr} \exp[-\mathscr{H}'(\{n_i\})/kT] \tag{2.13}$$

and the trace is taken over all configurations $\{n_i\}$ of the entire system. Assuming that the bulk gas is ideal, with the chemical potential μ_g related to the pressure p by the equation

$$\mu_g = \mu_g^0 + kT \ln p \tag{2.14}$$

we get the following general equation of the adsorption isotherm:

$$\ln p = -\mu_g^0/kT + \frac{1}{L^2 kT} \left(\frac{\partial F}{\partial \theta} \right)_T, \tag{2.15}$$

where L is the linear dimension of the lattice and it is assumed here that $L \to \infty$. One can also readily relate the thermal average of the occupation variable to the coverage θ. Namely for the lattice of L^2 sites we have

$$\theta = \frac{1}{L^2} \sum_{i=1}^{L^2} \langle n_i \rangle_T. \tag{2.16}$$

Similarly, the average potential energy per lattice site is given by

$$U = \langle \mathscr{H} \rangle_T / L^2 = V_0 + \frac{1}{2L^2} \sum_{i \neq j} u(r_{ij}) \langle n_i n_j \rangle_T. \tag{2.17}$$

It is also straightforward to obtain expressions for other thermodynamic quantities, such as the heat capacity

$$C = \frac{1}{kT^2 L^2} [\langle \mathscr{H}^2 \rangle_T - \langle \mathscr{H} \rangle_T^2] \tag{2.18}$$

and the isothermal compressibility

$$\kappa = \frac{1}{kTL^2} \left[\sum_i \langle n_i^2 \rangle - \left(\sum_i \langle n_i \rangle \right)^2 \right] \tag{2.19}$$

which carries the information about the density fluctuations in the adsorbed film.

The lattice gas model Hamiltonian (2.11) can be mapped on an equivalent Ising model Hamiltonian $\mathscr{H}_{\text{Ising}}$ [129]. The spin orientation at the ith site $S_i = \pm 1$ is related to the occupation variable n_i by

$$S_i = 1 - 2n_i \tag{2.20}$$

and it yields

$$\mathscr{H}' = \frac{1}{2} N(V_0 - \mu) + \frac{1}{4} \sum_{i \neq j} u(r_{ij}) + \mathscr{H}_{\text{Ising}} \tag{2.21}$$

with

$$\mathscr{H}_{\text{Ising}} = -H \sum_i S_i - \sum_{i \neq j} J_{ij} S_i S_j. \tag{2.22}$$

In the above

$$H = \frac{1}{4} \sum_{j(\neq i)} u(r_{ij}) + \frac{1}{2} (V_0 - \mu) \tag{2.23}$$

is the ''magnetic field'' related to the chemical potential and

$$J_{ij} = -\frac{u(r_{ij})}{4} \tag{2.24}$$

are the effective two-spin coupling constants. Representation of the lattice model in the ''magnetic language'' immediately brings out the symmetry properties of the Hamiltonian (2.22). Namely, it is invariant under the transformation

$$H, \quad \{S_i\} \rightarrow -H, \quad \{-S_i\}. \tag{2.25}$$

This implies that the adsorption isotherm is antisymmetric with respect to the point $\theta = 1/2$, $\mu = \mu_c$, where μ_c is the chemical potential value corresponding to $H = 0$.

The above model assumes that interactions in the system are pairwise additive. In many situations the inclusion of contributions due to non-pairwise interactions may be also needed [167,169]. For example,

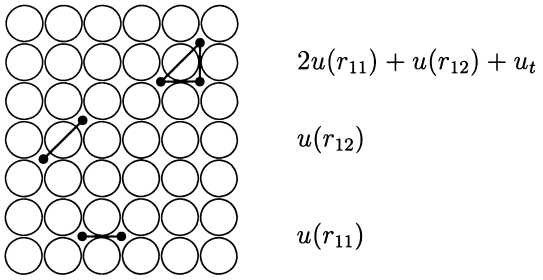

Fig. 2. Interaction energies on a square lattice. $u(r_i)$ represent pairwise interaction between the ith site and its nearest neighbors and u_t is the three-body energy.

the energy of the occupied triangle of neighboring sites Fig. 2 involves a three-body interaction term u_t and is equal to $2u(r_1) + u(r_2) + u_t$. The inclusion of three-body interaction modifies the expression for the configurational energy of the system (2.10) and gives

$$\mathscr{H} = V_0 \sum_i n_i + \frac{1}{2} \sum_{i \neq j} u(r_{ij}) n_i n_j + \sum_{i \neq j \neq k} u_t n_i n_j n_k. \tag{2.26}$$

The most important consequence of nonzero three-body interaction is the removal of above mentioned symmetry properties of the Hamiltonian.

Another possibility is to consider lattice gas models with anisotropic interactions in different directions [33,170]. Such a model may be used to mimic adsorption on rectangular lattices. This last model allows to consider the formation of both the commensurate as well as incommensurate phases. When the mutual occupation of adjacent sites is excluded (large size of adsorbate atoms), the surface lattice can be decomposed into a number (q) of sublattices, as it will be discussed in Section 3. Another possibility is to use the lattice gas model formalism to represent the properties of multilayer films [43,174–178] and to study wetting phenomena (see Section 4). In this case, the three-dimensional version of the lattice model is considered, with the surface potential represented as a function of the distance from the surface z. Of course, in the lattice gas model language this distance can assume only discrete values and is expressed in lattice spacings.

Several specific examples of lattice gas models used to represent adsorption on square and rectangular lattices will be considered in Section 4.

2.2.2. Early theories of adsorption on corrugated surfaces

It seems intuitively obvious that lattice gas models are best suited to represent low temperature adsorption on highly corrugated surfaces. Only in such cases, the effects due to surface diffusion of adatoms can be safely ignored. For example, the temperature dependence of the configurational heat capacity of a single atom adsorbed on a crystalline solid was found [179,180] to exhibit a broad peak with the maximum located at $T \approx 0.2V_D/k$, where V_D is the height of the potential barrier between adjacent sites. The position of that maximum only very slightly depends on the surface lattice symmetry and the size of adsorbed atoms. The appearance of that heat capacity peak results directly from a gradual transition from the regime of fully localized adsorption ($kT/V_D \ll 0.2$) to the regime of fully mobile adsorption ($kT/V_D \gg 0.2$). At the intermediate temperatures, the adsorption is neither

fully localized nor fully mobile and can be termed as partially localized. Of course, the degree of localization of adatoms is not entirely determined by the parameter kT/V_D, but depends also on the film density. Mutual interaction between the adsorbed atoms plays an important role in dense films and may stabilize commensurate structures, as well as lead to the formation of incommensurate films, as will be discussed in later sections of this article. Numerous experimental facts also support the concept of partially localized adsorption (see Ref. [181] and the references cited therein).

Assuming for a moment that the degree of localization is entirely determined by the height of potential barrier V_D and the temperature, it is possible to construct a simple model which assumes that the localized atoms are represented by the lattice gas model, while the mobile ones are treated as a two-dimensional uniform fluid. Within the mean field approximation, the localized atoms are represented in the framework of Bragg–Williams approximation and the mobile ones by a two-dimensional counterpart of the van der Waals fluid model. This approach leads to a simple equation of the adsorption isotherm in the form [182]

$$p = K(T)\frac{\theta}{1-\theta}\left(\frac{1-\theta}{1-f_\ell\theta}\right)^{f_\ell}\exp\left[\frac{f_m\theta}{1-\theta} - \alpha\theta/kT\right], \tag{2.27}$$

where $K(T)$ is the Henry law constant, θ the surface coverage, f_ℓ and f_m are the fractions of localized and mobile molecules, respectively, and the parameter α represents the effects of adsorbate–adsorbate interaction and is given by

$$\alpha = \alpha_m f_m(2-f_m) + \alpha_\ell f_\ell^2. \tag{2.28}$$

The constants α_m and α_ℓ represent the effect of adsorbate–adsorbate interaction in fully mobile and fully localized adsorption models, respectively. Note that both f_ℓ and f_m ($f_\ell + f_m = 1$) are functions of the temperature and the potential barrier V_D. One important property of the above model is that it predicts changes in the location of the critical point with V_D. In particular, the critical value of the surface coverage changes with the degree of localization. In the case of a simple lattice gas model with attractive interaction between the nearest neighbors, the critical density is equal to $\theta_c = 1/2$, while for the two-dimensional uniform van der Waals fluid it is equal to 1/3. In many experimental situations the value of θ_c lies between those two limiting values and the above model allows for a rough estimation of the degree of localization if θ_c is known [183].

A more realistic model which assumes that the degree of localization depends also on the film density has been also developed. Holland [184] considered adsorption of hard disks, and then Patrykiejew [185] extended the model by taking into account the effects of mutual attractive interaction between the adsorbed atoms. The contribution due to localized atoms was obtained by minimizing the Helmholtz free energy of the film with respect to the density of localized atoms (for a fixed total surface coverage). This model allows also to include the possibility of formation of other registered structures than a simple (1×1) phase. In the case of adsorption on a surface with a square symmetry and when the size of adsorbed atoms is too large for a mutual occupation of nearest neighbor sites, the registered ordered phase corresponds to the $c(2 \times 2)$ structure. In such a case the surface lattice can be considered as composed of two interpenetrating sublattices (Section 3.1) and the formation of $c(2 \times 2)$ phase is connected with a preferential occupation of only one sublattice. Within the mean field approximation, the above model leads to the following set of equations which define the adsorption isotherm:

$$p = K_{\mathrm{m}}(T)\frac{\theta-\theta_\ell}{1-\theta}\exp\left[\frac{\theta-\theta_\ell}{1-\theta}-\alpha_{\mathrm{m}}\theta/kT\right], \tag{2.29}$$

$$C(T) = \frac{(1-\theta_\ell)(\theta-\theta_\ell)}{(\theta_l^2-\delta^2)^{1/2}(1-\theta)}\exp[\Delta\alpha\theta/kT] \tag{2.30}$$

and

$$\delta = \begin{cases} 0, & \theta_\ell \le 2kT/D, \\ \dfrac{kT}{D}\ln\dfrac{\theta_\ell+\delta}{\theta_\ell-\delta}, & \theta_\ell > 2kT/D, \end{cases} \tag{2.31}$$

where $K_{\mathrm{m}}(T)$ is the Henry constant for mobile adsorption, the function $C(T)$ depends also on $V_{\mathrm{D}}, \Delta\alpha = \alpha_{\mathrm{m}} - \frac{1}{2}(\alpha_{ii}+\alpha_{ij}), D = \alpha_{ii}-\alpha_{ij}, \theta_\ell$ is the surface coverage corresponding to localized atoms and δ measures the asymmetry of occupation of different sublattices by the localized atoms. The parameters α_{ii} and α_{ij} represent the energies of interaction between localized atoms located on the same and different sublattices, respectively. Note that the values of α_{ii} and α_{ij} depend on the relative size of adatoms and the surface lattice unit cell.

The above model predicts that the distribution of adatoms between the sublattices is uniform when the total surface coverage is lower than

$$\theta^* = \frac{H(T)+2kT/D}{H(T)+1}, \tag{2.32}$$

where

$$H(T) = \frac{2kT}{2kT-D}C(T)\exp\{-2[\alpha_{\mathrm{m}}-\tfrac{1}{2}(\alpha_{ii}+\alpha_{ij})]/D\}. \tag{2.33}$$

The preferential occupation of one sublattice occurs for higher surface coverages ($\theta > \theta^*$).

The parameters $\Delta\alpha$ and D are primarily determined by the relative size of adsorbate atoms and lattice unit cell. Thus, one can relate them to the dimensional incompatibility between adsorbate and adsorbant I. The dependence of the film properties on the height of potential barrier for diffusion is carried by the parameter $C(T)$, which changes with V_{D} and T. At the low temperature limit $C(T) \to 0$, the adsorption is fully localized, while at the high temperature limit $C(T) \to \infty$ and adsorption is fully mobile. Depending on the values of I and V_{D} the model predicts four different types of phase diagrams for the adsorbed monolayer as shown in Fig. 3. It should be noted that all situations depicted in Fig. 3 resemble phase diagrams found in experimentally studied systems [166,187,188].

The main shortcoming of the above presented models is that they rest upon a very crude mean-field approximation and also do not take into account any possibility of the formation of dense incommensurate solid phases (Section 3.3). Observed qualitative similarities between the predictions of those models and experimental observations may be misleading. The model predicts that the high density (solid) phase is a registered $\mathrm{c}(2\times 2)$ phase, while experiments [108], as well as computer simulations [189], demonstrate clearly that the formation of registered (or partially registered) phase occurs at lower densities and is often followed by the transition to a still more dense incommensurate solid phase. Thus, the model does not correctly predict the topology of the phase diagram. Mean field character of the model leads also to a serious overestimation of the critical, triple and tricritical points so that any fit to experimental data is bound to give incorrect values of the parameters such as V_{D}.

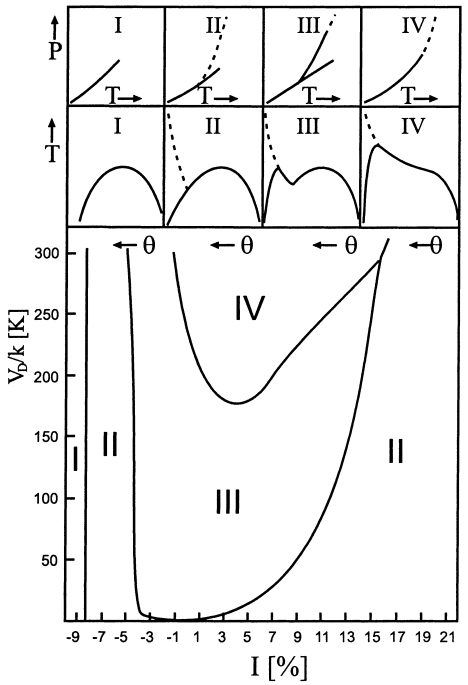

Fig. 3. Different types of the phase diagram (upper part) and the regions of the potential barrier for diffusion V_D and the dimensional incompatibility I corresponding to different phase behavior of adsorbed monolayer films (lower part) predicted by Eq. (2.29) (from ref. [186]).

Another simple model of monolayer adsorption on corrugated surfaces was proposed by Niskanen [190]. The model includes both commensurate and incommensurate solid phases in addition to gas and liquid phases. The fluid (gas and liquid) phases are represented by a lattice gas model while the solid phases (both commensurate and incommensurate) are described in terms of the Lennard-Jones–Devonshire cell model [191]. In order to construct phase diagrams the Helmholtz free energies of different phases as functions of film density (θ) have been calculated. For the solid phases, the cell model leads to the following simple expression for the free energy:

$$F_S(\theta, T) = \theta u_0 - \theta kT \ln [A_f(\theta, T)], \tag{2.34}$$

where u_0 is the ground state energy per atom, $A_f(\theta, T)$ is the free area of thermal oscillations and its analytic form is known [191]. It has been assumed that the surface corrugation does not affect the properties of the incommensurate solid. A commensurate phase has been assumed to be represented by the same model but for a specified density θ_C. The particular value of θ_C has been determined by the size of the surface unit cell. The effect of surface corrugation has been taken into account by assuming that it leads to a lowering of the ground state energy of the commensurate phase by Δu_0, so that the free energy for that phase reads

$$F_C(\theta_C, T) = F_S(\theta_C, T) - \theta_C \Delta u_0. \tag{2.35}$$

The properties of the gas and liquid phases, represented by the Ising model, were evaluated using approximate Kadanoff's variational method [192].

The above model predicts very rich phase diagrams. Their detailed structure depends on the assumed value of the commensurate phase density, which is determined by the size of adsorbed atoms, and the magnitude of surface corrugation. A mean field character of the model leads to severe underestimation of the entropy and predicts that all the observed transitions are first-order. In particular, in the case of triangular symmetry of substrate lattice considered by Niskanen, both solid phases are of the same symmetry, so that the transition is bound to be continuous (Section 3). The use of lattice gas model to represent fluid phases is also quite unrealistic for low surface corrugations as it ignores the effects of surface corrugation on the structure of liquid phase and the location of the critical point (Section 5). It was argued that the model can be also applied to substrates with square symmetry, but then the assumed cell model is a very poor representation for the incommensurate phase.

Although the approaches recalled above vastly oversimplify the reality and cannot be directly applied to quantitative analysis of experimental data, they clearly demonstrate that even simple methods of statistical mechanics allow to develop models which reveal the importance of the surface corrugation on the behavior of adsorbed films.

2.2.3. Continuous space models

In principle, the problem of gas adsorption on a crystalline surface characterized by finite corrugation of the surface potential can be approached with the use of theoretical methods similar to those developed for uniform systems.

In the most general case, a gas in contact with a solid surface can be considered as a fluid subjected to the external potential field [193,194]. Thermodynamic properties of such systems can be determined using various approaches such as virial series methods [21,193], integro-differential equations analogous to the Born–Yvon–Green hierarchy [195,196] and the density functional theory [197–200]. The quantities characterizing the adsorbed state are defined as surface excesses of the appropriate thermodynamic functions [193]. For example, the amount adsorbed Γ, is given by the surface excess of the density

$$\Gamma = \int_V [\rho(\boldsymbol{r}) - \rho_b]\, d\boldsymbol{r}, \tag{2.36}$$

where $\rho(\boldsymbol{r})$ is the local density at $\boldsymbol{r}$, ρ_0 is the corresponding bulk uniform fluid density

$$\rho_0 = \lim_{z\to\infty} \rho(\boldsymbol{r}) \tag{2.37}$$

and the integration in Eq. (2.36) is performed over the entire volume of the system. Note that for large distances from the surface the local density becomes independent of $\boldsymbol{\tau} = (x, y)$. At low film densities [193]

$$\rho(\boldsymbol{r}) \propto \exp[-\beta v(\boldsymbol{r})] \tag{2.38}$$

and we know that the variation of $v(\boldsymbol{r})$ with x, y ceases as the distance from the surface increases (Section 2.2).

In a similar fashion one can define the surface excess for any other thermodynamic quantity Y. Namely, defining the local density $y(\boldsymbol{r})$ of the quantity Y one obtains

$$y_{ex} = \int_V [y(\boldsymbol{r}) - y_0]\, d\boldsymbol{r}. \tag{2.39}$$

For example, when the adsorbate–adsorbate interaction is pairwise additive and represented by the potential $u(r)$ then the potential energy is represented by

$$E = \int_V e(\boldsymbol{r})\,\mathrm{d}\boldsymbol{r} \tag{2.40}$$

with the energy density $e(\boldsymbol{r})$ defined as

$$e(\boldsymbol{r}) = \rho(\boldsymbol{r})v(\boldsymbol{r}) + \frac{1}{2}\int_V n^{(2)}(\boldsymbol{r},\boldsymbol{r}')u(|\boldsymbol{r}-\boldsymbol{r}'|)\,\mathrm{d}\boldsymbol{r}'. \tag{2.41}$$

In the above, $n^{(2)}(\boldsymbol{r},\boldsymbol{r}')$ is the two-particle distribution function, which can be written as

$$n^{(2)}(\boldsymbol{r}_1,\boldsymbol{r}_2) = \rho(\boldsymbol{r}_1)\rho(\boldsymbol{r}_2)g_2(\boldsymbol{r}_1,\boldsymbol{r}_2), \tag{2.42}$$

where $g_2(\boldsymbol{r}_1,\boldsymbol{r}_2)$ is the two-particle correlation function. From the above equations it follows that evaluation of the thermodynamic quantities which characterize the system requires detailed knowledge about the local density as well as the two-particle correlation function. Evaluation of those quantities is a highly nontrivial problem and the vast majority of existing theories [196,198,201] rests upon the approximation

$$g_2(\boldsymbol{r}_1,\boldsymbol{r}_2) = g_2^0(|\boldsymbol{r}_1-\boldsymbol{r}_2|), \tag{2.43}$$

where $g_2^0(r)$ is the two-particle correlation function for a uniform system. This approximation is justified only when the effects of surface corrugation are negligible and the adsorbing surface can be considered as an attractive plane. When one is mostly interested in the effects due to surface corrugation on the behavior and properties of adsorbed films, the use of full three-dimensional version of the nonuniform fluid theory is not practical. Calculation of surface excesses of the thermodynamic quantities requires evaluation of multidimensional integrals over the entire volume. Periodic variation of the gas–solid potential affects the properties of the adsorbate at small distances from the surface (Section 2.2) and the potential barrier for surface diffusion is usually much lower than the adsorption energy. Since the gas–solid potential exhibits a rather sharp and deep minimum at a certain preferred distance from the surface, the adsorbed particles are rather tightly bound to the substrate. At low temperatures, where the surface corrugation effects are important, the interface between the adsorbed layer and the bulk (uniform) gas is usually well defined. This allows to consider the adsorbed monolayer film as a two-dimensional phase in equilibrium with a bulk (uniform) gas. Prasad and Toxvaerd [196] have presented a formal theory for such systems using the BBGKY hierarchy [195] of integro-differential equations.

Saam and Ebner [197] and Fairbent et al. [198] considered the density functional theory which assumes that the local density is represented by a superposition of gaussian functions. A similar theory was considered by Sokołowski and Steele [199] and then by Patrykiejew and Sokołowski [200]. Several perturbational theories have been also proposed [201,202]. In such cases, the effects of surface corrugation are assumed to be small enough to be treated as a perturbation to an otherwise uniform two-dimensional fluid subjected to a uniform surface potential

$$v_0 = \langle v(\boldsymbol{\tau})\rangle_{\boldsymbol{\tau}}. \tag{2.44}$$

Periodicity of the gas–solid potential allows to represent the Boltzmann function $e(\boldsymbol{\tau}) = \exp[-\beta v(\boldsymbol{\tau})]$ or

the local density $\rho(\boldsymbol{\tau})$ by the Fourier series

$$\gamma(\boldsymbol{\tau}) = \sum_{\boldsymbol{q}} \tilde{\gamma}_{\boldsymbol{q}} \exp[\mathrm{i}\boldsymbol{q}\cdot\boldsymbol{\tau}], \tag{2.45}$$

where γ stands for e or ρ. Then the properties of a nonuniform system are expanded with respect to the difference

$$\Delta\gamma(\boldsymbol{\tau}) = \gamma(\boldsymbol{\tau}) - \gamma_0, \tag{2.46}$$

where γ_0 corresponds to the uniform reference system.

For example, the perturbational expansion for the local density with respect to $\Delta e(\boldsymbol{\tau})$ reads [202]

$$\ln t(\boldsymbol{\tau}_1) = \rho_0 \int [g_{20}(\tau_{12}) - 1]\Delta e(\boldsymbol{\tau}_2)\,\mathrm{d}\boldsymbol{\tau}_2 + \frac{1}{2}\rho_0^2 \int [g_{30}(\boldsymbol{\tau}_1,\boldsymbol{\tau}_2,\boldsymbol{\tau}_3) - g_{20}(\tau_{13})g_{20}(\tau_{12}) - g_{20}(\tau_{23})]\Delta e(\boldsymbol{\tau}_2)\Delta e(\boldsymbol{\tau}_3)\,\mathrm{d}\boldsymbol{\tau}_2\,\mathrm{d}\boldsymbol{\tau}_3 + \cdots, \tag{2.47}$$

where $t(\boldsymbol{\tau}) = \rho(\boldsymbol{\tau})/e(\boldsymbol{\tau})$ and $g_{m0}(\boldsymbol{\tau}_1,\ldots,\boldsymbol{\tau}_m)$ is the m-particle correlation function of the reference fluid. Substituting Eq. (2.45) into the above expansion one gets

$$\ln t(\boldsymbol{\tau}) = \rho_0 \sum_{\boldsymbol{q}\geq 1} \tilde{e}_{\boldsymbol{q}} \exp(\mathrm{i}\boldsymbol{q}\cdot\boldsymbol{\tau})\tilde{G}_{20}(\boldsymbol{q}) + \frac{1}{2}\rho_0^2 \left\{ \sum_{\boldsymbol{q},\boldsymbol{q}'\geq 1} \tilde{e}_{\boldsymbol{q}}\tilde{e}_{\boldsymbol{q}'} \exp[\mathrm{i}(\boldsymbol{q}+\boldsymbol{q}')\cdot\boldsymbol{\tau}]\tilde{G}_{30}(\boldsymbol{q},\boldsymbol{q}') - \sum_{\boldsymbol{q}\geq 1} \tilde{e}_{\boldsymbol{q}} \exp(\mathrm{i}\boldsymbol{q}\cdot\boldsymbol{\tau})\tilde{G}_{20}(\boldsymbol{q}) \right\} + \cdots, \tag{2.48}$$

where $\tilde{G}_{20}(\boldsymbol{q})$ and $\tilde{G}_{30}(\boldsymbol{q},\boldsymbol{q}')$ are the Fourier transforms of the corresponding two-and three-particle correlation functions. Once the local density of the nonuniform fluid is determined one can readily calculate perturbational corrections to the system free energy and other thermodynamic quantities. Of course, the above expansion can be used only for fluid phases and to a commensurate solid phase. The symmetry properties of the incommensurate solid phase are usually different from the symmetry of solid surface. The unit cell of a solid phase is characterized by the reciprocal lattice vectors $\boldsymbol{k}_1$ and $\boldsymbol{k}_2$ which are different from the surface lattice reciprocal vectors $\boldsymbol{b}_1$ and $\boldsymbol{b}_2$ (cf. Eq. (2.3)). The Fourier expansion for the local density of incommensurate solid phase

$$\rho^{\mathrm{s}}(\boldsymbol{\tau}) = \sum_{\boldsymbol{k}} \rho^{\mathrm{s}}_{\boldsymbol{k}} \exp(\mathrm{i}\boldsymbol{k}\cdot\boldsymbol{\tau}), \tag{2.49}$$

where $\boldsymbol{k} = n_1\boldsymbol{k}_1 + n_2\boldsymbol{k}_2$ (n_1 and n_2 are integers), is rather poorly convergent and the use of perturbational as well as density functional theories requires additional simplifying assumptions. Fairbent et al. [197] proposed to represent the local density of a solid phase by a superposition of Gaussian functions. This approximation gives reasonable results only when the solid phase has the same symmetry as the symmetry of solid lattice and the difference between lattice unit cells of the adsorbed layer is not much different from the surface unit cell. Therefore, it is not appropriate to describe fluid–solid equilibria in adsorbed films on a square or rectangular lattice.

The fundamental problem that somewhat limits the applications of the above mentioned two-dimensional perturbational as well as density functional theories is connected with their mean field character. It is so because exact solutions for multiparticle correlation functions are not available.

Besides, when applied to adsorption on corrugated surfaces, those theories assume that the effects of surface corrugation are small and do not lead to any appreciable out-of-plane effects [203] and ignore, often present, nonuniform density modulations in the film (Section 5).

In fact, the only reliable methods which allow for investigation of adsorption on surfaces with finite corrugation of the gas–solid potential are computer simulations [30,34,131–133], discussed in detail in Section 5.

3. Theories of surface phase transitions

3.1. Ordered states and order–disorder transitions

In this section we wish to recall some basic aspects of the theory of phase transitions which are a necessary prerequisite in order to provide a framework for the discussion of various numerical results in the later sections. We shall emphasize features which distinguish the ordering of these (quasi-) two-dimensional adsorbed layers and the phase transitions which they can undergo from corresponding phenomena in the bulk. We assume some familiarity with the theory of phase transitions and critical phenomena in general (see e.g. [46,204,205] for more tutorial introductions).

At first sight one expects for an adsorbed monolayer all the phases which are familiar states of matter in three space dimensions: gas, fluid and various solid phases (Fig. 4). But there are important

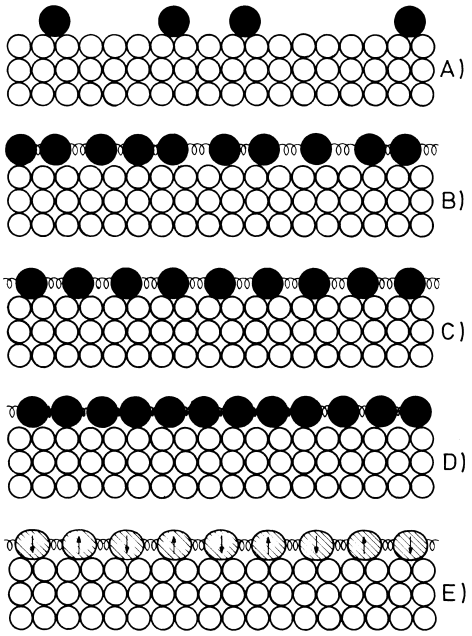

Fig. 4. Schematic cross section of a crystal surface with an adsorbed monolayer (substrate atoms are denoted as open circles, adsorbate atoms as full circles). Springs indicate adsorbate–adsorbate interactions. Lattice gas (A), fluid (B), commensurate (C) and incommensurate (D) solid phases are shown. While cases (A)–(D) assume adsorption of simple atoms, case (E) refers to adsorption of non-dissociated molecules, where internal degrees of freedom of the molecules may show an additional ordering (example: the antiferromagnetic structure of O_2 on graphite).

differences both due to the presence of the corrugation potential caused by the underlying substrate, and by the more profound effect of statistical fluctuations that destabilize certain orderings in two dimensions. If the periodic variation of the corrugation potential is very strong, in comparison with the interaction between adatoms, it may be appropriate to treat the ordering phenomena as a problem in lattice statistics. As discussed already in Section 2.2.1, one considers the ideal lattice formed by the minima of the corrugation potential (disregarding any defects or heterogeneities that may be present at surfaces of real crystals). Each lattice site can be occupied at most by one adatom. If the (pairwise) interaction between adatoms is purely attractive, the only phase which one expects is a lattice gas phase at low coverage, separated by a two-phase coexistence region from a ''lattice-fluid'' phase at higher coverage (Fig. 4A, B). This lattice fluid can be considered as a version of the registered (1×1) phase (where every available site of the lattice is occupied, corresponding to the maximum coverage $\theta = 1$ of the monolayer) diluted with vacancies.

In many cases of practical interest the adatom–adatom interactions are repulsive at least for nearest-neighbor distances on the lattice. Then at low enough temperatures registered superstructures (i.e. monolayers with a periodicity of their ordering that exceeds the lattice spacing a but is commensurate with it) occur (Fig. 4C), Fig. 5 shows examples for a square symmetry of the substrate surface (some other examples will be also invoked in Section 4).

If the potential binding the adlayer to the substrate surface would have vanishing corrugation, we would have to consider essentially ordering phenomena in continuous two-dimensional space. This limiting case is particularly interesting with respect to the liquid–solid transition and the nature of the two-dimensional solid in general. As will be discussed in Section 3.4, such two-dimensional solids possess no true long-range positional order in the usual sense [206], although they possess long-range orientational order. The melting then may occur via two continuous transitions, implying a so-called ''hexatic'' phase in between this unconventional solid and the liquid [39], see Section 3.4. These phenomena may persist in a weak corrugation potential as well (see also Section 5.3). Within the temperature region where solid phases are stable, suitable variation of parameters like coverage (or spreading pressure) and temperature may lead to phase transitions between these incommensurate solids and commensurate phases that are in registry with the substrate periodicity Section 3.3.

While most part of this section is devoted to a discussion of monolayer phase transitions, under suitable conditions also multilayer adsorption and wetting phenomena can be observed Section 3.5. Clearly, it is of interest to understand the relations between the phase behavior of an adsorbate–substrate system at low coverage to the phase behavior of multilayer films at high coverage in the same system.

We now start off with some general comments about order–disorder transitions in registered phases, while critical properties at these transitions will be reviewed in Section 3.2.

For lattice gas systems it is convenient to transform from the local occupation variable n_i $(= 0 \text{ or } 1)$ to a pseudospin variable $S_i = 1 - 2n_i$ $(= \pm 1)$ (see Section 4.1 for details). Then the coverage θ is related to the average magnetization of the pseudospins $m = \langle S_i \rangle_T$, $\theta = (1 - m)/2$. For describing the various orderings of Fig. 5, it is convenient to introduce sublattice magnetizations m_α defined as

$$m_\alpha = (1/M) \sum_{i \in \alpha} \langle S_i \rangle_T, \quad \alpha = a, b, c, d, \tag{3.1}$$

where M is the total number of sites but the sum is extended only over the $M/4$ sites of a particular

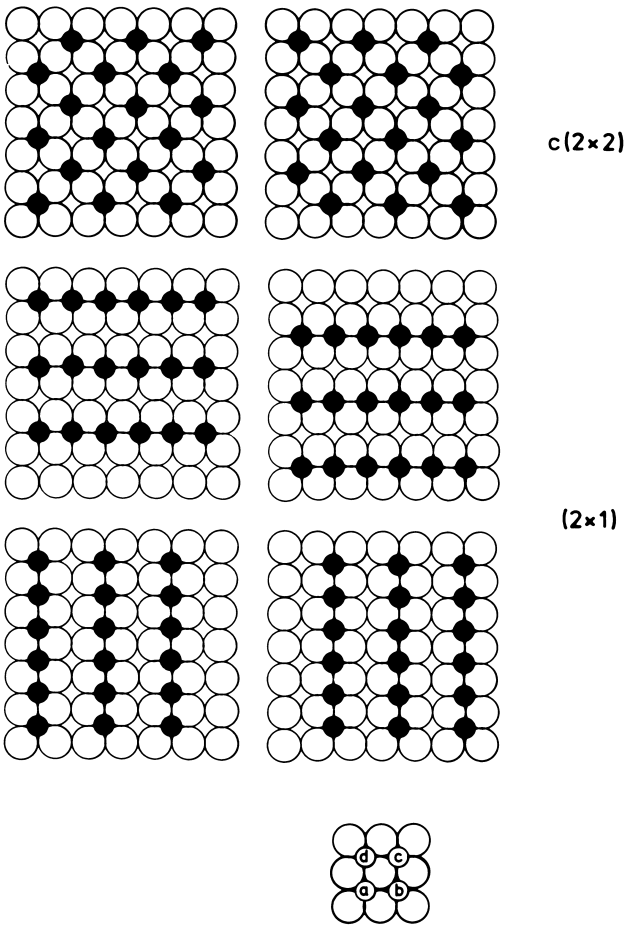

Fig. 5. Adsorbate superstructures on (100) surfaces of cubic crystals. Atoms in the top-layer of the substrate are shown as white circles, while adsorbate atoms are shown as full black circles. Upper part shows the two possible domains of the $c(2 \times 2)$ structure, obtained by dividing the square lattice of preferred adsorption sites into two sublattices following a checkerboard pattern: either the white sublattice or the black sublattice is occupied by the adatoms. In the (2×1) structure, however, full and empty rows alternate. These rows can be interchanged, and in addition they can be oriented either along the *x*-direction (middle part) or the *y*-direction (lower part). So four possible domains result, and one needs a two-component order parameter to describe this ordering, unlike the $c(2 \times 2)$ structure where a single-component (i.e., scalar) order parameter is appropriate. The lowest part of the figure indicates how one assigns 4 sublattices (a, b, c, d) to the square lattice.

sublattice α. Then the order parameter of the $c(2 \times 2)$ phase can be written as follows:

$$\Psi_{c(2\times2)} = m_a + m_c - (m_b + m_d). \tag{3.2}$$

The two types of domains shown on the top of Fig. 5 simply correspond to $\Psi_{c(2\times2)} = \pm 1$. Actually one can combine the sublattices a, c into a single sublattice, as well as the sublattice b and d, so the description of this structure would need only two sublattices. But the situation differs for the (2×1) structure, where two components are needed:

$$\Psi^{I}_{(2\times1)} = m_a + m_b - (m_c + m_d), \quad \Psi^{II}_{(2\times1)} = m_a + m_d - (m_b + m_c). \tag{3.3}$$

The domains shown in the middle of Fig. 5 correspond to $\Psi^{\mathrm{I}}_{(2\times1)} = \pm1$, $\Psi^{\mathrm{II}}_{(2\times1)} = 0$, while the domains shown in the lower part correspond to $\Psi^{\mathrm{I}}_{(2\times1)} = 0, \Psi^{\mathrm{II}}_{(2\times1)} = \pm1$. For the (2×2) structure on the square lattice (not shown in Fig. 5, but shown in Fig. 23 as the structure No. 3), where only one of the four sublattices (a, b, c, d) is occupied while the other three sublattices are empty, so that this ordering in the ideal case leads to a coverage $\theta = 1/4$, one needs three independent order parameter components, e.g.

$$\Psi^{\mathrm{I}}_{(2\times2)} = -m_a + m_b + m_c + m_d, \quad \Psi^{\mathrm{II}}_{(2\times2)} = m_a - m_b + m_c + m_d,$$
$$\Psi^{\mathrm{III}}_{(2\times2)} = m_a + m_b - m_c + m_d. \tag{3.4}$$

Note that due to the constraint $m_a + m_b + m_c + m_d = m$ there is no fourth independent component. The order parameter components defined in Eq. (3.4) thus do not bring out the symmetry properties of the structure in a natural way; thus in practice one often proceeds differently, by considering the expansion of the ordering in terms of mass density waves, as will be discussed below. Here we only emphasize that order parameters of the type considered in Eqs. (3.2), (3.3) and (3.4) are not only appropriate for lattice gas models, but can be used as well for any corresponding structure in the off-lattice case if it is commensurate with the square lattice of the substrate (100) surface. Analogous considerations can be made, of course, in the case where the substrate surface has (110) geometry, and the lattice of preferred sites then is a rectangular rather than a square lattice. Sublattices a, b, c, d may be introduced for the rectangular structure analogously, and the $\mathrm{c}(2 \times 2)$ structure described by $\Psi_{\mathrm{c}(2\times2)}$; the structure (2×1), described by $\Psi_{(2\times1)}$, exists as well. However, the two components written for the (2×1) structure in Eq. (3.3) are no longer equivalent, because the lattice spacing of the rectangular lattice is $\sqrt{2}a$ in the y direction and a in the x direction, and hence the adatoms for $\Psi^{\mathrm{I}}_{(2\times1)}$ (middle part of Fig. 5 could be a distance $2a$ apart along the x-axis, while for $\Psi^{\mathrm{II}}_{(2\times1)}$ (lower part of Fig. 5) they are a distance $a\sqrt{2}$ apart. Therefore the two cases $\Psi^{\mathrm{I}}_{(2\times1)}, \Psi^{\mathrm{II}}_{(2\times1)}$, really are to be considered as different structures, rather than as different components of thesame structure, and hence we rather have two distinct (2×1) structures on the rectangular lattice with a single order parameter component each (Fig. 6). Note that the structure where rows of occupied sites run in the x-direction is rather unlikely to occur, since it would imply a nearest neighbor distance of a in the x-direction but $2a\sqrt{2}$ in the y-direction, and hence could be stabilized only by very anisotropic adatom–adatom interactions. Therefore this structure is not considered in Fig. 6.

We now turn to a discussion of how these various orderings show up in reciprocal space, since experimental scattering techniques (such as low energy electron diffraction (LEED), elastic scattering of synchrotron radiation or neutrons, etc.) yield related information via superstructure Bragg spots and their intensities. As an example, the reciprocal lattice and the 1st Brillouin zones for the square and triangular lattices are shown in Fig. 7. Note that in the case of weak corrugation we expect a close-packed triangular structure of adatoms, with a lattice spacing incommensurate with the underlying substrate lattice, but rather given by the chosen coverage θ. In reciprocal space, this (1×1) triangular structure would cause Bragg spots according to the outer hexagon in the lower part of Fig. 7. Superstructures relative to this basic triangular lattice {such as $(\sqrt{3} \times \sqrt{3})R30^\circ$ and (2×2) structures, as included in Fig. 7} are not expected in this case; we expect such superstructures only for adsorption on close-packed (111) surfaces of cubic crystals or on hexagonal substrates (such as graphite, for instance), which are beyond the scope of the present treatment, however.

The superlattice Bragg spots of the $\mathrm{c}(2 \times 2)$ and (2×1) superstructures on the square lattice occur at special points at the boundary of the 1st Brillouin zone, as shown in Fig. 7. For instance, the $\mathrm{c}(2 \times 2)$

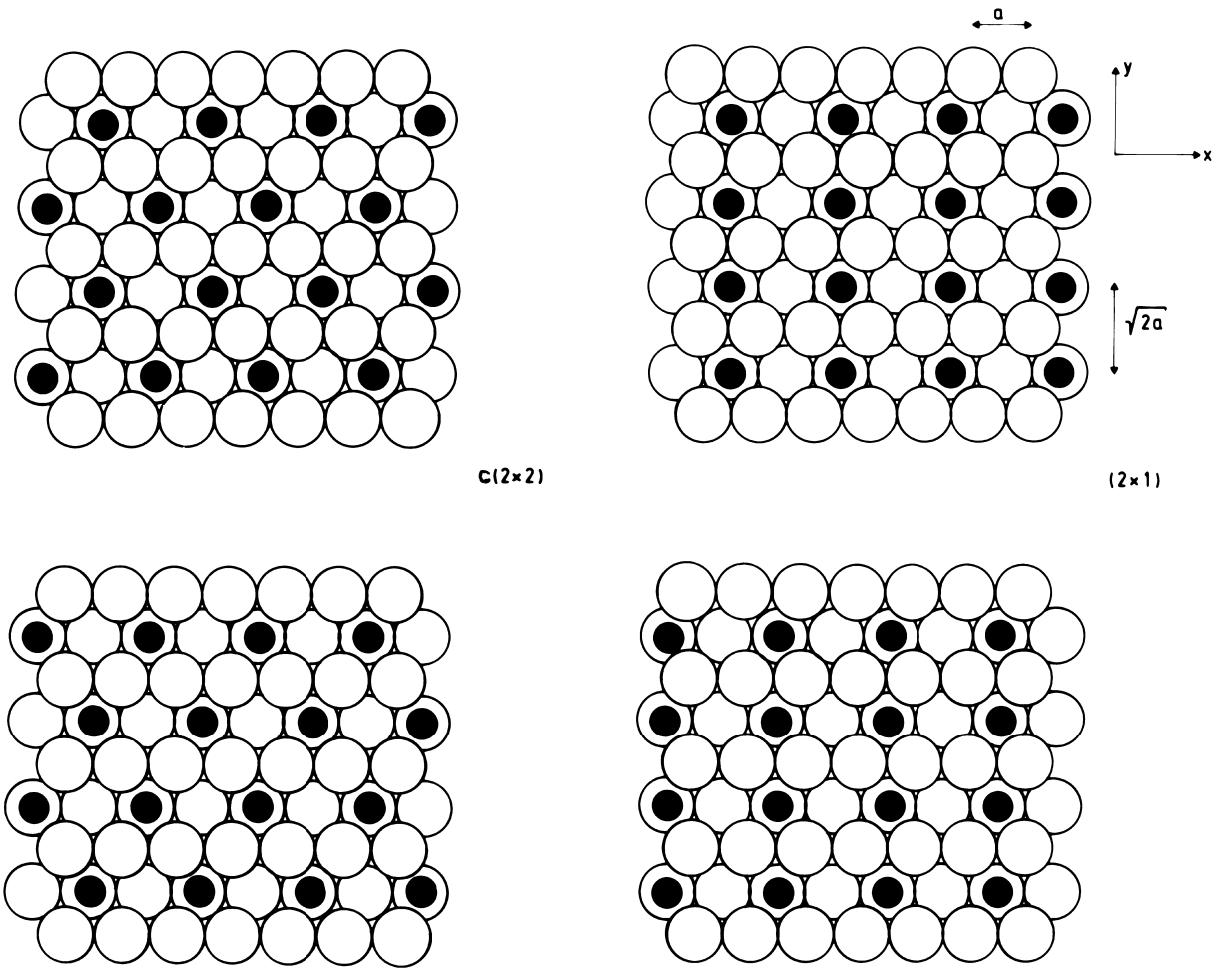

Fig. 6. Adsorbate superstructures on (110) surfaces of face-centered cubic crystals. Atoms in the two topmost layers of the substrate are shown as white circles, while adsorbate atoms are shown as full black circles. Left part shows the two possible domains of the c(2×2) structure, while the right part shows the two possible domains of the (2×1) structure (with rows of occupied sites running in the y-direction, so that the nearest adatoms are at distances $\sqrt{2}a$ and $2a$, respectively, when a is the lattice spacing of the rectangular lattice of preferred sites).

structure is characterized by the point $\boldsymbol{q}_0 = (\pi/a)(1,1)$, when a is the lattice spacing of the square lattice. Of course, other Bragg spots appear at additional positions such as $(\pi/a)(1,-1)$, $(\pi/a)(-1,-1)$, etc., but they need not be considered explicitly since they can be obtained from $\boldsymbol{q}_0$ by adding a suitable vector of the reciprocal lattice.

On the other hand, for the (2×1) structure two vectors $\boldsymbol{q}_1 = (\pi/a)(1,0)$ and $\boldsymbol{q}_2 = (\pi/a)(0,1)$ are required, they are not related by a reciprocal lattice vector of the original square lattice. In the general case one can find all l independent members of $\boldsymbol{q}_i$ (the so-called "star" of $\boldsymbol{q}_1$) by applying the point group operations of the lattice of adsorption sites to $\boldsymbol{q}_1$, and one keeps only those that are not related by a reciprocal lattice vector $\boldsymbol{G}$. Here we do not elaborate on these group-theoretical aspects of adsorbate layer ordering, but rather direct the reader to the appropriate literature [207,208].

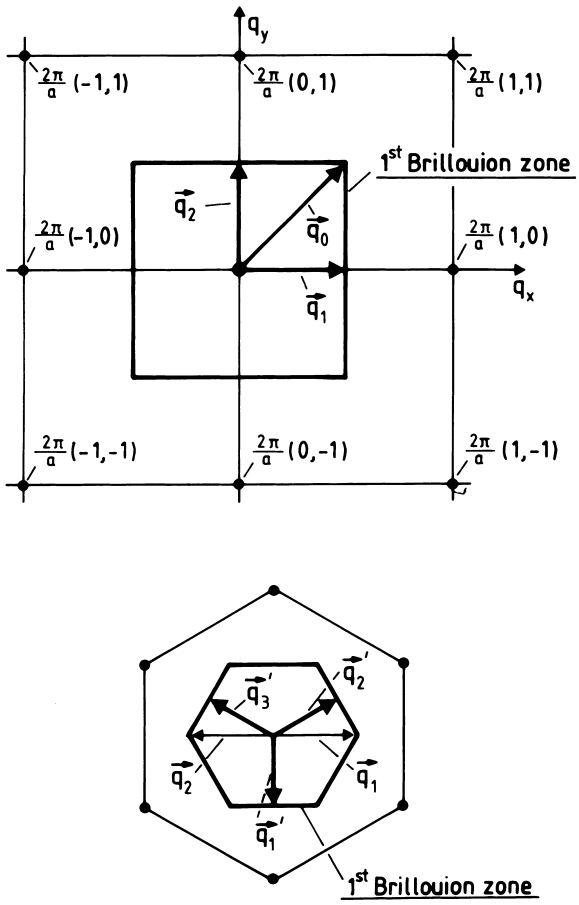

Fig. 7. Reciprocal lattice and the 1st Brillouin zone for the square lattice (upper part) and the triangular lattice (lower part). The c(2×2) structure is described by the single wave vector $\boldsymbol{q}_0$ in reciprocal space, while the (2×2) structure on the square lattice is described by a star $(\boldsymbol{q}_1, \boldsymbol{q}_2)$, as well as the $\sqrt{3} \times \sqrt{3}R30^\circ$ structure on the triangular lattice. The star of the (2×2) structure on the triangular lattice contains three members $\boldsymbol{q}_1$, $\boldsymbol{q}_2$, and $\boldsymbol{q}_3$.

If the star of $\boldsymbol{q}_1$ is known, the ordering can be described by an expansion of the local density $\langle \rho_j \rangle$ in mass density waves,

$$\langle \rho_j \rangle = \theta + \sum_{s=1}^{l} \rho(\boldsymbol{q}_s) \exp(\mathrm{i}\boldsymbol{q}_s \cdot \boldsymbol{R}_j), \tag{3.5}$$

$\boldsymbol{R}_j$ being the lattice vector of the site j. If some vector $\boldsymbol{G}$ of the reciprocal lattice connects $\boldsymbol{q}_s$ and $-\boldsymbol{q}_s$, the Fourier component $\rho(\boldsymbol{q}_s)$ is real and one has

$$\langle \rho_j \rangle = \theta + \sum_{s=1}^{l} \rho(\boldsymbol{q}_s) \cos(\boldsymbol{q}_s \cdot \boldsymbol{R}_j), \tag{3.6}$$

while otherwise one has to split $\rho(\boldsymbol{q}_s)$ into real and imaginary parts [46,207,208]. Assuming that

Eq. (3.6) holds, the order parameter components ϕ_s can be identified as

$$\phi = \frac{1}{N}\sum_j [\langle \rho_j \rangle - \theta] \cos(\boldsymbol{q}_s \cdot \boldsymbol{R}_j), \quad s = 1, \ldots, l. \tag{3.7}$$

As an illustration, we note for the square lattice that the lattice points $\boldsymbol{R}_j = (m, n)a$, with m, n integers. Using $\boldsymbol{q}_s = \boldsymbol{q}_0 = (\pi/a)(1, 1)$ for the $c(2 \times 2)$ structure in Eq. (3.7), we recover the single order parameter component

$$\phi = \frac{1}{N}\sum_j [\langle \rho_j \rangle - \theta](-1)^{m+n}, \tag{3.8}$$

which agrees with $\Psi_{c(2\times2)}$ (apart from a trivial normalization factor 2). For the (2×1) structure, we find two components, using $\boldsymbol{q}_1 = (\pi/a)(1, 0)$ and $\boldsymbol{q}_2 = (\pi/a)(0, 1)$,

$$\phi_1 = \frac{1}{N}\sum_j [\langle \rho_j \rangle - \theta](-1)^m, \quad \phi_2 = \frac{1}{N}\sum_j [\langle \rho_j \rangle - \theta](-1)^n, \tag{3.9}$$

again equivalent to $\Psi^{\mathrm{I}}_{(2\times1)}$, and $\Psi^{\mathrm{II}}_{(2\times1)}$ (Eq. (3.3)) as expected. Similar considerations can be performed for more complicated structures on the square lattice as well, and the treatment can be extended also to the rectangular lattice, of course.

The nature and symmetry properties of the order parameter (components) have consequences on the Landau expansion of the free energy $F\{\phi\}$ in terms of the order parameter. Although Landau theory has the character of a mean field theory [46,204,205] and hence is a bad guide, as far as the description of critical phenomena of adsorbed layers is concerned (see Section 3.2), it is nevertheless useful as a basis for the development of a classification scheme of the various superstructures into the appropriate "universality classes" [46,207]. E.g. for the $c(2 \times 2)$ structure (both on the square and the rectangular lattice) and for the (2×1) structure on the rectangular lattice we have a scalar (one-component) order parameter, which simply changes sign when we interchange occupied and empty sublattices. The free energy cannot depend on the particular way how sublattices have been assigned and must be independent of the resulting sign of the order parameter, of course. Thus only even terms can appear in the Landau expansion of these structures, F_0, r, u being constants,

$$F = F_0 + \tfrac{1}{2} r\phi^2 + \tfrac{1}{4} u\phi^4 + \cdots. \tag{3.10}$$

Eq. (3.10) is of the same form as the Landau expansion of an Ising ferromagnet (where ϕ corresponds to the magnetization). Thus Eq. (3.10) puts the corresponding adsorbate superstructures in the universality class of the two-dimensional Ising model (if they undergo in fact a second-order phase transition into the disordered phase, as the latter model does).

A different behavior results for the (2×1) structure on the square lattice, for which the Landau expansion takes the form [209]

$$F = F_0 + \tfrac{1}{2} r(\phi_1^2 + \phi_2^2) + \tfrac{1}{4}\left[u(\phi_1^4 + \phi_2^4) + u'(\phi_1^2\phi_2^2)\right] + \cdots. \tag{3.11}$$

If $u' = 2u$, the quartic term could be written as $\frac{1}{4}u(\phi^2)^2 = \frac{1}{4}u(\phi_1^2 + \phi_2^2)^2$, and we were to recover the Landau expansion of an isotropic two-component ferromagnet ("XY-model [46,204,205]). Actually, for the (2×1) structure such a full rotational symmetry in the plane of the order parameter components (ϕ_1, ϕ_2) is not found in general (and is also not expected). Clearly the two lattice axes (x, y) of the

square lattice single out four choices of (ϕ_1, ϕ_2) corresponding to the four kinds of domains shown in Fig. 5. As a result, the (2×1) structure on the square lattice belongs to the class of the "XY model with cubic anisotropy" [209]. Similar considerations leading to the appropriate Landau expansions are also possible for the more complicated orderings on the square lattice, as well as for the structures of interest on the rectangular lattice.

3.2. Critical phenomena in surface systems

A quantity of central interest for the discussion of critical phenomena of adsorbed layers is the structure factor $S(\boldsymbol{q})$, which is the (two-dimensional) Fourier transform of the pair correlation function of the adatom density $\rho(\boldsymbol{x})$ (note $\langle\rho(\boldsymbol{x})\rangle = \theta$)

$$S(\boldsymbol{q}) = \sum_{\boldsymbol{x}} \exp(\mathrm{i}\boldsymbol{q}\cdot\boldsymbol{x})G(\boldsymbol{x}), \quad G(\boldsymbol{x}) = \langle\rho(0)\rho(\boldsymbol{x})\rangle - \theta^2. \tag{3.12}$$

For a lattice gas system, the $\sum_{\boldsymbol{x}}$ extends over all lattice sites, of course; for an off-lattice description of adsorbed layers Eq. (3.12) applies also if the $\sum_{\boldsymbol{x}}$ is interpreted as an integration over continuous space $\boldsymbol{x}$. In the vicinity of any superlattice Bragg spot $\boldsymbol{q}_{\mathrm{B}}$, i.e. for $\boldsymbol{k} \equiv \boldsymbol{q} - \boldsymbol{q}_{\mathrm{B}}$ with $k = |\boldsymbol{k}| \ll |\boldsymbol{q}_{\mathrm{B}}|$, we can write $S(\boldsymbol{q})$ as follows:

$$S(\boldsymbol{q}) = \phi^2(T)\delta(\boldsymbol{k}) + S_T(\boldsymbol{q}_{\mathrm{B}})/\left[1 + k^2\xi^2\right], \quad k\xi \ll 1, \tag{3.13}$$

where $\phi(T)$ is the order parameter of the considered superstructure (for simplicity we treat here only a one-component order parameter), $S_T(\boldsymbol{q}_{\mathrm{B}})$ is the peak intensity of the thermal diffuse scattering, and ξ is the associated correlation length. If there is a second order phase transition at some critical temperature T_{c}, $\phi(T) \equiv 0$ for $T > T_{\mathrm{c}}$, of course, and thus Eq. (3.13) holds for both $T > T_{\mathrm{c}}$ and for $T < T_{\mathrm{c}}$, while right at the critical temperature a different behavior is predicted [46,204,205]:

$$S(\boldsymbol{q}) = S_{T\mathrm{c}}(\boldsymbol{q}) \propto k^{-(2-\eta)}, \tag{3.14}$$

η being a critical exponent related to the decay of critical correlations with distance $\{G(\boldsymbol{x}) \propto x^{-\eta}$ in $d = 2$ dimensions at $T_{\mathrm{c}}\}$. The behavior of $S(\boldsymbol{q})$ is plotted schematically in Fig. 8, where we have written $S_T(\boldsymbol{q}) = k_{\mathrm{B}}T\chi_T(\boldsymbol{k})$ to emphasize that in the pseudospin representation of a lattice gas $\chi_T(\boldsymbol{k})$ can be interpreted as a (staggered) susceptibility [46,204,205].

At a second order phase transition, one expects a critical temperature dependence of the order parameter $\phi(T)$, the diffuse scattering peak intensity and the correlation length ξ as follows:

$$\phi(T) = \hat{\phi}(-t)^{\beta}; \qquad S_T(\boldsymbol{q}_{\mathrm{B}}) = \hat{\Gamma}_{\pm}|t|^{-\gamma}; \qquad \xi = \hat{\xi}_{\pm}|t|^{-\nu}; \qquad t \to 0, \tag{3.15}$$

where $\hat{\phi}, \hat{\Gamma}_{\pm}$ and $\hat{\xi}_{\pm}$ are the appropriate "critical amplitudes" [46,204,205] (the signs $\pm$ refer to the signs of $t = T/T_{\mathrm{c}} - 1$).

A further critical exponent (α) is defined in terms of the specific heat singularity,

$$C = \left(\frac{\partial U}{\partial T}\right)_{\mu} = T\left(\frac{\partial^2 F}{\partial T^2}\right)_{\mu} = \hat{C}_{\pm}|t|^{-\alpha} + C_0 + C_1 t + \cdots, \tag{3.16}$$

where we assume an adsorbed system in equilibrium with surrounding gas (so that not the coverage θ of the adsorbed layer but rather the chemical potential μ is a given independent thermodynamic variable). Note that in addition to the singular term (again the two signs $\pm$ of the amplitude $\hat{C}_{\pm}$ refer to the sign of

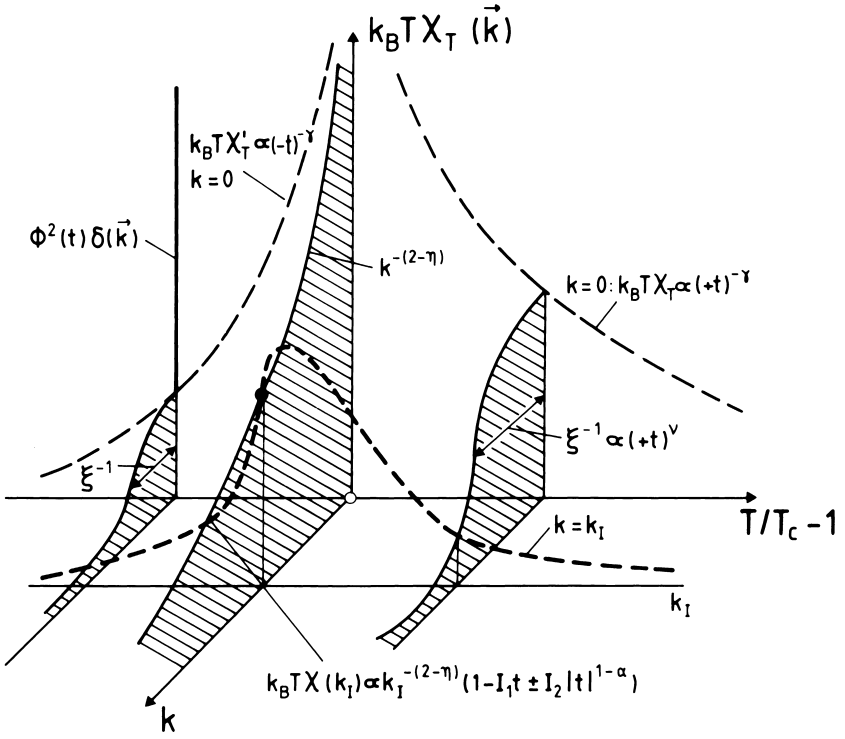

Fig. 8. Schematic plot of the scattering intensity $S(\boldsymbol{q})$ as a function of temperature distance k from a superstructure Bragg spot in reciprocal space. For $k = 0$ one observes a critical divergence according to the ordering "susceptibility" $S_T(\boldsymbol{q}_B) \equiv k_B T \chi_T(0) \propto |t|^{-\gamma}$, superimposed by a delta function whose weight is given by the square of the order parameter. For a non-zero wavenumber k_1, the scattering intensity has a maximum slightly above T_c, reflecting the smooth crossover from Ornstein–Zernike behavior for $k\xi \leq 1$ to the critical decay $k^{\eta-2}$ at T_c. Near T_c for $k \neq 0$, the intensity exhibits a singular temperature derivative due to the term $\pm I_2 |t|^{1-\alpha}$, as indicated in the figure. Note that the halfwidth of the Ornstein–Zernike peaks describing the diffuse scattering $\{S_T(\boldsymbol{q}) = S_T(\boldsymbol{q}_B)/(1 + k^2\xi^2)\}$ shrinks to zero as $T \to 0$, since the correlation length ξ diverges ($\xi \propto |t|^{-\nu}$). The critical exponents of the specific heat, ordering susceptibility and correlation length have been denoted as α, γ and ν, as usual [46,204,205].

t for $T > T_c$ and $T < T_c$, respectively) regular background terms, analytic in t, are added, since these terms often are not negligible, in the region of $|t|$ that can actually be reached.

While C can be measured for adsorbed layers on graphite (see e.g. [55] for a review), due to the favorable surface to volume ratio of this substrate, a direct measurement of C for monolayers adsorbed on metal surfaces is impossible. Here it is worth pointing out that one can estimate also the specific heat singularity from scattering, when one considers the integrated scattering intensity [210,211]. Actually, such an integration over a range of wavenumbers $0 < k < k_I$ always occurs, due to the finite resolution of the experimental setup (which we characterize by a wavenumber k_I here). Thus the intensity $I(q_B, k_I, t)$ can be written as

$$I(q_B, k_I, t) = \int_{k<k_I} d^2\boldsymbol{k} S(\boldsymbol{q}), \tag{3.17}$$

where $S(\boldsymbol{q})$ is given by Eq. (3.13) only for $k\xi \ll 1$ while in the opposite limit $k\xi \gg 1$ (and $T > T_c$) the result is written in terms of the scaling function $\tilde{S}(\zeta)$ as

$$S(\boldsymbol{q}) = k^{-(2-\eta)}\tilde{S}(k\xi) = S_0 k^{-(2-\eta)} + S_1 (k\xi)^{-(1-\alpha)/\nu} + \cdots, \tag{3.18}$$

where S_0 and S_1 are constants. The second term on the r.h.s. of Eq. (3.18), that generalizes Eq. (3.14), results from an energy-like singularity {note that the internal energy $U = U_0 + T_c[1/(1-\alpha)]\hat{C}_{\pm}|t|^{1-\alpha}\,\mathrm{sign}(t) + C_0 T + \cdots$, cf. Eq. (3.16)} of the order parameter pair correlation functions near T_c. Eqs. (3.17) and (3.18) then yield

$$I(\boldsymbol{q}_B, k_1, t) \propto 1 + I_1 t \pm I_2 |t|^{1-\alpha} \pm \cdots, \tag{3.19}$$

where I_1, I_2 are constants {and a term regular in t has been included in Eqs. (3.18) and (3.19), for the sake of consistency with Eq. (3.16)}.

A related energy-like singularity in fact is expected in the coverage $\theta(t,\mu)$ itself, if the system undergoes an order–disorder transition as a function of temperature at constant μ,

$$\theta = \theta_c(\mu) \pm \hat{\theta}(\mu)|t|^{1-\alpha} + \theta_1 t + \cdots, \tag{3.20}$$

where $\theta_c(\mu)$ is the coverage at the critical temperature $T_c(\mu)$, $\hat{\theta}_c(\mu)$ is another amplitude factor and θ_1 is a constant. Since in general $T_c = T_c(\mu)$ depends on μ, we can also probe the transition by varying μ at constant T (e.g., by controlling the gas pressure in a physi-sorption experiment). As long as one crosses the transition line $T_c(\mu)$ or its inverse function $\mu_c(T)$ at a finite angle, one still obtains the same exponents. Thus

$$\phi(\mu) \propto [\mu_c(T) - \mu]^{\beta}, \quad S(\boldsymbol{q}_B) \propto |\mu_c(T) - \mu|^{-\gamma}, \quad \ldots. \tag{3.21}$$

However, it is interesting to consider what Eq. (3.21), and the analog of Eq. (3.20), namely $\theta - \theta_c(T) \propto [\mu_c(T) - \mu]^{1-\alpha}$, imply when we rewrite the order parameter as a function of coverage at constant temperature. Thus (to leading order, assuming $\alpha > 0$) one gets

$$\phi(\theta) \propto [\theta_c(T) - \theta]^{\beta/(1-\alpha)}. \tag{3.22}$$

Again the same exponent applies whenever we cross the transition line $\theta_c(T)$ (or its inverse function $T_c(\theta)$) under a finite (nonzero) angle, and thus in an experiment at constant coverage one does not observe the exponent β quoted in Eq. (3.15) but rather $\beta_F = \beta/(1-\alpha)$. This effect is called "Fisher renormalization" [212]. A similar change applies to other quantities, too: $S(\boldsymbol{q}_B) \propto |t|^{-\gamma_F}$ with $\gamma_F = \gamma/(1-\alpha), C \propto |t|^{-\alpha_F}$ with $\alpha_F = -\alpha/(1-\alpha)$}. The Fisher renormalized exponents satisfy an analogous scaling law $(2 - \alpha_F = \gamma_F + 2\beta_F)$ as the original ones [46,204,205]

$$2 - \alpha = \gamma + 2\beta. \tag{3.23}$$

The above argument clearly does not work at the maximum of the transition line, $T_{\max}(\theta)$ defined by $\mathrm{d}T_c(\theta)/\mathrm{d}\theta = 0$, and in fact no Fisher renormalization does occur then. We also note that no Fisher renormalization occurs if $\alpha < 0$, since then the leading term in the relation between θ and t Eq. (3.20), or the analogous relation between θ and μ, is analytic. Note also that even for $\alpha > 0$ and $\mathrm{d}T_c(\theta)/\mathrm{d}\theta \neq 0$ this Fisher renormalization will be visible only if one is close enough to criticality so that the singular term in Eq. (3.20) dominates over the regular one. All these problems must be kept in mind if experiments on surface critical behavior in adsorbed layers are carried out to check the theoretical predictions. In the simulations one can choose to work either in the statistical ensemble at constant

coverage or at constant pressure, of course, and hence this problem of Fisher renormalization can be avoided.

For the sake of completeness, we mention that Eq. (3.23) is not the only scaling relation between critical exponents. Another one is readily found from Eq. (3.18), recognizing that $\tilde{S}(\zeta \to 0) \propto \zeta^{2-\mu}$, in order that powers of k cancel for $k \to 0$. This yields $S(\boldsymbol{q}_B) \propto \xi^{2-\mu} \propto |t|^{-\nu(2-\eta)}$ and hence, using Eq. (3.15), we conclude

$$\gamma = \nu(2-\eta). \tag{3.24}$$

Finally we mention the "hyperscaling relation" [72] involving the dimensionality d

$$2-\alpha = d\nu \quad (= 2\nu \text{ in } d=2). \tag{3.25}$$

Now a very important additional concept about critical phenomena is the idea of "universality" [46,72,204,205]. The universality principle states that as a rule, critical exponents, dimensionless critical amplitude combinations, and scaling functions (where "scale factors" have been absorbed in the variables) do not depend on the details of the system but are the same for a whole class of systems: the "universality class" to which a system belongs depends on the spatial dimensionality d, the number of order parameter components n, and certain general properties of the Hamiltonian like symmetry properties (e.g., the XY model with full rotational symmetry of the 2-component order parameter is one class, while addition of a fourfold anisotropy (square lattice) or sixfold anisotropy (triangular lattice) creates different universality classes [46,72,205,207]). Also the range of the (pairwise) interaction $v(\boldsymbol{r}_i - \boldsymbol{r}_j)$ matters: While typically all systems with short range interactions, for which the second moment of the interaction exists, defining the range R via

$$R^2 = \sum_{\boldsymbol{r}} r^2 v(\boldsymbol{r}) / \sum_{\boldsymbol{r}} v(\boldsymbol{r}), \tag{3.26}$$

belong to the same class, the situation differs for power law interactions

$$v(\boldsymbol{r}) = \hat{v} r^{-(d+\sigma)}, \quad 0 < \sigma < 2, \tag{3.27}$$

for which $R = \infty$ according to Eq. (3.26). One can show [213] that the behavior of such systems is mean field like for $0 < \sigma < d/2$ (for $d = 2$ this is the range $0 < \sigma < 1$) while a non-trivial critical behavior applies for $d/2 < \sigma < 1$ (at $\sigma = d/2 = 1$ power laws with mean-field exponents but logarithmic correction factors are expected).

At this point, we also emphasize that simple power laws as written in Eq. (3.15) represent the leading singular behavior in the limit $t \to 0$ only, and in practical cases when t is not so small one should take into account singular "corrections to scaling", e.g.

$$S_T(\boldsymbol{q}_B) = \hat{\Gamma}_{\pm} |t|^{-\gamma} \{1 + \hat{\Gamma}_{\pm}^{\text{corr}} |t|^{x_1^{\text{corr}}} + \cdots\}, \quad t \to 0, \tag{3.28}$$

where $\hat{\Gamma}_{\pm}^{\text{corr}}$ are the amplitude factors and x_1^{corr} is the critical exponent of the leading singular correction term. Often the accuracy of either experimental data or simulation does not allow to disentangle all these parameters (also T_c is usually not known in beforehand and has to be extracted from the fit together with the critical exponents). Then it is common to analyze such data in terms of "effective exponents" defined via a logarithmic derivative, e.g.

$$\gamma_{\text{eff}} \equiv -\mathrm{d} \ln S_T(\boldsymbol{q}_B) / \mathrm{d} \ln |t|. \tag{3.29}$$

This notation is particularly useful when one studies "crossover" [72,214] from one universality class to another, since varying a suitable parameter the correction amplitudes may become large and ultimately even divergent; e.g., a crossover between the critical behavior of the Ising model and mean-field critical behavior is observed when one studies systems with large but finite range R of the interaction [215,216]. One can then show that in $d = 2$ the crossover from the Ising exponent ($\gamma = 7/4$) to the mean field exponent ($\gamma = 1$) is described by

$$S_T(\boldsymbol{q}_B) = R^2 \tilde{\chi}(tR^2), \tag{3.30}$$

where $\tilde{\chi}(\zeta) \propto \zeta^{-7/4}$ for small ζ while $\tilde{\chi}(\zeta) \propto 1/\zeta$ for large ζ. The corresponding effective exponent decreases monotonically from $7/4$ to 1 for $T > T_c$ while for $T < T_c$ the variation is nonmonotonic, since $\gamma_{eff} \approx 0.85$ for $tR^2 \approx -1$ [215,216]. Note that in both cases the crossover from one limit to the other is not sharp but rather smooth, i.e. it smeared out over several decades in the crossover scaling variable ζ.

Similar crossover phenomena can also be discussed for other universality classes of critical phenomena. Consider, for instance a monolayer of magnetic atoms adsorbed in the (1×1) phase at full coverage at the rectangular lattice. Assuming further that there is a strong magnetic anisotropy forcing the spins of the atoms to lie in the xy-plane parallel to the substrate, a model Hamiltonian could be written as follows

$$\mathcal{H} = -J \sum_{\langle i,j \rangle} \left[S_i^x S_j^x + (1 - \Delta) S_i^y S_j^y \right], \tag{3.31}$$

where it is assumed that only nearest neighbor pairs $\langle i,j \rangle$ of spins on the lattice interact. The exchange constant is written as J for the x-components and $J(1 - \Delta)$ for the y-components of the spin (which for simplicity are treated as classical unit vectors here). If $\Delta = 0$ this model would be the XY-model of ferromagnetism, if $\Delta = 1$ it is the Ising model (extended to "classical" spins). On the rectangular lattice, x and y directions are not equivalent, and hence $\Delta \neq 0$ is a rather natural choice. If, however, Δ is small the system may still behave like an XY-model for not too small t: only for $t \to 0$ for any nonzero value of Δ a crossover to Ising-like behavior occurs. Similar crossovers can occur for many types of critical behavior.

Fig. 9 describes the generic situation of a crossover, where one assumes that the critical temperature $T_c(p)$ depends on a parameter p and ends at a value $p_m, T_m = T_c(p)$ in a "special" point. This special point may be the isotropic point ($\Delta = 0$) of the model, eq. (3.31), where then the coordinate g in Fig. 9 can be identified with Δ, or the mean-field limit $R^{-1} = 0$ of the medium-range Ising model of Eq. (3.30), or a "multicritical point" such as a tricritical point (Fig. 10 [127]). At a tricritical point, a line of second-order phase transitions ends and continues as a line of first-order transitions [217,218]. It is then advisable to define "scaling axes" (t, g) which are perpendicular (t) and parallel (g) to the critical line at the multicritical point (Fig. 9). Although for all $p < p_m$ the same type of critical behavior occurs, as it should be according to the universality principle, the region in the T–p-plane where it actually can be observed shrinks to zero smoothly as $p \to p_m$. Both the critical line and the center of the crossover region can be expressed in terms of the so-called "crossover exponent" φ [214],

$$t_c = g^{1/\varphi}/y_c, \quad t_{cross} = g^{1/\varphi}/y_{cross}, \tag{3.32}$$

y_c, y_{cross} being constants. The singular part of the free energy, which is a function of temperature T, the

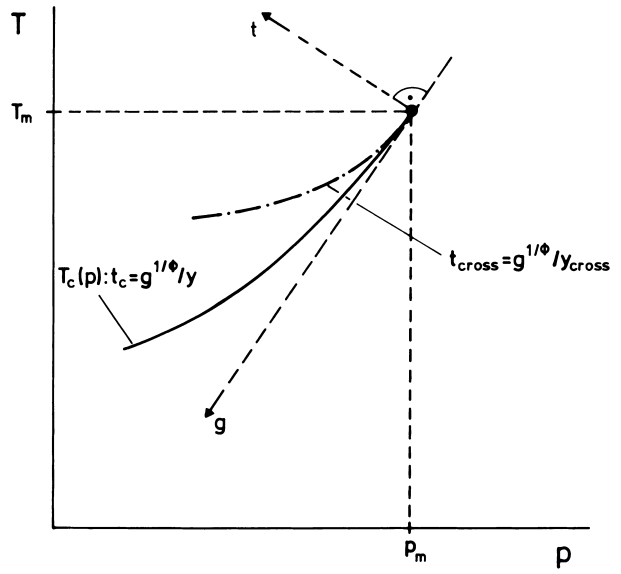

Fig. 9. Schematic phase diagram of a system exhibiting crossover between "ordinary" critical phenomena along the line $T_c(p < p_m)$ and the multicritical point $p = p_m$, $T_m = T_c(p_m)$. Considering the approach to the critical line along an axis parallel to the T-axis one will observe multicritical behavior as long as one stays above the dash-dotted curve $t_{cross} = g^{1/\phi}/y_{cross}$ describing the center of the crossover region. Only in between the dash-dotted curve and the critical line $T_c(p)$ (full curve) can the correct asymptotic behavior be seen.

field H conjugate to the order parameter, and the parameter p, near the multicritical point can be cast into a scaled form:

$$F^{sing}(T, H, p) = t^{2-\alpha_m} \tilde{F}\{Ht^{-(\beta_m+\gamma_m)}, g^{-1/\varphi}t\}. \tag{3.33}$$

Here $\alpha_m, \beta_m, \gamma_m, \ldots$ are the exponents (according to their usual meaning) at the multicritical point $(T_m, p_m,)$, and $\tilde{F}(x, y)$ is a scaling function. Since we have assumed in Eq. (3.32) that the critical singularities occur along the line $y = y_c = g^{1/\varphi}t_c$, it is implied that $\tilde{F}(x, y)$ has at $y = y_c$ singularities that yield the critical exponents at the critical line. For instance, using Eq. (3.33) yields for $t \to t_c$

$$\tilde{F}(0, y) \propto (y - y_c)^{2-\alpha} \Rightarrow C \propto (t - t_c)^{-\alpha} \quad \text{for } g > 0. \tag{3.34}$$

On the other hand, for large enough t (where $y = g^{-1/\varphi}t \gg y_{cross}$) we have $F^{sing}(T, 0, p) \propto t^{2-\alpha_m} \approx (t - t_c)^{2-\alpha_m}$ since then $t_c \ll t$. While the above description applies straightforwardly for the case of the medium range Ising model {defining the inverse interaction volume as the variable g, we have $\varphi = 1$ in Eq. (3.32)} and for the example of the tricritical point ($\varphi = 1/2$ in mean field theory, while for short range interactions as implied in Fig. 10 one has $\varphi = 4/9$ [219]), a special case occurs for the isotropic xy-model, Eq. (3.31) with $\Delta = 0$: in this case statistical fluctuations are so strong that the ordered state is destroyed completely, the system is at its "lower critical dimensionality" (lcd) [46,72,205]. For the Ising or Potts model [220,221] ferromagnet it is known that $lcd = 1$ so in $d = 2$ stable ordered phases are possible, but for the xy-model (without anisotropy) $lcd = 2$. Nevertheless, a continuous phase transition at a nonzero transition temperature T_{KT} occurs, but it is

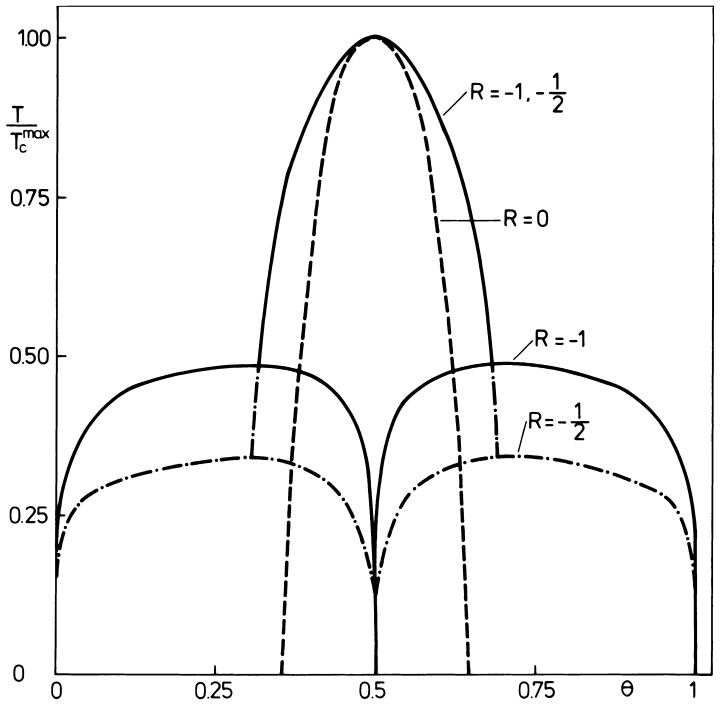

Fig. 10. Phase diagram for the square lattice gas with nearest neighbor repulsive interaction $u(r_{nn}) > 0$, and next nearest neighbor attractive interaction $u(r_{2nn}) \leq 0$, in the plane of variables coverage θ and temperature T (in units of the maximum transition temperature T_c^{max} of the order–disorder transition, which occurs for $\theta = 1/2$). Three choices of the ratio $R \equiv u(r_{2nn})/u(r_{nn})$ are shown. While above the transition lines in this phase diagram only the disordered phase of the lattice gas is thermodynamically stable, the $c(2 \times 2)$ structure is stable in the central part of the phase diagram underneath the (second-order) transition temperature $T_c(\theta)$. While these transition lines for $R = 0$ extend down to $T = 0\,\{T_c(\theta = \theta_c) = T_c(\theta = 1 - \theta_c) = 0$ with $\theta_c \approx 0.37$ [127]$\}$ for $R < 0$ the second-order transitions end at tricritical points $T_t(\theta = \theta_t)$ and $T_t(\theta = 1 - \theta_t)$, respectively. For $T < T_t$ and $\theta < 1/2$, one encounters a two-phase coexistence region between the $c(2 \times 2)$ phase and high-density lattice gas. Note that the phase diagram is strictly symmetric around $\theta = 1/2$, as is always implied for lattice gases with only pairwise interactions. From Binder and Landau [127].

not characterized by power laws but rather by an exponential divergence of the correlation length ξ [37]

$$\ln \xi = B/t^{\bar{\nu}}, \quad \bar{\nu} = 1/2, \quad t = (T - T_{KT})/T_{KT}, \tag{3.35}$$

where B is a (nonuniversal) constant. At the same time, Eq. (3.18) remains valid, so the susceptibility has also an exponential divergence, while the specific heat has an "essential" singularity, which is so weak that in practice it would hardly be observable either in an experiment or in a simulation

$$C^{sing} \propto \exp[-At^{-\bar{\nu}}], \quad t \to 0, \tag{3.36}$$

where A is another nonuniversal constant.

The power-law decay of the order parameter correlation function, Eq. (3.14), exists not only at the critical temperature T_{KT} but in the whole temperature regime for $0 < T < T_{KT}$, with a temperature-

Table 1
Critical exponents for various relevant universality classes in $d = 2$ dimensions

Critical exponents	Universality class			
	Ising criticality (short range)	Ising mean-field (long range)	Ising tricriticality (short range)	Tricriticality mean field (long range)
α	0 (log)	0 (jump)	8/9	1/2
β	1/8	1/2	1/24	1/4
γ	7/4	1	37/36	1
ν	1	1/2	5/9	1/2
δ	15	3	77/3	5
η	1/4	0	3/20	0

dependent exponent $\eta(T)$,

$$\left\langle \left(S_{ix}S_{jx} + S_{iy}S_{jy}\right)\right\rangle \propto |\boldsymbol{r}_i - \boldsymbol{r}_j|^{-\eta(T)}, \quad \eta(T) = T/(4T_{KT}). \tag{3.37}$$

Thus the regime of the ordered phase $(0 < T < T_{KT})$ can in a sense be considered as a line of critical points.

We conclude this section by quoting the exponent values of a few relevant models (or universality classes, respectively) in Table 1.

We have to add the following comments:

1. The critical exponent δ describes the response of the order parameter at T_c to the conjugate field,

$$\phi \propto H^{1/\delta}, \quad T = T_c. \tag{3.38}$$

   It is related to the other exponents via scaling relations, e.g. $\delta = (\gamma + \beta)/\beta$.
2. While short range Ising criticality is realized by the order–disorder transition of the $c(2 \times 2)$ structure on the square lattice or the (1×2) structure on the rectangular lattice {symmetry group p2mm}, the (2×1) structure on the square lattice (symmetry group p4mm) is *not* included in the table: the reason for this omission is that the *xy*-model with cubic anisotropy has non-universal critical exponents, due to the presence of a ''marginal operator'' in the Hamiltonian (in the sense of renormalization group theory [72]). We can realize the (2×2) structure also by a lattice gas with nearest (φ_{nn}) and next nearest neighbor interactions (φ_{nnn}), if both interactions are repulsive and if the ratio $R = \varphi_{nnn}/\varphi_{nn}$ exceeds $1/2$ [222]. It then turns out that not only the critical temperature T_c but also the critical exponent ν depends on R (Fig. 11), while the exponent $\eta = 1/4$, independent of R (all other scaling relations then follow from the scaling relations quoted above) [223–227].
3. On the first-order side of the tricritical point, another exponent β_2 can be defined, that describes how the two-phase coexistence region vanishes when the tricritical temperature T_t is approached from below, cf. Fig. 10,

$$\theta_{coex,2} - \theta_{coex,1} \propto (1 - T/T_t)^{\beta_2}. \tag{3.39}$$

   This exponent satisfies another scaling relation, involving the crossover exponent φ, namely

$$\beta_2 = (1 - \alpha_t)/\varphi. \tag{3.40}$$

   One finds $\beta_2 = 1$ for the mean-field case (which in $d = 2$ is realized only for long range forces,

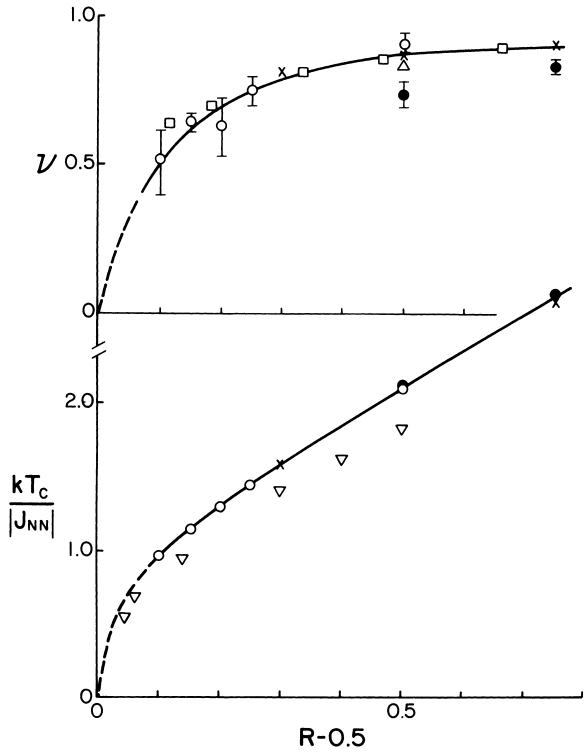

Fig. 11. Variation of the correlation length exponent ν (upper part) and the critical temperature T_c (lower part) of the lattice gas model with coverage $\theta = 1/2$ and repulsive interactions between nearest ($u(r_{nn})$) and next-nearest neighbors ($u(r_{2nn})$) with $R - 0.5$ (note that for $R \equiv u(r_{2nn})/u(r_{nn}) < 0.5$ the structure of the ordered phase is the c(2×2) structure in this model, only for $R > 0.5$ it is the (2×1) structure. Results of phenomenological finite size scaling renormalization group are shown by open circles [223], and the data collapsing finite size scaling method by an open triangle [222] in the upper part of the figure. Crosses denote Monte Carlo renormalization group estimates [224], open squares transfer matrix renormalization [225] and solid circles series extrapolations [226]. Open triangles in the lower part are due to real space renormalization [227]. From Landau and Binder [223].

unlike the case $d = 3$ [218]), while $\beta_2 = 1/4$ for the short range tricritical universality class of the Ising model.

3.3. Commensurate and incommensurate phases

We now return again to a distinction already made in Fig. 4: Given the fact that the corrugation potential due to the substrate defines a periodicity that the atoms in the adsorbate monolayer are exposed to, it is either possible that the periodicity describing the order of the monolayer is commensurate with the substrate (Fig. 4c) or incommensurate (Fig. 4d). In the first case, the ratio of the lattice spacing a_A and the lattice spacing a is a rational number ($a_A/a = m/n$ with m, n integers) while in the latter case this ratio is irrational. In this section, we are concerned with the peculiarities involved in the description of phase transitions between incommensurate and disordered phases as well as between incommensurate and commensurate phases, respectively. We shall briefly review the generic

phenomenological description of these transitions and introduce the basic microscopic models that have been studied in this context.

The first question that we ask is how can one incorporate incommensurate ordering into the description in the framework of Landau theory. For this purpose, it is useful to generalize the free energy expansion, Eq. (3.41), from a homogeneous order parameter ϕ to an inhomogeneous order parameter field $\phi(\boldsymbol{x})$,

$$F\{\phi(\boldsymbol{x})\} = F_0 + k_B T \int d\boldsymbol{x} \left\{ \frac{1}{2} r\phi^2(x) + \frac{1}{4} u\phi^4(\boldsymbol{x}) + \frac{1}{2} K_1 [\nabla\phi(x)]^2 + \cdots \right\}. \tag{3.41}$$

Note that in comparison with Eq. (3.10) we have slightly changed the normalization of the coefficients r, u which are dimensionless here when the free energy functional is extensive (proportional to the area taken by the adsorbate layer) and the order parameter field $\phi(x)$ is also dimensionless and normalized such that $|\phi(\boldsymbol{x})| \leq 1$ (e.g., for an Ising magnet $\phi(\boldsymbol{x})$ is obtained by normalizing the magnetization in units of its saturation value). The last term $\frac{1}{2} K_1 [\nabla\phi(\boldsymbol{x})]^2$ in Eq. (3.41) is called the "gradient energy" and describes the free energy cost in making the order locally inhomogeneous. In fact, one can show that the coefficient k_1 is related to the range of interaction R defined in Eq. (3.26) via $K_1 = R^2/d$ in d-dimensional systems [46,204,205].

However, there is no physical principle that requires that the interaction $v(\boldsymbol{r})$ in Eq. (3.26) is uniformly positive or uniformly negative; if $v(\boldsymbol{r})$ is nonuniform in sign, it may actually happen that R^2 as defined in Eq. (3.26) is negative. Then one cannot interpret R as an interaction range any longer, and also Eq. (3.41) must not be truncated after the gradient square term: for obtaining a physically meaningful free energy, a higher order gradient term must be included, assuming that the coefficient K_2 of this next term is positive [228]

$$\mathscr{F}\{\phi(\boldsymbol{x})\} = F_0 + k_B T \int d\boldsymbol{x} \left\{ \frac{1}{2} r\phi^2(\boldsymbol{x}) + \frac{1}{4} u\phi^4(\boldsymbol{x}) + \frac{1}{2} K_1 [\nabla\phi(\boldsymbol{x})]^2 + \frac{1}{4} K_2 [\nabla^2\phi(\boldsymbol{x})]^2 \right\}. \tag{3.42}$$

Considering the response of the order parameter to a conjugate field varying with a wave-vector $\boldsymbol{q}$, it is easy to show that the wave-vector dependent response function $\chi(\boldsymbol{q})$ or associated structure function $S(\boldsymbol{q}) = k_B T \chi(\boldsymbol{q})$ is no longer given by Eq. (3.13) but rather $S^{-1}(\boldsymbol{q})$ involves both terms in k^2 and in k^4:

$$S(\boldsymbol{q}) = (r + K_1 k^2 + K_2 k^4)^{-1}, \tag{3.43}$$

where $\boldsymbol{k} \equiv \boldsymbol{q} - \boldsymbol{q}_B$ as previously. Unlike Eq. (3.13) we here consider the disordered phase only.

If $K_1 > 0$ the first divergence of Eq. (3.41) occurs for $r = 0$, and writing hence $r = r't = r'(T/T_c - 1)$ Eq. (3.43) gets the Ornstein–Zernike form $S^{-1}(\boldsymbol{q}) = S^{-1}(\boldsymbol{q}_B)[1 + \xi^2 k^2 + \ldots], \xi = (K_1/r)^{1/2} = (K_1/r')^{1/2} t^{-1/2}$, the term with K_2 for $k\xi$ of order unity being a negligibly small correction and hence has been omitted.

However, if $K_1 < 0$ the first divergence of $S(\boldsymbol{q})$ no longer occurs for $T = T_c$ (or $t = 0$, respectively) and for $k = 0$, but rather a divergence occurs already at a higher temperature $t_c = K_1^2/4K_2 r'$ at a wavenumber $k = q^* \equiv \sqrt{-K_1/2K_2}$. Writing $t' = t - t_c$, Eq. (3.43) can be rewritten as

$$[S(\boldsymbol{q})]^{-1} = r't' + K_2 (k^2 - q^{*2})^2 \approx r't'[1 + \xi^2 (k - q^*)^2], \quad k \to q^*. \tag{3.44}$$

Now the mean field result for the correlation length ξ is no longer given by the result $\xi^2 = K_1/r$ which applies for $q^* = 0$ but rather by $\xi^2 = 4q^{*2} K_2/r = -2K_1/r$. Thus one finds that $S(\boldsymbol{q})$ has again a Curie–Weiss-like divergence, but it does not develop at the wavevector $\boldsymbol{q}_B$, corresponding to the Bragg spot of

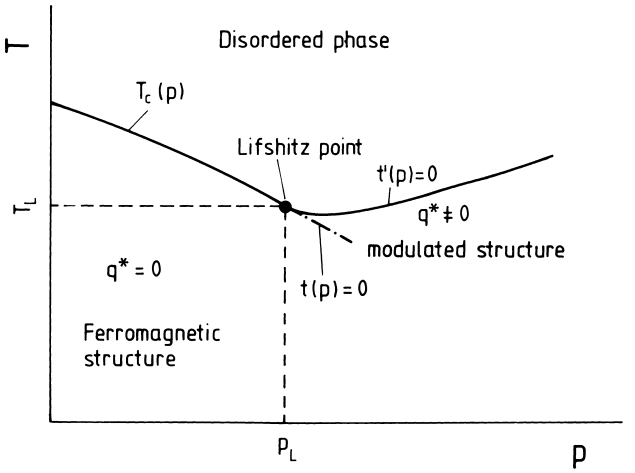

Fig. 12. Schematic phase diagram of a system where by a variation of a parameter p the coefficient $K_1(p)$ of the gradient energy (Eq. (3.42)) changes sign at a Lifshitz point $K_1(p_L) = 0, T_c(p_L) = T_L$. For $p < p_L$ one has a ferromagnetic structure while for $p > p_L$ where $K_1(p) < 0$ one has a modulated structure, with a characteristic wavenumber q^* describing the modulation. For $p \to p_L$ from above one has $q^* \propto (p/p_L - 1)^{\beta^*}$ with an exponent $\beta^*(\beta^* = 1/2$ in Landau theory).

the commensurate superstructure assumed by the choice of the order parameter ϕ, but rather long range order develops at a point a distance q^* away from the Bragg spot: i.e., the structure is modulated with a wavelength $\lambda^* = 2\pi/q^*$. The correlation function $\langle\phi(0)\phi(\boldsymbol{x})\rangle$ corresponding to $S(\boldsymbol{q})$ in real space {compare Eq. (3.12)} becomes, apart from power law prefactors,

$$\langle\phi(0)\phi(\boldsymbol{x})\rangle \propto \exp(-x/\xi)\cos(\boldsymbol{q}^* \cdot \boldsymbol{x}), \quad t' \to 0. \tag{3.45}$$

Now it turns out that it makes sense to consider the variation of a parameter p that has the effect that $K_1(p)$ somewhere changes sign (Fig. 12). The special point (p_L, T_L) where $K_1(p_L) = 0$ and hence $q^* = 0$ leads to another type of multicritical point, the so-called "Lifshitz point" [228], see Fig. 12. At the Lifshitz point, Eq. (3.44) gets replaced by

$$[S(\boldsymbol{q})]^{-1} = r + K_2 k^4 = r(1 + \xi^4 k^4), \quad \xi = (K_2/r)^{1/4} \propto t^{-1/4}, \ t \to 0. \tag{3.46}$$

At $T = T_L$ we have $r = 0$ and hence $S(\boldsymbol{q}) = K_2^{-1} k^{-4}$. Hence the predictions of the Landau theory for the critical exponents of an (isotropic!) Lifshitz point are

$$\alpha_L = 0, \ \beta_L = 1/2, \ \gamma_L = 1, \ \delta_L = 3, \ \nu_L = \tfrac{1}{4}, \ \eta_L = -4. \tag{3.47}$$

We note that thermal critical exponents are identical to normal critical behavior, and scaling relations expressed by Eqs. (3.23) and (3.24) hold. However, Eq. (3.47) is of no relevance for actual adsorbed layers on surfaces, because there are not any Lifshitz points at non-zero temperature in $d = 2$ dimensions [33,170].

Now the spatially isotropic form of the gradient expansion, Eq. (3.42), makes sense for adsorbed layers on (100) or (111) surfaces of cubic crystals, where the corrugation potential reflects the symmetry of the square or triangular lattices formed by the topmost layer of substrate atoms, but it is clearly not appropriate for (110) surfaces ,where x and y directions clearly are not equivalent, and one should allow for an anisotropic gradient energy term. Rather than the isotropic term $\frac{1}{2}K_1(p)[\nabla\phi(\boldsymbol{x})]^2$

one has

$$\text{Gradient energy} = \frac{1}{2}K_{1\parallel}(p)\left[\frac{\partial\phi(\boldsymbol{x})}{\partial y}\right]^2 + \frac{1}{2}K_{1\perp}(p)\left[\frac{\partial\phi(\boldsymbol{x})}{\partial x}\right]^2, \tag{3.48}$$

where we have assumed that it is the y-direction where $K_{1\parallel}(p)$ may change sign when p is varied, and then a term $\frac{1}{4}K_{2\parallel}(p)[\partial^1\phi(\boldsymbol{x})/\partial y^2]^2$ needs to be included. This case yields still a phase diagram of the type shown in Fig. 12, but with a uniaxial Lifshitz point [228]. The structure factor $S(\boldsymbol{q})$ then is no longer given by Eq. (3.46) but rather by (note that $K_{1\parallel}(p_L) = 0$ but $K_{1\perp}(p_L) > 0$ at the Lifshitz point)

$$[S(\boldsymbol{q})]^{-1} = r + K_{1\perp}k_\perp^2 + K_{2\parallel}k_\parallel^4 = r\left[1 + \xi_\perp^2 k_\perp^2 + \xi_\parallel^4 k_\parallel^4\right], \tag{3.49}$$

where the wavevector $\boldsymbol{k}$ has been split into parallel and perpendicular components, $\boldsymbol{k} = (k_x, k_y) = (k_\perp, k_\parallel)$. The correlation lengths defined in Eq. (3.49) then are $\xi_\parallel = (K_{2\parallel}/r)^{1/4}$, $\xi_\perp = (K_{1\perp}/r)^{1/2}$. Using $r = r't$, one thus concludes that at the uniaxial Lifshitz point there are two correlation lengths diverging with different exponents, $\xi_\parallel \propto t^{-\nu_\parallel}, \xi_\perp \propto t^{-\nu_\perp}$ with $\nu_\parallel = 1/4, \nu_\perp = 1/2$ in mean field theory [33,170,228].

Of course, it is possible to again illustrate these phenomenological considerations by constructing microscopic model Hamiltonians, that yield a phase diagram that qualitatively has the structure of Fig. 12, within mean field theory. A famous example is the ANNNI model [33,170] (axial next-nearest neighbor Ising model). In its standard version, this is a lattice gas model at the square (or rectangular, respectively) lattice with nearest neighbor interaction in the x-direction, while in the y-direction nearest and next nearest neighbor interactions compete. Writing then the index i representing a lattice site in terms of two coordinates $i = (i_x, i_y)$, in Ising spin representation the Hamiltonian becomes

$$\mathcal{H}_{\text{ANNNI}} = J_0 \sum_{i_x,i_y} S(i_x,i_y)S(i_x+1,i_y) - J_1 \sum_{i_x,i_y} S(i_x,i_y)S(i_x,i_y+1) - J_2 \sum_{i_x,i_y} S(i_x,i_y)S(i_x,i_y+2). \tag{3.50}$$

In principle, also a term $-H\sum_{i_x,i_y} S(i_x,i_y)$ should be added, representing a chemical potential controlling the coverage, but for simplicity this term has been omitted here (thus we consider the temperature driven phase transition at a coverage $\theta = 1/2$ in the lattice gas from the disordered phase to a phase separated state of two coexisting phases with high and low coverage for $p \le p_L$ here).

Denoting the ratio of the "exchange constants" $J_2/J_1 = K$, we obtain a phase diagram of the type shown in Fig. 12 in the molecular field approximation, identifying the parameter p with this ratio K (Fig. 13). The Lifshitz point occurs for $K = K_L = -1/4$ [33,170,229].

In Fig. 13 we have included a complication that has not been mentioned so far: there occurs a change in the character of the correlation function at the line $T = T_d(K)$ form an oscillatory decay in the y-direction

$$\langle\phi(0)\phi(y)\rangle \propto \exp(-y/\xi_\parallel)\cos(q^* y), \quad T > T_d(K), \tag{3.51}$$

to a monotonic decay,

$$\langle\phi(0)\phi(y)\rangle \propto \exp(-y/\xi_\parallel), \quad T_{cb}(K) < T < T_d(K), \ K/K_L < 1. \tag{3.52}$$

At fixed K the wavenumber q^* vanishes continuously as the disorder line is approached from above, $q^* \propto [T - T_d(K)]^{1/2}$.

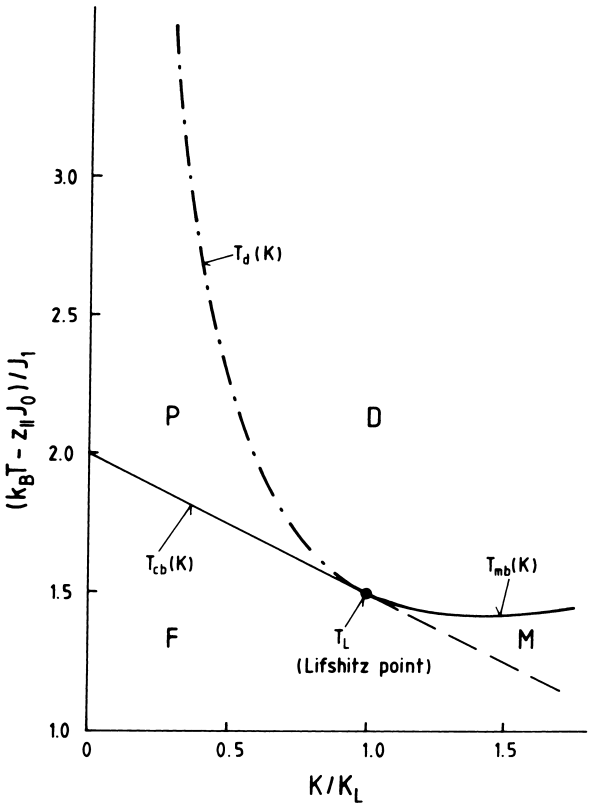

Fig. 13. Phase diagram of the ANNNI model (Eq. (3.50)) in the molecular field approximation, in the plane of variables reduced temperature k_BT/J_1 and coupling constant ratio ($K = J_2/J_1, K_L = -1/4$ is the value of K at the Lifshitz point). By subtracting a term $z_{\|}J_0/J_1$ ($z_{\|}$ is the coordination number in the direction (s) perpendicular to the modulation direction; $z_{\|} = 2$ for a square lattice) this phase diagram is identical for $d = 2$ and $d = 3$ dimensions. At the line $T = T_{cb}(K)$ a phase transition from the "paramagnetic" (P) phase to the "ferromagnetic" (F) occurs. At the "disorder line" $T_d(K)$ the decay of the correlation function changes from oscillatory ($\langle\phi(0)\phi(y)\rangle \propto \exp(-y/\xi_{\|})\cos(q^*y)$) to simple exponential ($\langle\phi(0)\phi(y)\rangle\exp(-y/\xi_{\|})$) again disregarding preexponential power laws. At the line $T = T_{mb}(K)$ the correlation length $\xi_{\|}$ diverges, and long range order of modulated type (M) sets in, characterized by an order parameter $\langle\phi(y)\rangle\cos(q^*y + \varphi)$, where φ is a phase factor. The lines separating the ferromagnetic phase from the modulated phase and higher order commensurate phases are not included on this phase diagram. Note that the transition from the region with oscillatory correlations (D) to the region with monotonically decaying correlations (P) at the disorder line $T_d(K)$ is not a phase transition in the thermodynamic sense. From Binder and Frisch [229].

However, we emphasize that this description of phase transitions between disordered, "ferromagnetic" and modulated phases is the result of the molecular field approximation, and the actual phase diagram of the ANNNI model in $d = 2$ dimensions, Eq. (3.50), is very different, as has been found by Monte Carlo [33,170] and transfer matrix calculations [230] (Fig. 14). Comparing Figs. 13 and 14 we see that mean field theory indeed is a very bad guide for the description of phase transitions in two-dimensional systems! First of all, statistical fluctuations have destabilized the Lifshitz point completely, it is suppressed to zero temperature. Secondly, the nature of the modulated phase has drastically changed: while in mean field theory one has true long range order described by an order parameter $\langle\phi(y)\rangle = A\cos(q^*y + \varphi)$, in reality $\langle\phi(y)\rangle \equiv 0$ in the modulated phase, one has a power law

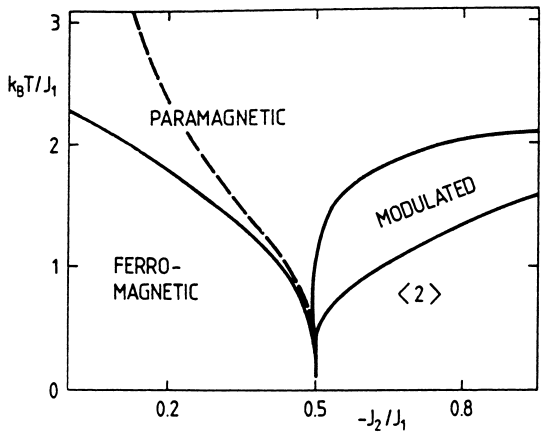

Fig. 14. Phase diagram of the two-dimensional ANNNI model as found from transfer matrix calculations. The broken curve in the paramagnetic phase is the disorder line $T_d(K)$, where $K = J_2/J_1$. Note that the Lifshitz point is suppressed, and rather all phase boundaries (and $T_d(K)$) merge at $T = 0$ in the point $K = -1/2$, where the ground state changes from the ferromagnetic phase (all spins up or all spins down) to the $\langle 2\rangle$ structure (2 rows of up spins alternate with two rows of down spins in the y direction). From Beale et al. [230].

decay of the correlation function:

$$\langle \phi(0)\phi(y)\rangle \propto y^{-\eta(T)} \cos(q^* y + \varphi). \tag{3.53}$$

The transition at $T = T_d(K)$ from exponentially decaying correlations (Eq. (3.51)) to this power law is a transition of the Kosterlitz–Thouless type [37], as it occurs in the two dimensional XY-model. Loosely speaking, one can draw an analogy between this ferromagnet with a two-component order parameter and the modulated phase because amplitude A and phase φ of the ordering also describe a two component order parameter space (recall that one can rewrite the magnetization of the XY model $\boldsymbol{M} = (M_x, M_y)$ as $\boldsymbol{M} = (A\cos\varphi, A\sin\varphi)$}.

Of particular interest, of course, is the transition from the modulated phase to the commensurate phase $\langle 2\rangle$ in Fig. 14, where two rows of up spins (the rows running in x-direction) alternate periodically with 2 rows of down spins. Thus when one proceeds in the y-direction the order is of the type $++--++--\cdots$. The transition from the phase $\langle 2\rangle$ to the modulated phase in the ANNNI model is a special case of a commensurate–incommensurate transition. Since commensurate–incommensurate transitions (Fig. 4c, d) are very common in monolayers adsorbed at surfaces, we now consider the phenomenological theory of such transitions in more detail.

We describe the modulation of the commensurate structure by two order parameter components ϕ_1, ϕ_2 in terms of an amplitude A and a phase φ ($\phi_1 = A_\ell^{i\varphi}, \phi_2 = A_\ell^{-i\varphi}$), assuming that the amplitude A is constant while $\varphi(x)$ may vary in x-direction in the considered uniaxial system. (Unlike for the ANNNI model above, we now assume it is the x-direction where an incommensurate modulation occurs, but the labeling of the coordinate axes is of course arbitrary.) Then a free energy can be postulated as [170,231–233]

$$\frac{\Delta\mathcal{F}}{k_B T} = \int \mathrm{d}x \left\{ \gamma A^2 \left(\frac{\mathrm{d}\varphi}{\mathrm{d}x}\right)^2 + 2\sigma A^2 \frac{\mathrm{d}\varphi}{\mathrm{d}x} + 2\omega A^n \cos[n\varphi(x)] \right\}, \tag{3.54}$$

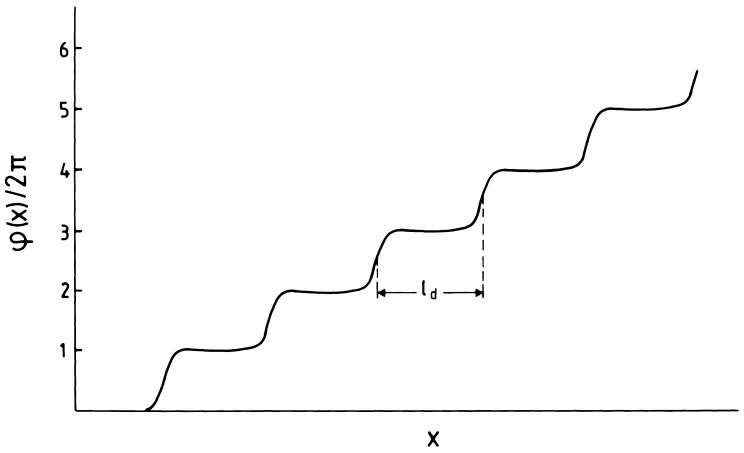

Fig. 15. Variation of the phase $\varphi(x)$ of a modulated structure near a commensurate–incommensurate phase transition. The structure can be characterized by a lattice of domain walls periodically spaced at a distance ℓ_d.

where γ, σ and ω are phenomenological coefficients, and different cases $n = 1, 2, \ldots$ can be distinguished. Minimizing this free energy functional with respect to $\varphi(x)$ yields an Euler–Lagrange equation:

$$\frac{d^2(n\varphi)}{dx^2} + v \sin[n\varphi(x)] = 0, \quad v \equiv n^2 \omega A^{n-2}/\gamma. \tag{3.55}$$

One can show that a commensurate–incommensurate transition occurs at $v_c = n^2\pi^2\sigma^2/16\gamma^2$. The incommensurate phase (for $v < v_c$) consists of a periodic arrangement of regions where the phase $\varphi(x)$ increases by $2\pi/n$ (see Fig. 15) for the case $n = 1$. This structure can be viewed as a domain wall lattice or "soliton lattice", whose lattice constant ℓ_d diverges logarithmically on approaching the commensurate–incommensurate transition, $\ell_d \propto |\ln(v_c - v)|$. However, a consideration of fluctuations (domain wall meandering, cf. Fig. 16 [234]) leads to a rather different result [235,236]

$$\ell_d \propto |\boldsymbol{q}^* - \boldsymbol{q}_B|^{-1} \propto (v_c - v)^{-1/2}. \tag{3.56}$$

If we would consider a single one-dimensional domain wall running along the y-axis on average, a consideration of fluctuations shows that over a distance L a root mean square displacement of this interface in the x-direction of order $w \propto \sqrt{L}$ would occur. In the domain wall lattice, these excursions of the interfaces give rise to an effective repulsive interaction (of entropic origin) between neighboring domain walls, which scales like $U(\ell_d) \approx k_B T(\xi/\ell_d)^2$ [235]. Treating the statistical mechanics of domain walls interacting with this potential yields Eq. (3.56).

Here we shall first describe in more detail the physics of the meandering of a single domain wall, which also is important for the description of phase coexistence in two-dimensional systems in general (Fig. 16). For this purpose, we derive the description of the free energy of an interface (or domain wall, respectively) in terms of the capillary wave Hamiltonian [236,237]. We consider the one-dimensional interface $x = h(y)$ and allow for the fact that the interfacial tensions f_{int} will (at least for a lattice system) depend on the angle θ between the tangent to the interface and the y-axis $[\theta = \arctan(dh/dy)]$. Then the total interfacial (free) energy can be found in terms of an integral along the contour of the

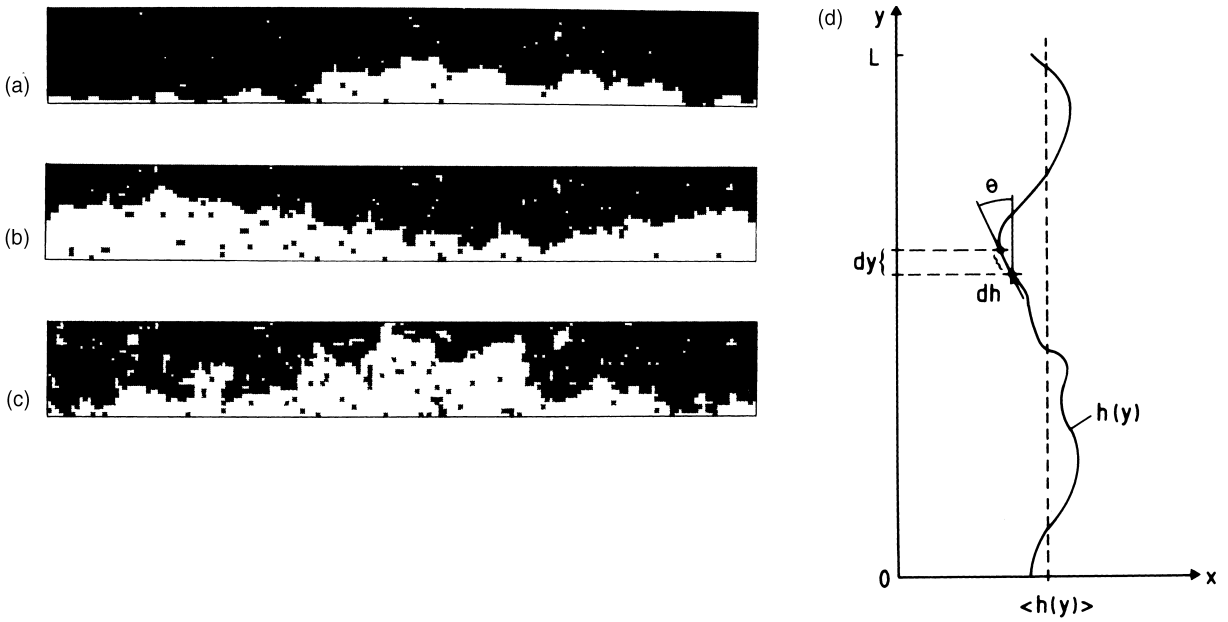

Fig. 16. Snapshot pictures of a meandering interface in the nearest neighbor lattice gas model, choosing a geometry $L \times 24$ in the x-direction across the interface, and $L_y = 228$ in the y-direction along the interface. At $x = 1$ and $x = L_x$ boundary fields $H_1 = -3J (H_{Lx} = +3J)$ are applied to stabilize the interface. Sites taken by adsorbed atoms are shown in black, empty sites are shown in white. Three temperatures are shown: $T = 0.68T_c$ (a), $0.78T_c$ (b) and $T = 0.88T_c$ (c). From [234]. Part (d) shows a coarse-grained description of an interface in the continuum limit, as assumed by capillary wave theory.

interface:

$$E_{\text{int}}/k_B T = \int \mathrm{d}\ell f_{\text{int}}(\theta)\sqrt{1 + (\mathrm{d}h/\mathrm{d}y)^2}. \tag{3.57}$$

Here we have used the fact that the line element $\mathrm{d}\ell$ along the interface satisfies $\mathrm{d}\ell^2 = (\mathrm{d}h)^2 + (\mathrm{d}y)^2$. Of course, in this coarse-grained description of the interface both overhangs and bubbles are deliberately ignored, and one even assumes that this coarse-grained interface is rather flat, such that $(\mathrm{d}h/\mathrm{d}y) \ll 1$ and hence one can expand $\sqrt{1 + (\mathrm{d}h/\mathrm{d}y)^2} \approx 1 + \frac{1}{2}(\mathrm{d}h/\mathrm{d}y)^2$, $f_{\text{int}}(\theta) = f_{\text{int}}(0) + f'_{\text{int}}(0)\mathrm{d}h/\mathrm{d}y + \frac{1}{2}f_{\text{int}}{}''(\mathrm{d}h/\mathrm{d}y)^2 + \cdots$. The linear term in $\mathrm{d}h/\mathrm{d}y$ yields only boundary terms to the integral, Eq. (3.57), and can thus be omitted. Thus one obtains

$$\frac{E_{\text{int}}}{k_B T} = f_{\text{int}}(0)\int \mathrm{d}y + \frac{\kappa}{2}\int \mathrm{d}y\left(\frac{\mathrm{d}h}{\mathrm{d}y}\right)^2, \tag{3.58}$$

where the coefficient $\kappa = f_{\text{int}}(0) + f_{\text{int}}{}''(0)$ is called the "interfacial stiffness". For the nearest neighbor Ising model, the temperature dependence of both $f_{\text{int}}(0)$ and k can be worked out, and behave qualitatively as shown in Fig. 17.

The second term in Eq. (3.58) is called the "capillary wave Hamiltonian". Introducing Fourier components of the height variable h, it is written as

$$\mathscr{H}_{\text{cw}}/k_B T = \frac{1}{2}\kappa\frac{1}{(2\pi)^{d-1}}\int \mathrm{d}^{d-2}q q^2 |h_{\boldsymbol{q}}|^2, \tag{3.59}$$

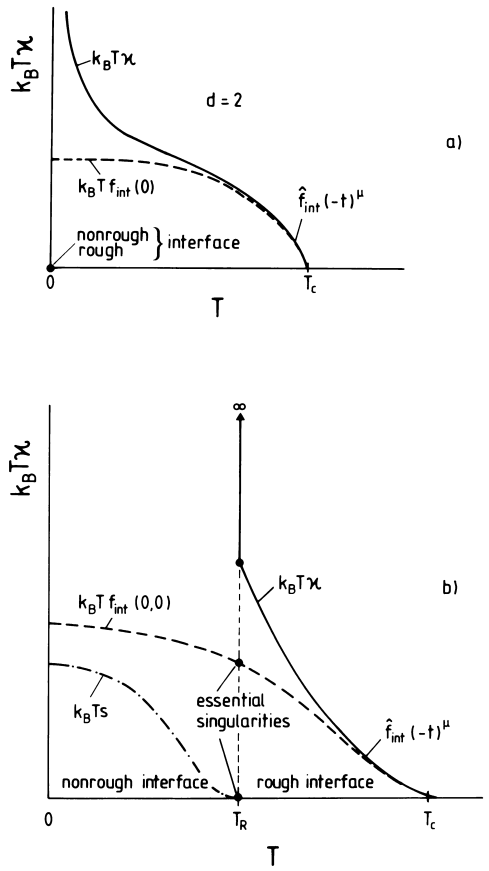

Fig. 17. Schematic temperature variation of interfacial stiffness $k_BT\kappa$ and interfacial free energy $k_BTf_{int}(0)$, for an interface oriented perpendicular to a lattice direction of a square (a) or simple cubic (b) Ising lattice, respectively. While for $d = 2$ dimensions the one-dimensional interface is rough for all nonzero temperatures, in $d = 3$ dimensions the two-dimensional interface is rough only for temperatures T exceeding the roughening transition temperature T_R. For $T < T_R$ there exists then a nonzero free energy k_BT_S of surface steps, which vanishes at $T = T_R$ with an essential singularity. While κ is infinite throughout the non-rough phase, $k_BT\kappa$ reaches a universal value as $T \to T_R^+$. Note that κ and f_{int} to leading order in their critical behavior become identical as $T \to T_c^-$, namely $f_{int} = \hat{f}_{int}(-t)^{\mu}$ with $t = T/T_c - 1$ and $\mu = (d-1)\nu$, i.e. $\mu = 1$ in $d = 2$ and $\mu \approx 1.26$ in $d = 3$, ν being the critical exponent of the correlation length.

where we have generalized the treatment to general dimensionality d (but note that for lattice systems, such as the Ising model in $d = 3$, Eq. (3.59) applies only for temperatures above the well-known interfacial roughening transition temperature T_R, cf. Fig. 17, while $\kappa = \infty$ for $T < T_R$).

Treating the statistical mechanics of Eq. (3.59), the problem is analogous to independent harmonic oscillators with spring constants κq^2. From the equipartition theorem one can then conclude that each degree of freedom has an average potential energy of $k_BT/2$, i.e.

$$k_BT\tfrac{1}{2}\kappa q^2\langle|h_{\boldsymbol{q}}|^2\rangle = \tfrac{1}{2}k_BT, \tag{3.60}$$

which implies $\langle|h_{\boldsymbol{q}}|^2\rangle = (\kappa q^2)^{-1}$. On the other hand, the mean square displacement of the interface is

$$w^2 = \langle h^2(y)\rangle - \langle h(y)^2\rangle = \frac{1}{(2\pi)^{d-1}}\int \mathrm{d}^{d-2}q\langle|h_{\boldsymbol{q}}|^2\rangle = \frac{1}{(2\pi)^{d-1}}\int \mathrm{d}^{d-2}q\frac{1}{\kappa q^2}. \tag{3.61}$$

Over a length scale L along the y-direction in $d = 2$, we hence obtain the power law

$$w^2(L) = \frac{1}{2\pi}\int_{2\pi/L}^{2\pi/\xi} \mathrm{d}q/(\kappa q^2) \approx L/\kappa, \tag{3.62}$$

where we have assumed that $L \gg \xi$, the correlation length in the bulk ($2\pi/\xi$ has to be used as an upper cutoff of the integration in q-space, since the coarse-grained description of the interface in Fig. 16d applies only after a coarse-graining of the Ising model such as in Fig 16a–c over a length scale ξ has been carried out). For completeness and later use, we mention that in $d = 3$ the capillary wave excitations still lead to a logarithmic divergence of the mean square displacement of the interfacial width w with L,

$$w^2(L) \propto \kappa^{-1}\ln(L/\xi). \tag{3.63}$$

After this digression on the physics of one meandering domain wall, we now consider the situation of a $p \times 1$ incommensurate phase showing meandering domain walls at mean spacing ℓ_d (Fig. 18). If $U(\ell_\mathrm{d})$ denotes the interaction of one domain wall per unit length with a neighbor at mean separation ℓ_d, the singular part of the free energy density near the commensurate–incommensurate phase transition can be estimated for n domain walls per length L_x as

$$f_\mathrm{sing}(T,\mu,\ell_\mathrm{d}) \approx L_x^{-1}[nf_\mathrm{int} + nU(\ell_\mathrm{d})/k_\mathrm{B}T]. \tag{3.64}$$

Here, $f_\mathrm{int} = f_\mathrm{int}(T,\mu)$ is the interfacial tension of an isolated domain wall parallel to the y-axis. In the commensurate phase the tension f_int is positive and an isolated wall is stable. However, as the commensurate–incommensurate transition is approached f_int vanishes and becomes negative in the incommensurate phase. The resulting instability causes the appearance of many walls. To leading order we assume a linear variation

$$f_\mathrm{int} \approx f_\mathrm{int}^*(1 - T/T_\mathrm{c}(\mu)), \tag{3.65}$$

with $T_\mathrm{c}(\mu)$ being the transition temperature of the commensurate–incommensurate transition, and f_int^* is some amplitude factor. Using the result $U(\ell_\mathrm{d}) \propto k_\mathrm{B}T(\xi/\ell_\mathrm{d})^2$ quoted above and noting that $n/L_x = \ell_\mathrm{d}^{-1}$, we find

$$f_\mathrm{sing}(T,\mu,\ell_\mathrm{d}) \approx f_\mathrm{int}^*(1 - T/T_\mathrm{c}(\mu))/\ell_\mathrm{d} + \xi^2/\ell_\mathrm{d}^3. \tag{3.66}$$

Note that in the second term on the right-hand side of Eq. (3.66) there clearly is a prefactor of order unity that we have suppressed here. Minimizing now $f_\mathrm{sing}(T,\mu,\ell_\mathrm{d})$ with respect to ℓ_d yields the distance between neighboring domain walls in thermal equilibrium,

$$\ell_\mathrm{d}^{-1} = (f_\mathrm{int}^*/3\xi^2)^{1/2}\sqrt{T/T_\mathrm{c}(\mu) - 1}, \tag{3.67}$$

which is the result announced in Eq. (3.56). Using this result in Eq. (3.66), one concludes that [239,240]

$$f_\mathrm{sing}(T,\mu) = \begin{cases} 0 & \text{for } T \le T_\mathrm{c}(\mu), \\ -\hat{A}(T/T_\mathrm{c}(\mu) - 1)^{3/2} & \text{for } T \ge T_\mathrm{c}(\mu), \end{cases} \tag{3.68}$$

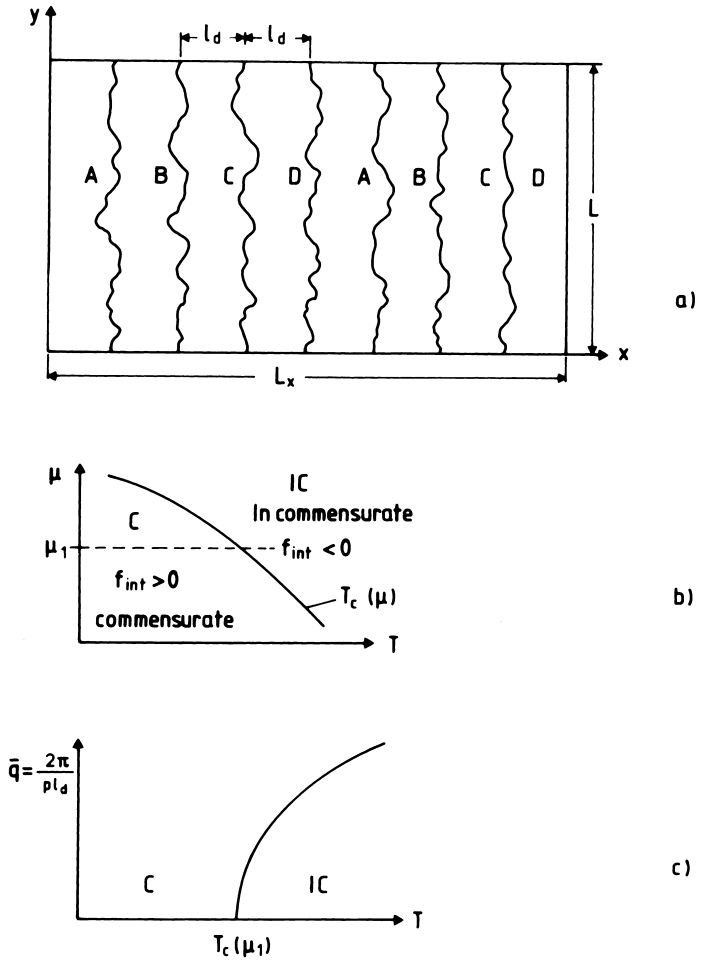

Fig. 18. (a) Schematic representation of a $p \times 1$ incommensurate phase for $p = 4$ showing meandering domain walls at mean spacing ℓ_d. The four types of domains are denoted as A, B, C and D, respectively. Eg. in the ANNNI model A can be represented by a sequence $\uparrow\uparrow\downarrow\downarrow\uparrow\uparrow \ldots$, while B, C and D represent the same sequence but shifted by one lattice unit, corresponding to a different assignment of the four sublattices of the $\langle 2 \rangle$ structure. (b) Phase diagram showing a commensurate (C)–incommensurate (IC) phase transition in the plane of variables μ (chemical potential) and temperature. (c) Variation of the "incommensurability" $\bar{q} = 2\pi/p\ell_d$ for the chemical potential μ_1. After Fisher [236], in changed form.

with $\hat{A} = 2(f_{int}^{*3}/3\xi^2)^{1/2}$. This result shows that the transition is a second-order transition, with a divergent specific heat ($C = T(\partial^2 f/\partial T^2)_\mu \propto (T/T_c(\mu) - 1)^{-1/2}$, i.e. $\alpha = 1/2$, cf. Eq. (3.16)).

However, there is *no divergence* on the commensurate side of the transition.

It is also of interest to discuss the correlation lengths of order parameter fluctuations in the incommensurate phase, noting that the situation considered in Fig. 18 is intrinsically anisotropic. The transverse correlation length $\xi_\perp$ is simply proportional to ℓ_d and hence [238]

$$\xi_\perp = \hat{\xi}_\perp (T/T_c(\mu) - 1)^{-\nu_\perp}, \quad \nu_\perp = 1/2. \tag{3.69}$$

From the diffusive character of the random-walk like one-dimensional interface in Fig. 16 or 18a we

conclude that

$$\xi_{||} = \text{const.}(\xi_{\perp})^2, \qquad \text{i.e. } \xi_{||} = \hat{\xi}_{||}(T/T_c(\mu) - 1)^{-\nu_{||}}, \quad \nu_{||} = 2\nu_{\perp} = 1. \tag{3.70}$$

These results can also be derived by a more rigorous analysis [239,240]. For this anisotropic situation, the hyperscaling relation (Eq. (3.25)) does not hold, and must be replaced by

$$2 - \alpha = \nu_{||} + \nu_{\perp}. \tag{3.71}$$

Next we consider the effect of dislocations in the incommensurate structure: these are topological defects where some domain walls merge in a point and terminate. In a $p \times 1$ structure Fig. 18a it is possible that p walls come together: so one could have the first four walls shown in Fig. 18a merge and thus the B, C, D domains terminate there as well and the first two A-domains merge thereafter. In the commensurate phase, where we may have a situation of only an A domain, for instance, this opens the possibility that local precursor-type fluctuations of the incommensurate phase occur already in the commensurate phase. These fluctuations may change the nature of the singularities at the transition, or even destroy the incommensurate phase altogether: renormalization group treatments show that [238,241–243] for $p = 1$ and $p = 2$ no incommensurate phase is possible: only a commensurate phase exists which must have a transition directly into the disordered phase, without an intervening incommensurate phase. In fact, the two-dimensional ANNNI model (Fig. 14) is an illustration of this finding, the ferromagnetic phase ($p = 1$) cannot make a transition to a modulated phase at all, while the phase $\langle 2 \rangle$ (which is of the type $p = 4$) can. In the commensurate phase, these dislocations are then responsible for singularities of the free energy $f_{\text{sing}}(T, \mu)$, so Eq. (3.68) gets modified: e.g., for $p = 3$ the specific heat gets a singularity of a cusp-type, $C \propto (1 - T/T_c(\mu)) \ln|1 - T/T_c(\mu)|$ for $T \leq T_c(\mu)$. Finally, we mention that the dislocations in the incommensurate phase also occur in bound pairs and their unbinding characterizes the ''melting'' of the incommensurate phase into the disordered phase via a Kosterlitz–Thouless type transition [52,170,244].

So far the only microscopic model exhibiting a commensurate–incommensurate phase transition, that we have discussed in this review, is the ANNNI model (Fig. 14).

However, due to the discrete spin nature of that model obviously no incommensurate phase can exist in that model in the ground state at $T = 0$, and in fact the phase diagram shows at $T = 0$ just the ferromagnetic phase and the commensurate $\langle 2 \rangle$ phase (Fig. 14).

However, this clearly is not the whole story, and for weak corrugation potentials it does make sense to consider models that do allow for the existence of incommensurate (IC) phases and *C–IC* phase transitions at $T = 0$. A model that is directly motivated by Fig. 4c, d is the Frenkel–Kontorova (FK) model [245]. Being interested in $T = 0$, it suffices (for an anisotropic substrate such as provided by (110) surfaces of cubic crystals) to consider the one-dimensional version only. Thus, we write down the potential energy of a harmonic chain of particles in an external sinusoidal potential (which represents the corrugation potential due to the substrate acting on the adatoms). The potential then is (κ is an effective ''spring constant'' describing the strength of interparticle interaction in the absence of the corrugation potential, A describes the strength of the corrugation potential, r_i is the position of particle i)

$$U = \frac{1}{2}k\sum_i (r_{i+1} - r_i - b)^2 + \frac{1}{2}A\sum_i \left(1 - \cos\frac{2\pi r_i}{a}\right). \tag{3.72}$$

The interatomic potential thus favors an interparticle spacing b, which in general differs from the distance a between the minima of the corrugation potential. To balance these competing interactions, the particles may choose non-trivial positions already in the ground state.

Of course, Eq. (3.72) is not used as a microscopically realistic description of a particular adsorbate–substrate system, but rather as a generic model suitable to develop the basic concepts and ideas. We proceed to obtain the solution that minimizes U (which is the relevant thermodynamic potential at $T = 0$). The condition $\partial U/\partial r_i$ has the interpretation that the force acting on each particle vanishes in equilibrium. This yields ($u_i = r_i/a$)

$$u_{i+1} - 2u_i + u_{i-1} = \frac{\pi}{2\ell_0^2} \sin(2\pi u_i), \quad \ell_0 = (ka^2/2A)^{1/2}. \tag{3.73}$$

Replacing differences by differentials Eq. (3.73) is reduced to the sine-Gordon equation [246]

$$\mathrm{d}^2u/\mathrm{d}n^2 = (\pi/2\ell_0^2) \sin(2\pi u). \tag{3.74}$$

One finds that the commensurate phase yields the absolute minimum of the energy for small enough misfit, $\delta \equiv |b - a|/a \leq \delta_c = 2/(\ell_0\pi)$; otherwise the ground state solution resulting from Eqs. (3.72)–(3.74) resembles Fig. (3.12) for $\varphi(x)/2\pi$, as expected, since Eq. (3.74) is identical with Eq. (3.55) for $n = 1$. For $\delta = \delta_c$, the solution of Eq. (3.74) reduces to the well-known ''domain-wall'' or ''kink'' or ''soliton'' solution,

$$u(n) = \frac{2}{\pi} \arctan\left[\exp\frac{\pi n}{\ell_0}\right]. \tag{3.75}$$

To create such a wall, one has to imagine that one particle has to be deleted (if b is less than a) or added (if b is larger than a). The thickness of the wall is ℓ_0. For larger misfits, $\delta > \delta_c$, the ground state consists of a lattice (''soliton lattice'') of regularly spaced domain walls of thickness $h\ell_0$, where h is given as the solution of the equation

$$\ell_0\delta = 2E(h)/(\pi h), \tag{3.76}$$

$E(h)$ being the complete elliptic integral of the second kind. The spacing ℓ_d of domain walls is given by

$$\ell_d = 2\ell_0 hK(h)/\pi, \tag{3.77}$$

with $K(h)$ being the complete elliptic integral of the first kind. The separation of particles on the average then is $a\ell_d/(\ell_d - 1)$. Since ℓ_d changes continuously with d, the ground states in general are incommensurate with respect to the sinusoidal potential. Thus at $\delta = \delta_c$ the $C \rightarrow IC$ transition takes place, with $\ell_d \propto |\ln(\delta - \delta_c)|$. However, it should be noted that in fact the continuum approximation made by replacing Eq. (3.73) by Eq. (3.74) in general is not valid, and on solving Eq. (3.73) one does not find a smooth variation of the wavenumber q of the structure with the misfit δ, but rather a discontinuous ''devil's staircase'' behavior is predicted, as the particles are not allowed to be at all possible ''heights'' of the potential U, but tend to stick to the bottoms of the potential wells, and thus the walls are ''locked'' to the lattice [170,247]. However, as most of the properties deriving from Eqs. (3.72), (3.73), (3.74), (3.75), (3.76) and (3.77) are substantially changed by thermal fluctuations at nonzero temperature, we do not go into further details here.

3.4. Melting phenomena

In this section we are concerned with the melting of two-dimensional solid phases which are incommensurate with the periodicity provided by the substrate (melting of commensurate solids in many aspects is not fundamentally different from the order–disorder transitions of the lattice gas models and variants thereof, as have been discussed already in Sections 3.1 and 3.2 of the present article). However, melting of incommensurate two-dimensional solids can have a character that is very different from these commensurate solids and from the melting transition of three-dimensional solids (which has to be a first-order transition, from general symmetry requirements [244]). However, in two dimensions it is conceivable that melting occurs via two consecutive Kosterlitz–Thouless-type [37] transitions: the first transition takes the solid (which in two dimensions lacks positional long-range order, though orientational long range order is still present!) to a hexatic phase [39]: while in the two-dimensional crystal the positional correlation function exhibits a power law decay, in the hexatic phase this correlation function already decays exponentially with distance, as it does in the ordinary disordered fluid phase. However, the correlation function of the orientational order parameter still shows a power law in the hexatic phase, and only via a second Kosterlitz–Thouless type transition does the system become an ordinary fluid where all correlation functions have an exponential decay.

This scenario of two-dimensional melting, as sketched above, is due to Halperin, Nelson and Young [38,39,244,248,249] and has been rather controversial until today, because the direct route from the crystal to the fluid via a single first order phase transition, as in the three-dimensional case, is not ruled out a priori: hence, the conditions under which two-dimensional melting is continuous and when it is first order are not yet clarified. Even for the simplest model of a two-dimensional melting transition, the hard disk fluid which is under study since the Monte Carlo and Molecular dynamics computer simulation methods where invented [250,251], the character of the transition is still under debate [252–254]. Nevertheless, we discuss this concept that melting is defect mediated here — even if it turns out that melting would occur via first order transitions in cases of practical interest, it is clear that these transitions are very weak first order transitions then, and although the relevant correlation lengths (and associated response functions) are not strictly divergent then at the transition point, they must become rather large. In addition, these defect concepts are rather useful also for some alternative theories describing melting as a first order transition: while the melting of the hexatic phase can be viewed as an ''unbinding transition'' of bound dislocation pairs with opposite Burgers vectors, the first order melting can be described [255,256] as a condensation of grain boundaries (via nucleation, just as at a first order condensation of liquid from saturated gas), and we recall that a grain boundary in $d = 2$ dimensions is nothing but a linear arrangement of dislocations.

After these introductory remarks we shall first describe the general ideas about Kosterlitz–Thouless transitions [37,58,244], using the plane rotator model [58] as a generic example, but we shall mention the generalization to solids whenever appropriate. The common feature about solids, plane rotator models (or isotropic XA magnets) and two-dimensional superfluids is that ordering of these systems involves the breaking of a continuous Abelian symmetry. In this general condition, long range order is destroyed by statistical fluctuations, but power-law decay of correlations still occurs [244].

The Hamiltonian of the plane rotator model, where each site i carries a planar unit vector with two components $(\cos\theta_i, \sin\theta_i)$, reads

$$\mathscr{H} = -J \sum_{\langle i,j \rangle} \cos(\theta_i - \theta_j), \tag{3.78}$$

where we assume the nearest neighbor exchange constant J ferromagnetic, $J > 0$. At very low temperatures spins at neighboring sites are strongly correlated and hence one may expand the cosine keeping only the quadratic term. For long wavelength fluctuations one may also make a continuum approximation, replacing the θ_i by $\theta(\boldsymbol{x})$ and hence $\{\theta_k$ is the Fourier transform of $\theta(\boldsymbol{x})\}$

$$\mathscr{H} = \frac{J}{2} \int \mathrm{d}\boldsymbol{x} [\nabla \theta(\boldsymbol{x})]^2 = \frac{J}{2} \int \frac{\mathrm{d}\boldsymbol{k}}{(2\pi)^2} k^2 |\theta_{\boldsymbol{k}}|^2. \tag{3.79}$$

If we also neglect the fact that $\theta_i + 2\pi n$ in Eq. (3.78) is equivalent to θ_i, for integer n, one finds by extending the range of integration over θ from $-\infty$ to $+\infty$ that the partition function can be written as functional integration, involving Gaussian integrals,

$$Z = \int_{-\infty}^{+\infty} \mathscr{D}\theta(\boldsymbol{x}) \exp\left\{ -\frac{J}{2k_{\mathrm{B}}T} \int \mathrm{d}\boldsymbol{x} [\nabla \theta(\boldsymbol{x})]^2 \right\}. \tag{3.80}$$

From this spin wave approximation [257] the correlation function

$$G(\boldsymbol{x}) = \langle \exp[i(\theta(\boldsymbol{x}) - \theta(0)] \rangle = \exp\{ -\tfrac{1}{2} \langle [\theta(\boldsymbol{x}) - \theta(0)]^2 \rangle \} \tag{3.81}$$

can be calculated (in the second step of Eq. (3.81) we have used already the Gaussian character of the Hamiltonian, Eq. (3.79)). We obtain [58]

$$\langle [\theta(\boldsymbol{x}) - \theta(0)]^2 \rangle = \int \frac{\mathrm{d}\boldsymbol{k}}{(2\pi)^2} |1 - \exp(\mathrm{i}\boldsymbol{k} \cdot \boldsymbol{x})|^2 \langle |\theta_{\boldsymbol{k}}| \rangle^2 \approx \frac{1}{2\pi} \int_{1/x}^{1/a} 2k \, \mathrm{d}k \langle |\theta_{\boldsymbol{k}}|^2 \rangle. \tag{3.82}$$

Here we have approximated the factor $|\exp(\mathrm{i}\boldsymbol{k}\boldsymbol{x}) - 1|^2$ by 2, its average value, in the interval $1/x < k < 1/a$ (a being the lattice spacing of the underlying lattice). Using now the equipartition theorem, $\langle |\theta(\boldsymbol{x})|^2 \rangle = k_{\mathrm{B}}T/Jk^2$, we find [58]

$$\langle [\theta(\boldsymbol{x}) - \theta(0)]^2 \rangle = \frac{k_{\mathrm{B}}T}{\pi J} \int_{1/x}^{1/a} \mathrm{d}k/k = \frac{k_{\mathrm{B}}T}{\pi J} \ln(x/a) \tag{3.83}$$

and hence, using Eq. (3.81)

$$G(\boldsymbol{x}) = x^{-\eta(T)}, \quad x \to \infty, \quad \eta(T) = k_{\mathrm{B}}T/(2\pi J). \tag{3.84}$$

Thus we see that at low temperatures — where the spin wave approximation is expected to be reasonable emdash there is no long range order as in $d = 3$ dimension (where $G(\boldsymbol{x}) \to \langle |\Psi| \rangle^2$ as $x \to \infty$, the square of the order parameter), but rather a power law decay of the correlation function, with an exponent that increases with temperature.

We now turn to the analog of these phenomena in crystals: there the phenomenological continuum Hamiltonian analog to Eq. (3.79) is simply given in terms of standard elasticity theory, described by the free energy functional [258]

$$\mathscr{F} = \frac{1}{2}\int \mathrm{d}\boldsymbol{x}\Big[2\eta u_{ij}^2(\boldsymbol{x}) + \lambda u_{kk}^2(\boldsymbol{x})\Big], \tag{3.85}$$

where η and λ are the Lamé coefficients, and $u_{ij}(\boldsymbol{x})$ is the symmetric strain tensor,

$$u_{ij}(\boldsymbol{x}) = \tfrac{1}{2}\big[\partial u_i/\partial x_j + \partial u_j/\partial x_i\big], \tag{3.86}$$

implying also the summation convention in Eq. ((3.85)). Now in a solid, the quantity of primary interest is the structure factor,

$$S(\boldsymbol{q}) = \sum_{\boldsymbol{x}} \exp(\mathrm{i}\boldsymbol{q}\cdot\boldsymbol{x})\langle e^{\mathrm{i}\boldsymbol{q}\cdot[\boldsymbol{u}(\boldsymbol{x})-\boldsymbol{u}(0)]}\rangle = \sum_{\boldsymbol{x}} \exp(\mathrm{i}\boldsymbol{q}\boldsymbol{x})\exp\left[-\frac{q^2}{4}\langle[\boldsymbol{u}(\boldsymbol{x})-\boldsymbol{u}(0)]\rangle^2\right]. \tag{3.87}$$

On the other hand, writing the density $\rho(\boldsymbol{x})$ of a collection of point particles at positions $\boldsymbol{R}(\boldsymbol{x}) = \boldsymbol{x} + \boldsymbol{u}(\boldsymbol{x})$ as $\rho(\boldsymbol{x}) = \sum_{\boldsymbol{x}} \delta[\boldsymbol{x} - \boldsymbol{R} - \boldsymbol{u}(\boldsymbol{x})]$, one recognizes that $S(\boldsymbol{q})$ is just the Fourier transform of the density–density correlation function, and defining [244]

$$\rho_{\boldsymbol{G}}(\boldsymbol{r}) = \exp[\mathrm{i}\boldsymbol{G}\cdot\boldsymbol{u}(\boldsymbol{r})], \tag{3.88}$$

where $\boldsymbol{G}$ is a vector of the reciprocal lattice associated with the lattice points $\{\boldsymbol{R}\}$, one sees that $S(\boldsymbol{q})$ is the Fourier transform of the Debye–Waller-factor

$$G(\boldsymbol{x}) = \big\langle \rho_G(\boldsymbol{x})\rho_{\boldsymbol{G}}^*(0)\big\rangle. \tag{3.89}$$

While in a three-dimensional crystal $G(\boldsymbol{x}\to\infty)$ tends to a nonzero constant, we here again encounter a power-law decay [244]

$$G(\boldsymbol{x}) \propto x^{-\eta_G(T)}, \quad \eta_{\boldsymbol{G}}(T) = \frac{k_{\mathrm{B}}T|\boldsymbol{G}|^2(3\mu+\lambda)}{4\pi\mu(2\mu+\lambda)}. \tag{3.90}$$

Note that $\eta_{\boldsymbol{G}}(T)$ depends on the temperature, on the Lamé coefficients, and on the particular reciprocal lattice vector involved — thus this behavior here is much less universal than in the plane rotator case. This power-law decay leads to power law singularities in $S(\boldsymbol{q})$ at the reciprocal lattice points $\{\boldsymbol{G}\}$. For $\boldsymbol{q}\approx\boldsymbol{G}$, one finds

$$S(\boldsymbol{q}) \sim |\boldsymbol{q}-\boldsymbol{G}|^{2-\eta_G(T)}. \tag{3.91}$$

Note that these singularities are the stronger the smaller the reciprocal lattice vectors $\boldsymbol{G}$ one is considering.

In Eqs. (3.85),(3.86),(3.87),(3.88),(3.89),(3.90) and (3.91), the effect of the periodic corrugation potential has been neglected completely. Although in an incommensurate solid the translational order of the substrate can be disregarded at long wavelengths, there is an orientational epitaxy [40]. To model induced orientational order in isotropic incommensurate adsorbed solid layers, the free energy functional of Eq. (3.85) must be replaced by [39,244]

$$\mathscr{F} = \frac{1}{2}\int \mathrm{d}\boldsymbol{x}\Big\{2\mu\big[u_{ij}(\boldsymbol{x})\big]^2 + \lambda[u_{kk}(\boldsymbol{x})]^2 - h\cos[p\theta(\boldsymbol{x})]\Big\}, \tag{3.92}$$

where the last term describes a p-fold symmetric term breaking the rotational invariance. The local

orientation angle $\theta(\boldsymbol{x})$

$$\theta(\boldsymbol{x}) \equiv \frac{1}{2}\left[\frac{\partial u_y(\boldsymbol{x})}{\partial x} - \frac{\partial u_x(\boldsymbol{x})}{\partial y}\right] \tag{3.93}$$

is measured from the direction of optimal alignment. The strength of this local orientational potential is given by h. Note that $p = 6$ for triangular solids resting on hexagonal substrates like graphite or (111) surfaces of $f.c.c.$ metals, while $p = 12$ for triangular solids on substrates with a square symmetry, however. We also note that the direction of optimal alignment need not coincide with a crystallographic axis of the substrate lattice.

Note that $\theta(\boldsymbol{x})$ as quoted in Eq. (3.93) plays a role in defining the (complex) local order parameters $\Psi_6(\boldsymbol{x}), \Psi_4(\boldsymbol{x})$ for orientational ordering

$$\Psi_6(\boldsymbol{x}) \equiv \exp[6\mathrm{i}\theta(\boldsymbol{x})], \qquad \Psi_4(\boldsymbol{x}) \equiv \exp[4\mathrm{i}\theta(\boldsymbol{x})]. \tag{3.94}$$

Here $\Psi_6(\boldsymbol{x})$ is appropriate for studying the melting of triangular lattices, since one is then only interested in bond order modulo 60° rotations, while $\Psi_4(\boldsymbol{x})$ would be appropriate for melting of a square lattice. We also note that $\theta(\boldsymbol{x})$ is well-defined not only for a continuum description (as invoked in Eq. (3.93)) but can also easily be defined for an atomistic model. One then defines $\theta(\boldsymbol{x})$ as the angle between the axis connecting an atom located at $\boldsymbol{x}$ and one of its 6 (triangular lattice) or 4 (square lattice) nearest neighbors relative to a reference axis (which is arbitrary in the case of a perfectly smooth substrate and the direction of optimal alignment in the case of a corrugated substrate). Since in a dense fluid also the notion of nearest neighbors of an atom is well defined (counting just those atoms which contribute to the first peak of the radial distribution function), one can consider these local order parameters $\Psi_6(\boldsymbol{x})$ and $\Psi_4(\boldsymbol{x})$ (Eq. (3.94)) even in the fluid phase, and study the respective correlation functions

$$G_6(\boldsymbol{x}) = \left\langle \Psi_6^*(\boldsymbol{x})\Psi_6(0)\right\rangle, \qquad G_4(\boldsymbol{x}) = \left\langle \Psi_4^*(\boldsymbol{x})\Psi_4(0)\right\rangle. \tag{3.95}$$

Of course, in the disordered fluid phase one expects that there is only short range orientational order, while at large distances one encounters an exponential decay:

$$G_6(\boldsymbol{x}) \propto \exp(-x/\xi_6), \qquad G_4(\boldsymbol{x}) \propto \exp(-x/\xi_4), \quad \text{fluid phase.} \tag{3.96}$$

While we have seen that in the solid phase the translational correlation function $G(\boldsymbol{x})$ (Eq. (3.89)) has a power law decay (Eq. (3.89), in the case of a smooth substrate), two-dimensional solids do exhibit true orientational long range order, i.e. (we specialize to the case of a triangular lattice here)

$$G_6(\boldsymbol{x}) \to \langle|\Psi_6|\rangle^2 \quad \text{for } x \to \infty, \quad \text{solid phase}, \tag{3.97}$$

which implies (cf. Eqs. (3.93) and (3.94)) that fluctuations in the local orientation angle $\theta(\boldsymbol{x})$ are finite [206,244]

$$\langle|\theta(\boldsymbol{x})|^2\rangle = \tfrac{1}{4}\langle|\nabla \times \boldsymbol{u}(\boldsymbol{x})|^2\rangle < \infty. \tag{3.98}$$

This behavior is in contrast to the diverging fluctuations in the displacement field (we have $\boldsymbol{u}(0) \equiv 0$ by arbitrarily putting the coordinate origin at one atom in the lattice)

$$\langle|\boldsymbol{u}(\boldsymbol{x})|^2\rangle \to \infty \quad \text{as } x \to \infty \tag{3.99}$$

noted already by Peierls and Landau [259,260]. At this point, we note that the hexatic phase is characterized by $\langle|\Psi_6|\rangle \equiv 0$ but a power-law decay rather than an exponential decay of $G_6(\boldsymbol{x})$,

$$G_6(\boldsymbol{x}) \propto x^{-\eta_6(T)}. \tag{3.100}$$

We now return to the effective Hamiltonian Eq. (3.92) describing the long wavelength properties of a solid monolayer exposed to the orientational potential due to the corrugated substrate crystal surface. Since the fluctuations in $\theta(\boldsymbol{x})$ are finite (Eq. (3.98)) and actually rather small, it is legitimate to expand the cosine function in Eq. (3.92) to quadratic order to obtain a generalized harmonic Hamiltonian [244]

$$\mathscr{F} = \frac{1}{2}\int \mathrm{d}\boldsymbol{x}\left\{2\mu\left[u_{ij}(\boldsymbol{x})\right]^2 + \lambda[u_{kk}(\boldsymbol{x})]^2 + \gamma\left(\frac{\partial u_y(\boldsymbol{x})}{\partial x} - \frac{\partial u_x(\boldsymbol{x})}{\partial y}\right)^2\right\} \tag{3.101}$$

with an "orientational elastic constant" $\gamma = hp^2/8$. The diverging Landau–Peierls fluctuations in the displacement field remain, the free energy Eq. (3.101) leads to the same algebraic decay of translational order as given in Eq. (3.90) but the exponent $\eta_{\boldsymbol{G}}(T)$ gets modified, for $x \to \infty$,

$$G(\boldsymbol{x}) \propto x^{-\eta_G(T)}, \frac{k_\mathrm{B}T|\boldsymbol{G}|^2(3\mu+\lambda+\gamma)}{4\pi(\mu+\gamma)(2\mu+\lambda)}. \tag{3.102}$$

Eqs. (3.85)–(3.91) or (3.97)–(3.102) are valid descriptions of the well-ordered solid phase on smooth or corrugated substrates, respectively. We now turn to the question how these phases decay into the less ordered hexatic and (finally) fluid phases. It turns out that these phase transitions are driven by the unbinding of topological defects, namely dislocations (solid) and disclinations (hexatic) [38,39,244,248,249]. The same problem of a defect-mediated phase transition already occurs in the simple example of the plane rotator model, Eq. (3.78), to which we return now.

The problem encountered by reducing Eq. (3.78) to Eqs. (3.79) and (3.80) obviously must arise from the fact that while $\exp(\mathrm{i}\theta) = (\cos\theta, \mathrm{i}\sin\theta)$ is a single valued function; the angle itself is multivalued — we may add or subtract multiples of 2π without changing the physics of the problem. In order to avoid complications due to this fact, it is convenient to work with the gradient of $\theta(\boldsymbol{x})$, which is single valued:

$$\boldsymbol{v}(\boldsymbol{x}) \equiv \nabla\theta(\boldsymbol{x}). \tag{3.103}$$

In the closely related problem of a superfluid film $\boldsymbol{v}(\boldsymbol{x})$ is proportional to the superfluid velocity, $\boldsymbol{v}_\mathrm{s} = (\hbar/m)\boldsymbol{v}$, m being the mass of the particles. Now the phase change of θ along any closed contour C

$$\oint_C \boldsymbol{v}(\boldsymbol{x})\cdot\mathrm{d}\ell = 2\pi s, \quad s = 0, \pm1, \pm2, \ldots. \tag{3.104}$$

If s is positive (negative) we call the corresponding excitation of the spin field a vortex (antivortex) of "charge" s (Fig. 19a). In practice, only the cases $s = \pm1$ need to be considered, if the contour encloses a single vortex or antivortex only. In the superfluid case, these excitations correspond to singularities in the flow field, due to a situation where the superflow is not strictly irrotational, $\nabla \times \boldsymbol{v}_\mathrm{s}(\boldsymbol{x}) \neq 0$, and Eq. (3.104) corresponds to the net circulation in the superflow, quantized as $\pm 2\pi\hbar/m$. In the superfluid, it is common to write the (complex) order parameter field $\Psi(x)$ in terms of amplitude and phase,

$$\Psi(\boldsymbol{x}) = |\Psi(\boldsymbol{x})|\exp[\mathrm{i}\theta(x)]. \tag{3.105}$$

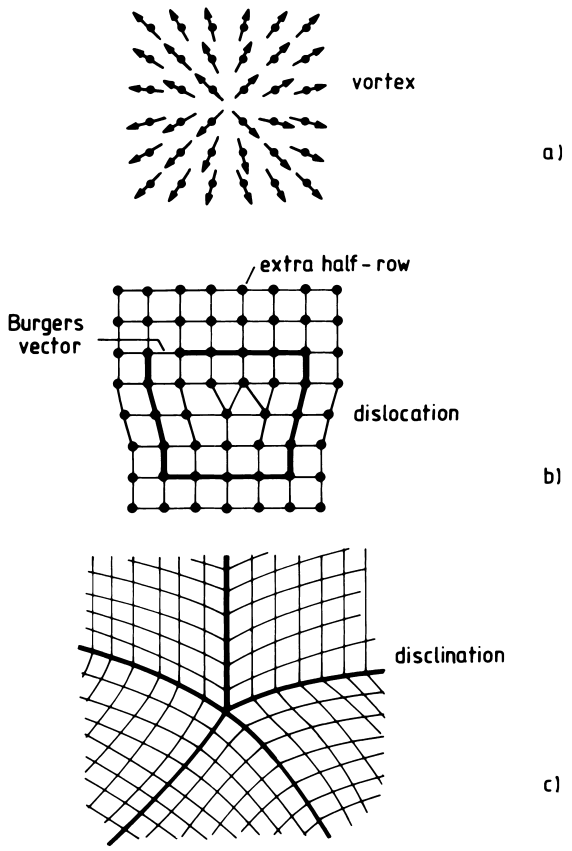

Fig. 19. Schematic pictures of topological excitations: (a) vortex in the plane rotator model on the square lattice (note that the corresponding antivortex is simply found by inverting the orientation of all the spins). (b) Dislocation on the square lattice, indicating the construction that yields the Burgers vector. (c) Disclination embedded in a square lattice.

The singular centers of the vortices (antivortices) are points where the amplitude vanishes, $\Psi(\boldsymbol{x}) = 0$. It is then convenient to allow for the situation where one has many vortices and antivortices in the system, and define a vortex charge density by

$$n(\boldsymbol{x}) = \sum_{\ell} s_{\ell} \delta(\boldsymbol{x} - \boldsymbol{x}_{\ell}), \tag{3.106}$$

where s_{ℓ} is the charge of the vortex (or antivortex) centered at point $\boldsymbol{x}_{\ell}$. Eqs. (3.104) and (3.106) also imply, $\hat{z}$ being a unit vector in z-direction perpendicular to the surface,

$$\nabla \times \boldsymbol{v}(\boldsymbol{x}) = 2\pi n(\boldsymbol{x})\hat{z}. \tag{3.107}$$

We now wish to study the effect of an assembly of vortices on the statistical mechanics. Following Kosterlitz and Thouless [37], we decompose $\boldsymbol{v}(\boldsymbol{x})$ into two parts,

$$\boldsymbol{v}(\boldsymbol{x}) = \nabla\tilde{\theta}(\boldsymbol{x}) + 2\pi(\hat{z} \times \nabla) \int \mathrm{d}\boldsymbol{x}' n(\boldsymbol{x}') G(\boldsymbol{x}, \boldsymbol{x}'), \tag{3.108}$$

where $\tilde{\theta}(\boldsymbol{x})$ is the non-singular phase function, and the Green's function $G(\boldsymbol{x},\boldsymbol{x}')$ satisfies

$$\nabla^2 G(\boldsymbol{x},\boldsymbol{x}') = \delta(\boldsymbol{x}-\boldsymbol{x}'). \tag{3.109}$$

It is easily checked from Eqs. (3.108) and (3.109) that Eq. (3.108) satisfies Eq. (3.107). Combining now Eq. (3.103) and Eq. (3.79) we see that the effective Hamiltonian can be broken into a piece due to regular spin waves and another piece due to vortices,

$$\frac{\mathscr{H}}{k_B T} = \frac{J}{2k_B T}\int \mathrm{d}\boldsymbol{x}\, \boldsymbol{v}^2 = \frac{J}{2k_B T}\int \mathrm{d}\boldsymbol{x}(\nabla\tilde{\theta})^2 + \frac{\mathscr{H}_{\mathrm{v}}}{k_B T} \tag{3.110}$$

with

$$\frac{\mathscr{H}_{\mathrm{v}}}{k_B T} = \frac{2\pi^2 J}{k_B T}\int \mathrm{d}\boldsymbol{x}\int \mathrm{d}\boldsymbol{x}_1 \int \mathrm{d}\boldsymbol{x}_2\, n(\boldsymbol{x}_1)n(\boldsymbol{x}_2)\nabla G(\boldsymbol{x},\boldsymbol{x}_1)\cdot\nabla G(\boldsymbol{x}_1\boldsymbol{x}_2). \tag{3.111}$$

Using the ''charge neutrality'' condition

$$\int \mathrm{d}\boldsymbol{x}\, n(\boldsymbol{x}) = 0 \tag{3.112}$$

one can reduce Eq. (3.111) to a simpler form by integration by parts and using the explicit form of the Green's function of the Laplacian in two dimensions,

$$G(\boldsymbol{x},\boldsymbol{x}') = \frac{1}{2\pi}\ln(|\boldsymbol{x}-\boldsymbol{x}'|/a) + C, \tag{3.113}$$

where C is a constant that will get the physical significance of the vortex core energy E_{c} here. As a result, one finds

$$\frac{\mathscr{H}_{\mathrm{v}}}{k_B T} = \frac{-J\pi}{k_B T}\int_{|\boldsymbol{r}-}\int_{\boldsymbol{r}'|>a} \mathrm{d}\boldsymbol{x}\,\mathrm{d}\boldsymbol{x}' n(\boldsymbol{x})n(\boldsymbol{x}')\ln(|\boldsymbol{x}-\boldsymbol{x}'|/a) + \frac{E_{\mathrm{c}}}{k_B T}\int \mathrm{d}\boldsymbol{x} n^2(\boldsymbol{x}). \tag{3.114}$$

So in addition to the spin wave part of the partition function due to $J/(2k_B T)\int \mathrm{d}\boldsymbol{x}(\nabla\tilde{\theta})^2$, which has been used in Eqs. (3.80),(3.81),(3.82) and (3.83) already, we have to consider the effects of the vortex part, Eq. (3.114). Basically, this is a Coulomb gas problem in $d = 2$ dimensions (where the electrostatic interaction is a logarithmic variation rather than $1/x$ as it would be in $d = 3$ dimensions).

We first estimate the energy of a single vortex, using directly Eq. (3.79) and noting that for a vortex configuration $|\nabla\theta(\boldsymbol{x})| = 1/\rho$, where ρ is the radial distance from the center of the vortex. This yields, assuming a total area πL^2 encircling the vortex,

$$E_{1\mathrm{vortex}} = \frac{1}{2}J\int \mathrm{d}\boldsymbol{x}[\nabla\theta(\boldsymbol{x})]^2 \approx \pi J\int_a^L \rho\,\mathrm{d}\rho\left(\frac{1}{\rho}\right)^2 = \pi J\ln(L/a). \tag{3.115}$$

Here we have neglected the case energy E_{c}.

Thus if the considered linear dimension $L\to\infty$, the energy of a single vortex would diverge! But in an area L^2 there are $(L/a)^2$ possibilities to put such a vortex, so the entropy is estimated as

$$S_{1\mathrm{vortex}} \approx 2k_B\ln(L/a). \tag{3.116}$$

The free energy excess needed to create an isolated vortex $F_{1\text{vortex}} = E_{1\text{vortex}} - TS_{1\text{vortex}}$ would hence become negative if T exceeds a critical value

$$k_B T_c = \pi J/2. \tag{3.117}$$

Thus the picture of the Kosterlitz–Thouless transition [37] emerges as follows: for $T < T_c$, one has only bound vortex–antivortex pairs, which have a finite excitation energy, depending on the separation ρ between their cores as given by Eq. (3.114)

$$E_{\text{vortexpair}} = 2E_c + 2\pi J \ln(\rho/a). \tag{3.118}$$

At low enough temperatures, only the smallest possible distance $\rho = a$ contributes and then the density of these tightly bound vortex–antivortex pairs is simply given by $n_{\text{vortexpair}} \propto \exp(-2\dot{E}_c/k_B T)$. As the temperature is raised towards T_c, not only the density of vortex pairs increases but also more and more vortex pairs with larger separation ρ appear, until at T_c free vortices (i.e., $\rho \to \infty$) can be generated by statistical fluctuations. In the Coulomb gas interpretation, the Kosterlitz–Thouless transition [37] hence gets the interpretation as a metal–insulator transition (free charges at $T > T_c$ imply a conducting state, while the phase for $T < T_c$ containing only bound dipoles is insulating). As mentioned above, a completely analogous treatment applies to the superfluid–normal-fluid transition in $d = 2$ dimensions as well: instead of Eq. (3.79), one has the Hamiltonian

$$H_{\text{superfluid}} = \frac{1}{2}\rho_s^{\circ}(T) \int \mathrm{d}\boldsymbol{x} |\boldsymbol{v}_s(\boldsymbol{x})|^2, \tag{3.119}$$

where $\rho_s^{\circ}(T)$ is the superfluid density. Using the equivalence that $\boldsymbol{v}_s = \hbar \boldsymbol{v}/m$, we can identify $\hbar^2 \rho_s^{\circ}(T)/m^2$ with J and then Eq. (3.117) gets replaced by

$$k_B T_c^{\text{superfluid}} = \frac{\pi}{2}\hbar^2 \rho_s^{\circ}(T)/m^2. \tag{3.120}$$

Of course, the arguments presented in Eqs. (3.115),(3.116),(3.117),(3.118),(3.119),(3.120) and () are plausibility arguments only, and can estimate the transition temperature only qualitatively but not quantitatively — for a quantitative treatment the statistical mechanics of the full Hamiltonian, Eq. (3.114) must be tackled, which requires renormalization group methods [261,262]. But the final answers for the transition temperature can be cast into a similar form as Eqs. (3.117) and (3.120) — only the ''coupling constants'' (J or $\hbar^2 \rho_s^{\circ}(T)/m^2$, respectively) get ''renormalized''. A spectacular consequence of this modified form of Eq. (3.120) is that the density of the superfluid vanishes discontinuously at T_c in $d = 2$ dimensions (since in the normal fluid we must have $\rho_s^{\circ}(T > T_c) \equiv 0$), and the magnitude of this jump in the superfluid density is universal [244,262].

We now return to the melting of two-dimensional crystals and consider the defects corresponding to the vortices of the plane rotator models: these are dislocations [263]. However, while in the continuum version of the plane rotator model, the basic field $\boldsymbol{v}(\boldsymbol{x}) = \boldsymbol{v}\theta(\boldsymbol{x})$ has a vector character, now the basic displacement field $u_{ij}(\boldsymbol{x})$ is a second rank tensor. So the scalar charges of the vortices get now replaced by a vector, the Burgers vector $\boldsymbol{b}$ characterizing a dislocation. We see this when we write down the relation corresponding to Eq. (3.104);

$$\oint_C \mathrm{d}\boldsymbol{u} = a\boldsymbol{b}(\boldsymbol{x}); \tag{3.121}$$

here we have defined the Burgers vector $\boldsymbol{b}(\boldsymbol{x})$ dimensionless and therefore the lattice spacing a is

written explicitly. Fig. 19b illustrates the discrete version of this construction, Eq. (3.121) on the square lattice. Note that a dislocation can be made by adding (or removing, respectively) extra half-rows of atoms on an otherwise perfect lattice. The Burgers vector itself must then also be a vector of the underlying lattice. Since dislocation pairs (with equal and opposite Burgers vectors) are known to interact logarithmically in two dimensions [263], it is plausible that dislocation unbinding drives the melting transitions of a two-dimensional solid [37].

Now continuum elasticity theory exhibits a second type of topological defects: disclinations [263] (Fig. 19c). The energy cost of a disclination grows much faster with the area of the region taken by the defect than the energy cost of a dislocation. However, these defects then play a basic role for the transition from the hexatic phase to the fully disordered fluid.

The effective Hamiltonian for interacting dislocations in two dimensions can be found analogously to the effective Hamiltonian for the interacting vortices discussed above. One decomposes the matrix of displacement derivatives into a smooth part and a part due to dislocations:

$$\frac{\partial u_j(\boldsymbol{x})}{\partial x_i} = \frac{\partial \theta_j(\boldsymbol{x})}{\partial x_i} + \left.\frac{\partial u_j(\boldsymbol{x})}{\partial x_i}\right|_{\text{sing}}, \tag{3.122}$$

and the analog of Eq. (3.110) becomes

$$\mathscr{H} = \mathscr{H}_0 + \mathscr{H}_{\text{dislocations}}, \tag{3.123}$$

with

$$\frac{\mathscr{H}_{\text{dislocations}}}{k_{\text{B}}T} = -\frac{1}{8\pi}\sum_{\boldsymbol{x}\neq\boldsymbol{x}'}\left\{K_1\boldsymbol{b}(\boldsymbol{x})\cdot b(\boldsymbol{x}')\ln(|\boldsymbol{x}-\boldsymbol{x}'|/a) - K_2\frac{[\boldsymbol{b}(\boldsymbol{x})\cdot(\boldsymbol{x}-\boldsymbol{x}')][\boldsymbol{b}(\boldsymbol{x}')\cdot(\boldsymbol{x}-\boldsymbol{x}')]}{|\boldsymbol{x}-\boldsymbol{x}'|^2}\right\} + \frac{E_c}{k_{\text{B}}T}\sum_{\boldsymbol{x}}|\boldsymbol{b}(\boldsymbol{x})|^2. \tag{3.124}$$

Here the coupling constants K_1 and K_2 are equal in the case of a smooth substrate and are given by

$$K_1 = K_2 = (4a^2/k_{\text{B}}T)\mu(\mu+\lambda)/(2\mu+\lambda), \tag{3.125}$$

the $\{\boldsymbol{b}(\boldsymbol{x})\}$ are dimensionless Burger's vectors of the form

$$\boldsymbol{b}(\boldsymbol{x}) = m(\boldsymbol{x})\boldsymbol{e}_1 + n(\boldsymbol{x})\boldsymbol{e}_2, \tag{3.126}$$

where $m(\boldsymbol{x})$ and $n(\boldsymbol{x})$ are integers, and $\boldsymbol{e}_1, \boldsymbol{e}_2$ are unit vectors spanning the underlying (triangular) lattice. E_{c} is the core energy of the dislocations, and again a renormalization group recursion relation for the "fugacity" $y = \exp(-E_{\text{c}}/k_{\text{B}}T)$ has to be constructed. Although due to the vector character of the Burgers vector (Eq. (3.126)) the Hamiltonian of this "vector Coulomb gas" (Eq. (3.124)) is more complicated than the scalar one, Eq. (3.114), the treatment can be carried over in a very similar manner [39,244]. One finds that the melting transition occurs via unbinding of dislocations, when the dimensionless elastic constants $\bar{\mu} = \mu a^2/k_{\text{B}}T, \bar{\lambda} = \lambda a^2/k_{\text{B}}T$) take a universal ratio [39,244]

$$\lim_{T\to T_{\text{m}}^-}\frac{\bar{\mu}_{\text{R}}(T)\left[\bar{\mu}_{\text{R}}(T)+\bar{\lambda}_{\text{R}}(T)\right]}{2\bar{\mu}_{\text{R}}(T)+\bar{\lambda}_{\text{R}}(T)} = 4\pi. \tag{3.127}$$

Here the index R indicates that the (final) "renormalized" values of the elastic constants μ, λ must be used in the harmonic part $\mathscr{H}_0$ (Eq. (3.123)), which is of the form of Eq. (3.85), which are taken at the

start of the renormalization group recursion. The theory also predicts cusp-like singularities of these renormalized elastic constants just below the melting temperature T_m [244]

$$\bar{\mu}_R(T) = \bar{\mu}_R(T_m)\left[1 + b(T_m - T)^{\bar{\nu}}\right], \quad \bar{\nu} = 0.3696\ldots. \tag{3.128}$$

The same exponent $\bar{\nu}$ also enters the critical behavior of the correlation length $\xi_+(T)$, which describes the average distance between free dislocations for $T > T_m$,

$$\xi_+(T) \propto \exp\left[b/(T - T_m)^{\bar{\nu}}\right], \quad T \to T_m^+. \tag{3.129}$$

At this point we emphasize that the exponent $\bar{\nu}$ in Eqs. (3.127) and (3.128) differs from the analogous result for the plane rotator model, for which $\bar{\nu} = 1/2$ [37]. The correlation length $\xi_+(T)$ has also a direct physical significance since it controls the growth of the pseudo-Bragg-singularities that develop at $\boldsymbol{q} = \boldsymbol{G}$ as $T \to T_m^+$,

$$S(\boldsymbol{q} = \boldsymbol{G}) \propto \xi_+^{2-\eta_G}, \tag{3.129}$$

where $\eta_{\boldsymbol{G}}$ is still given by Eq. (3.90) if one uses the renormalized elastic constants $\bar{\mu}_R(T_m), \bar{\lambda}_R(T_m)$ rather than the corresponding "bare" ones.

Above T_m there occurs still a nontrivial behavior of the orientational correlations. They can be treated by another effective Hamiltonian [39,244] with a nontrivial coupling constant $K_A(T)$,

$$\mathscr{H}_{\text{eff}}\{0\} = \frac{1}{2}K_A(T)\int \mathrm{d}\boldsymbol{x}(\nabla\theta)^2. \tag{3.131}$$

Noting the analogy with Eq. (3.79), we can immediately conclude that in the hexatic phase the orientational correlation $G_6(\boldsymbol{x})$ (Eq. (3.95)) should exhibit a power-law decay, Eq. (3.100), with

$$\eta_6(T) = 18k_BT/(\pi K_A(T)). \tag{3.132}$$

Now one can estimate that $K_A(T) \approx 2E_c a^2$ sufficiently above T_m, while near $T_m K_A(T)$ is divergent, $K_A(T) \propto [\xi_+(T)]^2$ [39,244]. This behavior results because free dislocations screen the interactions between dislocation pairs, and so this interaction gets unscreened as $T \to T_m^+$. On the other hand, at a temperature $T = T_i$, where $\eta_6 = 1/4$, the Kosterlitz–Thouless transition from the hexatic to the isotropic liquid phase occurs. Thus the coupling constant $K_A(T_i)$ exhibits at T_i a universal jump, analogous to the universal jump of the superfluid density at the two-dimensional superfluid to normal fluid transition.

We now discuss the question to what extent this behavior gets modified when the effect of substrate corrugation is taken into account. It is found [39,244] that the behavior of interacting dislocations in the presence of a periodic substrate potential is still described by the vector Coulomb gas Hamiltonian (Eq. (3.36)), but now the logarithmic coupling K_1 and the angular coupling K_2 are no longer equal and

$$K_1^R = \frac{4a^2}{k_BT}\left[\frac{\mu(\mu+\lambda)}{2\mu+\lambda} + \frac{\mu\gamma}{\mu+\gamma}\right], \qquad K_2^R = \frac{4a^2}{k_BT}\left[\frac{\mu(\mu+\lambda)}{2\mu+\lambda} - \frac{\mu\gamma}{\mu+\gamma}\right], \tag{3.133}$$

where the orientational elastic constant γ was specified in Eq. (3.101). It turns out that the difference between K_2^R and K_1^R has a marked influence on the exponent $\bar{\nu}$ controlling the exponential divergence of the correlation length $\xi_+(T)$ in Eq. (3.129) [248,249]: Depending on the ratio $\sigma = K_2^R(T_m^-)/K_1^R(T_m^-)$, $\bar{\nu}$ decreases smoothly from $\bar{\nu} = 2/5$ when $\sigma = 0$ to $\bar{\nu} = 0.3696$ when $\sigma = 1$. The dislocation unbinding

transition always occurs when the renormalized coupling constant $K_1^R = 16\pi$, as previously (Eq. (3.127)).

Although the melting of incommensurate solids into fluids in the presence of the periodic substrate potential hence is not very different from the smooth substrate case, a rather different behavior is found above the melting temperature. We can again use a Hamiltonian as written in Eq. (3.131), but must amend it by the orientational biasing potential $-h\cos(p\theta)$, as we did for the harmonic Hamiltonian described from elasticity theory for the solid phase, Eq. (3.92). Thus

$$\mathscr{H}_{\mathrm{eff}}(\theta) = \int \mathrm{d}\boldsymbol{x}\left\{\frac{1}{2}K_{\mathrm{A}}(T)[\nabla\theta(\boldsymbol{x})]^2 - h\cos[p\theta(\boldsymbol{x})]\right\}. \tag{3.134}$$

For melting of triangular lattices on a hexagonal substrate ($p = 6$), long range orientational order would be present even above T_{m} because of this term. Thus all fluids on such substrates are trivial examples for systems with hexatic order, and therefore the hexatic to liquid transition driven by disclination unbinding will be smeared out, it is a sharp transition for the smooth substrate case only. However, due to the Novaco–McTague effect [40] there are typically two symmetric degenerate orientational minima, a few degrees off perfect alignment. In the equilibrium incommensurate phase, there will be a symmetry breaking with respect to these two minima. This opens the possibility of an Ising-like transition at a temperature above T_{m}, where this symmetry is then restored. But the orientational order parameter $\langle 6^{\sigma i\theta}\rangle$ would still be nonzero even above this transition, however.

For melting of incommensurate triangular lattices on square substrates, an Ising transition is predicted [39,244] above T_{m} even in the absence of any Novaco–McTague effects. The substrate then presents a 12-fold symmetric potential, which acts like an Ising perturbation on $\exp[6i\theta(\boldsymbol{x})]$. Thus there should be an Ising-like transition, above which $|\langle\exp(6\mathrm{i}\theta)\rangle|$ vanishes. In contrast, $|\langle\exp(4\mathrm{i}\theta)\rangle|$ is nonzero for square substrates at all temperatures for square lattice substrates.

Finally we draw attention to the work by Ostlund and Halperin [264] who considered two-dimensional melting on uniaxial substrates.

3.5. Multilayer adsorption, wetting and interfacial phenomena

Since several decades it is known experimentally that adsorption at surfaces is not restricted to the formation of various monolayers, but rather a second layer can condense on the first one, a third on the second, etc., until ultimately thick ''wetting layers'' are formed. In this subsection, we shall discuss these phenomena from a very simplistic point of view, assuming a lattice gas model with a nearest neighbor attractive interaction. Thus, we disregard completely any effects due to a possible misfit between the lattice spacing of the substrate and the interatomic distances preferred by the adsorbate species, and also do not pay any attention to the effect that order–disorder phenomena possibly occurring in the first layer at low coverage could have on the adsorption of further layers at high coverage. Thus, the only transition that still is possible in the first monolayer is a (first order) transition from the lattice gas phase at low coverage to a ''lattice fluid'' phase (which for a square substrate is nothing but the (1×1) structure with some disorder due to residual empty lattice sites) at a coverage closer to the monolayer saturation coverage. Considering the adsorption isotherm, i.e. the coverage expressed as a function of the chemical potential of the adsorbate (cf. Section 2, Eqs. (2.12)–(2.15)), this condensation shows up as a step singularity, and actually the condensation of further layers show up as additional steps. Although this model is extremely crude, the resulting

adsorption isotherms closely resemble corresponding experimental results for multilayer adsorption (see Section 4).

In this subsection we only discuss the lattice gas model with an extremely short range binding potential due to the substrate, assuming that only the first layer adjacent to the wall is affected. In Ising spin representation, the Hamiltonian is

$$\mathscr{H} = -J \underbrace{\sum_{\langle i,j\rangle}}_{\text{interior layers}} S_i S_j - J_s \underbrace{\sum_{\langle i,j\rangle}}_{\text{surface layer}} S_i S_j - H \sum_i S_i - H_1 \underbrace{\sum_i}_{\text{surface layer}} S_i, \quad S_i = \pm 1. \tag{3.135}$$

Here $J > 0$ represents the attractive interaction between two adsorbate atoms which are nearest neighbors on the lattice; if both adsorbate atoms are in the surface layer $n = 1$, we assume in general a different interaction (J_s) to allow for a substrate-mediated force. As is well documented, the ''magnetic field'' H in spin language is related to the bulk chemical potential of the lattice gas, while the effect of the (short range) binding potential to the substrate is contained in H_1, the ''surface field'' acting on spins in layer $n = 1$ (see e.g. [5] or Section 2 of the present article).

The occurrence of multi-layer adsorption can already be deduced from Eq. (3.135) in the framework of the molecular field approximation [43,265]. If $q_{||}$ is the coordination number in the lattice planes parallel to the surfaces, molecular field theory amounts to the following set of coupled equations for the magnetizations $m_n = \langle S_i \rangle_{i \in n}$ of the nth layer:

$$m_n = \tanh\left[\frac{H}{k_B T} + \frac{q_{||} J}{k_B T} m_n + \frac{J}{k_B T}(m_{n-1} + m_{n+1})\right], \quad n \geq 2, \tag{3.136}$$

$$m_1 = \tanh\left(\frac{H}{k_B T} + \frac{H_1}{k_B T} + \frac{q_{||} J_S}{k_B T} m_1 + \frac{J}{k_B T} m_2\right). \tag{3.137}$$

Solving these equations numerically one can show that the sequence of layering transitions ends in critical points $T_c(n)$, with 43 $\lim_{n\to\infty} T_c(n) = T_c$, the bulk critical temperature of the three-dimensional Ising model. However, again the molecular field equation fails qualitatively: actually the layering transitions do not extend all the way up to the critical point, but rather they terminate near the roughening transition temperature T_R [43]. Fig. 20 shows schematically the expected phase diagrams: only if a characteristic temperature of the system, the wetting transition temperature T_W that we shall discuss below, falls underneath the roughening transition temperature T_R, layering transitions can be observed (while the molecular field theory implies $T_R = T_c$ and hence such a restriction does not exist). Asymptotically one expects an approach of $T_c(n)$ to T_R according to a logarithmic law [266]:

$$T_R - T_c(n) \propto (\ln n)^{-2}, \quad n \to \infty. \tag{3.138}$$

We now briefly explain the physics of the interfacial roughening transition, which is a singularity of the interfacial free energy f_{int} (Fig. 17) describing the free energy excess due to an interface between coexisting bulk low density and high density phases of the lattice gas. For $T < T_R$, such an interface (oriented normal to a lattice direction of the simple cubic lattice) is essentially flat, the mean square interfacial width $\langle w^2 \rangle$ is finite, and the long wavelength capillary-wave type excitations (Fig. 16d) do not occur, while they do occur for $T > T_R$, leading to a divergent interfacial width (Eq. (3.63)). Here we shall not go into any mathematical detail of the roughening transition, but rather we direct the reader to suitable reviews [46,71,267]. We only mention that the roughening transition also belongs to the class of Kosterlitz–Thouless [37]-type of phase transitions, which were discussed in the previous section.

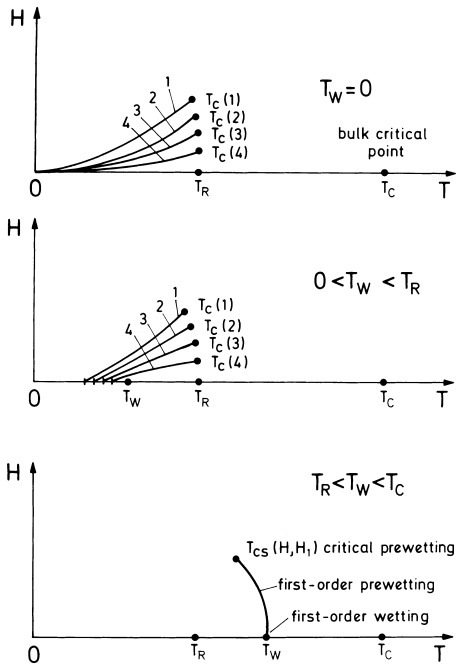

Fig. 20. Schematic phase diagrams of a semi-infinite Ising magnet as a function of bulk field H and temperature T. Three possible "scenarios" are shown (which of them is realized depends on the ratios between the surface and bulk interactions (J_s/J) and on the surface field H_1/J); note that additional scenarios can be thought of and it is not yet clear under which conditions these phase diagrams actually occur. In the language appropriate to adsorption problems, the upper phase diagram refers to a "strong substrate", the surface being wetted by the adsorbate material at all temperatures. The middle and lower phase diagrams correspond to "intermediate substrate systems", where the surface is only wet if T exceeds a certain temperature T_w. If T_w exceeds the roughening temperature T_R, one has just one first-order prewetting line ending in a prewetting critical point $T_{cs}(H, H_1)$ only if $T_w < T_R$ does one have an infinite sequence of first-order layering transitions (labelled by the numbers $n = 1, 2, 3, 4, \ldots$ of the layers in the figure). These layering transitions end in layering critical points $T_c(n)$, with $\lim_{n\to\infty} T_c(n) = T_R$. Note that in the case of $T_w > T_R$ it is also possible that the wetting transition observed when T increases towards T_w at $H = 0$ can also be second order ("critical wetting") rather than first order: then a prewetting transition line does not exist.

Thus one finds the analoguous exponential singularity of the correlation length ξ_{hh} of height–height correlations of the interface (and the step free energy s, cf. Fig. 17)

$$\xi_{hh}(T) \propto s^{-1}(T) \propto \exp\left[\frac{\text{const.}}{(T_R - T)^{1/2}}\right], \quad T \to T_R^- . \tag{3.139}$$

For $T > T_R$ the presence of capillary waves with arbitrary large wave lengths λ implies that $\xi = \infty$, of course (the height–height correlation function exhibits an algebraic rather than an exponential decay).

In order to understand the phase diagrams in Fig. 20 in more detail, we now turn to the wetting transition. Again a full account of wetting phenomena would require an extensive review of its own, and such reviews exist in the literature [45,268,269]; thus we restrict our treatment here to those salient features which are most relevant in the context of the simulations described in Sections 4 and 5. It turns out that wetting phenomena can also be understood in terms of a mean field theory for the Ising model,

but we have to work with a continuum rather than a lattice version. However, this continuum version is readily derived from Eqs. (3.136) and (3.137), replacing differences by differentials [68,270,271]:

$$m_{n\pm1} \approx m_n \pm a\left(\frac{\partial m_n}{\partial n}\right) + \frac{a^2}{2}\left(\frac{\partial^2 m_n}{\partial n^2}\right) \pm \ldots, \tag{3.140}$$

where we again have denoted the lattice spacing by a. It is then convenient to rescale the order parameter m_n in the nth layer by the bulk order parameter m_b in zero external field. We denote this rescaled order parameter $m_n/m_b = \mu(\zeta)$, ζ being the distance $(n-1)a$ from the surface plane rescaled by the correlation length ξ_b in the bulk. Eqs. (3.136) and (3.137) then lead to the following differential equation, when we also expand the tanh to third order [68,270,271]:

$$\frac{1}{2}\frac{\partial^2 \mu}{\partial \zeta} + \mu - \mu^3 + h = 0, \tag{3.141}$$

where h is the rescaled version of the magnetic field H, and a boundary condition [68,270,271]

$$\gamma \left.\frac{\partial \mu}{\partial \zeta}\right|_{\zeta=0} + h + h_1 + g\mu(\zeta = 0) = 0. \tag{3.142}$$

Here $\gamma = \xi_b/\left[a\sqrt{2(q_{||}+2)}\right], h_1$ is the rescaled surface field, $h_1 = H_1(\xi_b/a)^3\left[2(q_{||}+2)\right]^{3/2}/\sqrt{3}$ and the parameter g is related to the ratio J_S/J as $g = 1 + 2\xi_b^2(q_{||}J_S/J - q_{||} - 1)/a^2$. Alternatively, Eqs. (3.141) and (3.142) can be derived from a (rescaled) free energy functional describing a semi-infinite Ising-type system bounded by a surface at $\zeta = 0$ as follows:

$$\frac{F\{\mu(\zeta)\}}{k_B T_c} = \int_0^\infty d\zeta \left\{\frac{1}{2}\left(\frac{\partial \mu}{\partial \zeta}\right)^2 - \mu^2 + \frac{1}{2}\mu^4 - \mu h\right\} - \frac{h_1}{\gamma}\mu_1 - \frac{1}{2}\frac{g}{\gamma}\mu_1^2. \tag{3.143}$$

Here the first term is nothing but a rescaled version of the Ginzburg–Landau free energy functional presented in Eq. (3.41), restricting spatial variations to the direction normal to the substrate surface only, and the last two terms can be viewed as a phenomenological power series expansion of the (bare) surface free energy in terms of the local order parameter $\mu_1 \equiv \mu(\zeta = 0)$ at the substrate surface. Minimizing Eq. (3.143) with respect to $\mu(\zeta)$, Eqs. (3.141) and (3.142) follow as Euler–Lagrange equations of this variational problem.

The solution of Eqs. (3.141) and (3.142) leads to the surface phase diagram shown in Fig. 21. It is seen that the Ising model in mean field approximation leads to either second-order or first-order wetting transitions, depending on the choice of parameters h_1 and g (or H_1 and J_S/J, respectively). Note that in Fig. 21 the bulk field $H = 0$ has been put to zero, so one considers phase coexistence between liquid and gas in the bulk, and then wetting transitions can be observed by variation of the temperature T, the strength of the surface field H_1 or the ratio J_s/J. The phase diagram shown in the lowest part of Fig. 20 refers to one particular choice of H_1 and J_s/J, assuming that one is in a parameter region where then a variation of T yields a first order wetting transition at T_w. If T_w happens to be close enough to the critical temperature T_c in the bulk, then the above continuum theory equations (3.141),(3.142) and (3.143) make sense, and actually (in the framework of mean field theory) the three "control parameters" for the wetting transition (T, H_1 and J_s/J) can be incorporated into two scaled parameters only, namely h_1 and g (Fig. (3.18)).

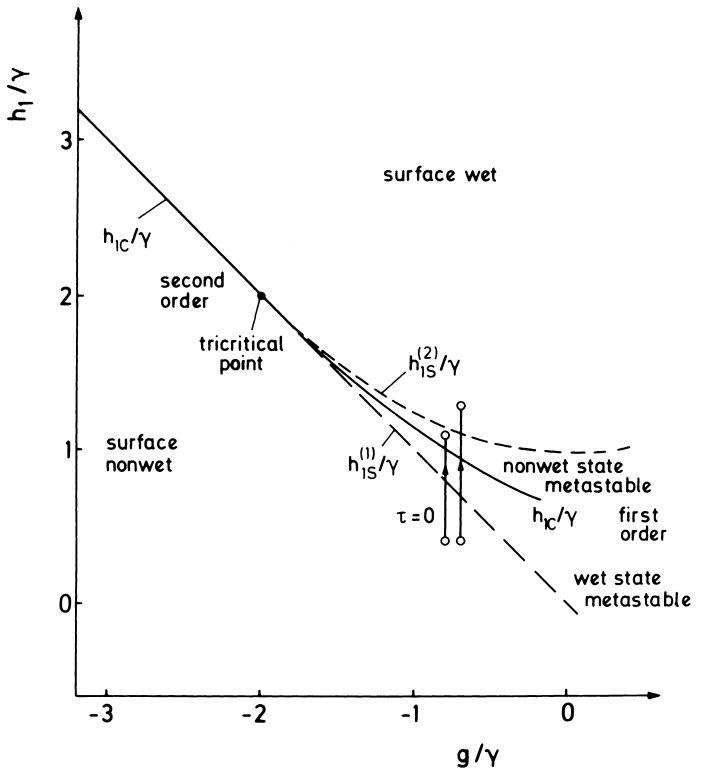

Fig. 21. Surface phase diagram of a nearest neighbor lattice gas model near its bulk critical temperature T_c in the mean field approximation. The coordinate axes are the rescaled surface field h_1/γ (ordinate) and rescaled surface enhancement parameter g/γ (abscissa). Above the full curve the surface is wet, i.e. a fluid film of macroscopic thickness has condensed at the substrate surface for $h = 0$ while in the bulk of the system ($\zeta \to \infty$) one still has the gas phase. Below the full curve the substrate surface is "nonwet" or "partially wet", i.e. a film of finite thickness only has condensed. For $g/\gamma < -2$ the wetting transition occurs along the straight line $h_{1c} = g$ and is second order, while for $g/\gamma > -2$ the wetting transition is first order. Thus, the special case $g_t/\gamma = -2, h_{1t} = -g_t$ is a tricritical wetting transition point. In the regime where the wetting transition is first order, mean field theory predicts metastable wet and nonwet regions limited by the two "surface spinodal" lines $h_{1s}^{(1)}$ and $h_{1s}^{(2)}$, respectively. For further explanation see the main text. From Schmid and Binder [68].

In a real system, of course, the strength of interactions between adsorbates and between adsorbates and the substrate is not a control parameter, but rather is fixed, and so wetting transitions can be observed varying T only. Therefore wetting transitions are difficult to observe in actual experiments, and computer simulations (where H_1 and J_s/J are convenient control parameters, see Section 4) have a definite advantage if one wishes to test the various theoretical concepts.

It is also instructive to consider the "translation" of the phase diagram of the considered lattice gas model in the lower part of Fig. 20 from the intensive variables (T, H) to the variables (T, ρ) where ρ is the density (Fig. 22. Such a choice of variables is very natural for a gas–liquid transition, of course. The basic quantity characterizing a wetting transition then is the surface excess density ρ_s, defined as

$$\rho_s = \int_0^\infty [\rho(z) - \rho(\infty)]\,\mathrm{d}z, \quad \rho(\infty) = \rho_{\mathrm{gas}}^{\mathrm{coex}} \text{ at coexistence.} \tag{3.144}$$

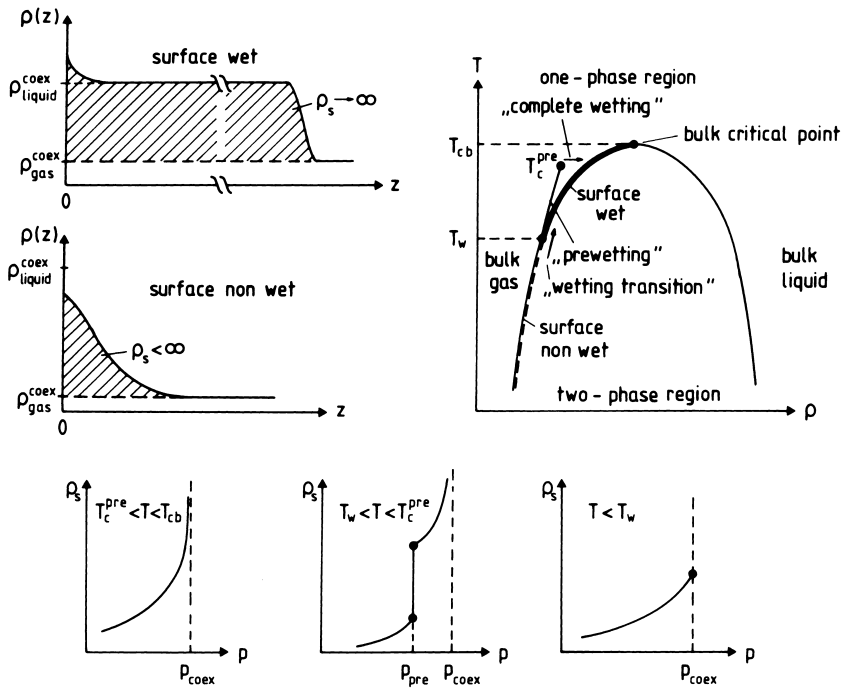

Fig. 22. Phase diagram of a semi-infinite fluid bounded by a wall in the plane of variable temperature T and density ρ. The gas–liquid coexistence curve separates bulk gas (left) from bulk liquid (right) and ends in a bulk critical point (T_{cb}). For $T > T_{cb}$, in the one phase region, no wetting phenomena can occur. The wetting transition (at temperature T_w) is encountered if one moves at gas–liquid coexistence along the gas branch of the coexistence curve. The left upper part of the figure compares schematically the density profiles that one finds then in the wet and nonwet states of the surface, respectively (z is the direction normal to the attractive wall which is located at $z = 0$, the shaded area indicates the definition of the surface excess density ρ_s). In the lower part of the figure, the variation of the surface excess density with gas pressure in the one phase region of the gas is shown, for temperatures exceeding the prewetting critical temperature T_c^{pre} (left part), in between T_w and T_c^{pre} (middle part) and for $T < T_w$ (lower part).

For a nonwet surface, we have ρ_s finite while in the wet case ρ_s is infinite. While for a second-order wetting transition ρ_s shows a critical divergence as $T \to T_w$ from below, ρ_s stays finite in this limit for a first-order wetting transition, and exhibits at T_w then a jump singularity (ρ_s jumps from a finite value to infinity).

In the lower part of Fig. 22, qualitative ''adsorption isotherms'' are shown when one traverses the one-phase region increasing the gas pressure p up to its value at gas–liquid coexistence. While for $T < T_w$, ρ_s then increases up to a finite value at $p = p_{coex}$, for $T > T_w$ one observes again a divergence of ρ_s as $p \to p_{coex}$. This divergence is termed ''complete wetting''. For temperatures in the region $T_w < T < T_c^{pre}$ the adsorption isotherm shows one jump, where the film thickness increases from a small value to a somewhat larger value. This singularity is the prewetting transition. As $T \to T_c^{pre}$, the magnitude of the jump smoothly vanishes (one expects that the phase transition for $T = T_c^{pre}$ falls in the universality class of the two-dimensional Ising model).

Of course, the description of wetting as given in Fig. 21 in terms of thin adsorbed films vs. macroscopically thick films can be easily related to the standard description in terms of the contact angle of droplets [272]. One considers the formation of fluid droplets of spherical cap-like shape sitting

on the wall and thin fluid layers spread out over the whole substrate surface as competing possibilities and asks which case yields the lower free energy. Three interfacial free energies play a role — the gas–liquid interfacial tension $f_{\rm int}$, as well as the surface free energy density $f_{\rm s}^{\ell}$ of the liquid in contact with the wall, and of gas in contact with the wall ($f_{\rm s}^{\rm g}$). The balance of forces on the contactline of a stable (''sessile'') drop at the wall with contact angle θ yields [272]

$$f_{\rm int}\cos\theta = f_{\rm s}^{\rm g} - f_{\rm s}^{\ell}. \tag{3.145}$$

Of course, this equation has a solution only for θ as long as $f_{\rm s}^{\rm gas} < f_{\rm s}^{\ell} + f_{\rm int}$: a surface that satisfies this condition is nonwet. In contrast, if $f_{\rm s}^{\rm gas} > f_{\rm s}^{\ell} + f_{\rm int}$, it is energetically more favorable for the droplet to completely spread out, and form a (thick) film of liquid phase, so there is no longer any direct contact between the gas and the wall because of the intruding liquid layer. As a result, in this wet region of the surface the actual surface energy of the gas is no longer given by the continuation of the branch $f_{\rm s}^{\rm g}$ from the nonwet region, but rather by $f_{\rm s}^{\rm g*} = f_{\rm s}^{\ell} + f_{\rm int}$.

We now consider the description of wetting phenomena in terms of the effective interface Hamiltonian [45,269]. This concept is inspired by the interpretation of a wetting transition as an interface unbinding transition, and the intrinsic profile of the interface is disregarded, only the local distance $\ell(\boldsymbol{\rho})$ of the interface from the wall at lateral distance $\boldsymbol{\rho} = (x, y)$ from the origin is considered (see Fig. 16d). Then the effective Hamiltonian becomes, in the spirit of Eq. (3.58)

$$\mathscr{H}_{\rm eff}^{\rm int}\{\ell(\boldsymbol{\rho})\} = \int {\rm d}\boldsymbol{\rho}\left[\frac{1}{2}f_{\rm int}(\nabla\ell)^2 + \Sigma\{\ell(\boldsymbol{\rho})\}\right], \tag{3.146}$$

where $\Sigma(\ell)$ is the effective interface potential due to the wall. Assuming short range forces and a second order wetting transition, $\Sigma(\ell)$ can be written as

$$\Sigma(\ell) = 2Hm_{\rm b}\ell - A\tau\exp(-\ell/\xi_{\rm b}) + B\exp(-2\ell/\xi_{\rm b}), \tag{3.147}$$

where A, B are positive constants and τ is the normalized distance from the wetting transition (e.g. $\tau = 1 - T/T_{\rm w}$ if one considers the temperature as the control parameter). If one disregards the capillary wave fluctuations described by the $(\nabla\ell)$H2 term in Eq. (3.146) (compare Eqs. (3.58)–(3.63)), the equilibrium average distance ℓ of the interface from the wall is found by minimizing the effective surface free energy density $\Sigma(\ell)$ with respect to ℓ. This yields

$$2Hm_{\rm b}\xi_{\rm b} = 2B\exp(-2\ell/\xi_{\rm b}) - A\tau\exp(-\ell/\xi_{\rm b}). \tag{3.148}$$

Studying the nonwet side of the transition, where $\tau > 0$, we find for $H = 0$ a logarithmic growth of the thickness ℓ of the wetting layer:

$$\ell = -\xi_{\rm b}\ln(A\tau/2B). \tag{3.149}$$

For $\tau < 0$ and $H = 0$ the minimum would occur for $\ell \to \infty$, the interface is not bound to the wall, the wall is ''wet''. Then it is of interest to consider the approach to this wet state of the surface as $H = 0$ (''complete wetting''), which again yields a logarithmic law:

$$\ell = -\xi_{\rm b}\ln H + {\rm const.}, \quad H \to 0. \tag{3.150}$$

This simple treatment can be generalized to long range wall potentials (then the exponentials in Eq. (3.147) have to be replaced by the appropriate power laws [45]), to first order wetting transitions (then $\Sigma(\ell)$ must lead to a minimum at $\ell_{\rm min}^{\rm w} < 0$ for which $\Sigma(\ell_{\rm min}^{\rm w}) = 0$ at $H = 0$ so a jump from $\ell_{\rm min}^{\rm w} < \infty$ to

$\ell \to \infty$ occurs at the transition, etc.). We shall not describe all these extensions here but rather refer the reader to the literature [45,268,269]. We emphasize, however, that for critical wetting with short range forces the simple mean field theory based on Eqs. (3.147) and (3.148) is not expected to be accurate, and capillary wave fluctuations need to be taken into account. However, it is still unclear whether the resulting theory based on a renormalization group treatment of Eq. (3.146) [273,274] can account for the actual behavior of the corresponding more microscopic model, Eq. (3.135) [175,275]. We do not describe the corresponding work, since real systems need to take into account long range forces between the substrate surface and the adsorbate [45,269] and then a mean field theory similar to Eqs. (3.147),(3.148),(3.149) and (3.150) is believed to work better.

As a final point of this subsection we mention that it is also interesting to consider wetting phenomena in semi-infinite two-dimensional lattice gas models bounded by a one-dimensional wall. This problem may be relevant for the adsorption of monolayers on stepped surfaces [276]. The change of the binding potential near the boundary of a terrace may give rise to preferential adsorption along this boundary. In this case, interfacial fluctuations near the wetting transition are far more relevant, cf. Eqs. (3.57),(3.58),(3.59),(3.60),(3.61) and (3.62) and Fig. 16. Using for this problem again the nearest neighbor Ising model, i.e. Eq. (3.135) but in one dimension less, a critical wetting transition can be found exactly [277] at

$$\exp(2J/k_BT)\{\cosh(2J/k_BT) - \cosh(2H_{1c}/k_BT)\} = \sinh(2J/k_BT), \tag{3.151}$$

and in this case Eq. (3.150) is replaced by a power law, $\ell \propto H^{-1/3}$ as $H \to 0$ [278,279].

4. Lattice gas models

Basic information about the lattice gas model description of adsorbed layers has been already presented in Sections 2.2.2 and 3.1. Wide popularity of that approach results from its flexibility and simplicity. By changing the parameters representing various interactions in the system one can determine how they influence the structure and stability of various ordered states (Section 3.1). In general, exact solutions of lattice gas models are seldom available [277,280] and various approximations must be used. Apart from the mean field type theories that can provide only crude and often qualitatively incorrect results [5,46], the transfer matrix method [281–285], the renormalization group method [41,285,286] and the coherent anomaly method introduced by Masuo Suzuki [173,287,288] have been applied to obtain solutions of various lattice gas models. Particularly interesting and abundant results have been obtained with the help of computer simulation methods, however [5,33,127–129,174,289–292].

In this section we concentrate the discussion on those applications of lattice gas models that have been directed towards understanding various adsorption phenomena on square and rectangular lattices.

4.1. Monolayers

The interaction between the particles adsorbed on a lattice can be represented by the potential $u(r)$, where r assumes discrete values:

$$r = \sqrt{k^2a_1^2 + l^2a_2^2}. \tag{4.1}$$

In the above, a_1 and a_2 are the lengths of the unit cell vectors and k and l are integers. In principle, all the properties of such lattice gas systems can be derived from the grand canonical potential, Eq. (2.11). The possible ordered structures that can appear in the system are primarily determined by the lattice symmetry and the properties of the potential $u(r)$. Usually, $u(r)$ is a sum of contributions arising from repulsive and attractive interactions. For example, assuming that $u(r)$ is given by the Lennard-Jones potential, the effect of repulsive forces can be related to the relative size of adatoms, measured by the parameter σ and the size of the surface unit cell, measured by the lattice constants a_1 and a_2. It is convenient to introduce the reduced quantities and express all the distances in units of, say, a_1. Note that in the case of a square lattice, e.g. (100) plane of the f.c.c. crystal, $a_2 = a_1$, while for the (110) plane of the f.c.c. crystal $a_2 = \sqrt{2}a_1$. Also, the energy-like quantities, as well as the temperature, can be expressed in units of ε.

In the ground state $(T = 0)$ the ordered structures can be usually readily determined. Any ordered superstructure, labelled by the lower index m, is characterized by the unit vectors $\boldsymbol{e}_{m,1}$ and $\boldsymbol{e}_{m,2}$ (Fig. 23) such that

$$\boldsymbol{e}_{m,i} = m_{i,1}\boldsymbol{a}_1 + m_{i,2}\boldsymbol{a}_2, \tag{4.2}$$

where $m_{i,1}$ and $m_{i,2}$ are integers. Each ordered state m is characterized by its density ρ_m and the energy $E_m^* = E_m/\varepsilon$ (per lattice site) given by

$$\rho_m = \frac{1}{M}\sum_i n_i, \tag{4.3}$$

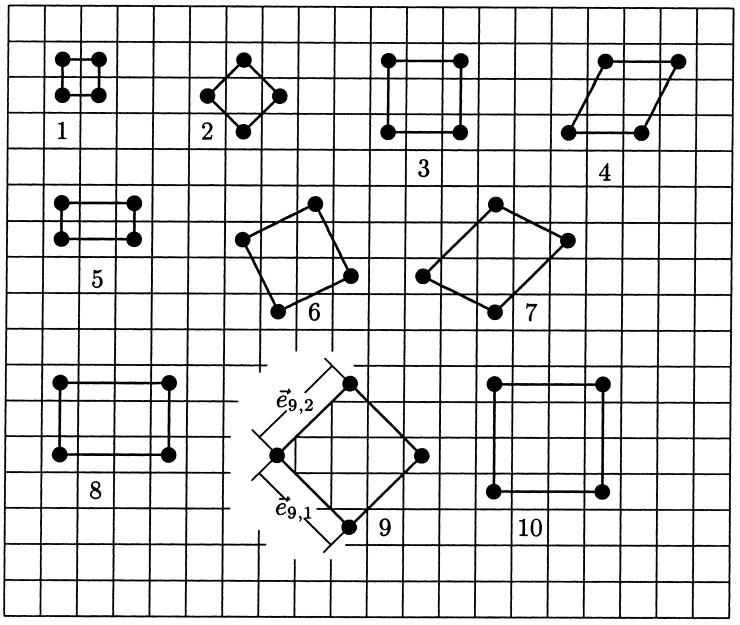

Fig. 23. Examples of different ordered superstructures on a square lattice. The adsorbate layer unit lattice cell vectors are shown for the structure 9.

where M is the total number of lattice sites in the system and

$$E_m^* = \frac{1}{2}\sum_k u^*(r_k)p_j. \tag{4.4}$$

In the last equation the distance r_j is measured from any chosen occupied site to the jth shell of the occupied neighbor sites and p_j is the number of particles in the jth shell of neighboring sites. Thus, the grand canonical potential (per lattice site) of any ordered structure m is equal to

$$g_m^*(\mu^*) = \rho_m E_m^* - \rho_m \mu^*. \tag{4.5}$$

The transition point between two different superstructures m and n occurs at the chemical potential equal to

$$\mu_{\mathrm{tr}}^*(m,n) = \frac{\rho_n E_n^* - \rho_m E_m^*}{\rho_n - \rho_m}. \tag{4.6}$$

In the above, the density of the final state n is assumed to be higher than the density of the initial state m. One also has to take into account the dilute gas phase g, which at the ground state has the density $\rho_g = 0$ and the energy $E_g^* = 0$.

The results of systematic study of the ground state properties of systems characterized by different symmetry of the surface lattice and different size of the adsorbed particles have been presented by Kaburagi [293] and by Borowski et al. [294]. An example of the results obtained for a square lattice is presented in Fig. 24. From the ground state calculations it follows that in the case of a square lattice, the systems with $\sigma^* = \sigma/a \leq 1.0033$ exhibit only two different phases: the dilute gas phase and a simple (1×1) ordered phase of density $\rho = 1$. As soon as σ^* becomes larger than 1.0033 the situation

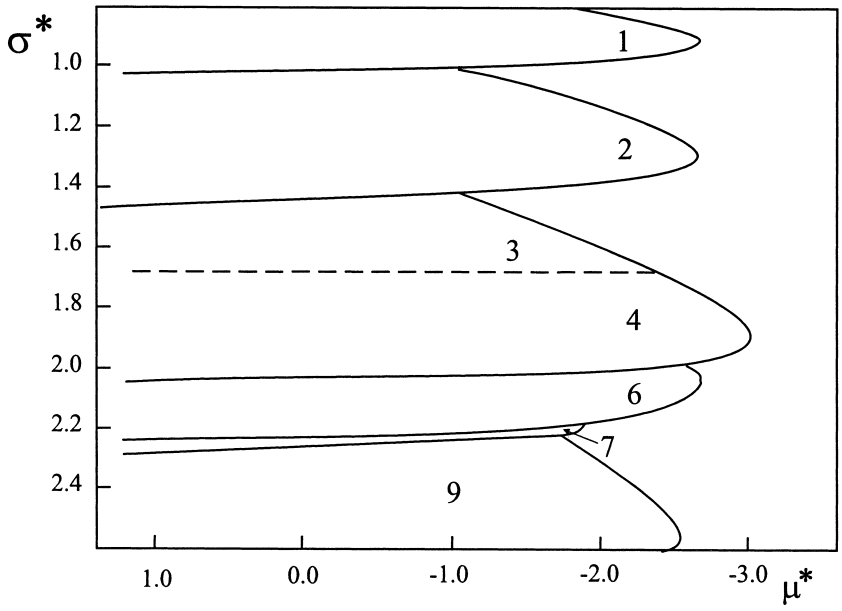

Fig. 24. Ground state phase diagram for the Lennard-Jones lattice gas on a square lattice (from Ref. [294]). The numbers mark the stability regions of different superstructures shown in Fig. 23.

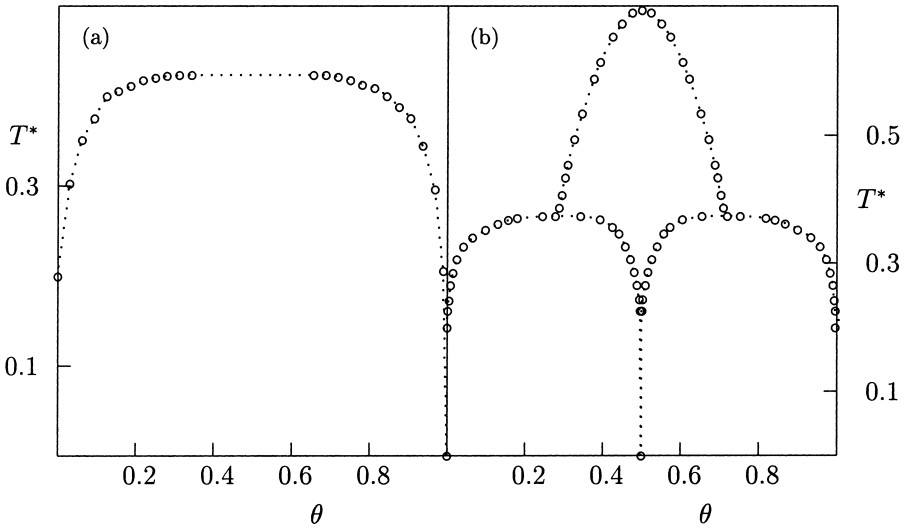

Fig. 25. Examples of phase diagrams for the two-dimensional square lattice gas model for Lennard-Jones particles of $\sigma^* = 1.0$ (a) and 1.02 (b) obtained from Monte Carlo simulation [295].

becomes a little more complex and the system exhibits additional $c(2 \times 2)$ ordered phase of the density $\rho = 0.5$. Due to the symmetry properties of the Hamiltonian, the phase diagram is symmetric around the point $\rho = 0.5$. Examples of phase diagrams corresponding to the above mentioned two regimes and determined by the Monte Carlo simulation are presented in Fig. 25. Note that the phase diagram shown in Fig. 25b is qualitatively the same as the phase diagram for the Ising model with the first nearest neighbor repulsive and the second nearest neighbor attractive interaction (cf. Fig. 10).

The lattice gas model provides a simple explanation for the experimentally observed changes in the critical temperature of adsorbed monolayers resulting from the changes of the dimensional incompatibility between adsorbate and adsorbent (cf. Eq. (2.9)). Note that in the case of a lattice gas model, a simple mean field approximation gives

$$T_c^{MF} = \frac{U_{sum}}{2k}, \tag{4.7}$$

where

$$U_{sum} = -0.5 \sum_j u(r_j) \tag{4.8}$$

and the sum runs over different shells of neighbors. In the particular case of the Lennard-Jones interaction potential, truncated at $2.5\sigma^*$, U_{sum} is given by [296]

$$U_{sum} = -8\varepsilon[C_{12}\sigma^{*12} - C_6\sigma^{*6}], \tag{4.9}$$

where $C_{12} = 1.015997141$ and $C_6 = 1.156625$.

Thus, the critical temperature is proportional to U_{sum}, which varies with σ^*. Of course, the same is true for more rigorous treatments, as is illustrated in Figs. 26a and b. The only available experimental data which clearly demonstrate changes of the two-dimensional critical temperature with dimensional

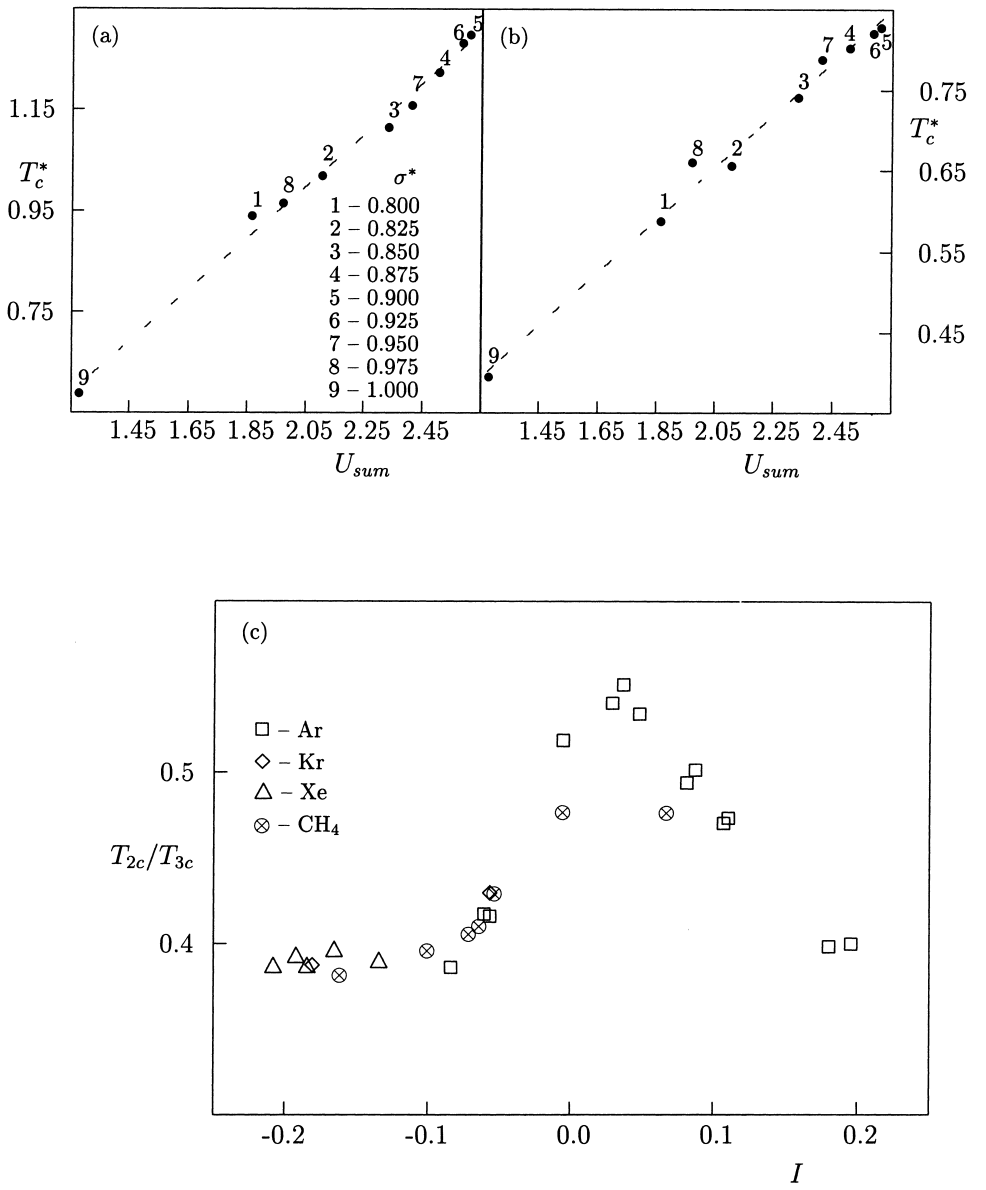

Fig. 26. Two-dimensional critical temperature versus U_{sum} for the Lennard-Jones particles of different diameter, $\sigma^* = \sigma/a$, (shown in the figure) on a square lattice, obtained from mean field approximation (a) and from the coherent anomaly theory (b); (c) shows the ratio of two-dimensional and three-dimensional (bulk) critical temperatures for simple gases adsorbed on lamellar dihalides plotted versus the dimensional incompatibility parameter defined by Eq. (2.9) (from Ref. [296]).

incompatibility correspond to adsorption on a honeycomb lattice of lamellar dihalides surface [138] (cf. Fig. 26c). Nevertheless, the qualitative picture should be the same in the case of adsorption on a square lattice. Of course, the predictions stemming from lattice gas models do not directly apply to adsorption on rather weakly corrugated surfaces of lamellar dihalides and are, at most, only qualitatively correct.

Lattice gas models work much better for strongly adsorbed (chemisorbed) species. Good examples of such a system are the monolayers of atomic hydrogen adsorbed on Pd(100) [16] and on W(100) [297], Cl adsorbed on Ag(100) [129] and O atoms adsorbed on Cu(100) [298]. It is particularly interesting that even very simple lattice models allow to obtain a rather good agreement with experimental data. For instance, hydrogen adsorbed on W(100) orders into $c(2 \times 2)$ phase at low temperatures. The simplest possible model which predicts that form of ordering is the Ising-like model with nearest-neighbor repulsive interactions only. Monte Carlo simulation for such a model [289] led to rather good agreement between the calculated and measured temperature changes of the intensity of a LEED spot for the $c(2 \times 2)$ phase.

A quite similar model was also found suitable to describe the dissociative adsorption of chlorine on the Ag(100) surface. A monolayer film of atomic Cl on Ag(100) was found to form the $c(2 \times 2)$ phase [298,299]. Taylor et al. [129] performed Monte Carlo simulations for a model with infinite nearest-neighbor repulsion on a 72×72 lattice and found a good agreement with experimental data. In particular, the calculated structure factor versus coverage reproduces quite well the measured LEED beam height (see Fig. 27). A rather convincing proof for the adequacy of the Ising model representation for that system is the ''Fisher renormalized'' exponent $\beta/(1-\alpha) \approx 0.12$ evaluated from experimental data and which agrees very well with the exact Ising value of 0.125 (cf. Section 3.2).

A similar system of H atoms adsorbed on Pd(100) surface, which was also found to exhibit the $c(2 \times 2)$ ordered structure, required a much more complicated model, however. LEED diffraction intensities measured as a function of temperature at different surface coverages [16] allowed to determine the phase diagram shown in Fig. 28. One important difference between the phase behavior of H/Pd(100) film with respect to H/W(100) system is a lack of symmetry about $\theta = 0.5$. Therefore, a lattice gas model with pairwise interactions only is evidently too simple to describe the phase diagram for H/Pd(100) system. A Monte Carlo study of Binder and Landau [127] for a model with 1st and 2nd nearest neighbor interactions supplemented by a three-body interaction term (cf. Section 2.2.1) allowed to reproduce well the phase diagram but only at temperatures near the maximum transition temperature (see Fig. 28). It was argued that the widening of the ordered phase regime resulted from the limited resolution of LEED experiments. In Monte Carlo simulation one can mimic this limited resolution by finite system size. Calculations performed for (40×40) lattice demonstrated that in this case the widening of the regime of ordered phase at low temperatures does occur as is demonstrated by Fig. 29. The phase diagram depicted in Fig. 29 was obtained for a simple model with the repulsive (attractive) first (second) nearest neighbor interaction and neglected three-body term and hence exhibits full symmetry with respect to the point $\theta = 0.5$ (cf. also Fig. 25). In general, addition of three-body interactions destroys the invariance of the Hamiltonian with respect to the particle–vacancy exchange (cf. Section 2.2.1).

Although the formation of the $c(2 \times 2)$ ordered phase is quite common in atomic monolayers on metals [299], there are also numerous examples of systems known which show other ordered phases. For example, atomic oxygen adsorbed on Rh(100) was found to form the $p(2 \times 2)$ structure of density 0.25 [111], which then undergoes a transition to a denser $c(2 \times 2)$ structure. The same behavior was found for O/Pd(100) [112] and Se/Ni(100) [130]. The phase diagram for the last system was evaluated by reflection high-energy electron diffraction (RHEED) [130] and was also studied by Monte Carlo simulation [130,300]. Analysis of experimental data, model calculations and symmetry arguments led to the conclusion that the Se/Ni(100) phase diagram is topologically equivalent to the Ashkin–Teller model [301]. In this model, each lattice site is characterized by two Ising spins, s_i and t_i, and the

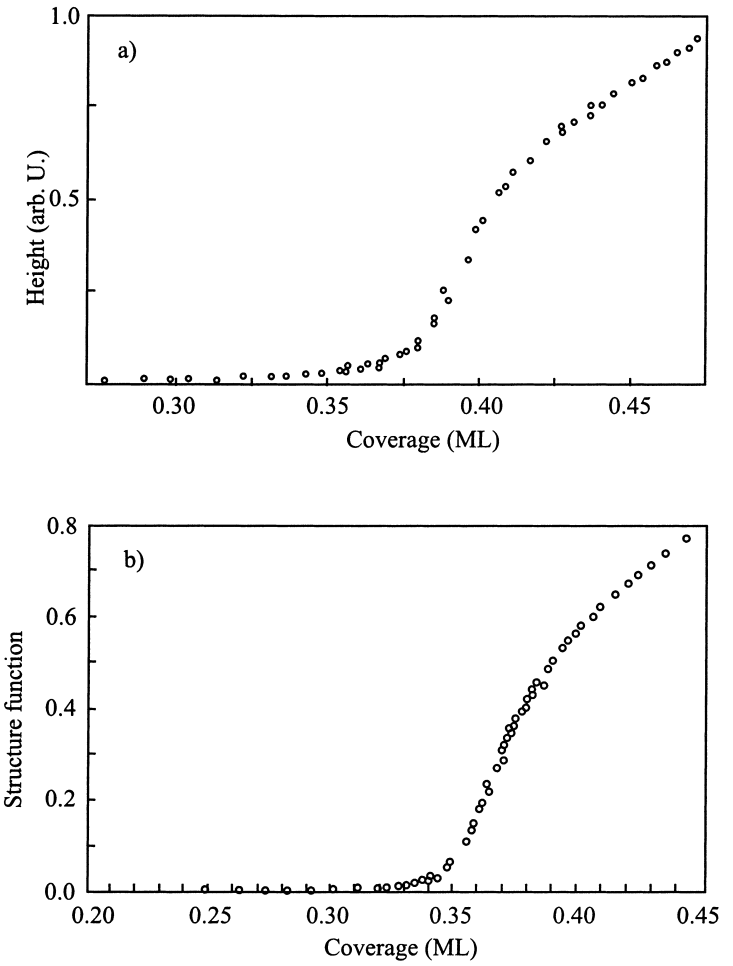

Fig. 27. Coverage dependence of the $(1/2, 1/2)$ LEED beam height at 300 K for the atomic Cl adsorbed on Ag(100) surface (a) and the structure factor obtained from Monte Carlo simulation on the 72×72 lattice (b). (Adapted from Ref. [129].)

Hamiltonian reads:

$$\mathscr{H} = -J \sum_{\langle i,j \rangle} (s_i s_j + t_i t_j) - \Lambda \sum_{\langle i,j \rangle} s_i t_i s_j t_j. \tag{4.10}$$

Critical properties of that model are believed to be non-universal and dependent on the ratio Λ/J. A Monte Carlo study was performed [130] for a simple lattice gas model with interactions up to fourth nearest neighbors which yields the phase diagram belonging to the universality class of the Ashkin–Teller model. This was obtained using the Hamiltonian given by Eq. (2.11) with $u(r_{1\mathrm{nn}}) = \infty$, $u(r_{2\mathrm{nn}}) = 1176\,\mathrm{K}$, $u(r_{3\mathrm{nn}}) = 0$ and $u(r_{3\mathrm{nn}} = 0.1u(r_{2\mathrm{nn}})$. Fig. 30 shows that the experimental Se/Ni(100) phase diagram and the phase diagram obtained for the above lattice gas (Ashkin–Teller-like) model are quite similar, indeed.

The structures $\mathrm{c}(2 \times 2)$ and $\mathrm{p}(2 \times 2)$ observed in the adsorption systems mentioned above are degenerate as the adsorbed species can occupy one of two or four sublattices, respectively. Thus,

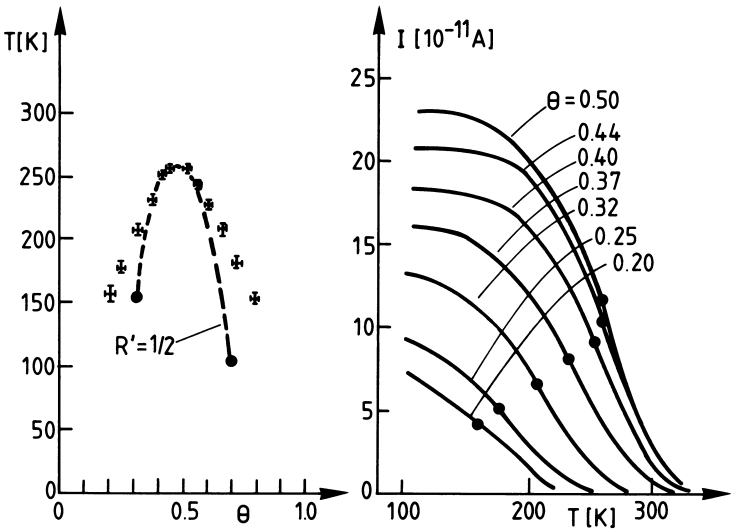

Fig. 28. (a) (left) Experimental phase diagram for H/Pd(100) — crosses, which denote the points $T_{1/2}$ where LEED intensities have dropped to one-half of their low-temperature values [16]. Dashed line is a theoretical phase diagram [127]. (b) (right) LEED intensities plotted versus temperature at various coverages (shown in the figure) (adapted from Ref. [16]).

domains of, say $c(2 \times 2)$ phase on different sublattices may appear and give rise to the formation of a network of light and heavy walls (cf. Fig. 31). It was argued by Baraldi et al. [109] that the transition between the $c(2 \times 2)$ and the denser (1×1) structures in O/Rh(100) film is governed by the formation of heavy wall-like defects. The presence of the domain-wall structure for the $p(2 \times 2)$ phase was clearly seen at the configurations obtained by Monte Carlo method by Bartelt et al. [300].

Such degenerate structures may in certain circumstances exhibit commensurate–incommensurate transitions. This transition has been found for the models with anisotropic interactions, such as the ANNNI model [33,170] (see Section 3.4) and the lattice gas model of Lennard-Jones particles on a rectangular lattice [292]. In the latter case anisotropy of interactions in x and y directions follows naturally from the differences in the distances between neighboring particles located along those two axes. Lennard-Jones particles on model rectangular lattices with the ratio of lattice constants $g = |a_2|/|a_1| = 1.1$ and 1.2 and for particles characterized by different size $\sigma^* = \sigma/a_1$ were studied by mean field theory and Monte Carlo simulation method by Patrykiejew et al. [292]. For sufficiently small σ^* the only stable ordered structure is a simple (1×1) phase independent of the magnitude of the ratio g and such systems correspond to the ordinary Ising ferromagnet. The increase of σ^* introduces a larger difference between the interaction energies in x and y directions which induces the formation of other ordered states of lower density such as the (2×1) and $c(2 \times 2)$ structures. In particular, one may obtain the situation where the nearest neighbor interaction along one, say the x, axis becomes repulsive while the interaction along the other (y) axis is still attractive.

From the ground state calculations it follows that the stability regions of (2×1) and $c(2 \times 2)$ structures are determined by the difference in their energies (per site)

$$\Delta u = u_{(2\times1)} - u_{c(2\times2)}. \tag{4.11}$$

For example in the Lennard-Jones particles adsorbed on a lattice with $g = 1.1$ it was found [292] that the system with $\sigma^* = 1.02$ should order into a simple (1×1) phase, the system with $\sigma^* = 1.03$ into the

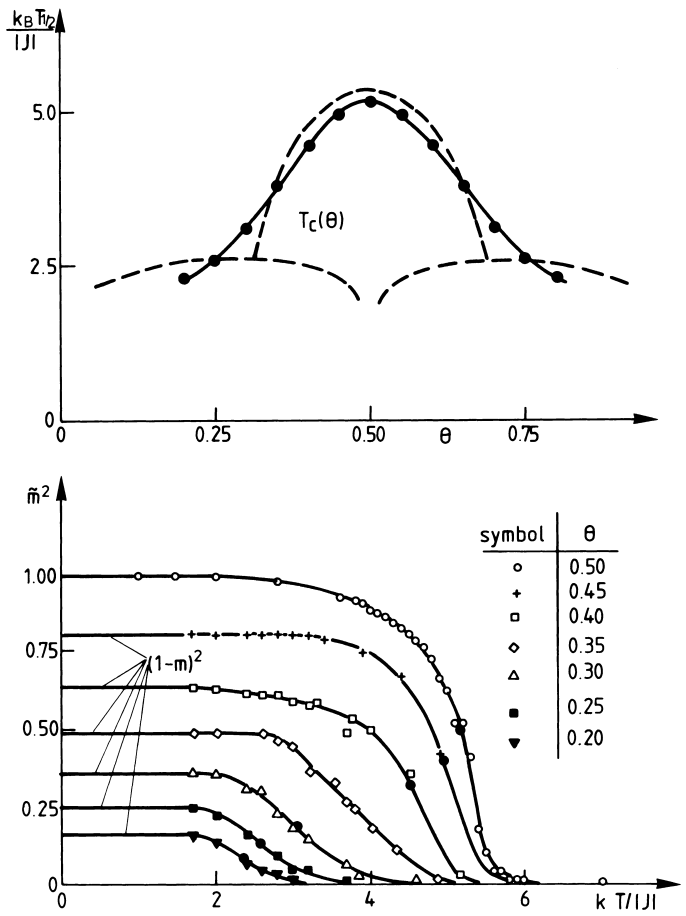

Fig. 29. (a) (top) Phase diagram for a simple lattice gas model with the first nearest neighbor repulsive and the second nearest neighbor attractive interactions $(R = u(r_{nnn})/u(r_{nn}) = -1)$ derived from the points at which the squared order parameter for the c(2×2) phase (shown in part (b) (bottom)) drops to 50% of its low temperature value (dots and full line) in comparison with the correct phase diagram (broken curves). (From Ref. [127].)

(2×1) structure while the system with a slightly larger value $\sigma^* = 1.05$ should already form the c(2×2) phase. Monte Carlo simulations confirmed that prediction very well. Fig. 32 shows snap-shots of configurations for the systems with $\sigma^* = 1.03$ and 1.05 which clearly demonstrate the formation of (2×1) and c(2×2) structures. One should note, however, that in the system with $\sigma^* = 1.05$ small domains of (2×1) structure are also present. Despite the apparent difference in the structure of the ordered phases, the phase diagrams for those two systems are very similar and in both cases look like that shown in Fig. 33. Also the critical point occurs at practically the same temperature of $T^* = kT/\epsilon \approx 0.235$.[1] Finite size scaling analysis of Monte Carlo data showed that both systems belong to the universality class of the two-dimensional Ising model (see Section 3.2).

[1] The total energy of attractive adsorbate–adsorbate interaction (per particle) is in both cases very similar and equal to about -1.39 (for $\sigma^* = 1.03$) and -1.32 (for $\sigma^* = 1.05$).

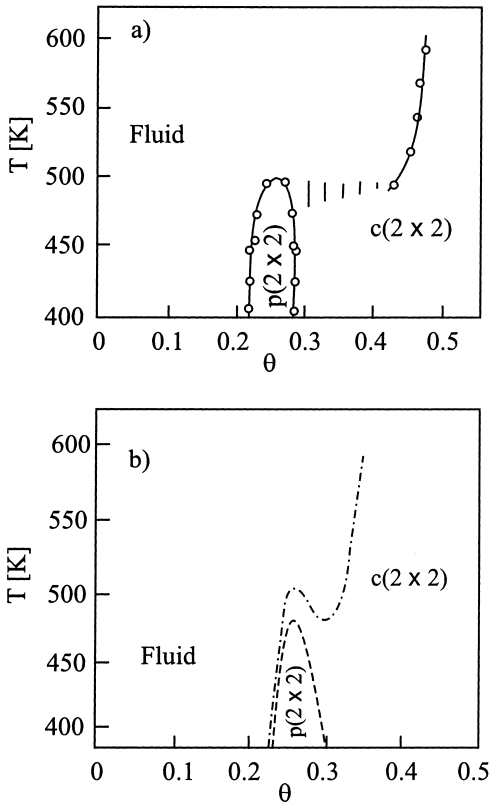

Fig. 30. A comparison of experimental phase diagram for selenium on Ni(100) surface (a) and the theoretical phase diagram for the Ashkin–Teller-like model (b) (adapted from Ref. [130]).

As it was already mentioned (Section 3.3), the appearance of $(p \times 1)$ order with $p \geq 3$ often induces the commensurate–incommensurate phase transition, which was particularly well demonstrated in numerous Monte Carlo studies of ANNNI model [170] (cf. Section 3.3), and was also observed in the lattice gas model of Lennard-Jones particles [292].

A lattice gas version of the ANNNI model with $J_2/J_1 = 0.3$ and $J_0/J_1 = -1.0$ was applied to evaluate the phase diagram for the O/Pd(110) adsorption system [302,303]. This system exhibits two different commensurate phases; (3×1) at the coverage around $1/3$ and (2×1) at higher coverages around $1/2$, with an intervening incommensurate structure between those two ordered states. The symmetry properties of the Hamiltonian for the lattice gas model with only pair interactions, which is invariant under the transformation $s_i \rightarrow -s_i$, give rise to the formation of another commensurate phase at the coverage around $2/3$, which is the same as the (3×1) phase but with inverted vacancy–particle occupations.

It has been already shown that the frequently observed asymmetry of phase diagrams for experimental systems can be taken into account by adding three-body interactions to the lattice gas models. Another possibility to explain this asymmetry is to go beyond the lattice gas model and allow the adsorbed particles to displace from lattice sites [116]. Such off-lattice models will be a subject of Section 5.

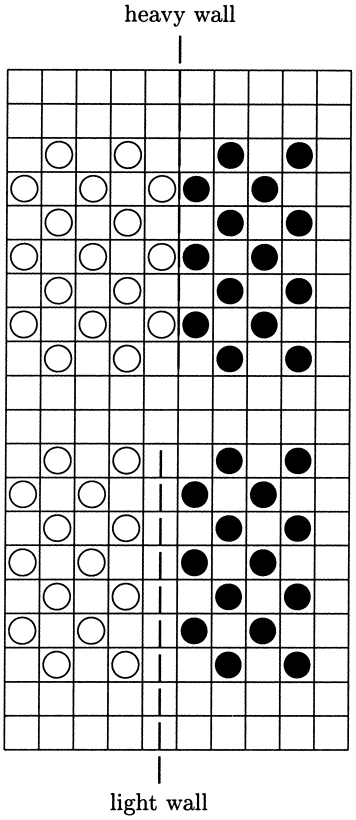

Fig. 31. Schematic representation of the formation of light and heavy walls between the domains of the c(2 × 2) phase formed on different sublattices.

4.2. Multilayer adsorption

Extension of the lattice gas formalism from two-to three-dimensional adsorption systems is straightforward [43,174]. Assuming that the adsorbate–substrate interaction is represented by the potential $v(z)$, where z is the distance from the surface, the Hamiltonian for such a model is obtained by replacing the constant term V_0 in Eq. (2.10) by $v(z)$, which gives

$$\mathscr{H} = \sum_i v(z_i)n_i + \frac{1}{2}\sum_{i\neq j} u(r_{ij})n_i n_j. \tag{4.12}$$

Note that in the lattice gas language, z_i can take up only discrete values determined by the distance of the ith site from the surface, given by the number of layers l. Depending on the properties of the potentials $v(z)$ and $u(r)$ the system shows different behavior [43,175,176,178,304–307].

Systematic analysis of the lattice gas model representation of multilayer adsorption was done by Pandit et al. [43] for the potential $v(z)$ given by

$$v(l) = V_0\delta_{l1} + Bl^{-3}, \tag{4.13}$$

where V_0 is the energy of adsorption for the first adsorbed layer.

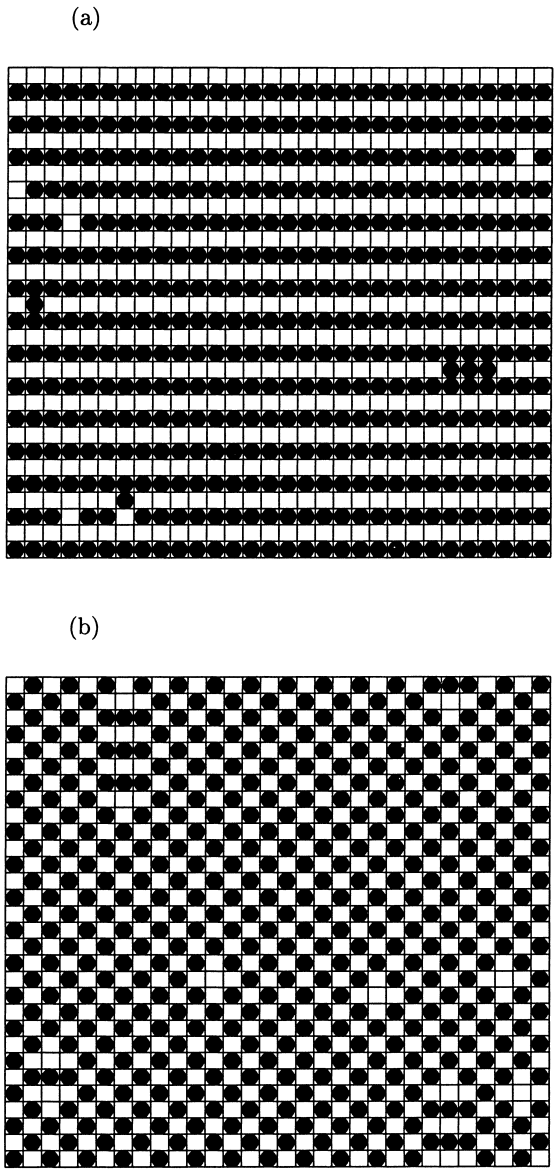

Fig. 32. Snap-shots of configurations for the system with $g = 1.1$ and $\sigma^* = 1.03$ at $T^* = 0.20$ and the chemical potential $\mu^* = \mu/\varepsilon = -1.0(\theta = 0.5001)$ (a) and $\sigma^* = 1.05$ at $T^* = 0.20$ and $\mu^* = -0.80(\theta = 0.492)$ (b). (From Ref. [292].)

Note that the above form of the adsorbate–substrate potential follows naturally from the assumption that the interaction between an adsorbate atom and a single atom of the substrate is represented by the (12,6) Lennard-Jones potential. In the case of a continuous space model, the interaction of an adsorbate atom with the entire substrate of uniform density gives [21] the potential in the form

$$v(z) = C_r z^{-9} - C_a z^{-3}, \tag{4.14}$$

where C_r and C_a (both being positive constants) determine the strength of repulsive and attractive

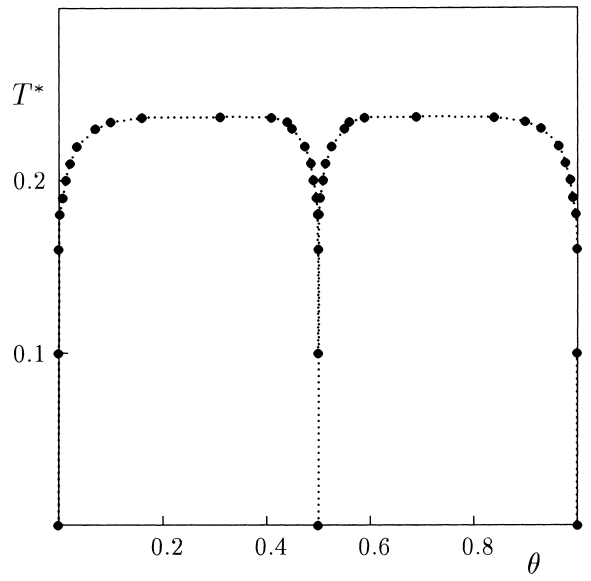

Fig. 33. Phase diagram for the Lennard-Jones lattice system for $g = 1.1$ and $\sigma^* = 1.03$ (from Ref. [292]).

interactions, respectively. In the lattice gas model language, one can drop the first (repulsive) term assuming that it is already taken into account by the assumption that the adsorbate particles occupy only the lattice sites above the surface.

A very elegant and detailed discussion of possible scenarios for the film growth was given by Pandit et al. [43], on the basis of a mean field theory for the lattice gas model, and more recently this problem was also considered by Prasad and Weichman [308], who used both the mean field theory and the renormalization group arguments.

Here we briefly discuss the main predictions stemming from the lattice gas model assuming that $B = V_0$ in Eq. (4.13) and neglecting all but the first nearest neighbor interactions between adsorbate atoms.

When the ratio V_0/u is sufficiently high, i.e., when the surface is highly attractive towards the adsorbate, the film grows in a layer-by-layer mode (see Fig. 34) which was observed in many real adsorption systems [3,51,108,138]. At low temperatures it corresponds to the presence of a series of layering transitions which terminate at the corresponding critical points $T_c(l)$ Section 3.5.

As the adsorbate–substrate interaction becomes weaker and the following condition is met

$$\frac{V_0}{u} < \left[\sum_{l=1}^{\infty} l^{-3}\right]^{-1} \tag{4.15}$$

the adsorbate does not wet the surface at $T = 0$, but may still exhibit complete wetting at the temperatures which exceed the wetting temperature T_w. Thus, below T_w the film thickness remains finite up to the bulk condensation point, while for $T > T_w$ we observe again the formation of macroscopically thick adsorbed film as the chemical potential approaches its bulk coexistence value. That change of the film behavior at T_w marks the so-called wetting transition which can be either the first-order or the continuous transition (critical wetting) depending on the value of V_0/u and on the

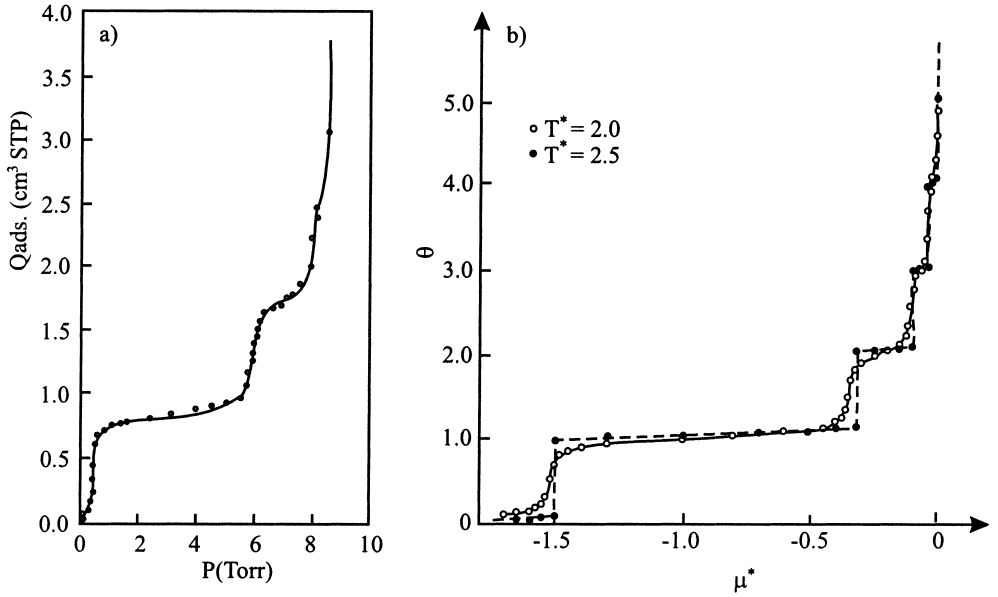

Fig. 34. An example of experimental adsorption isotherm for Ar on MgO at $T = 60.8$ K (adapted from Ref. [108]) (a) and isotherms obtained from Monte Carlo study (b) for a cubic lattice gas model (from Ref. [176]).

range of molecular interactions in the system [309]. When the wetting transition is first-order it is often preceded by the prewetting transition between the thin and thick films. The prewetting transition occurs at the chemical potential below the bulk coexistence value. As the temperature increases the prewetting transition terminates at the corresponding critical point. Due to the finite extent of thin and thick films, on both sides of the prewetting transition, it belongs to the universality class of the two-dimensional Ising model. This situation corresponds to the so-called intermediate substrate regime.

A tutorial discussion of the theoretical aspects of wetting phenomena was already given in Section 3.5, where it was also pointed out that all these phenomena can be modeled on a qualitative level by the Ising (lattice gas) model with nearest neighbor exchange $J > 0$ (i.e., attractive interaction in the lattice gas), if we add at the substrate surface a surface field H_1 (which models a short range attractive surface potential) that competes with the bulk field H (which is related to the gas pressure in the system: $H = 0$ means that one has gas–liquid coexistence in the bulk, see Section 3.5).

In Fig. 35a we present the section of the phase diagram for this model in the $H = 0$ plane, choosing the normalized inverse temperature J/kT_c as abscissa and the normalized enhancement of interaction J_s/J as ordinate variable, delimiting the regimes where different type of phase transitions at the substrate surface occur: to the right of the dashed vertical line (i.e., for temperatures $T < T_R$, the roughening transition temperature) layering transitions occur. The full curve is a projection of the line of tricritical wetting transitions into the shown plane: above this line the wetting transition (where one crosses a critical line $H_1 = H_{1c}(T)$ either by varying H_1 or by varying T at $H = 0$) is of first order, below the line the wetting transition is of second order. This tricritical line ends at the bulk critical temperature of the lattice gas in the so-called "special transition" point [175,275].

In the regime where first-order wetting occurs for $H = 0$, one expects to see prewetting phenomena for $H \neq 0$, and evidence for this prewetting transition is shown in Fig. 35b. Fig. 36a shows that the

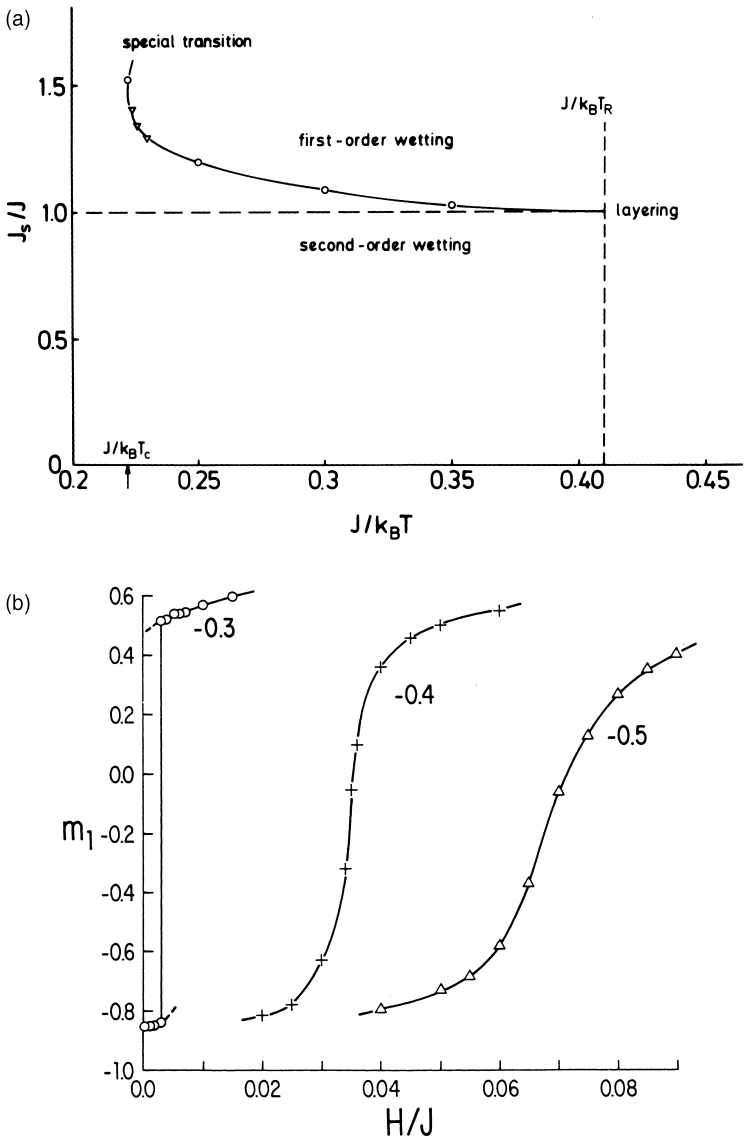

Fig. 35. (a) Phase diagram of the semi-infinite nearest-neighbor Ising model with exchange interaction J_s in the surface plane different from the bulk (J), showing different regimes of surface phase transitions as function of J_s/J and inverse temperature J/kT. The full curve is obtained from Monte Carlo simulations (from Ref. [275]). (b) Plot of the order parameter m_1 (layer magnetization of the first layer adjacent to the substrate, where the field H_1 acts) versus bulk field H, for the model of (a), and the choice of parameters $J_s/J = 1.3, J/kT = 0.25$ and three choices of H_1/J as indicated in the plot. The jump in the curve m_1 vs. H, for $H_1/J = -0.3$ is a first-order prewetting transition (from Ref. [175]).

model yields evidence predicted for the logarithmic growth of the thickness of the adsorbed layer (measured through the surface excess order parameter $m_s = \sum_n (m_n - m_b), m_n$ being the local order parameter in the nth layer away from the surface, m_b is the bulk order parameter). Both when one

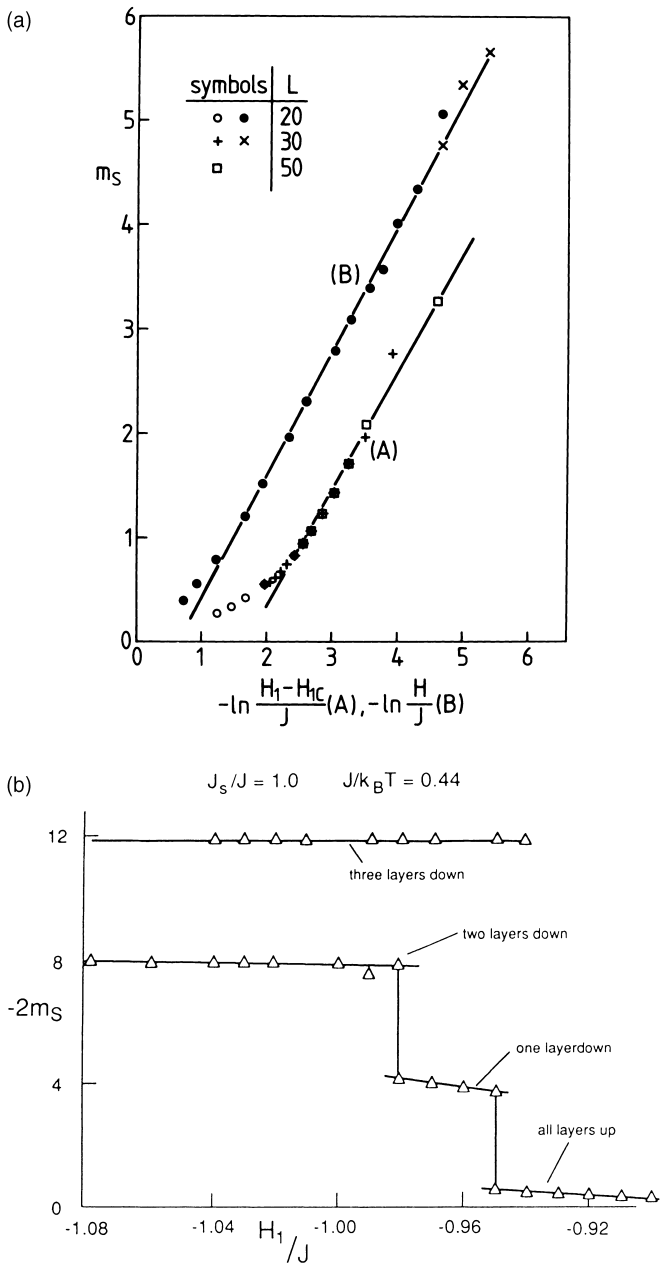

Fig. 36. (a) Semilog plot of the surface excess order parameter m_s vs. $(H_1 - H_{1c})/J$ (A) at $H = 0$, for the model of Fig. 35(a) and the choice of parameters $J_s/J = 1, J/kT = 0.3$ using $H_{1c}/J = 0.89$. Case (B) shows m_s plotted vs. H/J at $H_1 = H_{1c}$ for the same choice of parameters. Several choices of L (system geometry $L \times L \times D$ with $D = 40$) are shown (from Ref. [175]). (b) Surface excess order parameter m_s plotted vs. surface field H_1/J for $J_s/J = 1.0, J/kT = 0.44$ and $H = 0$, for a system with $L = 128, D = 40$. The state with all layers up (i.e., m_n near $m_n = +1$ for all layer numbers n) is that lattice gas phase where no condensation of any layer has as yet taken place, the state where m_1 is near $m_1 = -1$ (and hence $2m_s \approx -4$) means that the first layer has condensed at the substrate, etc. Note the strong hysteresis between the states where two or three layers have condensed (from Ref. [275]).

approaches the wetting transition for $H = 0$ varying H_1 and when one varies H for $H_1 = H_{1c}(T)$, a logarithmic variation is seen as predicted (Section 3.5).

We emphasize that these smooth logarithmic variations occur for $T > T_R$ only, while for $T < T_R$ the curve m_s vs. H shows an infinite sequence of steps as $H \to 0$ (multilayer adsorption), and also varying H_1 at $H = 0$ a number of steps in the curve m_s vs. H_1 is encountered Fig. 36b. The latter behavior is not theoretically well understood yet.

The wetting transition temperature grows as the ratio V_0/u becomes lower. When it reaches a certain limiting value, the wetting temperature reaches the bulk critical point of the adsorbate, and for still lower V_0/u one enters the so-called weak substrate regime. In this case the adsorbate does not wet the substrate under any conditions and adsorption is always finite.

Here we concentrate the discussion on a specific problem of layering transitions studied in the framework of lattice gas models of adsorption on a square lattice. More general discussion of multilayer adsorption and wetting phenomena can be found in specialized review articles [45,268,310].

Within the strong substrate regime the properties of adsorption systems appear to be very sensitive to even small changes in the relative strength of adsorbate–adsorbate and adsorbate–substrate interactions. Figs. 37 and 38 show examples of phase diagrams resulting from Monte Carlo study of a lattice gas model with nearest neighbor adsorbate–adsorbate interaction but long range surface potential (given by Eq. (4.13)) with $B = V_0$) [176]. In the case of strong substrate potential the film grows via a series of simple layering transitions involving condensation in one layer each. For a weaker surface potential one finds, however, a different sequence of layering transitions in which the first three layers condense together at low temperatures. This system shows also an example of a surface triple point at which the layering transitions of layers 1+2 and layer 3 coexist. Note that the critical point of the layering transition for layers 1+2 is considerably higher than the corresponding critical points for higher layers. This results from the enhanced effects of adsorbate–adsorbate interaction in the condensed two surface layers as compared with a single layer. Of course, even for a transition involving simultaneous condensation in several, but finite, number of layers the critical behavior corresponds to the universality class of a two-dimensional model, as the correlation length in the direction perpendicular to the surface stays finite.

A sufficient decrease of substrate potential finally leads to the crossover from the strong to the intermediate substrate regime. This crossover may be also induced by adding further neighbor (attractive) interactions between adsorbate particles [178]. Fig. 39 shows a comparison of the phase diagram obtained for a simple model with the first nearest neighbor interaction with the phase diagrams corresponding to the model with added interaction between the third nearest neighbors.

It is also of interest to consider the situation where the formation of a multilayer film is accompanied by the order–disorder transition in the adsorbed layer [306,311–314]. Ebner et al. [311] discussed a simple model with the first (second) nearest neighbor repulsive (attractive) interaction between the adsorbate particles and with the surface potential of the form (4.13). Although such a model is a little unrealistic with respect to the bulk fluid it shows many interesting surface properties which allow to explain some experimental data for adsorption of simple gases on graphite [315]. In particular, the assumption of repulsive first nearest neighbor interaction was found to inhibit wetting for a sufficiently strong substrate potential. Note that in such a model the completely filled first layer can exist only when the surface field is strong enough to overcome the effect of repulsive nearest neighbor interaction between the adsorbed particles. Whenever this happens all the sites in the second layer are subject to

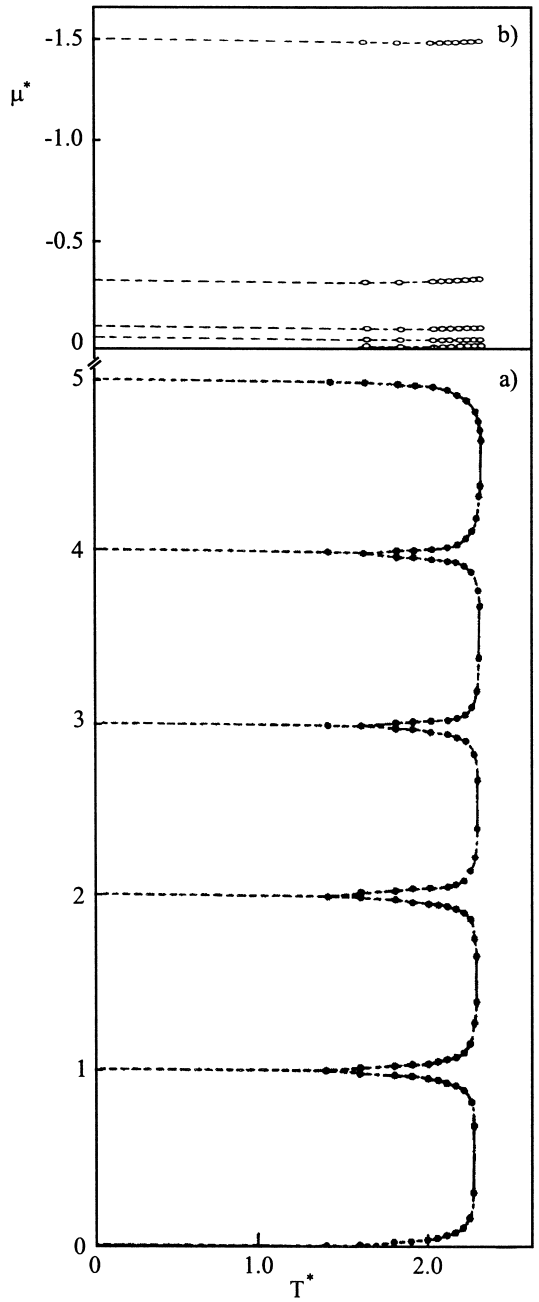

Fig. 37. (a) Phase diagram in the coverage (θ)–temperature ($T^* = kT/J$ where J is the exchange constant between nearest neighbors) plane of a nearest neighbor lattice gas model on a simple cubic lattice with a free surface, and a potential (4.13) with $B = V_0 = 2.5J$. (b) The corresponding phase diagram in the grand-canonical ensemble ($\mu' = (\mu - \mu_0)/J$, where μ_0 is the chemical potential at the bulk gas–liquid coexistence). Note that the adsorbate–substrate potential was cut off above the fourth layer, so that the curve for the layering transitions in the fifth and higher layers merge at the bulk coexistence curve (from Ref. [176]).

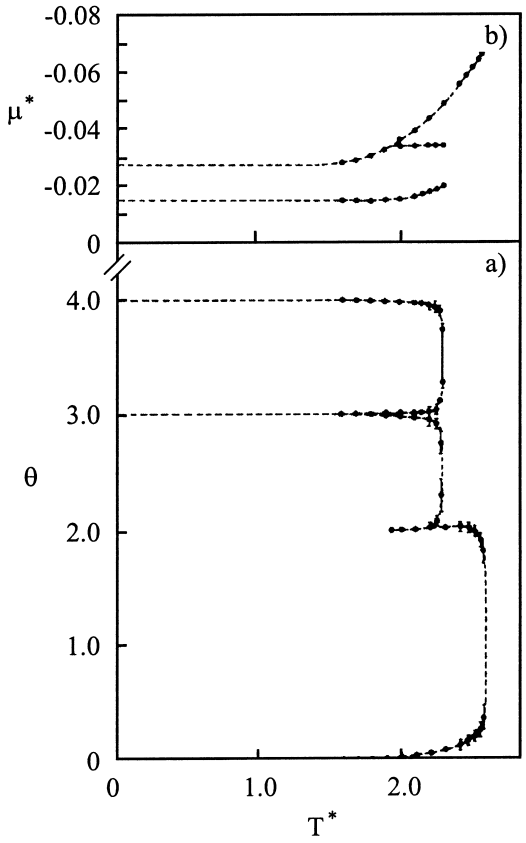

Fig. 38. The same as in Fig. 37 but for a weaker substrate potential with $V_0 = 0.93J$ (from Ref. [176]).

repulsive interaction and hence depopulate the second layer. This mechanism spreads to further layers as well and may prevent the system from complete wetting.

The supression of multilayer film formation due to ordering in the first adsorbed layer was also observed in a simple lattice model considered by Wagner and Binder [314]. Unlike in the above discussed situation the interaction between particles in the bulk were assumed to be attractive and the surface potential restricted to act only on the particles adsorbed on sites in the first layer and given by

$$v_i = w_0 + \tfrac{1}{2} w_1 [\cos(\pi x) + \cos(\pi y)] + w_2 \cos(\pi x) \cos(\pi y). \tag{4.16}$$

In the case of a square lattice with only one wavelength, twice the lattice spacing, x and y are integers and the surface lattice can be considered as composed of four sublattices with v_i^v acting on sites belonging to each sublattice v equal to:

$$v_i^1 = w_0 + w_1 + w_2, \quad v_i^2 = w_0 - w_2, \quad v_i^3 = w_0 - w_1 + w_2, \quad v_i^4 = w_0 - w_2.$$

This model was studied via mean field approximation and Monte Carlo simulation. It was found that for sufficiently high corrugation of the surface potential exceeding a certain critical value, the formation of the second as well as higher layers is suppressed at low temperatures. Fig. 40 presents the phase diagram for the case with additional repulsive next nearest neighbor interaction in the first

adsorbed layer. Instead of the usual first order layering transition at a particular chemical potential $\mu_c(1)$ one observes two second order transitions at $\mu_c^1(1)$ and $\mu_c^2(1)$. In the region between those values the adlayer forms the (2×1) ordered structure. Layering transitions in the second and higher layers all merge at the temperature marked by $T_w(2)$, so that at $T < T_w(2)$ only a monolayer film exists prior to the bulk adsorbate condensation.

The interplay between ordering in the first adsorbed layer and multilayer formation was observed experimentally [315–319], but such situations require different off-lattice models which will be the subject of the next section.

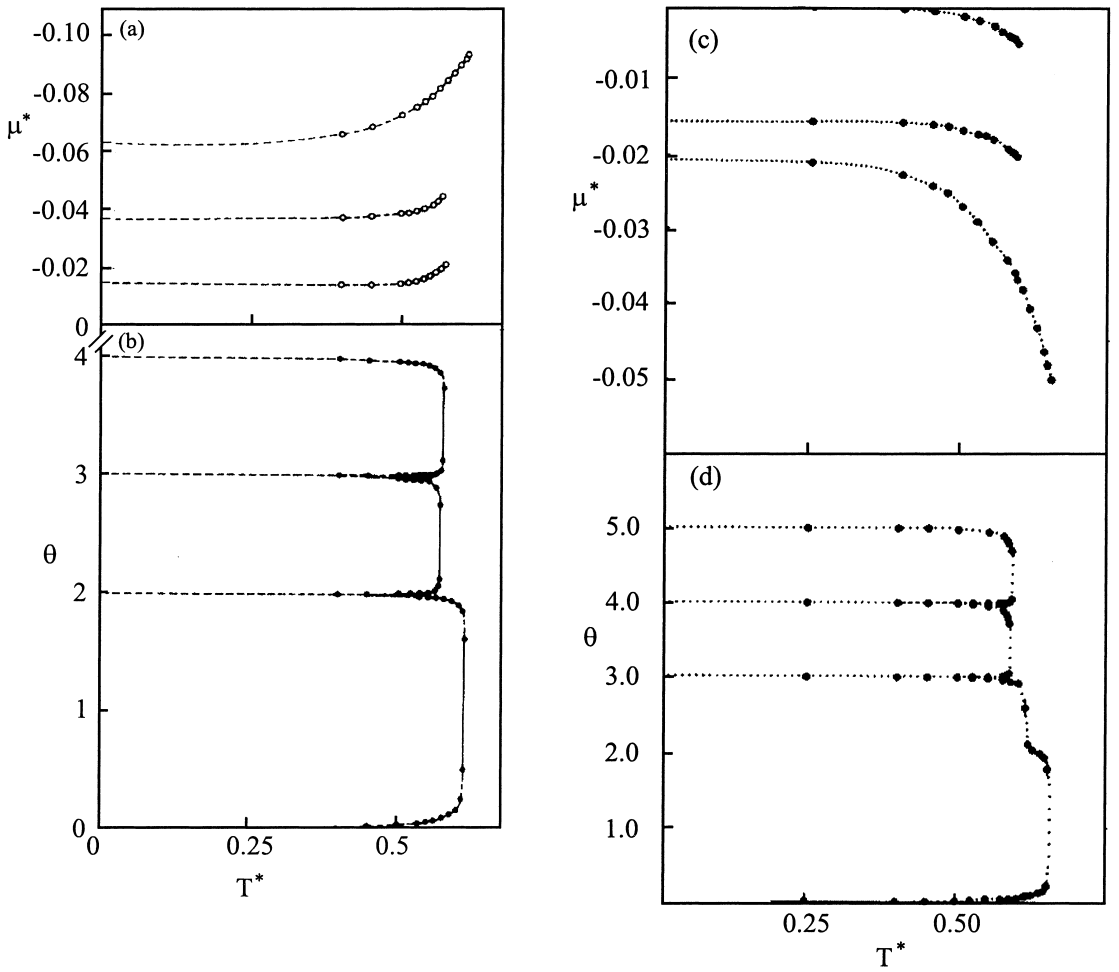

Fig. 39. A comparison of the phase diagram for the lattice gas models with the first nearest neighbor interaction (a, b) with the phase diagrams for the model with added second neighbor attractive interactions (c–f). (c–f) Results for $R = u(r_{nnn})/u(r_{nn}) = 0.05$ and 0.08, respectively. Parts (a), (c) and (e) show the phase diagrams in the coverage (θ) vs temperature $[T^* = kT/u(r_{nn})]$ plane, while (b), (d) and (f) show the corresponding phase diagrams in the chemical potential $[\mu^* = (\mu - \mu_0)/u(r_{nn})]$ vs temperature plane, where μ_0 is the chemical potential value at the bulk gas–liquid coexistence. Phase diagram in (a) and (b) was taken from ref. [176], while those shown in (c)–(f) from Ref. [178].

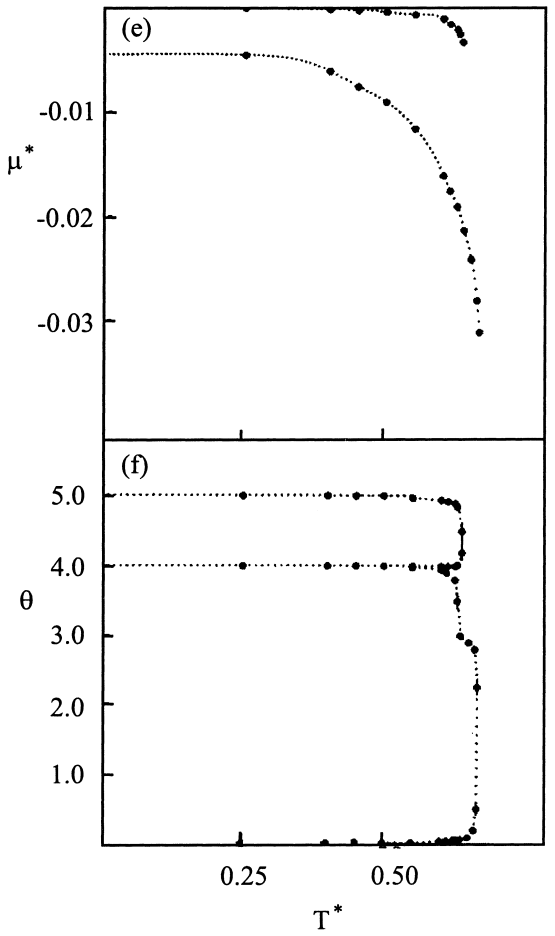

Fig. 39. (*Continued*).

5. Films on surfaces with finite corrugation

As it was already demonstrated in Section 2, atoms adsorbed on crystalline surfaces experience a corrugated surface potential. In case of physisorption periodic variations of the gas–solid potential are usually small as compared with the adsorption energy and often are also smaller than or comparable with the thermal energy of the adsorbed atoms. In such situations the lattice gas models discussed in the previous section do not describe well the properties of adsorbed layers. Off lattice movement as well as out-of-plane excitations of adsorbed atoms give rise to many new phenomena that cannot be included into the lattice gas formalism.

In this section we concentrate on the properties of films formed by the Lennard-Jones particles on surfaces with square and rectangular symmetry. Although the majority of the results reported here has been obtained with the help of computer simulation methods we also discuss several results of experimental studies as well as results stemming from analytical approaches.

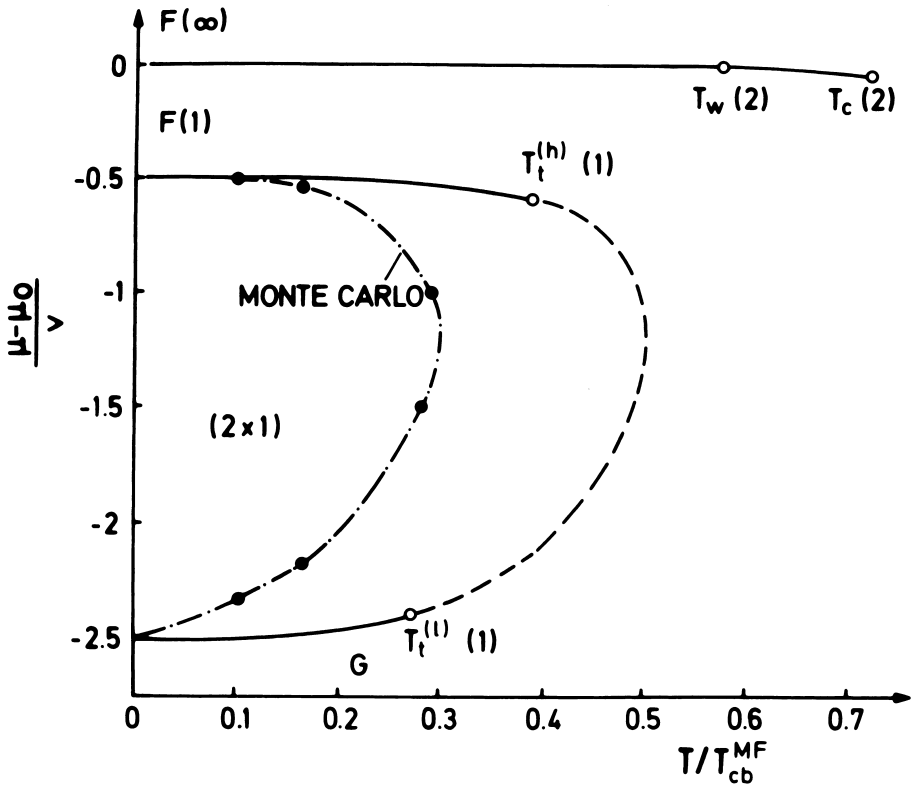

Fig. 40. Phase diagram of an adsorbed film in the simple cubic lattice from mean field calculations (full curves: first order transitions, broken curves: second order transitions) and from Monte Carlo simulation (dash-dotted curve: only the transition in the first layer is shown). Phases shown are the lattice gas (G), the ordered (2×1) phase in the first layer, lattice fluid in the first layer F(1) and in the bulk F(∞). For the sake of clarity, layering transitions in layers beyond the second layer (which nearly coincide with the layering of the second layer and merge at $T_w(2)$, are not shown. μ_0 is the chemical potential at the bulk gas–liquid coexistence, and T_{cb}^{MF} is the mean-field bulk critical temperature. While the layering transition of the second layer ends at the critical point $T_c(2)$, mean field theory predicts two tricritical points $T_t'(1)$ and $T_t^h(1)$ in the first layer (from Ref. [314]).

5.1. Adsorption on a noncorrugated substrate

To prepare a ground for a full appreciation of the surface corrugation effects on the behavior of films adsorbed on crystalline surfaces, we now briefly discuss the properties of films formed on a "flat" noncorrugated surface. When the surface potential possesses a deep minimum at a certain preferred distance from the surface, z_0, the adsorbed film is essentially two-dimensional at low temperatures. Deviations from planarity of the adsorbed layer may be due to temperature rise [203,320] and also may result from the formation of the second and higher layers [63].

The behavior of strictly two-dimensional Lennard-Jones systems has been intensively studied by various theoretical approaches [201,321–325] as well as by computer simulations [32,321,326–336]. In general, the phase diagram is quite well known. It has been found that it exhibits two-dimensional counterparts of all familiar states of matter in three-dimensional space: gas, liquid and solid (see

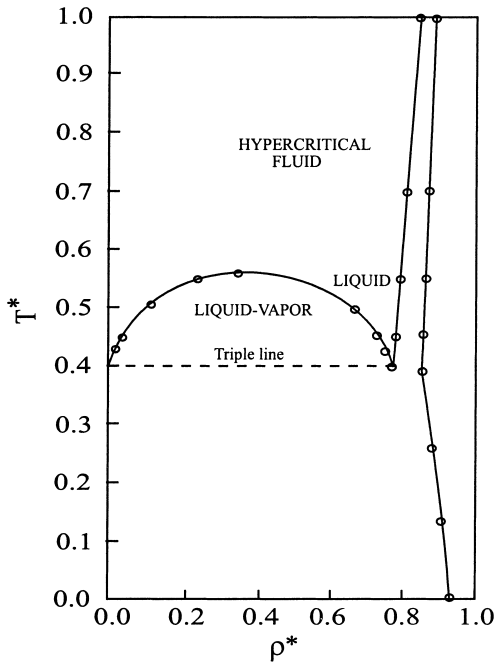

Fig. 41. Schematic representation of the phase diagram for the two-dimensional Lennard-Jones system.

Fig. 41). The triple point temperature has been estimated quite accurately as equal to $T_t^* = kT/\varepsilon = 0.40 \pm 0.015$ [321,330]. Existing estimations of the critical temperature [321,335] for that system are much less conclusive. From the theoretical calculations based on perturbation theory Barker et al. [321] have obtained $T_c^* \approx 0.56$, while Monte Carlo simulations performed by the same authors gave a lower value equal to about 0.533. A more recent Monte Carlo study due to Rovere et al. [335] has given a still lower value of 0.50 ± 0.02. Those rather large differences in the critical temperature estimations by different authors are not surprising. Computer simulations are difficult to interpret in the close vicinity of second-order phase transitions and suffer from considerably hindered speed of convergence, due to large effects of statistical fluctuation (critical slowing-down) as well as from the finite size effects which are particularly troublesome near the critical temperature [337]. Recent Monte Carlo studies in the Gibbs ensemble [338,339] have clearly demonstrated that the way one cuts off the interaction potential has also a big influence on the estimated critical temperature.

Another controversy about the properties of strictly two-dimensional Lennard-Jones system concerns the mechanism of melting. Already in the 1930s Peierls [259,260,340] argued that truly long-ranged positional order cannot exist in two-dimensional systems, so that two-dimensional crystalline order is impossible. This has been proved later by Mermin and Wagner [57]. In 1973 Kosterlitz and Thouless [37] proposed a theory of dislocation-mediated melting for a two-dimensional system. That theory has been later developed further by Halperin and Nelson [38,39] and by Young [248,249]. This theory is discussed in more detail in Section 3.4 of this article, and therefore here we recall only the salient features. From those theoretical works it follows that two-dimensional systems possess only quasi-long-ranged positional order characterized by algebraic decay of the two-particle correlation function. The KTHNY theory predicts that melting in two-dimensions occurs via two continuous phase transitions. In

the first transition, due to dissociation of dislocation pairs, the system looses the quasi-long-range positional order, but retains the quasi-long-range orientational order. This corresponds to the formation of the so-called hexatic phase. The second stage of melting is connected with the disclination-unbinding transition, occurring at higher temperature and leading to the formation of an isotropic two-dimensional liquid.

The scenario predicted by the KTHNY theory is considerably altered by the presence of periodic substrate potential and the actual mechanism of melting depends on the symmetry and size of the substrate surface as well as on the amplitude of the periodic surface potential [39]. We shall come back to this problem later in Section 5.2.

There are also other theories [255,256,341–343] that predict the usual first-order melting in two-dimensional systems. The concept of first-order melting was also advocated by Abraham [32,74], who argued that the loss of positional order is negligible in real systems due to their limited, though macroscopic, size.

Computer simulation studies [32,59,74,329,330,333] as well as experimental data [344–348] do not provide an univocal answer to the problem of melting in two-dimensions. In real adsorption experiments the assumption of two-dimensionality of adsorbed films is seldom fulfilled. Out-of-plane movement of adsorbed particles is expected to be an important factor which influences the properties and stability of all possible phases in monolayer films [63,203].

Monte Carlo simulations [131,320] and theoretical calculations [203,322] performed for monolayer systems in three-dimensional space at different film density clearly demonstrated that the critical as well as the triple point temperatures exhibit deviations from the values corresponding to strictly two-dimensional space.

For example, a Monte Carlo study by Patrykiejew et al. [131] has shown that the triple point of a monolayer allowed to relax along the axis perpendicular to the solid substrate surface is located at the temperature $T_t^* = 0.38 \pm 0.01$. This value is slightly lower than the value of about 0.4, found in two-dimensional systems as quoted above. Of course, this shift in the melting temperature may be also attributed to finite size effects and to the assumed rather small cut-off distance for the interaction potential (set at 2.5σ). It cannot be entirely ruled out, however, that the effects due to vertical motion of adatoms have any influence on the triple point temperature. It should be emphasized, however, that in the systems considered in Ref. [131] the adsorbed film was strongly pinned to the surface. Thus, even at the temperatures well above the triple point desorption and/or promotion of the second layer were not observed (cf. Fig. 42). On the other hand, a simulation run performed for the density $\rho^* = 0.81$, which is slightly higher than the triple point density of the two-dimensional Lennard-Jones system ($\rho_t^* \approx 0.79$ [329]), quite clearly demonstrated that the second layer promotion occurs at considerably lower temperature. This effect illustrates Fig. 43 which shows the temperature changes of the heat capacity for a series of systems with different density. Apart from a sharp peak at the temperature of $T^* \approx 0.38$, which marks the triple point melting, another broad maxima at considerably higher temperatures are present. These peaks are due to desorption from the first layer and the promotion of the second layer as confirmed by the density profiles calculated at different temperatures. In the case of a high density ($\rho^* = 0.81$) film, only one rather broad peak is found. In this case the promotion of the second layer as well as desorption both start at considerably lower temperatures than in the systems of lower density, while the melting point moves gradually towards higher temperatures for the densities exceeding the triple point value. Thus, the broad heat capacity peak is due to combined effects of melting, second layer promotion and desorption phenomena. Consequently, it is impossible to precisely locate the melting point from a study of the specific heat.

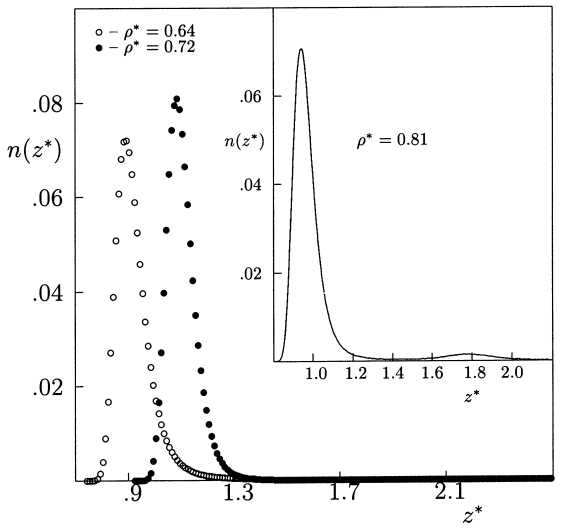

Fig. 42. Density profiles for the Lennard-Jones fluid in contact with a uniform attractive surface at the temperature $T^* = kT/\varepsilon_{gg} = 0.8$ and at different surface densities ρ^* shown in the figure. The results given in the inset correspond to the density exceeding the triple point density of the two-dimensional uniform Lennard-Jones system (adapted from Ref. [131]).

5.2. Films on square and rectangular lattices: experimental background

In the case when the gas–solid potential exhibits periodic variations due to the lattice structure of the surface, a competition between the surface corrugation and the adsorbate–adsorbate interactions becomes a major factor determining the structure of adsorbed layers. In general, the adsorbate–

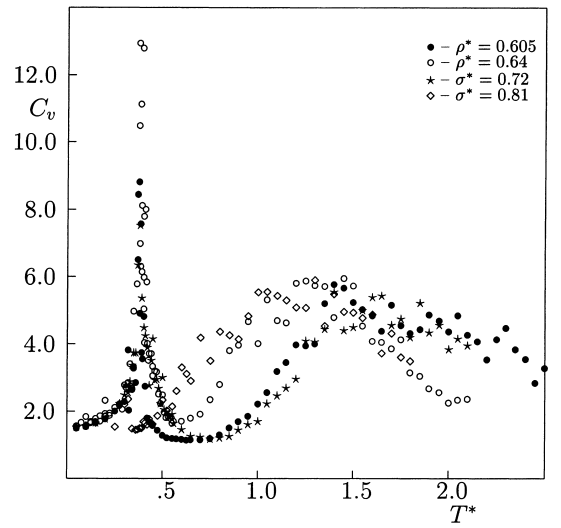

Fig. 43. The heat capacity curves for the Lennard-Jones fluid of different densities (shown in the figure) in contact with a uniform attractive surface (from Ref. [131]).

adsorbate interaction tends to enforce the formation of the hexagonal close-packed (h.c.p.) incommensurate solid phase in the monolayer film at low temperatures. On the other hand, the corrugated surface potential favors the formation of registered (or commensurate) structures. The actual structure of the film may be quite complicated and characterized by a highly nonuniform spatial distribution of adsorbed atoms within the film. In the most intensively studied case of adsorption on substrates with a hexagonal symmetry of the surface lattice, such as graphite [51,349–351], boron nitride [187,352], dense (111) plane of metal crystals (Pt, Cu, Ag) [14,19,353–356] and lamellar dihalides [138], both the commensurate and the incommensurate solid phases have the same symmetry and differ only by the spacing between neighboring atoms and by the orientation of the adsorbed layer lattice relative to the surface lattice [19,40,357–359]. In many cases the structure of the incommensurate phase can be described by the domain wall formalism [61,89] as already discussed in Section 3.3.

In the case of adsorption on surfaces of square and rectangular symmetry, such as low index planes ((100) and (110)) of the face centered crystals of various metals [20,94,97,106,360–362] or on the (100) plane of ionic regular crystals of MgO [108,363–367] and alkali halides [146,368,369], the situation looks quite different. Competing adsorbate–adsorbate and adsorbate–substrate interactions give rise to the formation of various registered superstructures [15], uniaxially ordered phases [370] as well as to various incommensurate phases [371].

For a rather weak physical adsorption on (100) planes of f.c.c. metal crystals, hexagonal structures in the monolayer films are usually found. Good examples of such systems are Xe films on Cu(100) [97,372] and Xe and Kr films on Pd(100) [94,95]. In some cases, however, different structures were also observed. Carbon monoxide adsorbed on Ni(100) and on Cu(100) [373], studied by LEED, Auger and work function measurements, was found to show the $c(2 \times 2)$ structure of square symmetry as well as an hexagonal structure. A recent infrared reflection–absorption studies [374] suggested that the (3×5) structure may be present at the surface coverage of 0.6 monolayer. Kr adsorbed on the Ir(100) surface [375] was also reported to form a (3×5) superstructure as well as a closed packed hexagonal phase.

A RHEED study of selenium adsorbed on Ni(100) [130] (see also Section 4.1) has shown the existence of the $c(2 \times 2)$ as well as the $p(2 \times 2)$ ordered commensurate structures in addition to various disordered phases. Symmetry arguments indicated that the phase diagram may belong to the universality class of the Ashkin–Teller model [301].

In the case of adsorption on the (100) plane of ionic crystals of metal oxides (MgO, NiO) and of alkali halides (NaCl, KCl, LiF, RbCl) the formation of various commensurate as well as incommensurate phases was observed, despite several problems with the preparation of substrates characterized by sufficiently high surface homogeneity [376–378]. One particular exemption is the MgO smoke particles, obtained by burning magnesium ribbons in a dry atmosphere, consisting of regular crystallites of the mean size about 2000 Å and with the predominantly exposed (100) plane [137] of the structure shown in Fig. 44.

Thermodynamic and structural studies of adsorption of noble gases (Ar, Kr and Xe) and small molecules of CH_4 [108,363–365] demonstrated important differences in their behavior. Low temperature adsorption isotherms for noble gases show the presence of two phase transitions which correspond to the 2D gas condensation followed by a transition between two condensed phases (see Fig. 45). Neutron diffraction measurements of Ar monolayer films allowed to identify two different ordered structures; the commensurate (2×3) phase which is stable for the surface coverages between

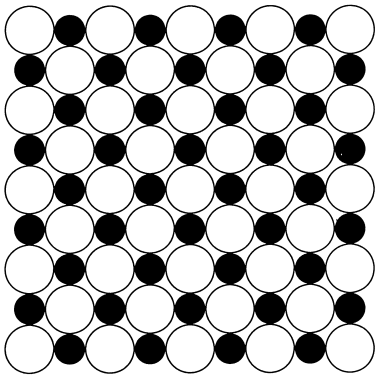

Fig. 44. Schematic representation of the (100) MgO surface. Mg^{2+} (of the size $d_{Mg^{2+}} = 1.72$Å) and O^{2-} (of the size $d_{O^{2-}} = 2.52$Å) ions are shown as filled and open circles, respectively.

0.5 and 0.8 and the denser incommensurate h.c.p. phase stable near the monolayer completion. Both Kr and Xe were found to form more or less distorted hexagonal incommensurate phases [363,379], so that the first transition can be interpreted as a 2D gas to 2D liquid condensation while the second transition is the 2D liquid to 2D incommensurate solid transition. In both cases the estimated triple point temperatures were found to agree quite well with the prediction $T_{t,2D}/T_{t,3D} = 0.61$ [380]. In the case of the CH_4/MgO system, the adsorption isotherms exhibit only one step connected with the transition from 2D dilute gas to the condensed commensurate $c(2 \times 2)$ structure, as indicated by neutron diffraction [365], LEED [381] and helium scattering [382] studies. Neutron scattering data also allowed

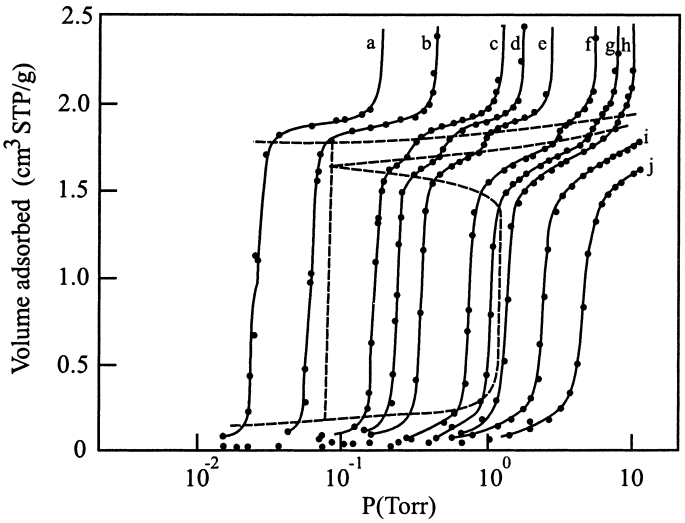

Fig. 45. Examples of adsorption isotherms for Xe/MgO system at different temperatures (adapted from Ref. [108]): (a) T=96.86 K; (b) 100.47 K; (c) 106.20 K; (d) 108.44 K; (e) 111.02 K; (f) 116.14 K; 118.72 K; (h) 121.15 K; (i) 126.17 K and (j) 131.19 K. Dashed lines show the estimated phase boundaries between the gas, liquid and solid monolayer phases. (Adapted from Ref. [108].)

to establish that the bilayer film of methane retains a commensurate structure at low temperatures up to 10 K [365]. The stability of the commensurate structure of CH_4 on MgO is surely connected with the surface corrugation and a rather good agreement occurs between the geometric surface lattice structure, with the second nearest neighbor distance equal to 4.21 Å, and the methane molecule diameter equal to 4.17 Å [383].

Apart from adsorption of simple spherical molecules the adsorption of various linear molecules such as N_2, C_2H_2, CO, CO_2 on MgO was also studied [108,367,384–386]. Some aspects of structural properties of such films and in particular orientational ordering of adsorbed molecules will be considered in Section 5.5.

Adsorption on ionic crystals of alkali halides concentrated mostly on molecular adsorbates [99,100,387,388], though some examples of detailed studies of simple atomic adsorbates (noble gases) were reported as well [376,389–393]. In such cases the adsorbed monolayers were observed to form distorted axially ordered hexagonal lattices [392].

A much stronger tendency towards axial ordering was found in adsorption on surfaces of rectangular shape of the unit cell, such as the (110) plane of f.c.c. metal crystals [17,18,20,103,360,394–398]. The Xe/Ag(110) monolayer was found to form an axially ordered hexagonal lattice [360], while the Xe/Cu(110) film orders into a $c(2 \times 2)$ commensurate phase which transforms into a more dense, also axially ordered hexagonal lattice [20,360]. LEED measurements for nitrogen adsorbed on Ni(110) [18] showed the formation of a commensurate (2×1) structure at low densities, a fluid (disordered) phase at intermediate densities and an incommensurate solid phase at high densities. A recent He atom diffraction study of nitrogen adsorbed on the Cu(110) surface [23] demonstrated the formation of a high-order commensurate pinwheel structure (see Fig. 46), earlier observed for CO adsorption on graphite [399]. This experimental observation was also confirmed by a molecular dynamics simulation [23]. Axially ordered structures were also observed by Fan and Ignatiev [400] in K and Cs monolayers on Cu(110).

LEED [401] and electron energy-loss spectroscopic [402] studies of O/Mo(110) showed the formation of the ordered $p(2 \times 2)$ structure.

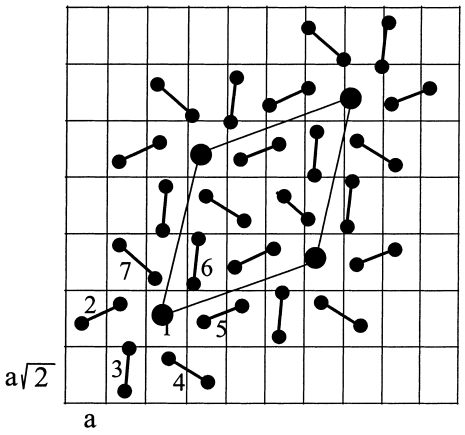

Fig. 46. Schematic representation of the high-order commensurate pinwheel structure of N_2 on Cu(110) surface proposed by Zeppenfeld et al. [23].

A common feature of all the adsorption systems mentioned above is that the size of the adsorbed atoms and molecules is so large that it does not allow for the formation of the (1×1) structure. In the case of nitrogen adsorbed on Ni(110), LEED studies indicated, however, that such a dense ordered structure may be stable under suitable conditions [18].

In the following sections we shall discuss theoretical and computer simulation studies for several model and experimental systems which exhibit different ordered structures.

5.3. Two-dimensional films on lattices with square and rectangular symmetry

Understanding the behavior of truly two-dimensional systems is of fundamental interest for the theory of phase transitions [72] and provides the ground for the development of methods which may allow to characterize better the surface properties of various materials. In Section 5.1 we have already discussed the properties of two-dimensional layers on flat, noncorrugated surfaces. Here we shall consider the effects of surface corrugation on the behavior of such systems. Our discussion heavily rests upon the results stemming from Monte Carlo simulation and theoretical studies.

Important information about the ordering in two-dimensional films formed on crystalline surfaces can be derived from the ground state calculations [112,131]. Knowledge about the ground state properties of adsorbed films is of interest by itself [112,113,294,403,404], and it provides important information for the appropriate use of computer simulations at finite temperatures. In particular it allows construction of the starting configurations that are close to the equilibrium arrangement of adsorbed species at low temperatures.

Bruch and Venables [112] considered the relation between the surface lattice and the adsorbed layer geometry in two-dimensional films adsorbed on crystals of different symmetry. They concentrated the discussion on the effects due to the corrugation potential and formulated explicit conditions for uniaxial registry. In that treatment the adsorbed film was assumed to be uniform in a sense that it was strictly two-dimensional and possessed a well defined lattice structure. The results obtained by Bruch and Venables must be considered as a sort of zeroth-order approximation only, since they did not attempt to minimize the system total energy, but rather focused on the calculations of the registry energy exerted by the surface corrugation potential only.

Determination of stable structures that may appear in two-dimensional adsorbed layers subjected to the surface potential of finite corrugation is not a trivial task even at zero temperature. In the case of a well defined lattice structure of the adsorbed layer its geometry and relation to the structure of the underlying substrate lattice can be expressed by Eq. (2.8) where the matrix elements α_{ij} are given by [405]:

$$\alpha_{11} = \alpha_1 \sin(\phi - \vartheta)/a_1 \sin(\phi), \quad \alpha_{12} = \alpha_1 \sin(\vartheta)/a_2 \sin(\phi), \tag{5.1}$$

$$\alpha_{21} = \alpha_2 \sin(\phi - \vartheta - \eta)/a_1 \sin(\phi), \quad \alpha_{22} = \alpha_2 \sin(\vartheta + \eta)/a_2 \sin(\phi). \tag{5.2}$$

When the potentials representing the adsorbate–adsorbate interaction, $u(r)$, and the adsorbate–substrate interaction, $v_{2D}(\boldsymbol{\tau})$, are specified, then the stable film structure can be obtained by minimizing the system energy with respect to the angles η and ϑ as well as with respect to α_1 and α_2.

Some simple examples of such calculations were reported by Patrykiejew et al. [131,133] in the case of adsorption on model (100) and (110) planes of atomic face centered cubic crystals, assuming that the adsorbed film forms a regular hexagonal lattice or simple registered phases such as $(1 \times 1), \mathrm{c}(2 \times 2)$ and (2×1). It was assumed that the adsorbate–adsorbate interaction potential $u(r)$ is given by the

Lennard-Jones function while $v_{2D}(\boldsymbol{\tau})$ was represented as

$$v_{2D}(\boldsymbol{\tau}) = \min_{z}[v(\boldsymbol{\tau}, z)] \tag{5.3}$$

with $v(\boldsymbol{\tau}, z)$ given by Eq. (2.6).

In the case of an incommensurate hexagonal phase consisting of N atoms, the energy corresponding to a given distance between the first nearest neighbors (α_1^*) and to a specified orientation of the adsorbed film with respect to the surface lattice (ϑ) is given by

$$e^*(\alpha_1^*, \vartheta) = 12[C_{12}^{o}(\sigma^*/\alpha_1^*)^{12} - C_6^{o}(\sigma^*/\alpha_1^*)^6] + \frac{1}{N}\sum_{i=1}^{N} v_{2D}^*(\boldsymbol{\tau}_i^*), \tag{5.4}$$

where all energies are expressed in units of ε_{gg} and all lengths in units of the surface lattice unit vector length a_1. This energy must be then minimized with respect to both α_1^* and ϑ in order to find the stable configuration. One readily observes that in the thermodynamic limit ($N \to \infty$) such a perfect, incommensurate, hexagonal phase has no preferred orientation [359] and the energy is given by

$$e^*(\alpha_1^*) = 12[C_{12}^{o}(\sigma^*/\alpha_1^*)^{12} - C_6^{o}(\sigma^*/\alpha_1^*)^6] + v_{2D,0}^*, \tag{5.5}$$

where $v_{2D,0}^*$ is the zeroth-order Fourier coefficient of $v_{2D}^*(\boldsymbol{\tau}^*)$ given by

$$v_{2D,0}^* = \frac{1}{a_s}\int_{a_s} v_{2D}(\boldsymbol{\tau}^*)\,\mathrm{d}\boldsymbol{\tau}, \tag{5.6}$$

where the integration is performed over the surface lattice cell of area a_s. The parameters C_{12}^0 and C_6^0 can be readily evaluated and their values depend on the assumed range of molecular interaction. In particular, assuming that the adsorbate–adsorbate interaction is cut off at the distance equal to 2.5σ one has [132]

$$C_{12}^{o} = 1.001632882 \quad \text{and} \quad C_6^{o} = 1.058492141 \tag{5.7}$$

and the nearest neighbor distance which minimizes the energy is equal to

$$\alpha_1^* = \sigma^*(2C_{12}^{o}/C_6^{o})^{1/6}. \tag{5.8}$$

Here we should mention that the problem of epitaxial rotation, i.e., the estimation of the angle ϑ was theoretically studied by Novaco and McTague [40,357], Shiba [85,86], Leatherman et al. [19], Hillier and Ward [405] and by Vives and Lindgård [359]. Those theories were quite successfully used for describing structural properties of simple atomic films on graphite. Bruch and Venables [112] applied the theory of Novaco and McTague [40] to adsorption on metals with a rectangular symmetry of the surface lattice.

In the case of registered phases, in which all adsorbed atoms are located directly above the surface potential minima $\{\boldsymbol{\tau}_s^* = (0.5, 0.5)a_2^*\}$ we have

$$e_r^*(\sigma^*) = 8[C_{12}^r\sigma^{*12} - C_6^r\sigma^{*6}] + v_{2D}^*(\boldsymbol{\tau}_s^*), \tag{5.9}$$

where the magnitudes of the parameters C_{12}^r and C_6^r depend on the assumed commensurate structure r. In particular, for the (1×1), $c(2\times2)$ and (2×1) phases we have

$$C_{12}^{(1\times1)} = 1.015997141 \quad \text{and} \quad C_6^{(1\times1)} = 1.156625, \tag{5.10}$$

$$C_{12}^{c(2\times2)} = 0.01587295532 \quad \text{and} \quad C_6^{c(2\times2)} = 0.142578125, \tag{5.11}$$

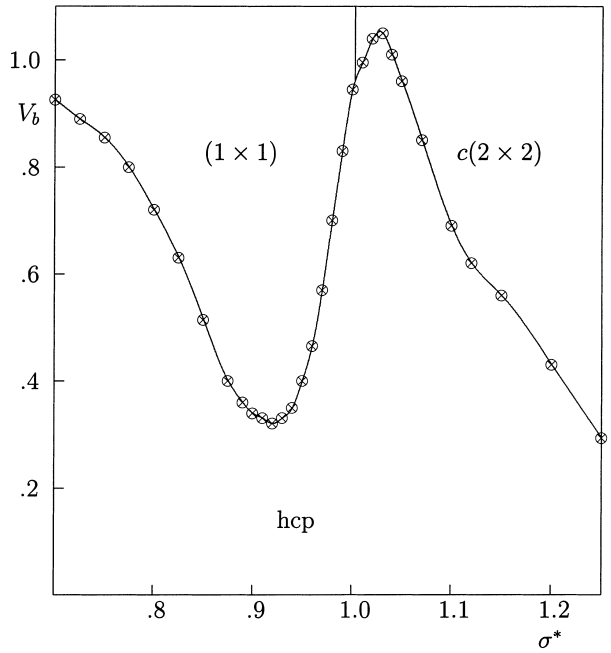

Fig. 47. Regions of stability of different surface phases for the Lennard-Jones particles adsorbed on the (100) plane of model f.c.c. crystals deduced from the ground state calculations for systems of number density equal 1.0 (from Ref. [131]).

and

$$C_{12}^{(1\times2)} = 0.01591578 \quad \text{and} \quad C_6^{(1\times2)} = 0.1518373843. \tag{5.12}$$

Using the above expressions regions of stability have been estimated corresponding to the h.c.p. phase and the above registered phases for adsorption on the (100) and (110) planes of an f.c.c. crystal, for the systems characterized by different sizes of the adsorbate atoms, given by σ^*, and with different corrugation of the surface potential [131,133] (see Fig. 47). Of course, such calculations do not provide any exact solution to the problem of ground state properties of incommensurate phases as they ignore lattice distortions which arise from defects and local elastic relaxations, as discussed by Vives and Lindgård [359] as well as from the formation of a domain-wall network structure [42]. The aim of the calculations performed by Patrykiejew et al. [131,133] was only to make a rough estimation of the adsorbed layer structures that would be best as starting configurations for the Monte Carlo calculations.

A systematic finite temperature canonical ensemble Monte Carlo simulation study was carried out for adsorption on the (100) [60,132] and (110) [133] planes of f.c.c. model crystals characterized by different corrugation of the surface potential, measured by the parameter V_b in Eq. (2.6).

All the calculations were performed for a fixed film number density corresponding to the density of fully occupied registered films. Thus, in the case of small adsorbed atoms, which can form the (1×1) structure, the number density $\rho_0 = N/M$, where N is the number of atoms and M the number of lattice sites, was equal to 1.0, while for larger atoms, for which ordering into c(2×2) and (2×1) structures occurs, the number density was equal to 0.5.

Now we briefly discuss the results obtained for adsorption on the (100) plane of an f.c.c. crystal [132] and begin with the highly corrugated systems of adatoms with $\sigma^* = 1.2$, which order into the $c(2 \times 2)$, and $\sigma^* = 0.9$, which form the (1×1) registered phase. From the ground state calculations already mentioned it was found that for the chosen parameters of the interaction potentials and for the densities not exceeding the density of a fully filled registered layer, the system with $\sigma^* = 1.2$ forms a stable $c(2 \times 2)$ phase for the corrugation parameter V_b greater than about 0.55. In order to obtain information about the internal structure of the adsorbed layer, and in particular to distinguish the well defined ordered structures and the disordered (fluid) phases it is convenient to define appropriate bond-orientational order parameters, which are frequently used to study and characterize ordering in various physical systems [59,407]. The adlayers with a four-fold symmetry, as in the case of both (1×1) and $c(2 \times 2)$ phases, and the layers with a six-fold symmetry can be characterized by the following bond-orientational order parameters [60,132], see also Section 3.4,

$$\psi_k = \left| \frac{1}{N_b} \sum_i \sum_j \exp[ik\phi_{ij}] \right|, \quad k = 4, 6. \tag{5.13}$$

In order to detect axially ordered hexagonal phase one can define the bond-orientational order parameter of the form

$$\psi_6^e = \left| \frac{1}{N_b} \sum_i \sum_j \cos[6\phi_{ij}] \right|. \tag{5.14}$$

Basically, in an ideal situation, when only pure phases are present, one can determine their nature looking at the behavior of those order parameters, the corresponding susceptibilities

$$\chi_i = \frac{L_x L_y}{T^*} [\langle \psi_i^2 \rangle - \langle \psi_i \rangle^2], \tag{5.15}$$

where L_x and L_y are the linear dimensions of the system in the x and y directions, and the fourth-order cumulants [5,46,60,132]

$$U_i = 1 - \frac{\langle \psi_i^4 \rangle}{3\langle \psi_i^2 \rangle^2}, \tag{5.16}$$

where the subscript i labels the above defined three bond-orientational order parameters ψ_4, ψ_6 and ψ_6^e.

When the adsorbed layer is in a disordered fluid state, the bond-orientational order parameters ψ_6, ψ_6^e defined above should be equal to zero since all possible mutual orientations of "bonds" appear in the system with the same probability. The bond order parameter ψ_4 is at all temperatures nonzero on a square substrate, since the corrugation potential acts then like a field conjugate to ψ_4, and thus causes a positive though small response (which only vanishes as $T \to \infty$). In the case of registered phases of square symmetry, ψ_4 is expected to be equal to unity, while the remaining order parameters ψ_6 and ψ_6^e should be equal to zero. In the hexagonal close packed phase ψ_4 should approach zero while ψ_6 should be equal to unity. The behavior of ψ_6^e depends on the orientation of the adsorbed layer with respect to the surface lattice and may assume different values. When the film exhibits uniaxial registry but retains perfect hexagonal structure than $\psi_6^e = 1.0$. On the other hand, when the hexagonal arrangement is not perfect, we expect nontrivial behavior of ψ_6^e, as well as of ψ_4 and ψ_6. Examples of the changes of ψ_4 and ψ_6 with temperature for adsorbed films formed on highly corrugated systems of different size are

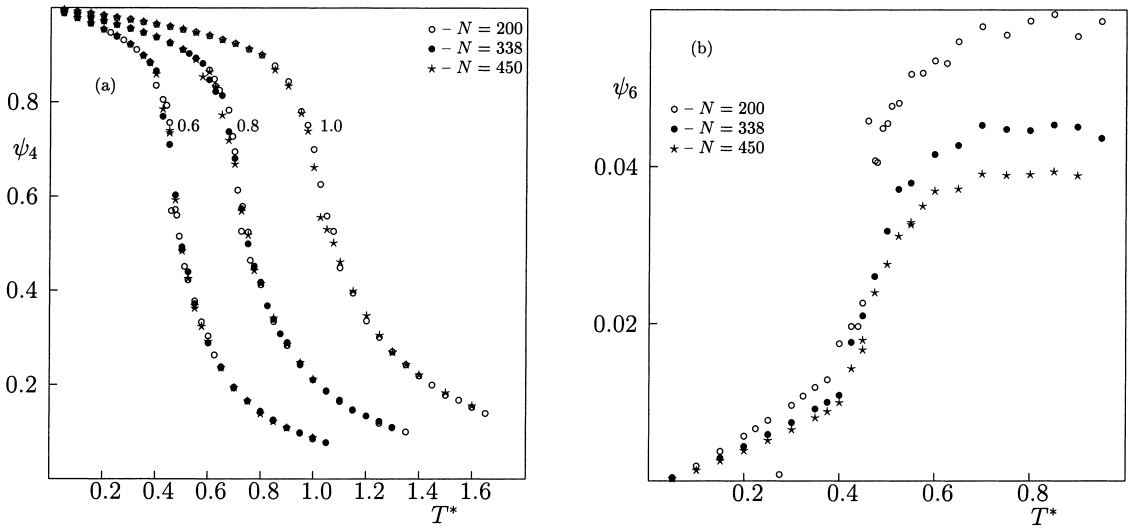

Fig. 48. Bond-orientational order parameters ψ_4 (a) and ψ_6 (b). The results shown in part (a) correspond to the systems with $\sigma^* = 1.20$, three different values of the corrugation parameter V_b and three different system sizes (shown in the figure) while the results shown in part (b) were obtained for $V_b = 0.6$ and three different system sizes (also shown in the figure) (from Ref. [132]).

shown in Fig. 48. It is quite clear that in all cases the adsorbed layers exhibit square symmetry at low temperatures and undergo rather abrupt, though continuous, disordering as the temperature increases. The absence of any finite size effects is a clear evidence that no longwavelength fluctuations develop. The finite size effects are only manifested in the behavior of residual ψ_6 (cf. Fig. 48b), but this merely reflects the gradual approach towards the thermodynamic limit.

The situation looks quite different for a weakly corrugated surface, characterized by the corrugation parameter of $V_b = 0.2$, as is demonstrated in Fig. 49. Now the low temperature phase exhibits hexagonal symmetry and it is also evident that this phase is axially ordered, since ψ_6^e approaches unity at low temperatures. In this case, disordering occurs via a sharp phase transition and it was identified as a melting transition. The behavior of the bond-orientational parameters for this system demonstrates also that the film looses axial ordering prior to the melting transition. The melting occurs at the temperature equal to about 0.385, while already at $T^* = 0.375$ the order parameter ψ_6^e drops to about 0.2. A rather convincing proof that the system remains in the solid state was provided by the calculations of the radial distribution function at different temperatures (see Fig. 50), which look practically the same at $T^* = 0.375$ and at lower temperatures. On the other hand, already at $T^* = 0.4$ the radial distribution function shows the behavior typical for a fluid phase. The estimation of the epitaxial rotation angle at different temperatures was done by the analysis of several configurations recorded during the simulation, and it was found that at $T^* = 0.3$ it is equal to about 1.9^o and jumps to about $16.7 \pm 0.2^\circ$ at $T^* = 0.375$.

Another type of behavior was observed for the system with intermediate corrugation of the surface potential ($V_b = 0.4$). In this case the low temperature phase has perturbed hexagonal symmetry and exhibits axial ordering, but along the line $x = y$, and hence the epitaxial rotation angle is equal to 45°. The bond-orientational order parameters show different behavior compared to the previous case (see Fig. 51). In particular, ψ_6 shows quite large deviations from unity already at low temperatures, while ψ_6^e

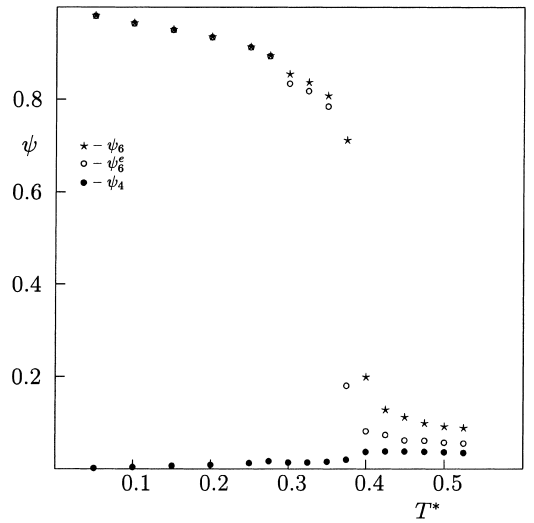

Fig. 49. Bond-orientational order parameters ψ_6, ψ_6^e and ψ_4 for the system of 450 particles with $\sigma^* = 1.2$ adsorbed on a weakly corrugate surface with $V_b = 0.20$ (from Ref. [132]).

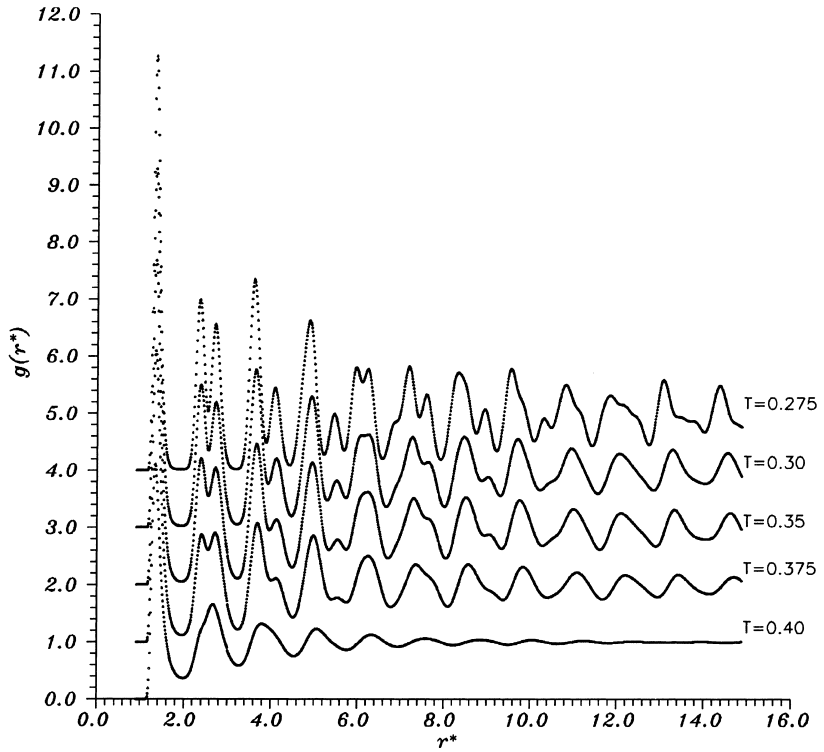

Fig. 50. Radial distribution functions for the same system as in Fig. 49 at different temperatures (shown in the figure). Note that the curves for different temperatures (apart from the one corresponding to $T^* = 0.40$, are shifted upwards by one unit with respect to each other (from Ref.[132]).

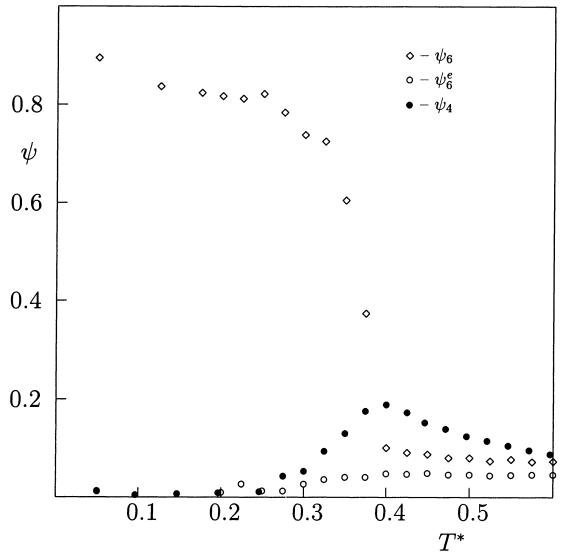

Fig. 51. Bond-orientational order parameters ψ_6, ψ_6^e and ψ_4 for the systems with $\sigma^* = 1.20$, and weakly corrugated surface with $V_b = 0.4$ (from Ref. [132]).

is very small. An interesting property of this system is a clearly seen increase of the bond-orientational order parameter ψ_4 upon melting, so that the liquid phase shows some remnants of a square order due to large effects of surface corrugation.

Still another important effect of the surface corrugation on the behavior of adsorbed films was found from the study of systems with different densities. As we know from the earlier discussion of a two-dimensional uniform Lennard-Jones system in Section 5.1, the melting transition of the hexagonal phase occurs at a constant (triple point) temperature of about $T_t^* = 0.40$, as long as the density is lower than the triple point density. In the case of corrugated surfaces it was found that the triple point temperature changes. In particular, corrugation lowers the triple point temperature. As long as the density is lower than the triple point density ρ_t the melting transition occurs at a constant temperature T_t^* (Fig. 52). Only when the density becomes very high the melting transition is shifted towards higher temperatures. This picture holds as long as the surface corrugation is low enough so that the solid phase is incommensurate. Fig. 52 includes also the locations of heat capacity maxima for highly corrugated systems which order into the $c(2 \times 2)$ phase. In such a situation the system undergoes rather an order–disorder transition than the melting and the disordering temperature appears to change continuously with the film density. For comparison Fig. 52 also shows the positions of the heat capacity peaks calculated for a singe particle, using the method of Doll and Steele [180] As discussed earlier in Section 2.2.2 the appearance of that maximum results from a gradual transition from localized to mobile adsorption and occurs at the temperature determined by the height of the potential barrier for diffusion. It is quite clearly seen that in all cases this transition region is located at considerably lower temperatures than the melting of the hexagonal phase and the disordering of the registered phase.

From the discussion presented above it follows that two main regimes of the film behavior can be identified, with respect to the amplitude of the corrugation potential. These are the strongly and weakly corrugated regimes. In the first case the adsorbed film forms registered structures while in the second

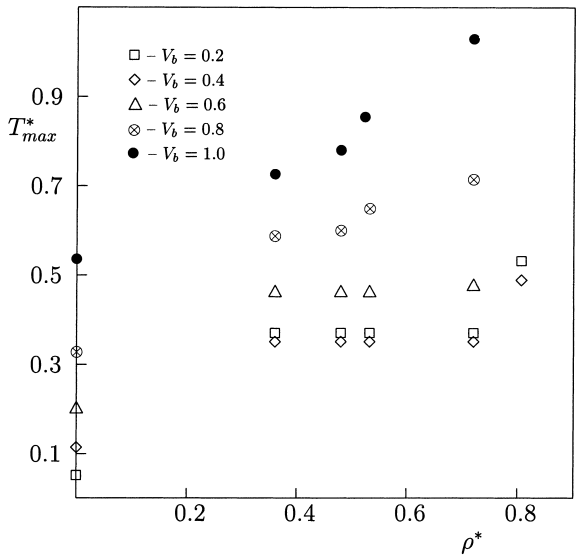

Fig. 52. Changes in the melting and disordering temperatures with the film density estimated from Monte Carlo simulation for 450 particles of $\sigma^* = 1.20$ for monolayer films on surfaces with different values of the corrugation parameter (shown in the figure). The data points at $\rho^* = 0$ mark the locations of the heat capacity maxima associated with the localized-to-mobile transition for a single adsorbed atom (from Ref. [132]).

the formation of a more or less perturbed hexagonally ordered incommensurate solid phase occurs at low temperatures.

Similar Monte Carlo calculations were performed for a series of systems with $\sigma^* = 0.9$ which is predicted to form a simple (1×1) ordered structure when the surface corrugation is high enough. It was also found that the films formed on highly corrugated surfaces disorder gradually, while those on weakly corrugated surfaces undergo a sharp melting transition. One particular problem addressed in that study [60] was the nature of the melting transition.

As discussed in Section 3.4, the mechanism of melting in two-dimensional systems is a subject of considerable current interest and hot controversy [59,407,408]. One of the still open questions is the adequacy of the picture provided by the KTHNY theory (Section 3.4) to real experimental systems. The hitherto collected experimental data [1,59,138,344] as well as the results of numerous computer simulations [32,59,131,253,406] seldom lead to unambiguous conclusions. The KTHNY theory predicts a two-step melting in the case of a flat, noncorrugated surface, as discussed earlier (Section 3.4). This scenario is considerably altered by the presence of a periodic substrate potential and the actual mechanism of melting depends on the symmetry and amplitude of the corrugation potential [38,39]. In general, surface corrugation is expected to wash-out the disclination-unbinding transition, and hence the melting becomes a one-step process. This transition may be continuous, as for the flat surface, or first-order. The only exception is the melting of an hexagonal adsorbate film on a square lattice characterized by weak corrugation of the adsorbate–substrate potential. In this case the theory proposed by Nelson and Halperin [38,39] predicts that the disclination-unbinding transition is replaced by an Ising-like transition. Thus, one expects to observe two liquid-like phases with different orientational symmetry.

Monte Carlo simulations performed for a series of two-dimensional systems of Lennard-Jones particles with $\sigma^* = 0.9$ on surfaces with different corrugation [60] demonstrated that the mechanism of melting is indeed considerably affected by the surface corrugation. In particular, the calculations were performed for two different systems belonging to the weakly corrugated regime. In order to determine the order and nature of the melting transition the behavior of the fourth-order cumulants of the bond-orientational order parameters, as defined by Eq. (5.16), for systems of different size was studied.

It is well known [64,409] that in the case of a second order phase transition the cumulants reach a trivial limit of $2/3$ at the temperatures well below the transition point and zero at the temperatures well above the transition point. At the transition temperature the cumulants for different system sizes should reach a common nontrivial intersection point U^* with the magnitude of U^* depending on the universality class of the phase transition. The results presented in Fig. 53 seem to confirm the predictions of the KTHNY theory. At the temperature $T^* \approx 0.4$ the bond-orientational order parameters ψ_6 and ψ_6^{e} both exhibit a sudden, though small, drop. Thus, above that temperature the system retains a considerable orientational order. According to the KTHNY theory this first transition, due to dissociation of dislocation pairs, transforms the solid phase into an hexatic phase. Then a second transition occurs at the temperature of about 0.485, which leads to the loss of orientational order in the system. The behavior of U_{L}, also depicted in Fig. 53, shows that the cumulants for different systems sizes do show a common intersection at U^* close to 0.61. This value of the cumulant fixed point corresponds to the universality class of the Ising model [64], exactly what the theory predicts for this case (Section 3.4).

The above conclusion must be treated with some care. The simulation studies were carried out for rather modest system sizes and no attempts were made to determine the real nature of the intervening phase, which appears between the solid and fluid phases. A possible answer to this problem might be obtained by the calculations of the bond-orientational correlation function, successfully used in the case of uniform two-dimensional systems [59].

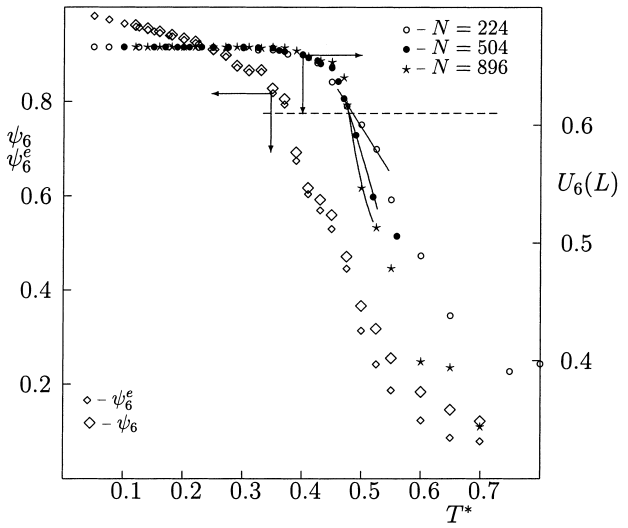

Fig. 53. Bond-orientational order parameters ψ_6 and ψ_6^{e} for the two-dimensional system of 894 particles with $\sigma^* = 0.9$ adsorbed on the surface of low corrugation, characterized by $V_{\mathrm{b}} = 0.1$, and the size of 32×28 surface unit cells as well as the fourth-order cumulants $U_6(L)$ for different system sizes obtained from Monte Carlo simulation (from Ref. [60]).

Similar studies were carried out for two-dimensional films formed on the (110) plane of f.c.c. model crystals of different corrugation [132]. In such a case, the corrugated surface potential has quite different properties than that corresponding to the (100) plane. In particular, the potential barriers for diffusion in the x and y directions are different, so that one can expect a strong tendency towards the formation of uniaxially ordered phases, as observed in numerous experimental studies [18,20,103,395–397] and predicted by theoretical calculations [112,113]. Note that the potential barriers for diffusion do not scale linearly with the corrugation parameter V_b, but rapidly decrease with V_b.

Another consequence of the difference in the surface lattice structure is the possibility that different registered phases form, namely (2×1) and $c(2 \times 2)$, of the same number density equal to 0.5. The ground state calculations, performed in a similar way as in the case of the (100) substrate lattice, allowed to estimate the regimes of σ^* and the corrugation parameter V_b in which those registered structure are more stable than the hexagonal phase (Fig. 54). In order to determine the internal structure of the ordered phases as well as to locate any possible phase transitions, the above defined bond-orientational order parameters were supplemented by the additional bond-orientational order parameter

$$\psi_r = \left| \frac{1}{N_b} \sum_i \sum_j \cos\left[w\phi_{ij}\right] \right| \tag{5.17}$$

with

$$w = 2\pi/\alpha_0, \quad \alpha_0 = \cos^{-1}(1/\sqrt{3}) \approx 0.95531662 \tag{5.18}$$

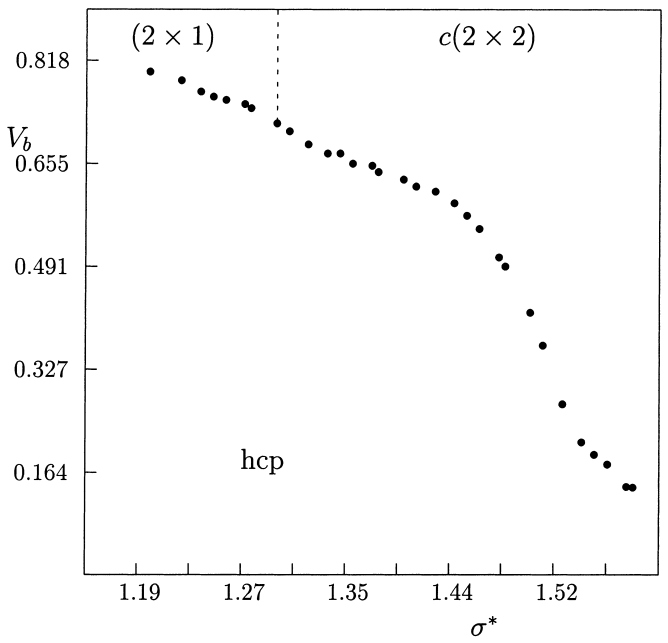

Fig. 54. Regions of stability of different surface phases for the Lennard-Jones particles adsorbed on the (110) plane of model f.c.c. crystals deduced from the ground state calculations for systems of number density 0.5 (from Ref. [133]).

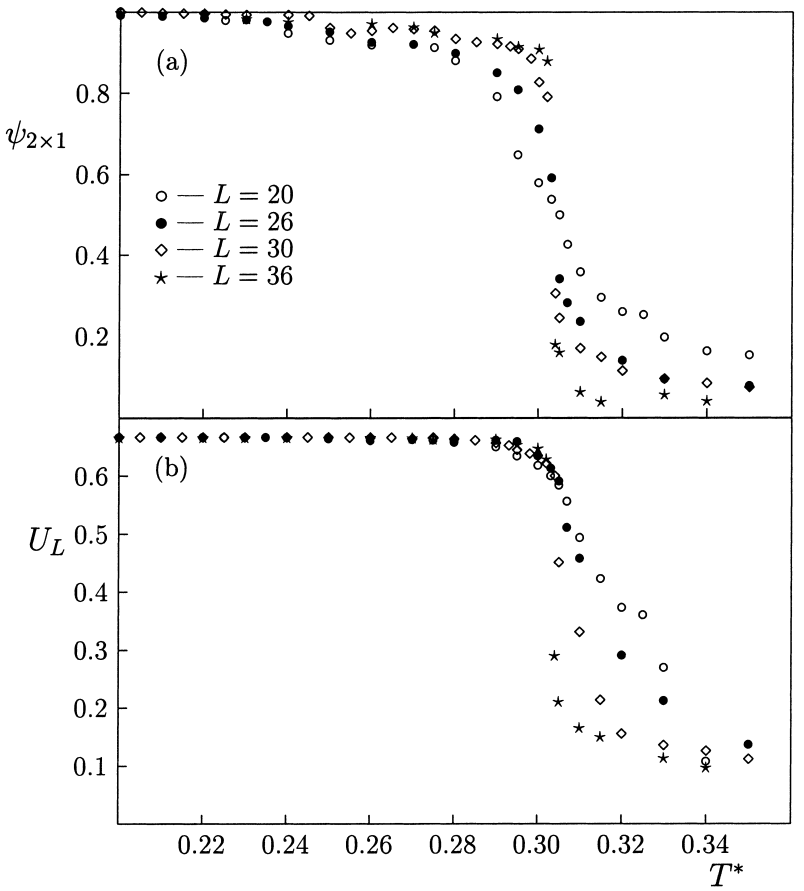

Fig. 55. Plots of the Ising-like order parameter $\psi_{(2\times1)}$ (a) and the corresponding fourth-order cumulant (b) versus temperature for the system of Lennard-Jones particles with $\sigma^* = 1.20$ adsorbed on the (110) plane of a model f.c.c. crystal with the corrugation parameter $V_b = 1.0$ and for different sizes of the simulation cell. Note that the number density in all systems is the same and equal to 0.5 (from Ref. [133]).

which was specifically constructed to indicate the presence of the $c(2 \times 2)$ phase on the rectangular lattice of the (110) plane of an f.c.c. crystal.

Another possibility of detecting the registered (2×1) and $c(2 \times 2)$ phases and to study the nature of the possible order–disorder transitions is to take into account that the surface can be considered as composed of four interpenetrating sublattices (see Section 3.1) and apply Ising-like order parameters, defined by Eqs. (3.2) and (3.3), and the appropriate fourth-order cumulants, defined in the same way as those given by Eq. (5.16).

Monte Carlo simulations performed for the systems, which according to the ground state predictions should order into the (2×1) and $c(2 \times 2)$ structures demonstrated rather unexpected differences in their behavior. While the system with the (2×1) ordered state was found to show an Ising-like order–disorder transition (Fig. 55), the system ordering into the $c(2 \times 2)$ structure exhibited gradual disordering, without any trace of a phase transition (Fig. 56). A possible explanation of the gradual disordering of the $c(2 \times 2)$ structure can be given by taking into account a large difference between the

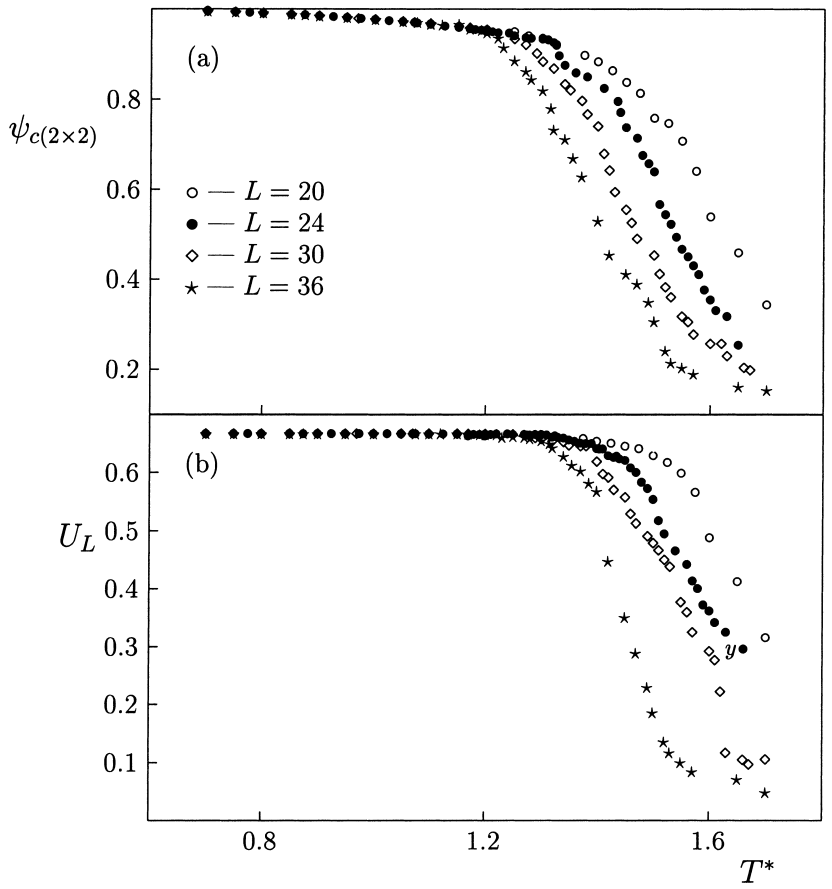

Fig. 56. Plots of the Ising-like order parameter $\psi_{c(2\times2)}$ (a) and the corresponding fourth-order cumulant (b) versus temperature for the system of Lennard-Jones particles with $\sigma^* = 1.55$ adsorbed on the (110) plane of a model f.c.c. crystal with the corrugation parameter $V_b = 1.0$ and for different sizes of the simulation cell. Note that the number density in all systems is the same and equal to 0.5 (from Ref. [133]).

potential barriers for diffusion in the x and y directions. In particular it was found that disordering is mostly associated with a gradual increase of the translational freedom along the x direction only, and hence looks very similar to that predicted by the one-dimensional Frank–van der Merwe theory [246]. Uniaxial ordering appeared to be also present in the films formed on weakly corrugated surfaces. The structure of the adsorbate lattice was found to be rectangular rather than hexagonal and its disordering occurs via rather sharp transitions at temperatures depending on the surface corrugation as well as the relative size of adsorbed atoms and the surface unit lattice cell. For sufficiently low surface corrugation the adsorbed film was observed to be incommensurate in the x direction as is demonstrated by Fig. 57 which shows the behavior of the density Fourier coefficients

$$\rho_{\boldsymbol{q}_{k_x,k_y}} = \left| \sum_{\boldsymbol{r}_i} \exp[\mathrm{i}\boldsymbol{r}_i \cdot \boldsymbol{q}_{k_x,k_y}] \right|, \tag{5.19}$$

where $\boldsymbol{q}_{k_x,k_y}$ denote the reciprocal surface lattice vectors

$$\boldsymbol{q}_{k_x,k_y} = 2\pi(k_x\boldsymbol{b}_1, k_y\boldsymbol{b}_2), \tag{5.20}$$

where k_x and k_y are integers.

The internal structure of the low temperature phases may be quite complex and cannot always be represented by a simple well defined lattice. Fig. 58a shows the example of a typical configuration recorded during the Monte Carlo simulation at a very low temperature of $T^* = 0.05$, which shows the formation of incommensurate strip-like structure with the rotational alignment of the solid phase and the presence of frozen-in gas–solid coexistence. The estimated tilting angle for the solid phase (see Fig. 58b) was found to be equal to about $71 \pm 1^\circ$ for this particular example. It is interesting that rather simple ground state calculations for a model strip-like structure of different width (cf. Fig. 58b) allowed to estimate the tilting angle. It occurred that the system energy reaches a minimum for the tilting angle just about 71° irrespective of the strip width (see Fig. 58c). Also, the asymptotic ($T^* \to 0$) behavior of the appropriate bond-orientational order parameters ψ_6, ψ_6^e and ψ_4 was found to be in a good qualitative agreement with the assumption of that value for the tilting angle.

5.4. Dense monolayer and bilayer films on a square lattice

Real adsorption systems usually show some effects of out-of-plane motion of adsorbed particles, even at low temperatures. The increase of the pressure, or the chemical potential, for the monolayer film may induce many new phenomena. What actually happens to the film depends crucially on the strength of the adsorbate–adsorbate and the adsorbate–adsorbent interaction, as already discussed in Section 4.2. Also the surface corrugation is expected to be a very important factor influencing the film behavior.

Possible scenarios may include the appearance of layering transitions leading to the formation of compact three-dimensional crystallites, promotion of the second layer due to melting and disordering of the first adsorbed layer as well as simple desorption of particles due to an increase in their kinetic energy. Also, the structure of adsorbed layers adjacent to the substrate surface may change upon the formation of higher layers, so that various commensurate–incommensurate transitions may occur in the film.

The problem of monolayer stability is closely related to the wetting of a substrate by an adsorbed film. In a recent paper by Phillips [410] is was demonstrated via the molecular dynamics simulation and analytic solution of the elastic continuum models that three different mechanisms may be responsible for the instability of the adsorbed monolayer and the promotion of the second, as well as higher, layers. In a strongly adsorbed film, the promotion of the second layer, under the specified thermodynamic conditions of temperature and pressure, occurs mostly due to migration of the atoms located at the edges of adsorbed islands of a compact two-dimensional solid layer. This process may be also accompanied by, much more rarely occurring, movements of individual atoms from the interior of the island to the second layer, if they happen to gain enough kinetic energy. These two mechanisms were observed also in the case of melting in dense monolayer films as will be discussed later. The third possible mechanism leading to the promotion of higher layers may be a sudden promotion of groups of adsorbed atoms due to the response to structural instability in the highly compressed solid layer. This last mechanism is most likely to occur in dense and relatively weakly adsorbed films in which stresses and strains are of particular importance.

Of course, the above mentioned effects are most likely to occur in adsorbed films formed on rather weakly corrugated surfaces, since such systems are most likely to form islands of a high density solid phase. In the case of strongly corrugated surfaces, on which the registered films are usually found, the promotion of the higher layers is not likely to occur. It can be rather expected that only a sufficient increase in the temperature may induce disordering which is accompanied and/or followed by desorption.

Model Monte Carlo studies of such systems were performed by Patrykiejew et al. [63,163], for a series of very similar systems as those described in the previous section, but assuming a full three-dimensional nature of the system. It was observed that monolayer films of number density equal to a fully filled registered (1×1) phase as well as films of higher density formed on highly corrugated

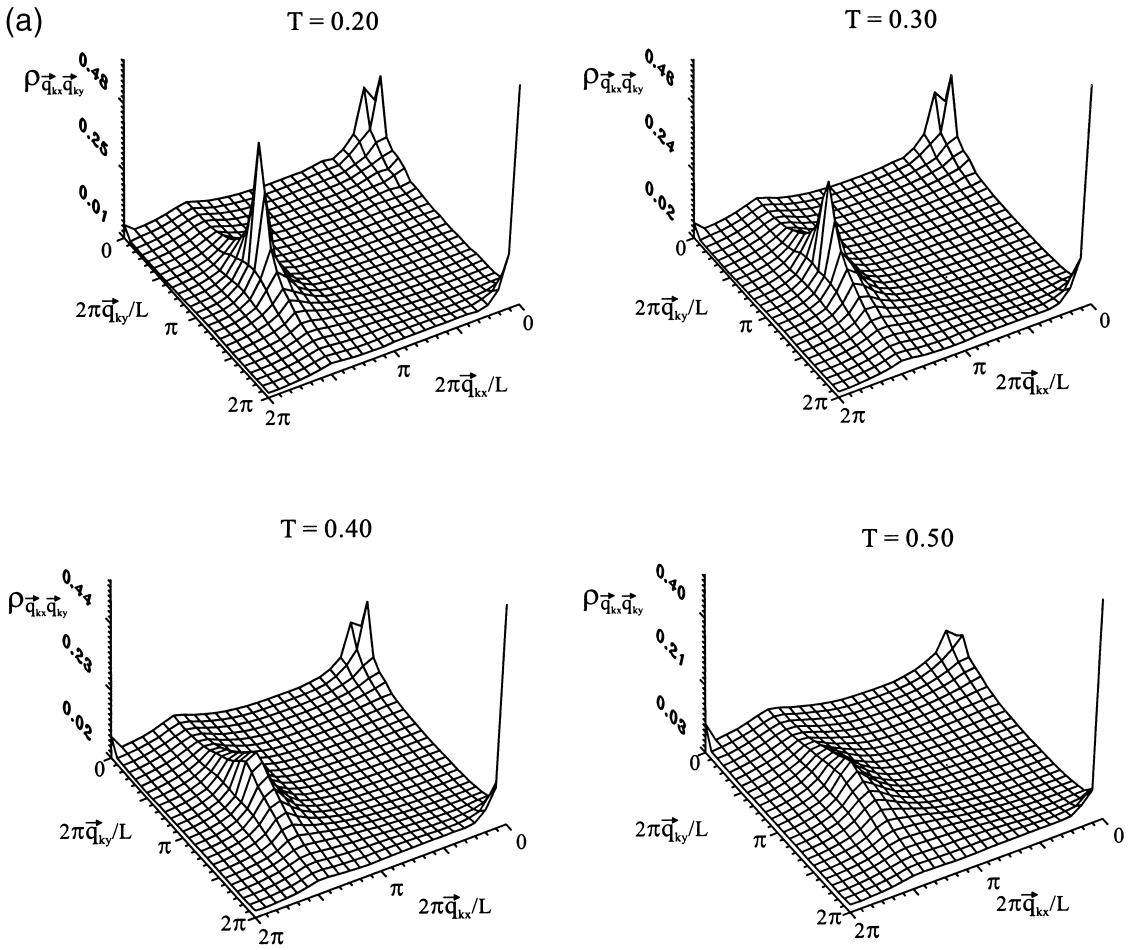

Fig. 57. The behavior of the density Fourier coefficients $\rho_{q_{k_x,k_y}}$ for the system of 450 Lennard-Jones particles adsorbed on the (110) plane of a model f.c.c. crystal surface of the size 30×30 unit lattice cells and the corrugation parameter $V_b = 0.4$ at different temperatures shown in the figure (a). (b) Same as (a) but for a highly corrugated surface ($V_b = 1.0$). The results for the two lowest temperatures correspond to the ordered (2×1) structure (from Ref. [133]).

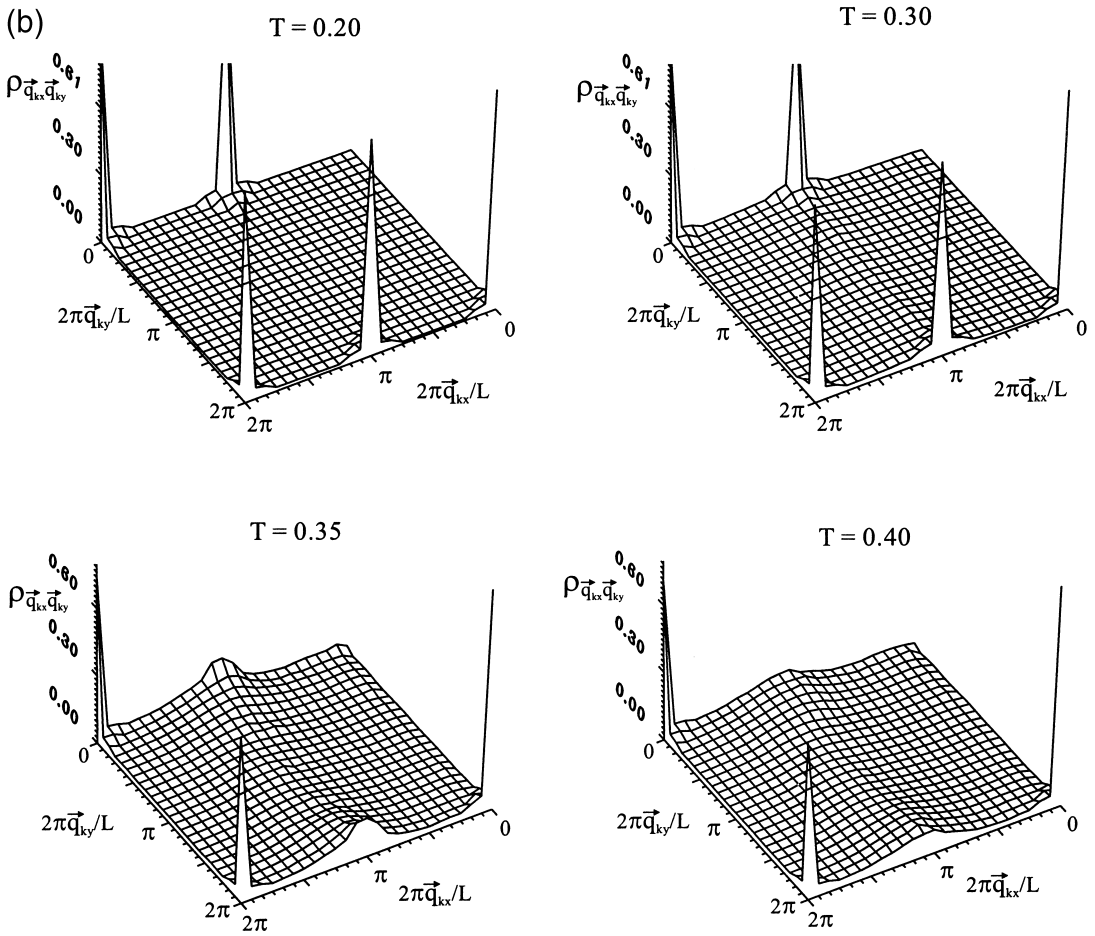

Fig. 57. (*Continued*).

surfaces do not exhibit any phase transition due to the possible order–disorder transition but the loss of epitaxial ordering occurs gradually at rather high temperatures and is accompanied by desorption (Fig. 59). In the case of films with the density exceeding the density of the (1×1) structure, the excess particles form the second layer which appears to also order into the (1×1) structure with the adsorbed particles located over the centers of squares formed by the particles of the first layer. Fig. 59b demonstrates that desorption from the second layer of a dense bilayer system starts at considerably lower temperatures than from the first layer. This figure also shows that the presence of a dense second layer stabilizes the first adsorbed layer.

The stability of the ordered (1×1) structure in the first layer is quite sensitive to even small changes of the surface corrugation as well as to the density changes in the film. Already, for the corrugation parameter equal to 0.9 and as soon as the film number density becomes larger than 1.0 the adsorbed layer shows a quite high tendency to form an uniaxially ordered phase in the first layer. Only when the film density becomes sufficiently high the adsorption in the second layer occurs. It is interesting to note that the formation of the second layer causes gradual restructuring of the first layer, which recovers the

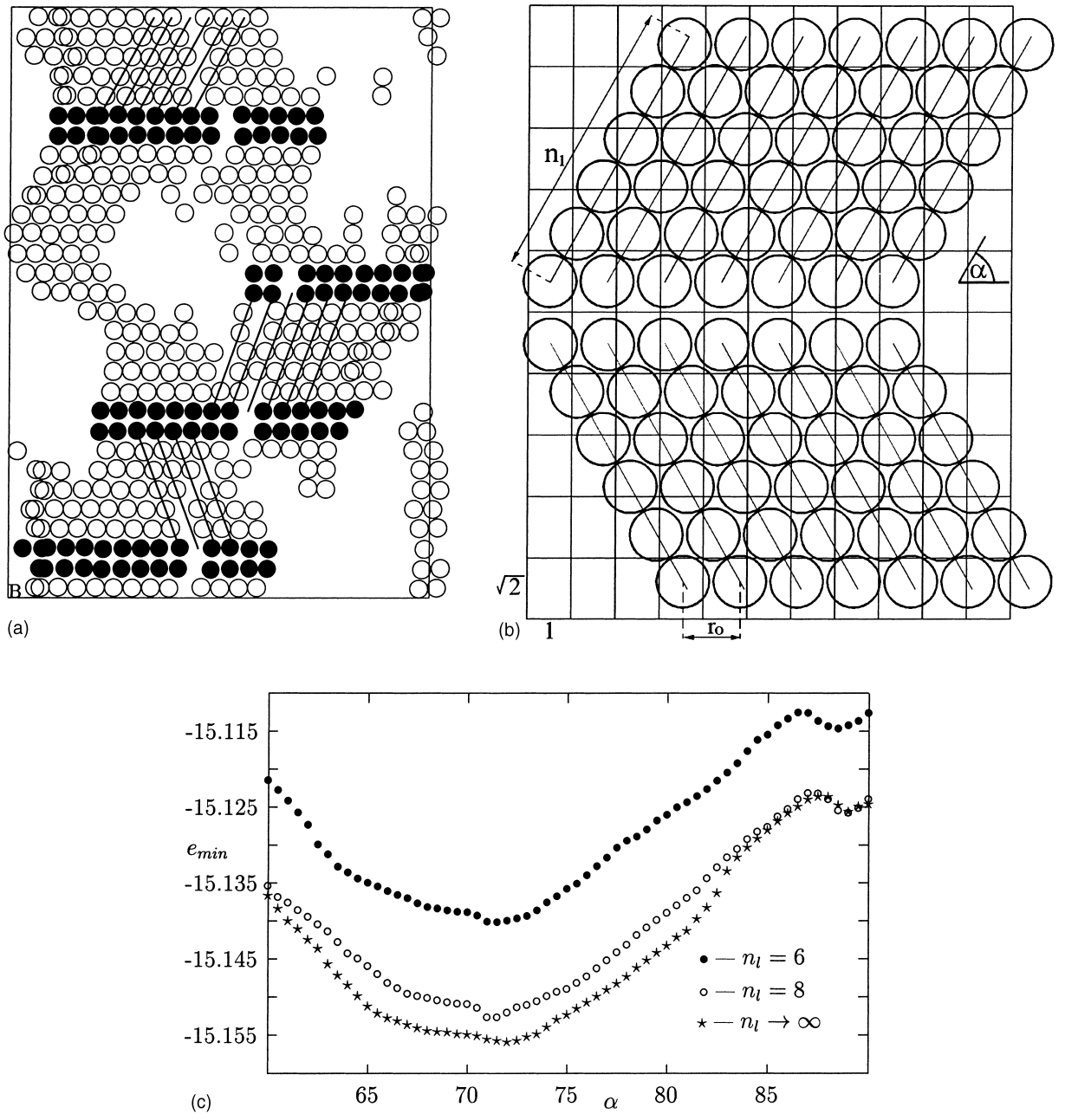

Fig. 58. (a) A snap-shot of the equilibrium configuration for the system of 200 Lennard-Jones particles with $\sigma^* = 1.20$, adsorbed on the (110) plane of a model f.c.c. crystal surface characterized by the corrugation parameter $V_b = 0.8$ at the temperature of $T^* = 0.05$. Particles separating differently oriented domains are shown as filled circles and lines show the orientation of different domains. (b) Schematic representation of the orientationally aligned striplike structure used in the ground state calculations of the tilting angle ϑ. (c) Changes of the energy of the structure depicted in (b) with the tilting angle and obtained for different number of particles in a single strip (n_l) (from Ref. [133]).

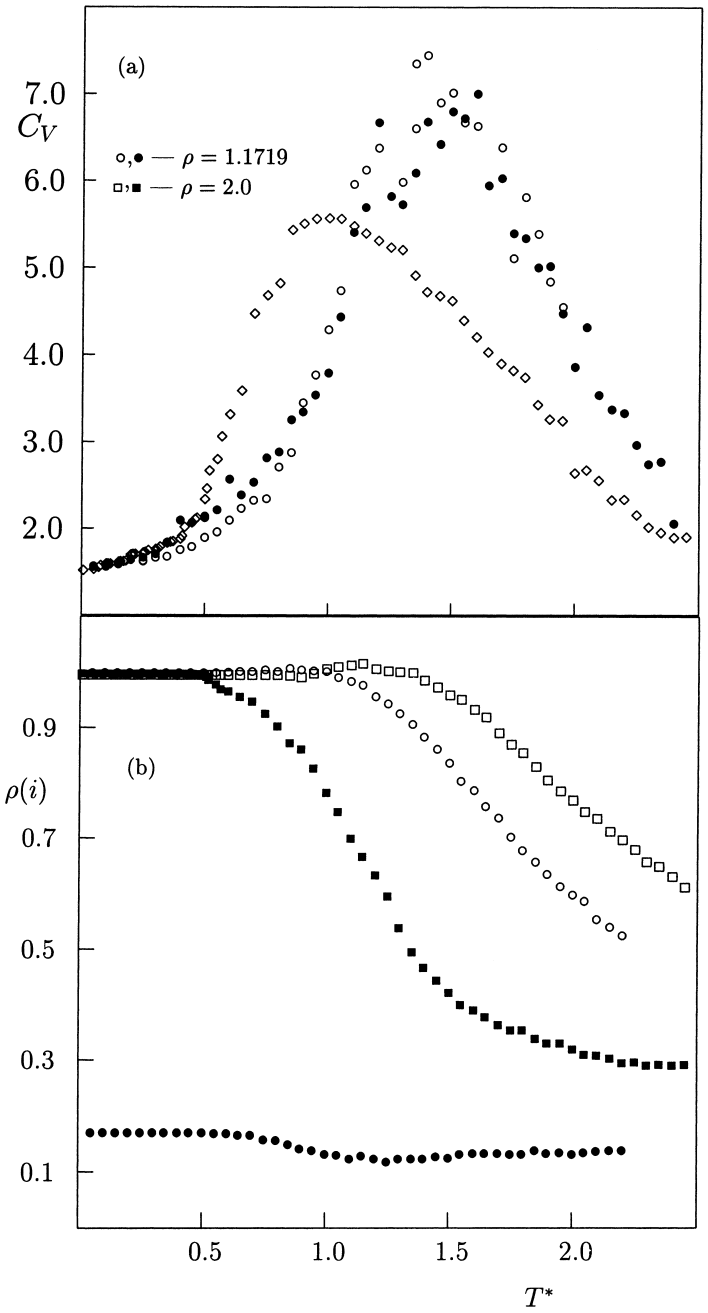

Fig. 59. Temperature changes of the heat capacity (a) and the layer densities (b) for the adsorbed films of Lennard-Jones particles of $\sigma^* = 0.8$ of different number density (shown in the figure) formed on the (100) plane of a model f.c.c. crystal characterized by the high corrugation of the surface potential (corrugation parameter $V_b = 1.0$) obtained from a Monte Carlo simulation performed for the system of size $16 \times 16 \times 10$ (from Ref. [163]).

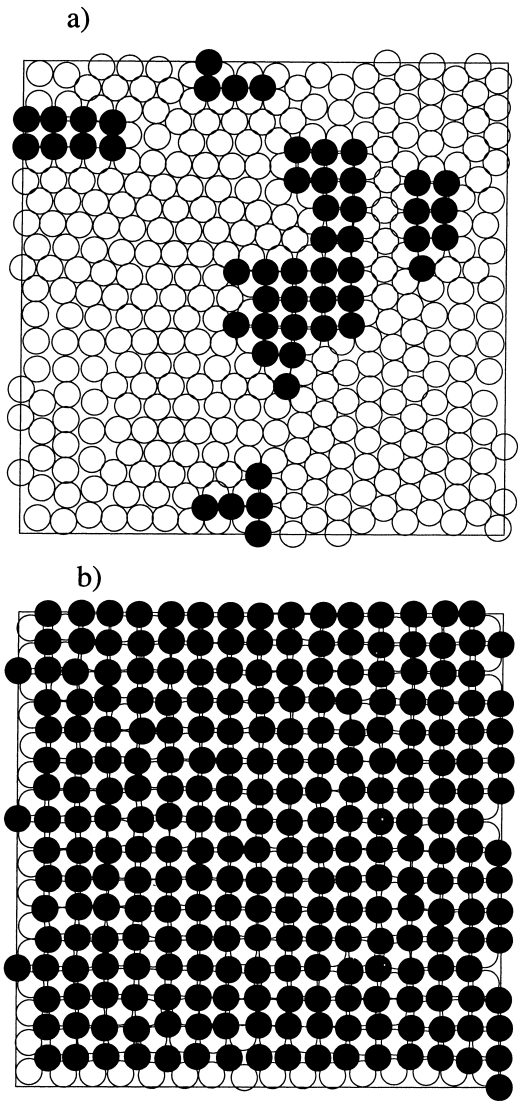

Fig. 60. Snap shot configurations for the adsorbed layer of Lennard-Jones particles of $\sigma^* = 0.8$ on the (100) plane of the model f.c.c. crystal with the corrugation parameter $V_b = 0.9$ recorded at the temperature $T^* = 0.02$ and the total film number density equal to $\rho_n = 1.5625$ (a) and 2.0 (b). Particles located in the first layer are represented by open circles while those from the second layer by filled circles (from Ref. [163]).

ordered (1×1) structure (see Fig. 60). Thus, the appearance of the second layer exerts a force which pushed the adsorbed atoms from the first layer back into the registry positions. The question of the equilibria involving monolayer and bilayer systems was addressed in experimental [411] as well as in theoretical [91,92,412] and computer simulation [63,162,413] studies. The systems that have been studied theoretically and with the help of computer simulations were quite different, however. The substrate was assumed to be either noncorrugated [91,92] or to possess a graphite-like structure [162]. The available experimental data refer only to adsorption on graphite [411] and such systems are beyond

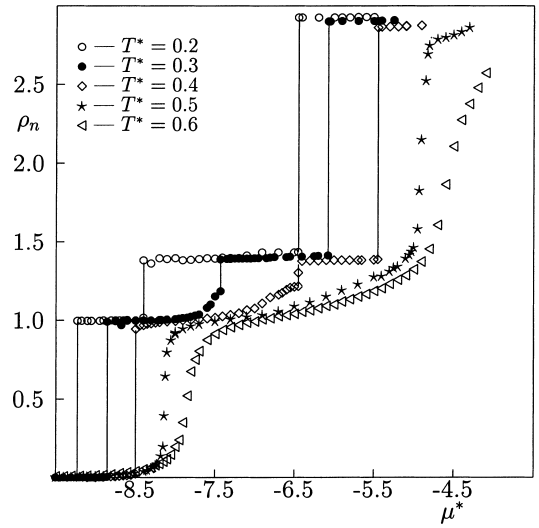

Fig. 61. Adsorption isotherms obtained from grand canonical Monte Carlo calculations for a model system of Lennard-Jones fluid in contact with the (100) plane of f.c.c. crystal of the size 20×20 lattice sites and characterized by the corrugation parameter $V_b = 0.8$ at different temperatures (shown in the figure). (From Ref. [63].)

the scope of our article. We mention here only that in general the formation of the second, as well as the higher layers was found to be a very important factor determining the structure of the lower layers and, in some cases, it was found to lead to the commensurate–incommensurate transition between layers [162].

Instead of working in the canonical ensemble, with a fixed total density and temperature, in many cases a new important insight into the properties of adsorbed systems can be obtained from simulations carried out in the grand canonical ensemble, in which the controlling intensive variable is the chemical potential. Fig. 61 shows typical examples of adsorption isotherms for the Lennard-Jones fluid in contact with the (100) plane of an f.c.c. crystal characterized by the corrugation parameter $V_b = 0.8$ at different temperatures and obtained from Monte Carlo simulations [63]. These isotherms demonstrate the formation of the registered (1×1) structure of number density $\rho_n = 1.0$ at low temperatures, the transition to a much denser incommensurate solid monolayer as well as the layering transition due to the condensation of the second layer. The identification of the different monolayer phases mentioned above was done by the calculation of the average nearest neighbor distances between the adsorbed atoms, the calculation of the density profiles as well as by a direct inspection of the configurations recorded during the simulation runs. Fig. 62 (a), (b) presents examples of the configurations corresponding to the registered (1×1) structure and to the incommensurate phase of hexagonal symmetry, while (c) shows the density profiles corresponding to those two phases. In the case of the incommensurate phase the locations of adsorbed particles show pronounced deviations from planarity.

This system also shows that the formation of a second layer considerably affects the structure of the first adsorbed layer. A dense incommensurate monolayer does not show a perfect hexagonal structure, but always exhibits local distortions and defects (see Fig. 63a). On the other hand, dense bilayer films appear to be nearly perfectly hexagonally ordered (see Fig. 63b) and exhibit only a small rotation with respect to the underlying substrate lattice. It was also shown that the low temperature monolayer has a little lower density than the first layer in a dense bilayer system. The compression of the first layer due

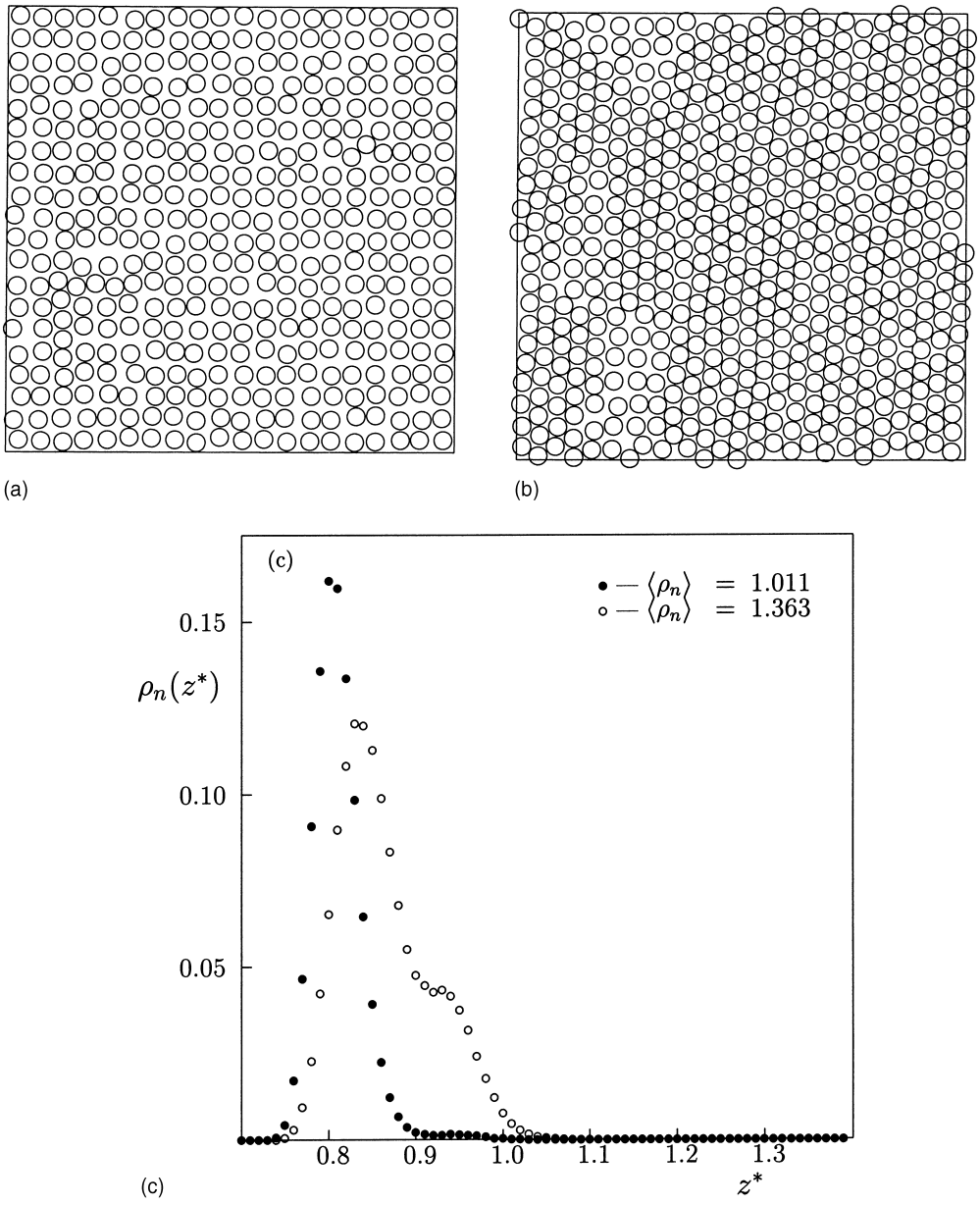

Fig. 62. (a), (b) Examples of configurations for the same system as in Fig. 61, recorded at the temperature $T^* = 0.2$ and the chemical potential $\mu^* = \mu/\varepsilon = -8.45$ on both sides of the commensurate (a) to the incommensurate (b) transition. (c) The corresponding local density profiles (averaged over the entire surface) for both phases ((•) commensurate phase and (○) incommensurate phase). Average densities of both phases are given in the figure. (From Ref. [63].)

to the formation of a second layer, lowers the average nearest neighbor distance by about 1% and this value is considerably greater than predicted by theoretical calculations [92] for hexagonal films formed on a flat surface.

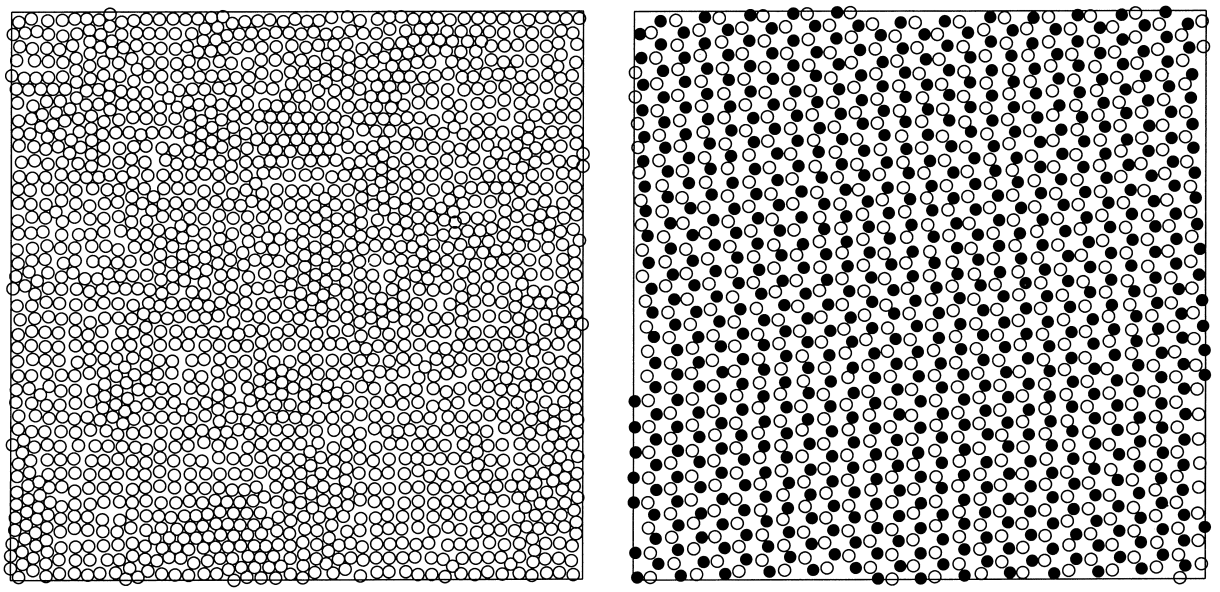

Fig. 63. Examples of configurations for the dense monolayer film at $T^* = 0.3$ and $\mu^* = -7.5$ (a) and bilayer film at $T^* = 0.15$ and $\mu^* = -6.40$ (b) recorded for the same system as in Fig. 61, but for a larger surface size equal to 40×40. (From Ref. [63].)

Fig. 64 shows the phase diagram for the system discussed above and obtained from the both grand canonical and canonical ensemble Monte Carlo simulations. The locations of phase transitions were established from the adsorption isotherms (cf. Fig. 61) and from the temperature changes of the heat capacity (in the canonical ensemble), which enables to locate the melting in the first as well as in the second layer (see Fig. 65).

The data shown in Fig. 65 demonstrate that the temperature of the melting transition of the incommensurate monolayer solid phase moves towards higher values when the density of that phase increases. Only for the films which exhibit the formation of the second layer the melting temperature is constant and equal to about 0.5. A quite similar effect was found experimentally for nitrogen adsorbed on graphite [55]. It was demonstrated that it is connected with a different mechanism of the melting transition in submonolayer and dense monolayer solid films. A submonolayer solid does not occupy the entire surface but rather forms high density islands which coexist with a dilute phase. Upon melting the more or less uniform fluid phase is formed and spreads over the entire surface. This cannot happen in an already dense monolayer since there is not enough space for the fluid phase. The only possibility for the liquid monolayer to appear is the decrease of the density in the first layer by the promotion of the second layer. This mechanism was found in the computer simulation studies for methane films on graphite [159] and for argon films on (100)MgO [414]. Note that this last system is characterized by the square symmetry of the surface lattice. In the case of the model systems discussed above, it was also found that submonolayer films melt without any effects due to the promotion of the second layer, while the melting of a dense monolayer solid is accompanied by the transfer of particles from the first to the second layer (see Fig. 66). In the case of surfaces with lower corrugation of the surface potential the

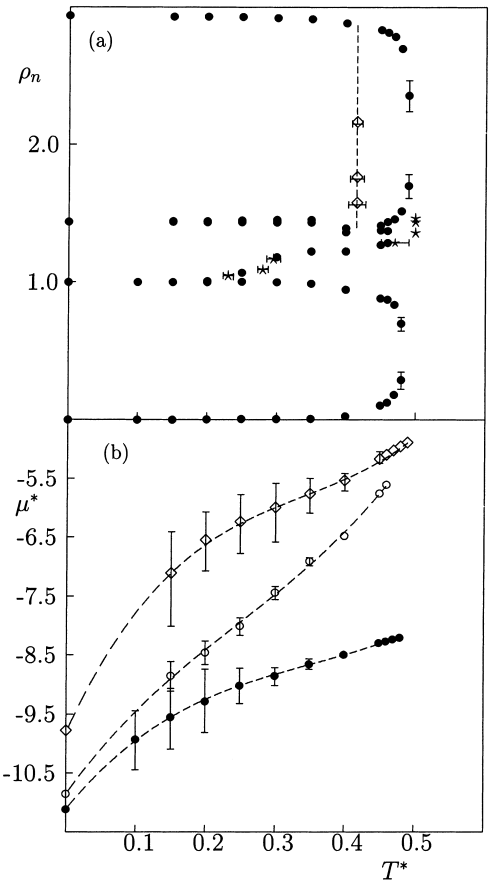

Fig. 64. Phase diagram for the Lennard-Jones adsorbed bilayer film formed on the (100) plane of an f.c.c. crystal characterized by the corrugation parameter $V_b = 0.8$. (a) The phase diagram in the plane (ρ_n, T^*). Filled points are the results of grand canonical Monte Carlo calculations, while stars and diamonds correspond to the canonical ensemble calculations. The triple line of the solid–liquid–gas coexistence in the second layer is shown as a broken vertical line. (b) Phase diagram in the (μ^*, T^*) plane derived from the grand canonical ensemble Monte Carlo simulation. The gas–commensurate (1×1) phase transition points are shown as filled points, the commensurate–incommensurate transition points in the first layer are represented by open points, while the layering transition points in the second layer are marked by open diamonds. The location of the gas–(1×1) phase transition at zero temperature was obtained from the ground state calculations, while the locations of the commensurate–incommensurate and layering transitions at zero temperature were estimated by extrapolation of the results obtained for finite temperatures. (From Ref. [63].)

same changes in the mechanism of melting were found [132], but the phase behavior of such systems shows new features. In particular, it was found that the low temperature adsorption isotherms did not show the presence of two phase transitions in the monolayer regime, but rather a single transition corresponding to the gas–incommensurate solid coexistence (see Fig. 67). Only at sufficiently high temperatures two different phase transitions are observed. The first transition corresponds to the gas–liquid condensation, while the second transforms the liquid phase into an incommensurate solid phase. The regimes corresponding to one and two phase transitions in the first adsorbed layer meet at the triple point temperature T_t^* (see Fig. 68). Calculations performed for a series of systems with gradually

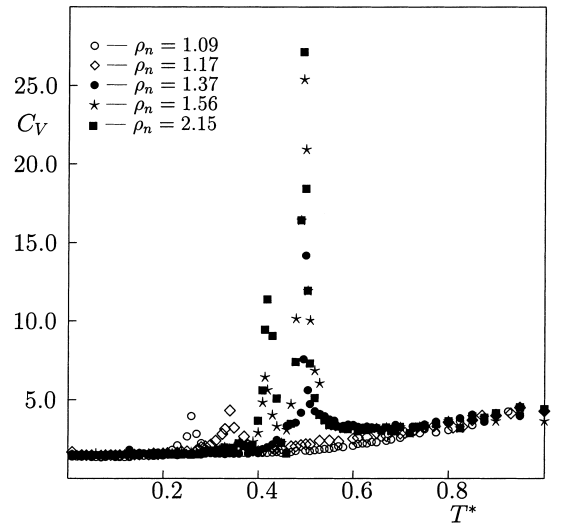

Fig. 65. The heat capacity curves for the Lennard-Jones adsorbed films of different density (shown in the figure) formed on the (100) plane of f.c.c. crystal characterized by the corrugation parameter $V_b = 0.8$ The peaks at the temperature of about $T^* = 0.4$ obtained for the systems with the two highest values of the density correspond to the triple-point melting of the second layer, while the remaining peaks result from the melting of the monolayer incommensurate solid phase. (From Ref. [63].)

decreasing surface corrugation demonstrated that the triple point temperature converges to the value corresponding to the adsorption on a flat surface, which is equal to about 0.4, quite the same as found for a strictly two-dimensional and uniform Lennard-Jones system (cf. Section 5.1). It should be noted

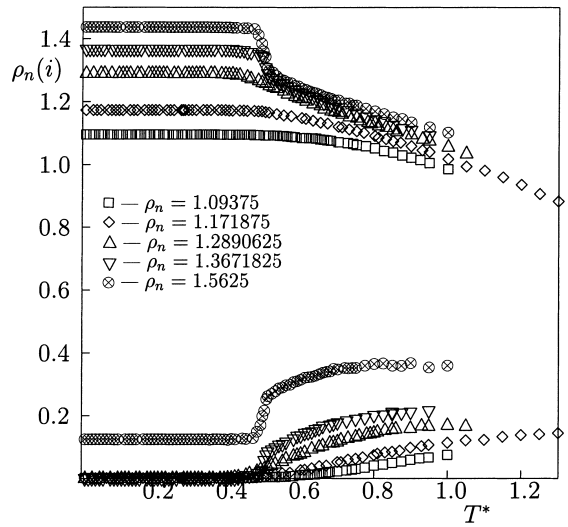

Fig. 66. Temperature changes in the densities of the first and second layers in the films of different total number densities (shown in the figure) formed on the (100) plane of f.c.c. model crystal characterized by the corrugation parameter $V_b = 0.8$ and obtained from the canonical ensemble Monte Carlo simulation study. The upper (lower) family of curves corresponds to the first (second) layer. (From Ref. [63].)

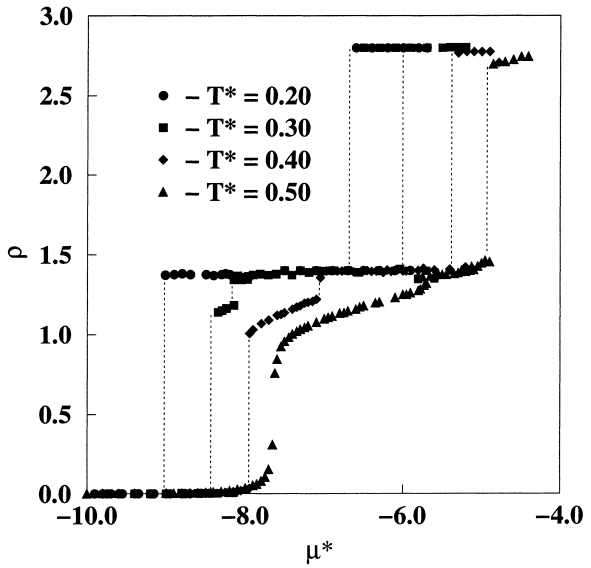

Fig. 67. Adsorption isotherms obtained from grand canonical Monte Carlo calculations for a model system of Lennard-Jones fluid in contact with the (100) plane of a f.c.c. crystal of the size 20×20 lattice sites and characterized by the corrugation parameter $V_b = 0.6$ at different temperatures (shown in the figure). (From Ref. [163].)

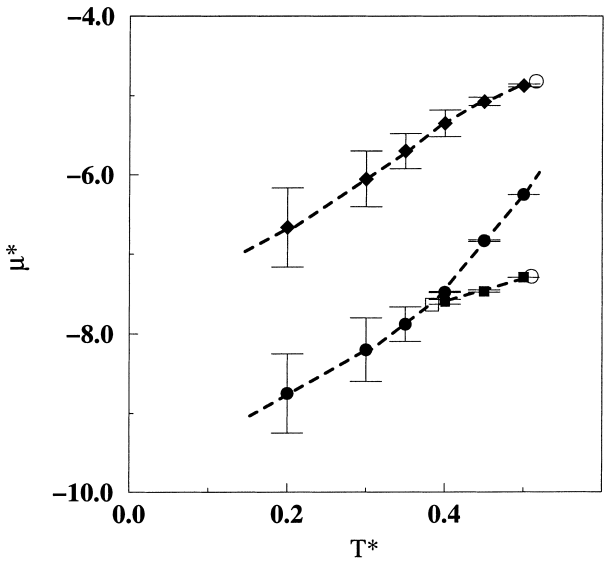

Fig. 68. Phase diagram for the Lennard-Jones adsorbed bilayer film formed on the (100) plane of an f.c.c. crystal characterized by the corrugation parameter $V_b = 0.6$ in the (μ^*, T^*) plane derived from the grand canonical ensemble Monte Carlo simulation. The gas–incommensurate solid and the liquid–incommensurate solid transition points are marked by filled circles, the gas–liquid transition points are represented by filled squares and the layering transition in the second layer by filled diamonds. The critical points for the condensation in the first and in the second layer are shown as open circles, while the triple point in the monolayer is marked by an open square. (From Ref. [163].)

that the behavior of adsorption isotherms as those shown in Fig. 67 is very often observed in real systems [51,108,138]. Of course, the results presented above do not correspond directly to any real situation, primarily because the assumed relative size of the adsorbed atoms and the surface unit cell is much smaller than in most experimental systems. As it was already shown in Section 5.2, the adsorbed atoms are usually too large to order into the (1×1) structure. Both experimental [108] and theoretical [15] studies of even quite small argon atoms adsorbed on the (100) plane of MgO crystals pointed out that the adsorbed films order into the (2×3) high order commensurate phase at low temperatures. Meichel et al. [15] presented theoretical calculations of the ground state energy for different high-order commensurate superstructures formed by noble gases (Ar, Kr, Xe) on the (100)MgO surface and found that in the case of Kr and Xe the most stable state corresponds to the (2×2) structure, though it was also shown that some other high-order commensurate structures may also occur. At finite temperatures, the stability of the (2×3) structure for Ar was found to be limited only to submonolayer coverages and at the onset of the second layer formation a little denser (2×4) structure is formed. This was demonstrated by LEED measurements and supported by theoretical calculations. In the case of krypton, both experiment and theory showed that the (2×2) structure competes with the (2×8) structure. In the case of the largest Xe atoms, the LEED experiments suggested that the monolayer film is incommensurate with the substrate and shows hexagonal packing.

5.5. Orientational effects in molecular films

Considering the adsorption of nonspherical molecules on crystalline surfaces one faces additional complications due to possible orientational ordering of the adsorbed molecules. Such effects were demonstrated to be of great importance for the structure and thermodynamic properties in many experimental systems [55,147,415–418]. The most thoroughly studied systems are the monolayer films of carbon monoxide and nitrogen on graphite [55]. The phase diagram for a monolayer of nitrogen on graphite is probably the best characterized case in molecular adsorption. Numerous experimental [415–417,419,420], theoretical [418,421–424] and computer simulation [55,425–428] studies were carried out in order to understand the role played by molecular nonsphericity in such films. As compared to the films of simple spherical adsorbates, in particular noble gases, which already exhibit very complex phase behavior of adsorbed layers (see previous sections), the adsorbed films consisting of nonspherical molecules show many new features.

Already the mean field theory applied to study orientational effects in two-dimensional point quadrupoles arranged on an hexagonal lattice under the influence of a uniform substrate field predicted the appearance of four distinct orientationally ordered phases [421]. Experiments for nitrogen and carbon monoxide films on graphite revealed the presence of three of them [400,416,418,419,429,430]. Only the so-called ''ferro'' phase was not found, but it is not physically feasible to occur in such systems as its formations requires rather strongly repulsive surface potential. Experimental findings were also supported by computer simulations [55,425–428,431,432].

Strong orientational effects were also found in numerous experimental [23,433–435], theoretical [387,422–424,435,436] and computer simulation [23,437–439] studies of linear molecules adsorbed on various surfaces characterized by square and rectangular symmetry.

In this section we briefly discuss the behavior of selected adsorbed films formed on crystals with a square symmetry of their surfaces, such as ionic alkali halides and MgO crystals, and on the (110) plane of metal crystals. Then we consider some simple theoretical approaches based on the lattice gas model,

which demonstrate that monolayer films of linear molecules do undergo various phase transitions connected with a different orientational ordering. Finally, we concentrate on computer simulation studies of models and of real adsorbed films formed on square surfaces with a finite corrugation of the substrate potential.

The interaction of multiatomic adsorbates with a solid surface is much more complex than in the case of simple atomic gases. Note that to specify the location of a simple homonuclear diatomic molecule with respect to the solid surface requires a set of five coordinates, three of them are the coordinates of the center of mass and the remaining two specify the orientation of the molecular axis. Thus, in order to calculate thermodynamic properties of an isolated molecule in the vicinity of the solid surface one needs to evaluate five-fold integrals. For instance, the Henry constant for a fluid of diatomic molecules in contact with a corrugated surface is given by [440]

$$K_{\mathrm{H}}(T) = \frac{1}{A}\int \{\exp[-\beta v(\boldsymbol{r}_{\mathrm{c}}, \vartheta, \varphi)] - 1\}\, \mathrm{d}\boldsymbol{r}_{\mathrm{c}}\, \mathrm{d}\vartheta\, \mathrm{d}\varphi, \tag{5.21}$$

where $\boldsymbol{r}_{\mathrm{c}} = (x_{\mathrm{c}}, y_{\mathrm{c}}, z_{\mathrm{c}})$ specifies the location of the center of mass relative to the substrate and the angles ϑ and φ specify the orientation of the molecular axis with respect to the substrate. The theoretical description of dense systems requires the inclusion of the adsorbate–adsorbate interactions and this introduces further complexity. The energy of interaction between a pair of simple diatomic molecules depends of their distance and relative orientations so that evaluation of thermodynamic properties of adsorption systems requires very tedious calculations. Various theoretical approaches and approximations have been reviewed by Patrykiejew and Sokołowski [441].

Among the most intensively studied adsorption systems characterized by a square symmetry of the surface lattice are CO_2 and CO on (100)NaCl surface [101,387,437,439]. Those systems were mostly studied by helium scattering [99,433] and particularly intensively by infrared spectroscopy [101,368,387,442–444]. Also, theoretical [436] and computer simulation [437–439] studies were reported in the literature.

Low temperature infrared measurements of Heidberg et al. [368] demonstrated that CO_2 adsorbed on NaCl undergoes a first-order phase transition between the two-dimensional gas and the commensurate solid phase. This solid phase corresponds to the (2×1) structure in which the molecules are tilted relative to the surface at the angle ϑ close to 60°. A similar conclusion was reached by Lange et al. [433] who used helium scattering and by Schimmelpfennig et al. [445] from LEED measurements. Liu et al. [446] also studied monolayers of CO_2 on NaCl by Helium scattering and found that dense monolayer films order into the $(2\sqrt{2} \times 2\sqrt{2})R45°$ structure. Recent molecular dynamics calculations of Vigiani et al. [438] demonstrated also the formation of the (2×1) herringbone commensurate phase with the tilting angle of the molecular axis about 60°. They have performed calculations for finite patches of adsorbed CO_2 films as well as for a system with periodic boundary conditions and found quite important differences in the equilibrium structure of the low temperature phase. Though in both cases the (2×1) herringbone phase was observed, in the case of finite patches they found differently oriented domains shown schematically in Fig. 69, while in the simulation with periodic boundary conditions only one orientation of the ordered phase was observed. The domains of differently oriented herringbone structure are separated by walls, which were found to be very stable and did not vanish under repeated annealing. This high stability of walls was found to be directly connected with a strong corrugation of the adsorbate–substrate potential. Quite similar calculations performed in the case of only weakly corrugated surfaces inevitably led to the formation of one-domain structure after repeated

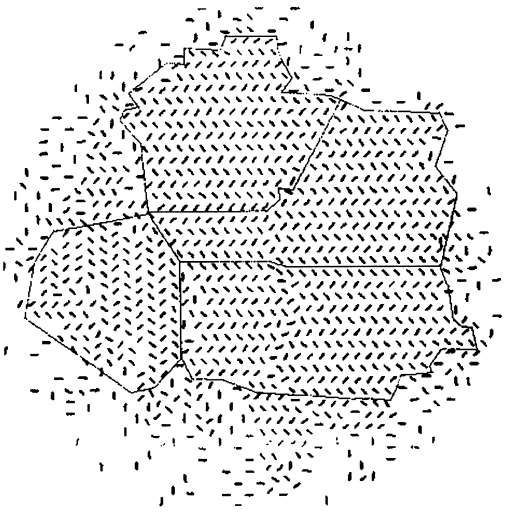

Fig. 69. The domain structure of the CO_2 monolayer on the NaCl crystal (from Ref. [438]).

annealing of the sample. While discussing the properties of CO_2 films on NaCl it is noteworthy that a similar system of three-atomic OCS molecules was also found to exhibit the (2×1) structure, as deduced from the helium atom diffraction measurements [435]. Energy minimization calculations indicated that the adsorbed molecules are only slightly tilted with respect to the solid surface with molecular axes parallel to each other, but with alternate orientation (O–C–S and S–C–O) on each sublattice.

Monte Carlo simulations for the carbon monoxide monolayer on NaCl [437] demonstrated the formation of the $p(2 \times 1)$ structure with a glide plane and with the carbon atom end down and pointing towards an Na^+ ion and the tilt angle of about 24° at low temperatures. As the temperature increases, this orientationally ordered phase undergoes a transition to the orientationally disordered (1×1) structure. The results of Monte Carlo simulations were found to be quite consistent with experimental data [447,448] and with theoretical calculations [436,449,450]. The transition temperature was estimated to lie in the range between 30° and 35° K, and above the transition temperature the adsorbed films were observed to be localized.

Highly ordered structures were also observed in monolayer films of various molecular adsorbates on (100)MgO [366,451] and on (100) and (110) planes of metal crystal surfaces [18,23,452–456]. In most cases chemisorption rather than physical adsorption occurs and is often accompanied by the dissociation of adsorbed molecules [454]. Such systems are beyond the scope of the present review. Here we just mention recent molecular dynamics simulation study of water adsorption on the (100)MgO surface performed by Girardet et al. [456]. From the ground state calculations, based on the energy minimization for various high order commensurate structures, it was found that the most stable configuration corresponds to the (1×1) structure. It should be noted that experimental studies [457–459] pointed out that the monolayer film of water forms a very stable (3×2) structure as well as a denser structure of unknown internal structure that is stable only at sufficiently low temperatures below 180 K. Molecular dynamics simulation confirmed the existence of the (3×2) structure at low temperatures with the water molecules oriented parallel to the surface and the water molecular symmetry axis pointing to $\pm 45°$ and $\pm 135°$. Upon the increase of the total density of admolecules in

the system the structure of the adsorbed monolayer started to change and complicated structures with domains of the $(1 \times 1), (2 \times 1)$ as well as (3×2) phases were observed. When the second layer was formed on the top of the first layer, it was found to exhibit hexagonal symmetry. For still higher water concentration, the second and higher layers started to develop an ice-like three-dimensional structure without any visible effect on the structure of the first layer. This peculiar behavior was attributed to the lack of hydrogen bonds between the molecules of the second and the first layers, while the molecules located in the second and higher layers are evidently subject to weak association through hydrogen bonds.

In general the orientational transitions observed in various adsorbed films of heteroatomic molecules on ionic crystals usually occur at considerably lower temperatures than the localized-to-mobile transition, so that the adsorbed molecules remain tightly bonded to adsorption sites at the temperatures well above the orientational transition. Similar behavior was also observed for simple homonuclear molecules adsorbed on graphite [55]. This allows to use a lattice gas model formalism to investigate orientational transitions in adsorbed films [55,421–424,460,461]. A simple theoretical model for adsorption of diatomic molecules adsorbed on a square lattice was considered by Patrykiejew [422–424]. The model assumed that each adsorbed molecule was placed over an adsorption site with a certain ''reference'' point chosen within a molecule placed directly above the center of the adsorption site. This reference point was either the center of mass of a molecule or the center of one of the atoms. In either case the potential of interaction between a molecule and the substrate is a function of the orientation only. Also, the potential of interaction between a pair of molecules adsorbed on adjacent sites depends only on their relative orientation. Note that the periodic variation of the surface potential gives rise to the appearance of a certain potential barrier for rotation. The state of a single adsorption site is given by

$$\rho_i^{(1)}(\omega_i) = n_i(\omega_i), \tag{5.22}$$

where $n_i = 0(1)$ when the ith site is empty (occupied) and $\omega_i = (\vartheta, \varphi)$ represents the orientation of a molecule adsorbed on the site i. In the framework of a mean-field approximation the behavior of the adsorbed film can be deduced from the one-particle orientation-dependent distribution function

$$h^{(1)}(\theta, \omega) = \theta \tilde{h}^{(1)}(\omega), \tag{5.23}$$

where θ is the surface coverage. With the above assumptions one readily obtains the expression for the Helmholtz free energy of the film (per particle)

$$f = kT\left(s_0 + \int \mathrm{d}\omega\, \tilde{h}^{(1)}(\omega)\left[\ln \tilde{h}^{(1)}(\omega) + \frac{1}{kT} v(\omega) + \frac{2\theta}{kT}\int \mathrm{d}\omega'\, \tilde{h}^{(1)}(\omega') u(\omega, \omega')\right]\right\}, \tag{5.24}$$

where

$$s_o = \frac{1}{\theta}\ln(1-\theta) + \ln\left(\frac{\theta}{1-\theta}\right) \tag{5.25}$$

and $u(\omega, \omega')$ represents the interaction potential acting between a pair of nearest neighbor admolecules. To determine the form of the orientation distribution function and then the thermodynamic properties of the system one can minimize the free energy, which is a functional of $\tilde{h}^{(1)}(\omega)$, with respect to $\tilde{h}^{(1)}(\omega)$, which yields

$$kT \ln\left[\tilde{h}^{(1)}(\omega)\lambda\right] = -v(\omega) - 2\theta \int \mathrm{d}\omega \tilde{h}^{(1)}(\omega) u(\omega, \omega) \tag{5.26}$$

with

$$\lambda = \int \mathrm{d}\omega \exp\left\{ -\left[v(\omega) + 2\theta \int \mathrm{d}\omega' \tilde{h}^{(1)}(\omega') u(\omega, \omega') \right] / kT \right\}. \tag{5.27}$$

In the limit of $\theta \to 0$, i.e., for a single molecule, it was found that the surface corrugation influences molecular orientation in a very much similar way as it affects atomic diffusion from one site to another. In particular, the configurational heat capacity was found to exhibit a broad peak with the maximum at the temperature equal to

$$kT_{\max}/V_{\mathrm{r}} = 0.2 \pm 0.01, \tag{5.28}$$

where V_{r} is the potential barrier for rotation. Relationship (5.28) was found to hold independently of the elongation of adsorbed molecules and the size of constituting atoms with respect to the size of the surface unit cell.

When the density of the adsorbed film increases, the lateral interactions between admolecules begin to contribute to the total energy of the film and may lead to the shift of the heat capacity maxima towards higher temperatures or to exhibit discontinuities, indicating the presence of first-order orientational phase transitions [423,424]. The nature of those changes depend primarily on the elongation of the adsorbed molecules. In the high density films of such elongated molecules the effective potential barrier for rotation is rather due to admolecule–admolecule interaction than merely due to surface corrugation. An example of the phase diagram obtained from such mean-field calculations is presented in Fig. 70.

Of course, the observed structural changes are, to a high extent, connected with the assumed rigid lattice structure of the film. In a real situation it is quite likely that the adsorbed molecules would start to assume off-lattice positions prior to the rotational transition predicted for the lattice gas model, in particular, in the case of adsorbed films weakly bonded to the substrate surface.

Continuous space Monte Carlo simulations in the canonical ensemble have been performed for a monolayer of homonuclear diatomics of different elongation adsorbed on the (100) plane of an f.c.c. crystal of varying surface corrugation [462]. The simulation method was the same as used in the study of previously discussed adsorbed films of monoatomic adsorbates (see Section 5.4). Thus, the adsorbate molecules could move freely in the three-dimensional space above the crystal surface, which was assumed to be a source of the potential given by Eq. (2.2).

The calculations were carried out for small molecules built of two identical atoms of diameter σ bonded together at the distance d and for the total density of admolecules corresponding exactly to one completely filled registered layer with one molecule per surface unit lattice cell.

It was found that the properties of the adsorbed layer are very sensitive to even small changes of the molecular elongation and that for small elongations orientational disordering occurs at much lower temperatures than positional disordering of registered structures.

Even for small molecules with $\sigma^* = \sigma/a = 0.8$ and of elongations $d^* = d/a = 0.1$ and 0.2, which at sufficiently low temperatures assume parallel orientation relative to the substrate surface with the molecular axes along the symmetry axes of the crystal ($\varphi = k\varphi/2$ ($k = 0, 1$)) and form a simple (1×1) structure with the molecular center of mass located directly above the center of the surface unit lattice cell, the Monte Carlo simulations clearly demonstrated that nonsphericity plays an important role and both systems behave quite differently. Fig. 71 shows examples of the temperature changes of the heat capacity for both systems and it is clear that the shorter molecules exhibit only a rather small and broad

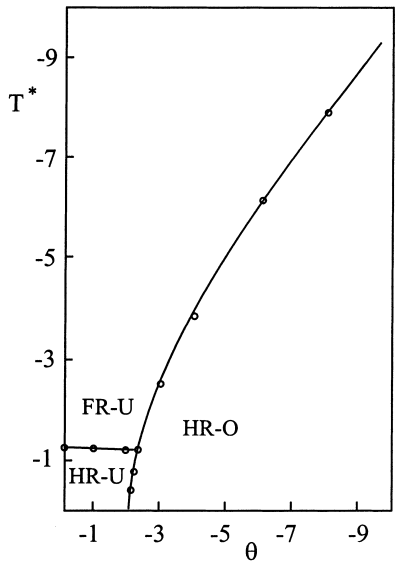

Fig. 70. Phase diagram in the coverage (θ) – reduced temperature ($T^* = kT/\varepsilon_{gg}$) plane for a model of diatomic molecules of $\sigma^* = 1$ and the elongation $d^* = d/a = 0.5$ adsorbed on the (100) plane of an f.c.c. crystal. In the calculations it was assumed that one atom of each adsorbed molecule is located directly over the center of the surface unit lattice cell. The symbols FR-U, HR-U and HR-O mark the regions of stability of different phases. FR-U corresponds to the $c(2 \times 2)$ phase with free rotation, HR-U corresponds to the $c(2 \times 2)$ phase with frozen rotational movement (all molecules assume vertical orientation with respect to the surface), while HR-O is the orientationally ordered $c(2 \times 2)$ phase consisting of two sublattices of differently oriented molecules; on one sublattice the adsorbed molecules are oriented nearly perpendicularly to the surface, while on the other sublattice the molecules exhibit only a slight tilt and are all oriented along one of the symmetry axes of the crystal (from Ref. [423]).

maximum, while the longer ones yield a sharp peak, which indicates the presence of a phase transition. The calculations of the distribution functions of the orientation angles ϑ and φ demonstrated that in both systems the loss of orientational ordering is a gradual process (see Fig. 72) and hence do not allow to explain the anomalous behavior of the heat capacity for the system with $d^* = 0.2$. A deeper insight into the structure of the adlayer can be gained, however, if one probes the short range correlations between orientations of the adsorbed molecules and considers the behavior of the appropriate order parameters, such as

$$P_\vartheta = \langle |\cos \vartheta_{ij}| \rangle = \left\langle \frac{1}{N} \sum_{i=1}^{N} \frac{1}{n_i} \sum_{j(\mathrm{nn})} |\cos(\vartheta_i - \vartheta_j)| \right\rangle \tag{5.29}$$

and

$$P_\varphi = \langle |\cos \varphi_{ij}| \rangle = \left\langle \frac{1}{N} \sum_{i=1}^{N} \frac{1}{n_i} \sum_{j(\mathrm{nn})} |\cos(\varphi_i - \varphi_j)| \right\rangle, \tag{5.30}$$

where the first sum runs over all N molecules in the adsorbed layer and the second sum is taken over all n_i nearest neighbors of the molecule at site i. In both the above cases the order parameter P_φ was found

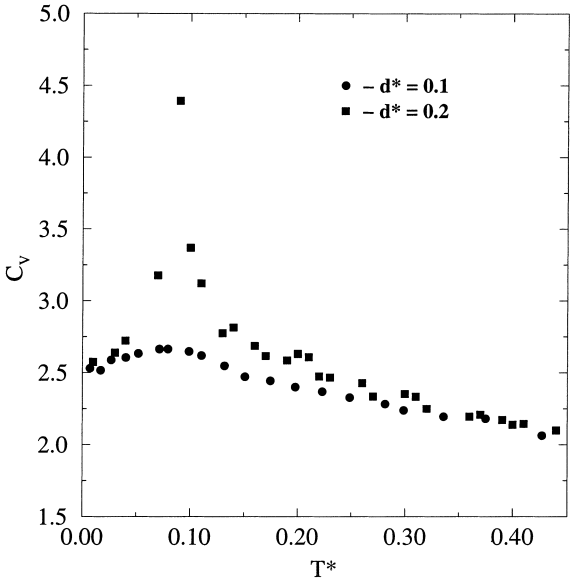

Fig. 71. Temperature changes of the heat capacity for the model monolayer films of homonuclear diatomic molecules of $\sigma^* = 0.8$ and two different elongations d^* (shown in the figure) adsorbed on the (100) plane of a f.c.c. crystal as obtained from Monte Carlo simulation (from Ref. [462]) Note that because of the use of classical (rather than quantum-mechanical) statistical mechanics C_V tends to $5/2$ (in units of the Boltzmann constant) rather than zero as $T \to 0$.

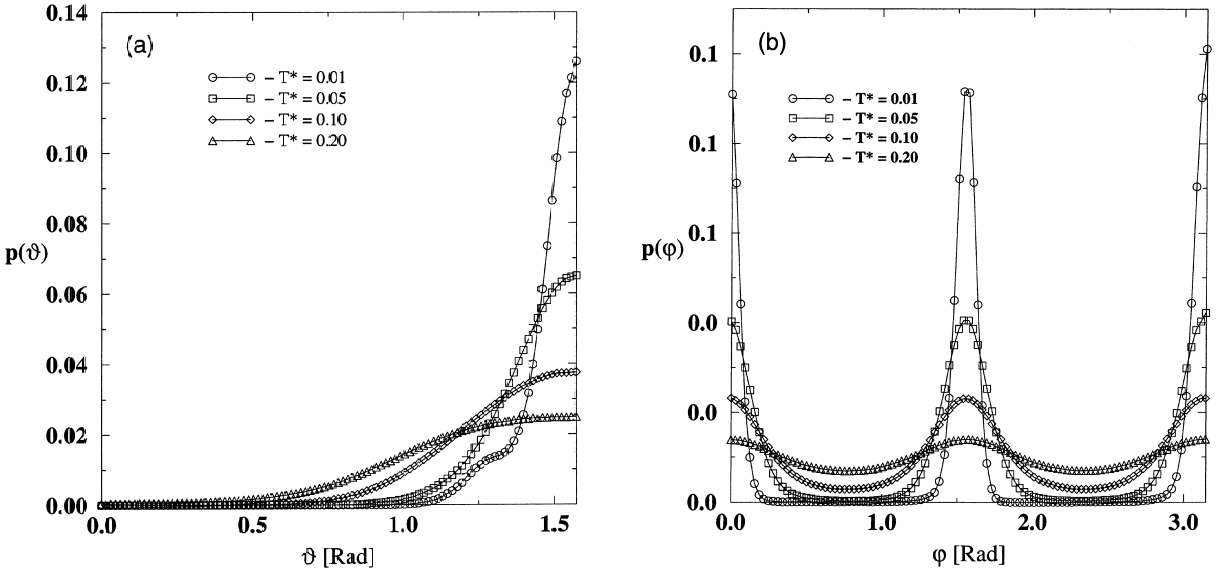

Fig. 72. The angular distribution functions $p(\vartheta)$ (a) and $p(\varphi)$ (b) for the model monolayer film of homonuclear diatomic molecules of $\sigma^* = 0.8$ and the elongation $d^* = 0.2$ adsorbed on the (100) plane of an f.c.c. crystal, obtained from the simulations at different temperatures (shown in the figure). From. Ref. [462].

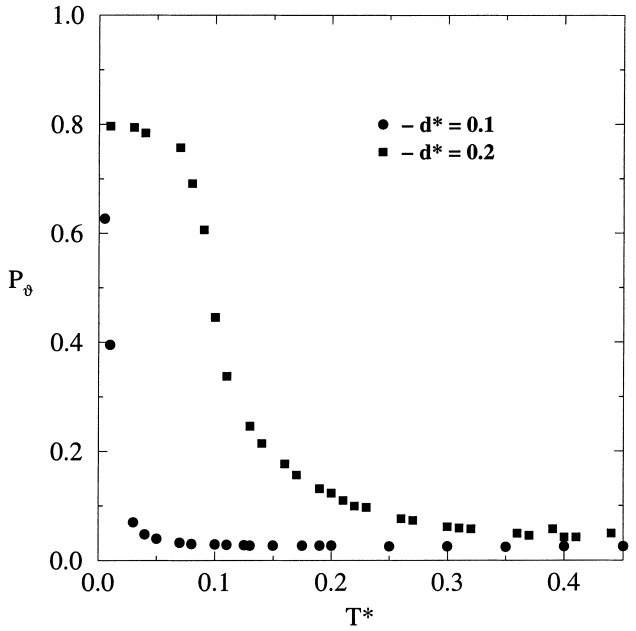

Fig. 73. Temperature changes of the order parameter P_ϑ for the same systems as in Fig. 72 obtained from Monte Carlo simulation (from Ref. [51]).

to change smoothly with temperature, while the behavior of the order parameter P_ϑ indicates that the observed transition for the system with $d^* = 0.2$ can be attributed to a quite abrupt loss of mutually parallel alignment of neighboring molecules (see Fig. 73).

Another type of orientational behavior develops in systems of molecules with larger elongation. Surface corrugation dominates only the positional ordering of the adsorbed film and ensures registry, while the orientational properties of the film are dominated by the admolecule–admolecule interaction. In particular, for the molecules of elongation $d^* = 0.4$ the in-plane orientation of the molecular axes does not agree with the symmetry axes of the surface lattice. Instead, the preferred values of the azimuthal angle are, at sufficiently low temperatures, 45° and 135° (see Fig. 74a), and the molecules are tilted with respect to the surface; the distribution function for the angle ϑ exhibits two maxima at about 34° and 57° (see Fig. 74b). This system was also found to exhibit a sharp orientational transition at the temperature of about $T^* = 0.19$. A direct inspection of the configurations recorded during the simulation runs showed that the system exhibits quite well formed domains of the (2×1) structure, which are not observed at the temperatures above the transition temperature. It should be noted that those domains of the (2×1) structure were found to exhibit different mutual orientation and were separated by walls, quite similar as found in the earlier discussed simulations of CO_2 films on MgO [438].

As it was shown above the identification of orientational ordering in molecular films studied by computer simulations can be done by the calculation of the angular distribution functions and the angular correlation functions. In some cases, however, one needs more detailed information about the system structure to identify the form of both orientational and positional ordering in the film. For instance, in Fig. 75 we present the distribution functions of the angles ϑ and φ for the CO adsorbed on

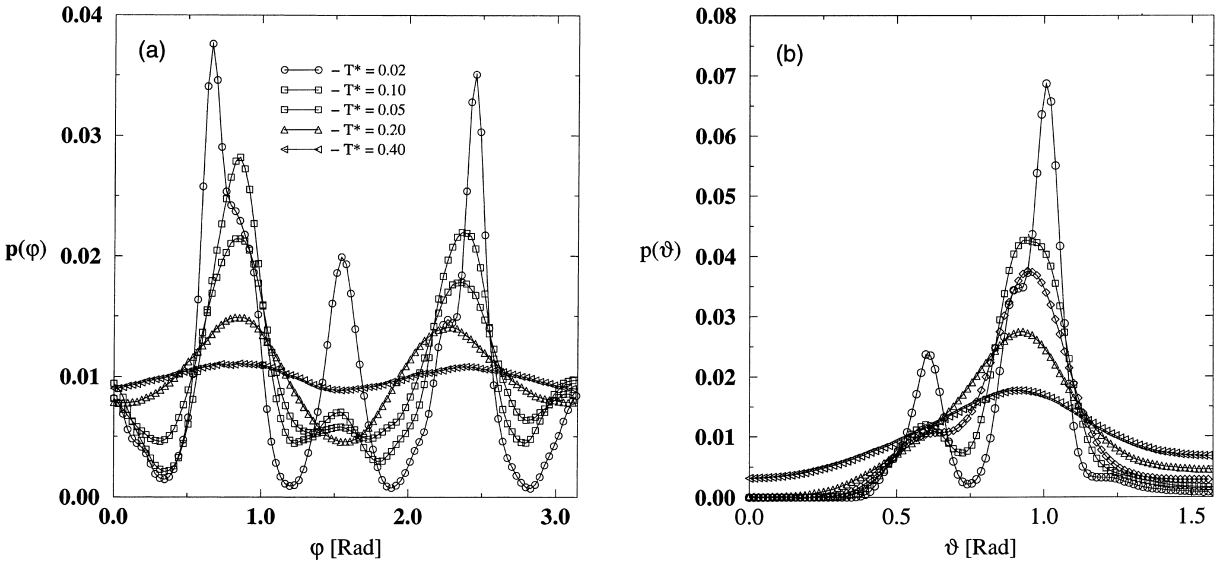

Fig. 74. The angular distribution functions $p(\vartheta)$ (a) and $p(\varphi)$ (b) for the model monolayer film of homonuclear diatomic molecules of $\sigma^* = 0.8$ and the elongation $d^* = 0.4$ adsorbed on the (100) plane of an f.c.c. obtained from simulations at different temperatures (shown in the figure). From. Ref. [462].

MgO, derived from the simulation due to Vu et al. [437] and obtained for a model system of homonuclear diatomic molecules of $\sigma^* = 0.9$ and the elongation $d^* = 0.4$ [462]. It is quite evident that the orientational behavior of both systems is strikingly similar, despite the differences in the structure of the adsorbate molecules. In particular, the distributions $p(\vartheta)$ (Figs. 75b and d) are practically the same. On the other hand, the distributions $p(\varphi)$ (Figs. 75a and c) show that the CO molecules adsorbed on the NaCl are oriented along one of the symmetry axes of the crystal surface, while the model system of homonuclear molecules exhibits the orientation of the adsorbed molecules along the diagonals of the surface unit lattice cells. In the case of CO/MgO system it was shown that the film orders into the (2×1) phase with two sublattices, while our model system shows a quite different sublattice structure. One can probe the sublattice structure of the film by recording the appropriately defined orientational order parameters (for each sublattice) and the angular distribution function $p_0(\vartheta, \varphi)$. It is also possible to investigate positional ordering of the adsorbed molecules by the calculation of the average displacements of the molecular center of mass from the center of the surface unit lattice cell in the x and y directions (Δx and Δy) in different sublattices as well as by the calculation of the corresponding distribution functions for those displacements $p_{\mathrm{p}}(\Delta x, \Delta y)$. Fig. 76 shows the behavior of the distribution functions $p_0(\vartheta, \varphi)$ and $p_{\mathrm{p}}(\Delta x, \Delta y)$ obtained for the above mentioned model system of homonuclear molecules. It is quite evident that one can identify four sublattices. A direct evaluation of the temperature changes of the average displacements $\langle \Delta x \rangle$ and $\langle \Delta y \rangle$ also demonstrated that the low temperature ordered state exhibits a four-sublattice structure and that disordering destroys this sublattice structure (see Fig. 77). Thus, despite the similarity of the angular distribution functions for the above two systems, as demonstrated by Fig. 75, the actual structures of the low temperature ordered states are quite different in both cases. In particular, our model system orders into the (2×2) structure rather than into the (2×1) structure.

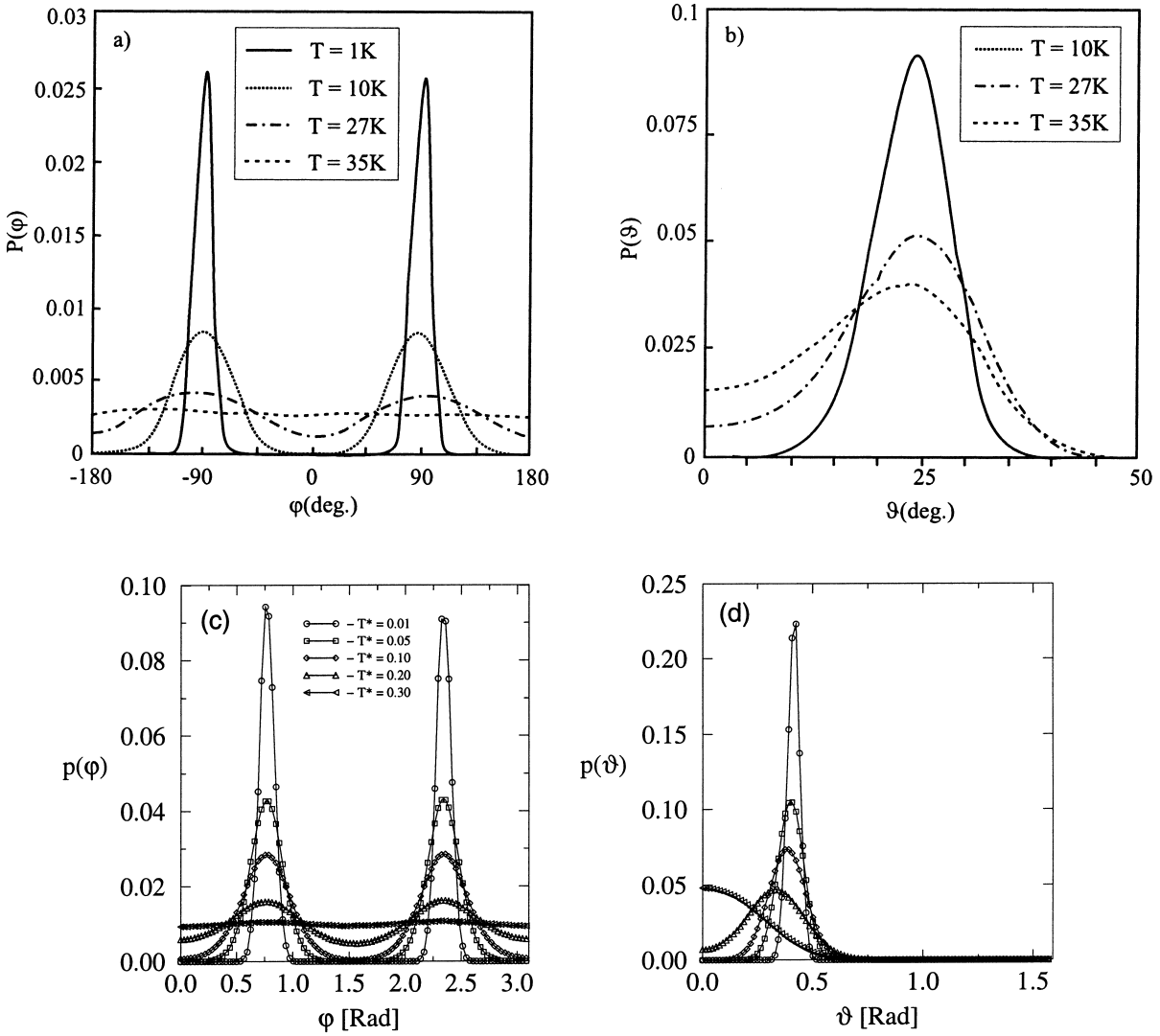

Fig. 75. The angular distribution functions $p(\varphi)$ and $p(\vartheta)$ obtained from the Monte Carlo simulation of CO film on the (100)NaCl surface [437] and the same obtained for a model film of homonuclear diatomic molecules of $\sigma^* = 0.9$ and the elongation $d^* = 0.4$ adsorbed on the (100) plane of an f.c.c. crystal [462].

6. Final remarks

Single crystals with an orientation of their surface plane chosen such that their topmost layer, which provides a substrate for adsorbed films, has a square or rectangular symmetry provide a fascinating "laboratory" for the study of phase transitions and critical phenomena in two dimensions. If the strength of the corrugation potential due to the substrate surface is so strong that adsorbate atoms can be adsorbed only in the centers of the potential wells, the lattice gas model of adsorbed monolayers can be

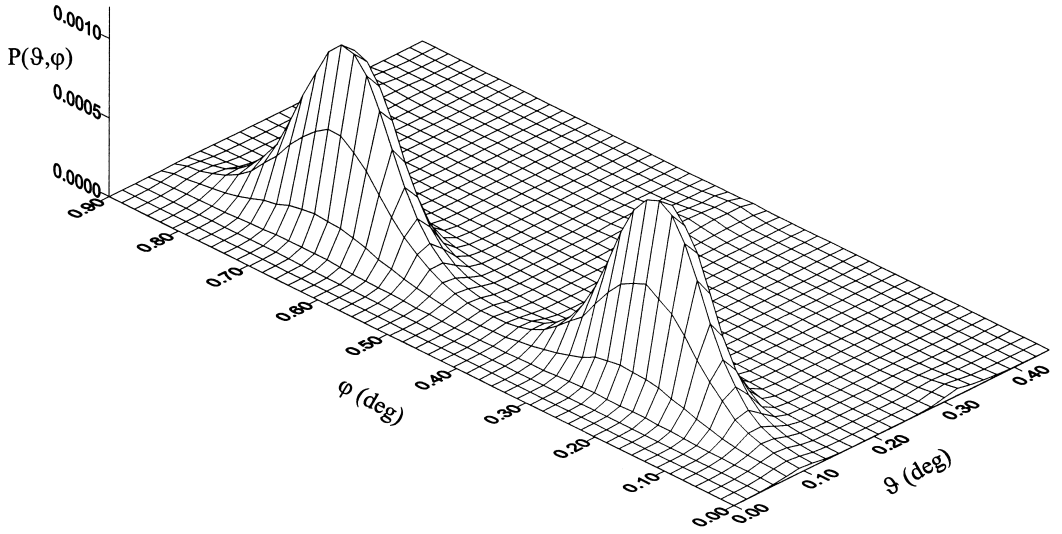

Fig. 76. Two-dimensional distribution function $p_{\mathrm{p}}(\Delta x, \Delta y)$ obtained from Monte Carlo simulation for a model film of homonuclear diatomic molecules of $\sigma^* = 0.9$ and the elongation $d^* = 0.4$ adsorbed on the (100) plane of an f.c.c. crystal at the temperature $T^* = 0.10$ (from Ref. [462]).

realized, and this simple description (Section 2) indeed is a reasonable approximation for several adsorbate systems on surfaces of cubic metals. Depending on the character of the lateral interactions between the adatoms, superstructures of various symmetry can be realized; the order–disorder transitions of these structures provide realization of unique universality classes of critical phenomena,

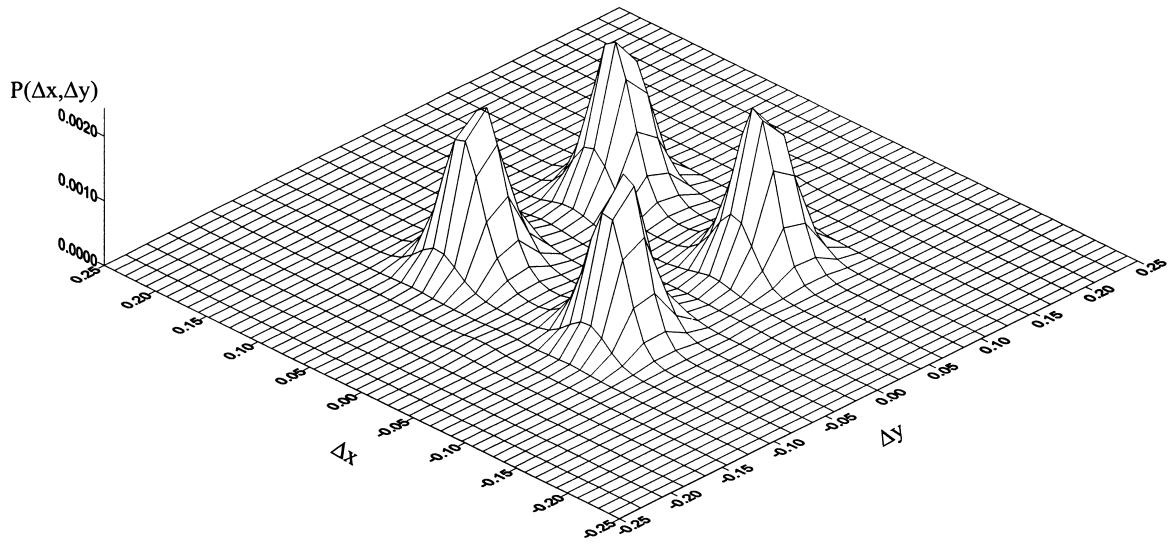

Fig. 77. Two-dimensional distribution function $p_0(\vartheta, \varphi)$ obtained from Monte Carlo simulation for a model film of homonuclear diatomic molecules of $\sigma^* = 0.9$ and the elongation $d^* = 0.4$ adsorbed on the (100) plane of an f.c.c. crystal at the temperature $T^* = 0.10$ (from Ref. [462]).

that have no counterpart in three dimensions at all (Section 3). Although experimental realizations for this wealth of phenomena predicted by analytical considerations and verified by Monte Carlo simulations of corresponding models are still scarce, these phase transitions are of basic interest for statistical mechanics and their application in surface science. Given the extraordinary progress in preparation of well-characterized clean surfaces, and the similarly impressive progress in structure analysis and microscopic observation of adsorbed layers, we are optimistic that many more experimental realizations of such orderings and their phase transitions will be found in the future. Thus we have described in the present article the necessary theoretical background and some illustrative model calculations in detail, in the hope that this treatise will be understandable to the experimentalist, and provide useful guidance and stimulation for a study of such phenomena in experiment. At this point, we must emphasize most strongly that for simplicity the model calculations reviewed here (Section 4) were examples just taken from the author's research groups. By no means would it have been possible to provide an equally deep coverage of all the work that exists in the field; we wish to apologize to all colleagues whose work is mentioned here only briefly or even not at all — this neglect should by no means be taken to imply that we rate the quality of their work less highly: but necessarily a biased selection had to be made, and we clearly could provide a more focused presentation of our own previous studies rather than providing a then necessarily rather incoherent review of the research from other groups, that adresses many different questions, including some which are completely outside the scope of this review (such as effects of surface heterogeneities and other types of quenched disorder, adsorbate–induced surface reconstruction, collective dynamic phenomena associated with phase transitions at surfaces, surface diffusion and growth phenomena, etc.).

While the lattice gas (Ising) model in its many variations plays for statistical mechanics a similar role as the fruitfly does for genetics, it must be emphasized that there are many phenomena expected in adsorbed layers that are beyond the realm of a lattice gas description. For instance, only off-lattice systems can show in the groundstate commensurate–incommensurate transitions via formation of soliton lattices, and allow a test of the famous theories of defect-mediated melting in two dimensions. We have reminded the reader on the basic theoretical concepts on both incommensurate phases and related ideas (e.g. domain-wall meandering, etc.) and we have presented a brief summary of the Kosterlitz–Thouless–Halperin–Nelson–Young theory of two dimensional melting as well (Section 3). It must be recalled, however, that for a treatment of each of these problems in full depth a lengthy review article of its own would have been required — and such reviews already exist and have been quoted in the reference list. Rather the purpose of the present survey was to give a tutorial introduction and allow the reader a substantially better understanding of the model studies described in Section 5. Note that the square and rectangular surface lattices with rather weak corrugation potentials provide a fascinating situation of conflict between the substrate potential symmetry and the tendency of the adsorbed layer to form a triangular structure (as it would if the corrugation of the substrate were completely turned off). In the model calculations reviewed here, both the corrugation strength and the misfit between the lattice spacing, that the adsorbate would take on a flat structureless substrate, and the lattice spacing of the substrate lattice were used as control parameters. It was shown that a wealth of phase transitions does occur, many of which provide examples for the general theoretical concepts discussed before, but some phenomena may need new developments in the model building considered by analytical theory as well. Again we hope that these studies will stimulate corresponding experimental work in the future, although clearly the off-lattice simulations are much less complete than the work based on lattice gas models.

Finally we have allowed for two more complications — multilayer adsorption or wetting, respectively, and effects of orientational order in adsorbed films of diatomic molecules. The corresponding subsections are particularly brief and show very few examples only — both topics deserve detailed independent reviews, and are rapidly developing fields, and it was rather intended to give a stimulating outlook on these fields, rather than provide a representative coverage.

Thus, despite the length of this article, only selected topics of the very broad field could be covered! But we do hope that the present emphasis on simulations guided by a tutorial overview of analytical theory with occasional outlook on experiments makes this article readable and useful for a wide audience.

Acknowledgements

We gratefully acknowledge partial support from the Volkswagen-Stiftung under grant No. I/71809 as well as the Committee for Scientific Research (Poland) under grant No. 3T09A 08216. K.B. thanks D.P. Landau for a fruitful interaction on some of the problems reviewed here. We are also grateful to T. Zientarski for a pleasant collaboration and several of the original papers on which this review is based.

References

[1] J.G. Dash, Films on Solid Surfaces, Academic Press, New York, 1975.
[2] S.K. Sinha (Ed.), Ordering in Two-dimensions, North-Holland, Amsterdam, 1980.
[3] J.G. Dash, R. Ruvalds (Eds.), Phase Transitions in Surface Films, Plenum, New York, 1980.
[4] H. Taub, G. Torzo, H.J. Lauter, S.C. Fain Jr. (Eds.), Phase Transitions in Surface Films 2, Plenum, New York, 1991.
[5] K. Binder, D.P. Landau, in: K.P. Lawley (Ed.), Advances in Chemical Physics, Wiley, Chichester, 1989, p. 91.
[6] H. Taub, K. Carneiro, J.K. Kjems, L. Passell, J.P. McTague, Phys. Rev. B 16 (1977) 4551.
[7] S.K. Sinha, in: D.L. Price, K. Sköld (Eds.), Methods of Experimental Physics, vol. 23, Neutron Scattering, Part B, Academic Press, San Diego, 1987, p. 1.
[8] H.J. Lauter, H. Godfrin, V.L.P. Frank, P. Leiderer, in: H. Taub, G. Torzo, H.J. Lauter, S.C. Fain Jr. (Eds.), Phase Transitions in Surface Films 2, Plenum, New York, 1991, p. 135.
[9] C.J. Wright, C.M. Sayers, Rep. Prog. Phys. 46 (1983) 773.
[10] L.J. Clarke, Surface Crystalography, Wiley, Chichester, 1985.
[11] F. Jons, J.A. Strozier, W.S. Yang Jr., Rep. Prog. Phys. 45 (1982) 527.
[12] K. Heinz, Rep. Prog. Phys. 58 (1995) 637.
[13] P.I. Cohen, J. Unguris, M.B. Webb, Surf. Sci. 58 (1976) 429.
[14] J. Unguris, L.W. Bruch, E.R. Moog, M.B. Webb, Surf. Sci. 87 (1979) 415.
[15] T. Meichel, J. Suzanne, C. Girard, C. Girardet, Phys. Rev. B 38 (1988) 3781.
[16] R.J. Behm, K. Christmann, G. Ertl, Surf. Sci. 99 (1980) 320.
[17] R. Imbihl, R.J. Behm, K. Christmann, G. Ertl, T. Matsushima, Surf. Sci. 117 (1982) 257.
[18] M. Grunze, P.H. Kleban, W.N. Unertl, F.S. Rys, Phys. Rev. Lett. 51 (1983) 582.
[19] G.S. Leatherman, R.D. Diehl, M. Karimi, G. Vidali, Phys. Rev. B 56 (1997) 6970.
[20] A. Glachant, M. Jaubert, M. Bienfait, G. Boato, Surf. Sci. 115 (1981) 219.
[21] W.A. Steele, The Interaction of Gases with Solid Surfaces, Pergamon Press, New York, 1974.
[22] K. Kern, G. Comsa, in: K.P. Lawley (Ed.), Advances in Chemical Physics, Wiley, Chichester, 1989.
[23] P. Zeppenfeld, J. George, V. Diercks, R. Halmer, R. David, G. Comsa, A. Marmier, C. Ramseyer, C. Girardet, Phys. Rev. Lett. 78 (1997) 1504.
[24] R. Morck, O. Shahal, Surf. Sci. Lett. 177 (1986) L963.

[25] N.S. Sullivan, J.M. Vaissiere, Phys. Rev. Lett. 51 (1983) 658.
[26] M. Bretz, J.G. Dash, D.C. Hickernell, E.O. McLean, O.E. Vilches, Phys. Rev. A 8 (1973) 1589.
[27] M. Lysek, P. Day, M. LaMadrid, D. Goodstein, Rev. Sci. Instrum. 63 (1992) 5750.
[28] F.T. Jensen, R.E. Palmer, Surf. Sci. 233 (1990) 269.
[29] K. Binder (Ed.) The Monte Carlo Method in Statistical Physics, Springer, Berlin, 1979.
[30] K. Binder (Ed.) Applications of the Monte Carlo Method in Statistical Physics, Springer, Berlin, 1984.
[31] M.P. Allen, D.J. Tildesley, Computer Simulation of Liquids, Clarendon Press, Oxford, 1987.
[32] F.F. Abraham, Phys. Rep. 80 (1981) 339.
[33] W. Selke, Phys. Rep. 170 (1988) 213.
[34] M.P. Allen, D.J. Tildesley (Eds.) Computer Simulation in Chemical Physics, Kluwer, Dortrecht, 1993.
[35] W. Selke, in: K. Binder (Ed.), The Monte Carlo Method in Condensed Matter Physics, Springer, Berlin, 1992, p. 329.
[36] D.P. Landau, in: K. Binder, G. Ciccotti (Eds.), Monte Carlo and Molecular Dynamics of Condensed Matter Systems, Italian Physical Society, Bologna, 1996.
[37] M. Kosterlitz, P.J. Thouless, J. Phys. C 6 (1973) 1181.
[38] B.I. Halperin, R.D. Nelson, Phys. Rev. Lett. 41 (1978) 121.
[39] R.D. Nelson, B.I. Halperin, Phys. Rev. B 19 (1979) 2457.
[40] A.D. Novaco, J.P. McTague, Phys. Rev. Lett. 38 (1977) 1286.
[41] S. Ostlund, A.N. Berker, Phys. Rev. B 21 (1980) 5410.
[42] F.D.M. Haldane, J. Villain, J. Phys. Paris 42 (1981) 1673.
[43] R. Pandit, M. Schick, M. Wortis, Phys. Rev. B 26 (1982) 5112.
[44] H. Nakanishi, M. Fisher, Phys. Rev. Lett. 49 (1982) 1565.
[45] S. Dietrich, in: C. Domb, J.L. Lebowitz (Eds.), Phase Transitions and Critical Phenomena, vol. 12, Academic Press, London, 1988, p. 1.
[46] K. Binder, in: F.R. de Boer, D.G. Pettifor (Eds.), Cohesion and Structure of Surfaces, Elsevier, Amsterdam, 1995, p. 121.
[47] A. Thomy, X. Duval, Colloq. Int. CNRS Nancy 132 (1965) 81.
[48] A. Thomy, X. Duval, J. Chim. Phys. Chim. Biol. 66 (1969) 1966.
[49] A. Thomy, X. Duval, J. Chim. Phys. Chim. Biol. 66 (1969) 286–1101.
[50] A. Thomy, X. Duval, C.R. Hebd, Seances Acad Sci. 259 (1964) 407.
[51] A. Thomy, X. Duval, J. Regnier, Surf. Sci. Rep. 1 (1981) 1.
[52] P. Bak, Rep. Prog. Phys. 45 (1982) 587.
[53] M.H.W. Chan, in: H. Taub, G. Torzo, H.J. Lauter, S.C. Fain Jr. (Eds.), Phase Transitions in Surface Films 2, Plenum, New York, 1991, p.1.
[54] R. Marx, Phys. Rep. 125 (1985) 1, and references cited therein.
[55] D. Marx, H. Wiechert, Adv. Chem. Phys. 95 (1996) 213, and references cited therein.
[56] R.J. Birgeneau, P.M. Horn, Science 232 (1986) 329.
[57] N.D. Mermin, H. Wagner, Phys. Rev. Lett. 17 (1966) 1133.
[58] A.P. Young, in: T. Riste (Ed.), Strongly Fluctuating Condensed Matter Systems, Plenum Press, New York, 1980.
[59] K.J. Strandburg, Rev. Mod. Phys. 60 (1988) 161.
[60] A. Patrykiejew, T. Zientarski, K. Binder, Acta Phys. Polon. 89 (1996) 735.
[61] J. Villain, Surf. Sci. 97 (1980) 219.
[62] M. den Nijs, in: C. Domb, J.L. Lebowitz (Eds.), Phase Transitions and Critical Phenomena, vol. 12, Academic Press, London, 1988, p. 219.
[63] A. Patrykiejew, S. Sokołowski, T. Zientarski, K. Binder, Surf. Sci. 421 (1999) 308.
[64] K. Binder, Z. Phys. B 43 (1981) 119.
[65] V. Privman (Ed.), Finite Size Scaling and Numerical Simulation of Statistical Systems, World Scientific, Singapore, 1990.
[66] M.S.S. Challa, D.P. Landau, K. Binder, Phys. Rev. B 34 (1986) 1841.
[67] J.W. Cahn, J. Chem. Phys. 66 (1977) 3667.
[68] I. Schmidt, K. Binder, Z. Phys. B 67 (1987) 1486.
[69] C. Ebner, W.F. Saam, Phys. Rev. 38 (1977) 1486.
[70] R. Lipovsky, J. Appl. Phys. 55 (1984) 2485.

[71] J.W. Weeks, in: Ordering in Strongly Fluctuating Condensed Matter Systems, T. Riste (Ed.), Plenum Press, New York, 1980, p. 293.
[72] M.E. Fisher, Rev. Mod. Phys. 46 (1974) 587.
[73] J.L. Cardy, in: C. Domb, J.L. Lebowitz (Eds.), Phase Transitions and Critical Phenomena, vol. 11, Academic Press, London, 1987, p. 55.
[74] F.F. Abraham, Phys. Rev. Lett. 44 (1980) 463.
[75] F.F. Abraham, Phys. Rev. Lett. 50 (1983) 978.
[76] S.W. Koch, F.F. Abraham, Phys. Rev. B 27 (1983) 2964.
[77] V. Bhethanabotla, W.A. Steele, J. Chem. Phys. 92 (1988) 3285.
[78] H.-Y. Kim, W.A. Steele, Phys. Rev. B 45 (1992) 6226.
[79] E. Vives, P.-A. Lindgård, Surf. Sci. 284 (1993) L449.
[80] D. Marx, S. Sengupta, P. Nielaba, Ber. Bunsenges. Phys. Chem. 98 (1994) 525.
[81] D. Marx, P. Nielaba, J. Chem. Phys. 102 (1995) 4538.
[82] D. Marx, S. Sengupta, P. Nielaba, K. Binder, Surf. Sci. 321 (1994) 195.
[83] C. Peters, M.L. Klein, Phys. Rev. B 32 (1985) 6077.
[84] V. Pereyra, P. Nielaba, K. Binder, J. Phys. Condens. Matter 5 (1993) 6631.
[85] H. Shiba, J. Phys. Soc. Japan 46 (1979) 1852.
[86] H. Shiba, J. Phys. Soc. Japan 48 (1980) 211.
[87] F.F. Abraham, W.E. Rudge, D.J. Auerbach, S.W. Koch, Phys. Rev. Lett. 52 (1984) 445.
[88] M. Kardar, A.N. Berker, Phys. Rev. Lett. 48 (1982) 1552.
[89] J. Villain, in: T. Riste (Ed.), Ordering in Strongly Fluctuating Condensed Matter Systems, Plenum, New York, 1980, p. 221.
[90] M. Schoebinger, F.F. Abraham, Phys. Rev. B 31 (1985) 4590.
[91] L.W. Bruch, M.S. Wei, Surf. Sci. 100 (1980) 481.
[92] M.S. Wei, L.W. Bruch, J. Chem. Phys. 75 (1981) 4130.
[93] J.M. Dickey, H.H. Farrell, M. Strongin, Surf. Sci. 23 (1970) 448.
[94] P.W. Palmberg, Surf. Sci. 25 (1971) 598.
[95] E.R. Moog, M.B. Webb, Surf. Sci. 148 (1984) 338.
[96] M.A. Chester, M. Hussain, J. Pritchard, Surf. Sci. 28 (1971) 460.
[97] A. Glachant, W. Bardi, Surf. Sci. 87 (1979) 187.
[98] J.P. Bibérian, M. Huber, Surf. Sci. 55 (1976) 259.
[99] D. Schmicker, J.P. Toennies, R. Vollmer, H. Weiss, J. Chem. Phys. 95 (1991) 9412.
[100] D. Scarano, A. Zucchina, J. Chem. Soc. Faraday Trans. I 82 (1986) 3611.
[101] J. Heidberg, E. Kampshoff, R. Kühnemuth, O. Schönekäs, Surf. Sci. 269/270 (1992) 120.
[102] J.P. Coulomb, T.S. Sullivan, J.B. Hastings, L. Passell, Surf. Sci. Lett. 150 (1985) L82.
[103] J. Küppers, F. Nitschke, K. Wandelt, G. Ertl, Surf. Sci. 87 (1979) 295.
[104] C. Rosmeyer, C. Girardet, P. Zeppenfeld, J. George, M. Büchel, G. Comsa, Surf. Sci. 313 (1994) 251.
[105] J. George, P. Zeppenfeld, M. Büchel, R. David, G. Comsa, Surf. Sci. 331-333 (1995) 1038.
[106] C. de Beauvais, D. Rouxel, B. Mutaftschiev, B. Bigeard, Surf. Sci. 272 (1992) 73.
[107] B.M. Ocko, O.M. Magnussen, J.X. Wang, Th. Wandlowski, Phys. Rev. B 53 (1996) R7654.
[108] J.P. Coulomb, in: H. Taub, G. Torzo, H.J. Lauter, S.C. Fain Jr. (Eds.), Phase Transitions in Surface Films 2, Plenum Press, New York, 1991, p. 113.
[109] A. Baraldi, V.R. Dhanak, G. Comelli, K.C. Prince, R. Rosei, Phys. Rev. B 56 (1997) 10511.
[110] S.-L. Chang, P.A. Thiel, J. Chem. Phys. 88 (1988) 2071.
[111] D.-H. Wei, D.C. Sketton, S.D. Kevan, J. Chem. Phys. 105 (1996) 7808.
[112] L.W. Bruch, J.A. Venables, Surf. Sci. 148 (1984) 167.
[113] L.W. Bruch, Surf. Sci. 150 (1985) 503.
[114] J.A. Snyman, J.H. Van der Merwe, Surf. Sci. 45 (1974) 619.
[115] J.A. Snyman, H.C. Snyman, Surf. Sci. 105 (1981) 357.
[116] B.N.J. Persson, Surf. Sci. 258 (1991) 451.
[117] T. Yamamoto, T. Izuyama, J. Phys. Soc. Japan 55 (1986) 4194.
[118] C. Ramseyer, C. Girardet, J. Chem. Phys. 103 (1995) 5767.

[119] S. Briquez, C. Girardet, J. Goniakowski, C. Noguera, J. Chem. Phys. 105 (1996) 676.
[120] D. Sahu, S.C. Ying, J.M. Kosterlitz, in: J.F. van der Veen, M.A. Van Hove (Eds.), The Structure of Surfaces II, Springer, Berlin, 1988, p. 470.
[121] L.L. Boyer, Phys. Rev. B 53 (1996) 3145.
[122] T.L. Einstein, Langmuir 7 (1991) 2520.
[123] J.W. Evans, D.E. Sanders, Phys. Rev. B 39 (1989) 1587.
[124] N.C. Bertelt, L.D. Roelofs, T.L. Einstein, Surf. Sci. 221 (1989) L750.
[125] Z. Zhang, K. Huang, H. Metiu, J. Chem. Phys. 93 (1990) 3614.
[126] C. Uebing, Surf. Sci. 272 (1992) 247.
[127] K. Binder, D.P. Landau, Surf. Sci. 108 (1981) 503.
[128] W. Kinzel, W. Selke, K. Binder, Surf. Sci. 121 (1982) 13.
[129] D.E. Taylor, E.D. Williams, R.L. Parc, N.C. Bertelt, T.L. Einstein, Phys. Rev. B 32 (1985) 4653.
[130] P. Bak, P. Kleban, W.N. Unertl, J. Ochab, G. Akinci, N.C. Bartelt, T.L. Einstein, Phys. Rev. Lett. 54 (1985) 1539.
[131] A. Patrykiejew, S. Sokołowski, T. Zientarski, K. Binder, J. Chem. Phys. 102 (1995) 8221.
[132] A. Patrykiejew, S. Sokołowski, T. Zientarski, Langmuir 13 (1997) 1036.
[133] A. Patrykiejew, S Sokołowski, T. Zientarski, K. Binder, J. Chem. Phys. 108 (1998) 5068.
[134] G.C. Wang, T.M. Lu, M.G. Legally, J. Chem. Phys. 69 (1978) 479.
[135] S. Ross, J.P. Olivier, On Physical Adsorption, Interscience, New York, 1964.
[136] J.D. Dash, R.D. Puff, Phys. Rev. B 24 (1981) 295.
[137] J.P. Coulomb, O.E. Vilches, J. Phys. Paris 45 (1984) 1381.
[138] Y. Larher, in: G. Benedek (Ed.), Surface Properties of Layered Structures, Kluwer, Dordrecht, 1992, p. 261.
[139] E.V. Albano, K. Binder, D.W. Heermann, W. Paul, J. Chem. Phys. 91 (1989) 3700.
[140] J. Merikoski, J. Timonen, K. Kaski, Phys. Rev. B 50 (1994) 7925.
[141] V. Pouthier, C. Ramseyer, C. Girardet, K. Kuhnke, V. Marsico, M. Blanc, R. Schuster, K. Kern, Phys. Rev. B 56 (1997) 4211.
[142] R.C. Nelson, T.L. Einstein, S.V. Khare, P.J. Rous, Surface Sci. 295 (1993) 462.
[143] W.A. Steele, Surf. Sci. 36 (1973) 317.
[144] J.O. Hirschfelder, C.F. Curtiss, R.B. Bird, Molecular Theory of Gases and Liquids, Wiley, New York, 1954.
[145] A. Vernov, W.A. Steele, Langmuir 8 (1992) 155.
[146] T. Hayakawa, Bull. Chem. Soc. Japan 30 (1957) 124, 236, 243, 332, 337, 343.
[147] F.Y. Hansen, L.W. Bruch, H. Taub, Phys. Rev. B 54 (1996) 14077.
[148] A. Luntz, L. Mattera, M. Rocca, S. Terreni, F. Tommasini, U. Valbusa, Surf. Sci. 126 (1983) 695.
[149] J. Perreau, J. Lapujoulade, Surf. Sci. 119 (1982) L292.
[150] J.F. Annett, R. Haydock, Phys. Rev. Lett. 53 (1984) 838.
[151] J.F. Annett, R. Haydock, Phys. Rev. B 34 (1986) 6860.
[152] D. Drakora, G. Doyen, F.V. Trentini, Phys. Rev. B 32 (1985) 6399.
[153] J.E. Müller, Phys. Rev. Lett. 65 (1990) 3021.
[154] K. Kern, R. David, P. Zeppenfeld, G. Comsa, Surf. Sci. 195 (1988) 353.
[155] J.R. Chen, R. Gomer, Surf. Sci. 94 (1980) 456.
[156] L.W. Bruch, in: H. Taub, G. Torzo, H.J. Lauter, S.C. Fain Jr. (Eds.), Phase Transitions in Surface Films 2, Plenum Press, New York, 1991, p. 67.
[157] H.-Y. Kim, W.A. Steele, Phys. Rev. B 44 (1991) 8962.
[158] C.D. Hruska, J.M. Phillips, Phys. Rev. B 37 (1988) 1988.
[159] J.M. Phillips, C.D. Hruska, Phys. Rev. B 39 (1989) 5425.
[160] J.M. Phillips, Langmuir 5 (1989) 571.
[161] J.M. Phillips, T.R. Story, Phys. Rev. B 42 (1990) 6944.
[162] J.M. Phillips, N. Shrimpton, Phys. Rev. B 45 (1992) 3730.
[163] A. Patrykiejew, S. Sokołowski, T. Zientarski, K. Binder, Langmuir 15 (1999) 3642.
[164] R.L. Park, H.H. Madden, Surf. Sci. 11 (1968) 188.
[165] S. Aubry, in: Solitons in Condensed Matter Physics, Springer, Heidelberg, 1978, p. 264.
[166] Y. Nardon, Y. Larher, Surf. Sci. 42 (1974) 299.
[167] K. Binder, D.P. Landau, Surf. Sci. 61 (1976) 577.

[168] K. Binder, W. Kinzel, D.P. Landau, Surf. Sci. 117 (1982) 232.
[169] K. Binder, in: Trends in Physics, Proceedings of the Fourth EPS Gen Conference, York, 1979, p. 164.
[170] W. Selke, in: C. Domb, J.L. Lebowitz (Eds.), Phase Transition and Critical Phenomena, vol. 15, Academic Press, London, 1992, p. 1.
[171] K. Binder, Adv. Colloid Interface Sci. 7 (1977) 279.
[172] A. Patrykiejew, Thin Solid Films 139 (1986) 209.
[173] A. Patrykiejew, P. Borowski, Phys. Rev. B 42 (1990) 4670.
[174] M.J. de Oliveira, R.B. Griffiths, Surf. Sci. 71 (1978) 687.
[175] K. Binder, D.P. Landau, Phys. Rev. B 37 (1988) 1745.
[176] A. Patrykiejew, D.P. Landau, K. Binder, Surf. Sci. 238 (1990) 317.
[177] A. Patrykiejew, K. Binder, Surf. Sci. 273 (1992) 413.
[178] M. Kruk, A. Patrykiejew, S. Sokołowski, Thin Solid Films 238 (1994) 302.
[179] R.H. van Dongen, Ph.D. Thesis, Technische Hogeschool, Delft, 1972.
[180] J.J. Doll, W.A. Steele, Surf. Sci. 44 (1974) 449.
[181] A. Patrykiejew, M. Jaroniec, Adv. Colloid Interface Sci. 20 (1984) 273.
[182] A. Patrykiejew, M. Jaroniec, Thin Solid Films 67 (1980) 187.
[183] A. Patrykiejew, M. Jaroniec, A.W. Marczewski, Thin Solid Films 76 (1981) 247.
[184] B.W. Holland, Trans Faraday Soc. 61 (1965) 546–555.
[185] A. Patrykiejew, Thin Solid Films 81 (1981) 89.
[186] A. Patrykiejew, Thin Solid Films 105 (1983) 259.
[187] J. Regnier, A. Thomy, X. Duval, J. Colloid Interface Sci. 70 (1979) 105.
[188] A.D. Migone, M.H.W. Chan, K.J. Niskanen, R.B. Griffiths, J. Phys. C 16 (1983) L1115.
[189] A. Patrykiejew, submitted for publication.
[190] K.J. Niskanen, Phys. Rev. B 33 (1986) 1830.
[191] J.A. Barker, Lattice Theories of the Liquid State, MacMillan, New York, 1963.
[192] L.P. Kadanoff, A. Houghton, M.C. Yalabik, J. Stat. Phys. 14 (1976) 171.
[193] W.A. Steele, M. Ross, J. Chem. Phys. 33 (1960) 464.
[194] D. Henderson (Ed.), Fundamentals of Inhomogeneous Fluids, Marcel Dekker, New York, 1992.
[195] C.A. Croxton, Liquid State Physics — A Statistical Mechanical Introduction, Cambridge Univ. Press, Cambridge, 1974.
[196] S.D. Prasad, S. Toxvaerd, J. Chem. Phys. 72 (1980) 1689.
[197] M.F. Saam, C. Ebner, Phys. Rev. A 15 (1977) 2566.
[198] D.K. Fairbent, W.F. Saam, L.M. Sander, Phys. Rev. B 26 (1982) 179.
[199] S. Sokołowski, W.A. Steele, J. Chem. Phys. 82 (1985) 2499.
[200] A. Patrykiejew, S. Sokołowski, Thin Solid Films 150 (1987) 105.
[201] P.A. Monson, W.A. Steele, D. Henderson, J. Chem. Phys. 74 (1981) 6431.
[202] S. Sokołowski, A. Patrykiejew, Z. phys. Chem. Leipzig 268 (1987) 583.
[203] P.A. Monson, M.W. Cole, F. Taigo, W.A. Steele, Surface Sci. 122 (1982) 401.
[204] H.E. Stanley, An Introduction to Phase Transitions and Critical Phenomena, Oxford Univ. Press, Oxford, 1971.
[205] J. Yeomans, Statistical Mechanics of Phase Transitions, Oxford Univ. Press, Oxford, 1992.
[206] N.D. Mermin, Phys. Rev. 176 (1968) 250.
[207] M. Schick, Progr. Surf. Sci. 11 (1981) 245.
[208] T.L. Einstein, in: R. Vanselov, R. Howe (Eds.), Chemistry and Physics of Solid Surfaces IV, Springer, Berlin, 1982, p. 251.
[209] S. Krinsky, D. Mukamel, Phys. Rev. B 16 (1977) 2313.
[210] N.C. Bartelt, T.L. Einstein, L.D. Roelofs, Surface Sci. 149 (1985) L47.
[211] N.C. Bartelt, T.L. Einstein, L.D. Roelofs, Phys. Rev. B 32 (1985) 2933.
[212] M.E. Fisher, Phys. Rev. 176 (1968) 257.
[213] M.E. Fisher, S.-K. Ma, B.G. Nickel, Phys. Rev. Lett. 29 (1972) 917.
[214] E. Riedel, F. Wegner, Z. Phys. 225 (1969) 195.
[215] E. Luijten, H.W.J. Blöte, K. Binder, Phys. Rev. Lett. 79 (1997) 561.
[216] E. Luijten, H.W.J. Blöte, K. Binder, Phys. Rev. E 56 (1997) 6540.

[217] R.B. Griffiths, Phys. Rev. Lett. 24 (1970) 715.
[218] S. Sarbach, I.D. Lawrie, in: C. Domb, J.L. Lebowitz (Eds.), Phase Transitions and Critical Phenomena, vol. 9, Academic Press, London, 1984, p. 1.
[219] B. Nienhuis, J. Phys. A 15 (1982) 199.
[220] R.B. Rotts, Proc. Camb. Philos. Soc. 48 (1952) 106.
[221] F.Y. Wu, Rev. Mod. Phys. 54 (1982) 235.
[222] K. Binder, D.P. Landau, Phys. Rev. B 21 (1980) 1941.
[223] D.P. Landau, K. Binder, Phys. Rev. B 31 (1985) 5946.
[224] R.H. Swendsen, S. Krinsky, Phys. Rev. Lett. 43 (1979) 177.
[225] M.P. Nightingale, Phys. Lett. A 59 (1977) 486.
[226] J. Oitmaa, J. Phys. A 14 (1981) 1159.
[227] M. Nauenberg, B. Nienhuis, Phys. Rev. Lett. 33 (1974) 941.
[228] R.M. Hornreich, M. Luban, S. Shtrikman, Phys. Rev. Lett. 35 (1975) 1678.
[229] K. Binder, H.L. Frisch, Eur. Phys. J. B 10 (1999) 71.
[230] P.D. Beale, P.M. Duxbury, J.M. Yeomans, Phys. Rev. B 31 (1985) 7166.
[231] I.E. Dzyaloshinskii, Zh. Eksp. Teor. Fiz. 35 (1964) 1518.
[232] P.G. de Gennes, Solid State Commun. 6 (1968) 163.
[233] P. Bak, V.J. Emery, Phys. Rev. Lett. 36 (1976) 968.
[234] E.V. Albano, D.W. Heermann, K. Binder, W. Paul, Surf. Sci. 223 (1989) 151.
[235] V.L. Pokrovskii, A.L. Talapov, Zh. Eksp. Teor. Fiz. 75 (1978) 1151.
[236] M.E. Fisher, J. Stat. Phys. 34 (1984) 687.
[237] F.P. Buff, R.A. Lovett, F.H. Stillinger, Phys. Rev. Lett. 15 (1965) 621.
[238] D.A. Huse, M.E. Fisher, Phys. Rev. B 29 (1984) 239.
[239] H.J. Schulz, Phys. Rev. B 22 (1980) 5274.
[240] H.J. Schulz, Phys. Rev. Lett. 46 (1981) 1685.
[241] S.N. Coppersmith, D.S. Fisher, B.I. Halperin, P.A. Lee, W.F. Brinkman, Phys. Rev. Lett. 46 (1981) 549.
[242] S.N. Coppersmith, D.S. Fisher, B.I. Halperin, P.A. Lee, W.F. Brinkman, Phys. Rev. B 25 (1982) 349.
[243] J. Villain, P. Bak, J. Phys. Paris 42 (1981) 657.
[244] D.R. Nelson, in: C. Domb, J.L. Lebowitz (Eds.), Phase Transitions and Critical Phenomena, vol. 7, Academic Press, London 1983, p. 1.
[245] J. Frenkel, T. Kontorova, Phys. Z. Sowjet. 13 (1938) 1.
[246] F.C. Frank, J.H. van der Merwe, Proc. Roy. Soc. London A 198 (1949) 205–216.
[247] S. Aubry, in: C. Godreche (Ed.), Structures Instabilities, Les Editions de Physiques, Les Ulis, 1986, p. 73.
[248] A.P. Young, J. Phys. C 11 (1978) L453.
[249] A.P. Young, Phys. Rev. B 19 (1979) 1855.
[250] N. Metropolis, M.N. Rosenbluth, A.H. Rosenbluth, A. Teller, E. Teller, J. Chem. Phys. 21 (1953) 1087.
[251] B.J. Alder, T.E. Wainwright, Phys. Rev. 127 (1962) 359.
[252] J.A. Zollweg, G.V. Chester, Phys. Rev. 46 (1992) 11187.
[253] H. Weber, D. Marx, K. Binder, Phys. Rev. B 51 (1995) 14636.
[254] A. Jaster, Europhys. Lett. 42 (1998) 277.
[255] S.T. Chui, Phys. Rev. Lett. 48 (1982) 933.
[256] S.T. Chui, Phys. Rev. B 28 (1983) 178.
[257] F.J. Wegner, Z. Physik 206 (1967) 465.
[258] L.D. Landau, E.M. Lifshitz, Theory of Elasticity, Pergamon, New York, 1970.
[259] R. Peierls, Ann. Inst. Henri Poincaré 5 (1935) 177.
[260] L.D. Landau, Phys. Z. Sowjetunion 2 (1937) 26.
[261] J.M. Kosterlitz, J. Phys. C 7 (1974) 1046.
[262] D.R. Nelson, J.M. Kosterlitz, Phys. Ref. Lett. 39 (1977) 1201.
[263] F.R.N. Nabarro, Theory of Dislocations, Clarendon Press, Oxford, 1967.
[264] S. Ostlund, B.I. Halperin, Phys. Rev. B 23 (1981) 335.
[265] R. Pandit, M. Wortis, Phys. Rev. B 25 (1982) 3226.
[266] M.P. Nightingale, W.F. Saam, M. Schick, Phys. Rev. B 30 (1984) 3830.

[267] H. van Beijeren, I. Nolden, in: W. Schommers, P. Blanckenhagen (Eds.), Structure and Dynamics of Surfaces II, Springer, Berlin 1987, p. 259.
[268] D.E. Sullivan, M.M. Telo da Gama, in: C.A. Croxton (Ed.), Fluid Interfacial Phenomena, Wiley, New York, 1986, p. 45.
[269] M. Schick, in: Liquids at Interfaces, Elsevier, Amsterdam, 1990.
[270] K. Binder, P.C. Hohenberg, Phys. Rev. B 6 (1972) 3461.
[271] K. Binder, P.C. Hohenberg, Phys. Rev. B 9 (1974) 2194.
[272] T. Young, Philos. Trans. Roy. Soc. London 95 (1805) 65.
[273] E. Brézin, B.I. Halperin, S. Leibler, Phys. Rev. Lett. 50 (1983) 1387.
[274] R. Lipovsky, M.E. Fisher, Phys. Rev. B 36 (1987) 2126.
[275] K. Binder, D.P. Landau, S. Wansleben, Phys. Rev. B 40 (1989) 6971.
[276] E.V. Albano, K. Binder, D.W. Heermann, W. Paul, Surf. Sci. 223 (1989) 151.
[277] D.B. Abraham, Phys. Rev. Lett. 44 (1980) 1165.
[278] D.B. Abraham, E.R. Smith, J. Stat. Phys. 43 (1986) 621.
[279] D.B. Abraham, J. Phys. A 21 (1988) 1741.
[280] L. Onsager, Phys. Rev. 65 (1944) 117.
[281] M.P. Nightingale, Physica A 83 (1976) 561.
[282] K. Kaski, W. Kinzel, J.D. Gunton, Phys. Rev. B 27 (1983) 6777.
[283] F. Buda, G.M. Florio, P.V. Giaquinta, Phys. Rev. B 35 (1987) 2021.
[284] B. Dünweg, A. Milchev, P.A. Rikvold, J. Chem. Phys. 94 (1991) 3958.
[285] M. Schick, J.S. Walker, M. Wortis, Phys. Rev. B 16 (1977) 2205.
[286] A.N. Barker, S. Ostlund, F.A. Putnam, Phys. Rev. B 17 (1978) 3650.
[287] M. Suzuki, J. Phys. Soc. Japan 55 (1986) 4205.
[288] M. Suzuki, M. Katori, X. Hu, J. Phys. Soc. Japan 56 (1987) 3092.
[289] G. Doyen, G. Ertl, M. Plancher, J. Chem. Phys. 62 (1975) 2957.
[290] K. Binder, D.P. Landau, Surface Sci. 151 (1985) 409.
[291] D.P. Landau, Phys. Rev. B 27 (1983) 5604.
[292] A. Patrykiejew, S. Sokołowski, R. Zagórski, Thin Solid Films 254 (1995) 116.
[293] M. Kaburagi, J. Phys. Soc. Japan 44 (1978) 54–394.
[294] P. Borowski, A. Patrykiejew, S. Sokołowski, Thin Solid Films 177 (1989) 333.
[295] A. Patrykiejew, P. Borowski, Thin Solid Films 195 (1991) 367.
[296] A. Patrykiejew, in: A. Dąbrowski, V.A. Tertykh (Eds.), Adsorption on New and Modified Inorganic Sorbents, Studies in Surface Science and Catalysis, vol. 99, Elsevier, Amsterdam, 1996.
[297] P.J. Estrup, in: The Structure and Chemistry of Solid Surfaces, Ed. G.A. Somorjai, Wiley, New York, 1969.
[298] Y. Tu, J.M. Blakely, Surf. Sci. 85 (1979) 276.
[299] H. Ohtani, C.-T. Kao, M.A. Van Hove, G.A. Somorjai, Progr. Surf. Sci. 23 (1987) 155.
[300] N.C. Bartelt, L.D. Roelofs, T.L. Einstein, Surf. Sci. Lett. 221 (1989) L750.
[301] J. Ashkin, E. Teller, Phys. rev. 64 (1943) 178.
[302] G. Ertl, J. Küppers, Surface Sci. 21 (1970) 61.
[303] P. Rujan, W. Selke, G.V. Uimin, Z. Phys. B 53 (1983) 221.
[304] I.M. Kim, D.P. Landau, Surface Sci. 110 (1981) 415.
[305] C. Ebner, Phys. Rev. B 28 (1983) 2890.
[306] W.F. Saam, Surf. Sci. 125 (1983) 253.
[307] C. Ebner, Phys. Rev. A 22 (1980) 2776.
[308] A. Prasad, P.B. Weichman, Phys. Rev. 57 (1998) 4900.
[309] S. Dietrich, M. Schick, Phys. Rev. B 33 (1986) 4952.
[310] G. Forgacs, R. Lipovsky, Th.M. Niewenhuizen, in: C. Domb, J.L. Lebowitz (Eds.), Phase Transitions and Critical Phenomena, vol. 14, Academic Press, London, 1991, p. 135.
[311] C. Ebner, C. Rottman, M. Wortis, Phys. Rev. B 28 (1983) 4186.
[312] D.A. Huse, Phys. Rev. B 30 (1984) 1317.
[313] S.J. Kennedy, J.S. Walker, Phys. Rev. B 30 (1984) 1498.
[314] P. Wagner, K. Binder, Surf. Sci. 175 (1986) 421.

[315] J.L. Seguin, J. Suzanne, M. Bienfait, J.G. Dash, J.A. Venables, Phys. Rev. Lett. 51 (1983) 122.
[316] J.W. White, R.K. Thomas, I. Marlow, G. Bomchil, Surf. Sci. 76 (1978) 13.
[317] J. Suzanne, E. Lerner, J. Krim, J.G. Dash, Phys. Rev. B 29 (1984) 983.
[318] Y. Larher, D. Haranger, Surf. Sci. 39 (1973) 100.
[319] S. Ramesh, J.D. Maynard, Phys. Rev. Lett. 49 (1982) 47.
[320] A. Patrykiejew, S. Sokołowski, Thin Solid Films, 128 (1985) 171.
[321] J.A. Barker, D. Henderson, F.F. Abraham, Physica A 106 (1981) 226.
[322] J.R. Klein, M.W. Cole, Faraday Discuss. Chem. Soc. 80 (1985) 71.
[323] F. Cuadros, A. Mulero, Chem. Phys. 177 (1993) 53.
[324] F. Cuadros, A. Mulero, J. Phys. Chem. 99 (1995) 419.
[325] X.C. Zeng, J. Chem. Phys. 104 (1996) 2699.
[326] F. Tsien, J.P. Valleau, Mol. Phys. 27 (1974) 177.
[327] S. Toxvaerd, Mol. Phys. 29 (1975) 273.
[328] S. Toxvaerd, Phys. Rev. A 24 (1981) 2735.
[329] J.M. Phillips, L.W. Bruch, R.D. Murphy, J. Chem. Phys. 75 (1981) 5097.
[330] J. Tabochnik, G.V. Chester, Phys. Rev. B 25 (1982) 6778.
[331] S. Toexvard, Phys. Rev. Lett. 51 (1983) 1971.
[332] C. Udink, D. Frenkel, Phys. Rev. B 35 (1987) 6933.
[333] C. Udink, J. van der Elsken, Phys. Rev. B 35 (1987) 279.
[334] M. Rovere, P. Nielaba, K. Binder, Z. Phys. B 90 (1993) 215.
[335] M. Rovere, D.W. Heermann, K. Binder, J. Phys.: Condens. Matter 2 (1990) 7009.
[336] M. Li, W.L. Johnson, W.A. Goddard III, Phys. Rev. B 54 (1996) 12067 .
[337] K. Binder, Rep. Prog. Phys. 60 (1997) 487.
[338] B. Smit, D. Frenkel, J. Chem. Phys. 94 (1991) 5663.
[339] A.Z. Panagiotopoulos, Mol. Simul. 9 (1992) 1.
[340] R.E. Peierls, Helv. Phys. Acta 7 (Suppl. II) (1934) 81.
[341] T.V. Ramakrishnan, Phys. Rev. Lett. 48 (1982) 541.
[342] H. Kleinert, Phys. Lett. A 95 (1983) 381.
[343] B. Joos, M.S. Duesbery, Phys. Rev. Lett. 55 (1985) 1997.
[344] P.A. Heiney, P.W. Stephans, R.J. Birgeneau, M.P. Horn, D.E. Moncton, Phys. Rev. B 28 (1983) 6416.
[345] S.E. Nagler, P.M. Horn, T.F. Rosenbaum, R.J. Birgeneau, M. Sutton, S.G.J. Mochrie, D.E. Moncton, R. Clarke, Phys. Rev. B 32 (1983) 7373.
[346] J.P. McTague, J. Als-Nielsen, J. Bohr, M. Nielsen, Phys. Rev. B 25 (1982) 7765.
[347] A.D. Migone, Z.R. Li, M.H.W. Chan, Phys. Rev. Lett. 53 (1984) 1133.
[348] J.A. Litzinger, G.A. Stewart, in: S.K. Sinha (Ed.), Ordering in Two Dimensions, North-Holland, Amsterdam, 1980, p. 147.
[349] Y. Larher, J. Chem. Phys. 68 (1978) 2257.
[350] M.D. Chinn, S.C. Fain, Phys. Rev. Lett. 39 (1977) 146.
[351] D.E. Johnson, J.M. Phillips, J.Z. Larese, Phys. Rev. B 56 (1997) 6462.
[352] C. Bockel, A. Thomy, X. Duval, Surf. Sci. 90 (1979) 109.
[353] J. Unguris, L.W. Bruch, M.B. Webb, J.M. Phillips, Surf. Sci. 114 (1982) 219.
[354] J.M. Gottlieb, Phys. Rev. B 42 (1990) 5377.
[355] J.C. Tully, Surf. Sci. 226 (1991) 461.
[356] R.D. Diehl, in: H. Taub, G. Torzo, H.J. Lauter, S.C. Fain Jr. (Eds.), Phase Transitions in Surface Films 2, Plenum, New York, 1991, p. 97.
[357] J.P. McTague, A.D. Novaco, Phys. Rev. B 19 (1979) 5299.
[358] F. Gray, J. Bohr, in: H. Taub, G. Torzo, H.J. Lauter, S.C. Fain Jr. (Eds.), Phase Transitions in Surface Films 2, Plenum, New York, 1991, p. 83.
[359] E. Vives, P.A. Lindgård, Phys. Rev. B 47 (1993) 7431.
[360] M.A. Chesters, M. Hussain, J. Pritchard, Surf. Sci. 35 (1973) 161.
[361] C. Ramsayer, C. Girardet, P. Zeppenfeld, J. George, M. Büchel, G. Comsa, Surf. Sci. 313 (1994) 251.
[362] K. Kern, R. David, P. Zeppenfeld, R. Palmer, G. Comsa, Solid State Commun. 61 (1987) 391.

[363] J.P. Coulomb, T.S. Sullivan, O.E. Vilches, Phys. Rev. B 30 (1984) 4753.
[364] M. Bienfait, J.P. Coulomb, J.P. Palmari, Surf. Sci. 182 (1987) 557.
[365] J.P. Coulomb, K. Madih, B. Croset, H.J. Lauter, Phys. Rev. Lett. 54 (1985) 1536.
[366] M. Sidoumou, T. Angot, J. Suzanne, Surf. Sci. 272 (1992) 347.
[367] D. Ferry, J. Suzanne, Surf. Sci. 345 (1996) L19.
[368] J. Heidberg, E. Kampshoff, O. Schönekäs, H. Stein, H. Weiss, Ber. Bunsenges. Phys. Chem. 94 (1990) 118.
[369] J. Dericbourg, Surf. Sci. 269/270 (1992) 1157.
[370] J.M. Gottlieb, L.W. Bruch, Phys. Rev. B 44 (1991) 5759.
[371] C. Ramseyer, P.N.M. Hoang, C. Girardet, Surf. Sci 265 (1992) 293.
[372] M. Chesters, J. Pritchard, Surf. Sci. 28 (1971) 460.
[373] J.C. Tracy, J. Chem. Phys. 56 (1972) 2736–2748.
[374] A. Grossmann, W. Erley, H. Ibach, Surf. Sci. Lett. 330 (1995) L646.
[375] K.O. Legg, F. Jona, D.W. Jepsen, P.M. Marcus, Phys. Rev. B 16 (1977) 5271.
[376] T. Takaishi, M. Mori, J. Chem. Soc. Faraday Trans. I 68 (1972) 1921.
[377] S. Ross, H. Clark, J. Am. Chem. Soc. 76 (1954) 4291.
[378] J.G. Dash, R. Ecke, J. Stoltenberg, O.E. Vilches, O.J. Whitemore, J. Phys. Chem. 82 (1978) 1450.
[379] J.L. Jordan, J.P. McTague, L. Passell, J.B. Hastings, Bull. Am. Phys. Soc. 28 (1983) 874.
[380] C. Tessier, Y. Larher, in: S.K. Sinha (Ed.), Ordering in Two Dimensions, North-Holland, New York, 1980, p. 163.
[381] T. Meichel, J. Suzanne, J.M. Gay, C. R. Acad. Sci. Paris 11 (1988) 989.
[382] D.R. Jung, J. Cui, D.R. Frankl, G. Ihm, H.Y. Kim, M.C. Cole, Phys. Rev. B 40 (1989) 11893.
[383] D.R. Baer, B.A. Fraass, D.H. Riehl, R.O. Simmons, J. Chem. Phys. 68 (1978) 1411.
[384] J.W. He, C.A. Estrada, J.S. Corneille, M.C. Wu, D.W. Goodman, Surf. Sci. 261 (1992) 164.
[385] V. Panella, J. Suzanne, P.N.M. Hoang, C. Girardet, J. Phys. I 4 (1994) 905.
[386] D.L. Meixner, D.A. Arthur, S.M. George, Surf. Sci. 261 (1992) 141.
[387] G.E. Ewing, Int. Rev. Phys. Chem. 10 (1991) 391.
[388] D.J. Dai, G.E. Ewing, J. Chem. Phys. 98 (1993) 5050.
[389] W.A. House, M.J. Jaycock, J. Colloid Interface Sci. 59 (1977) 266.
[390] A. Glachant, J.P. Coulomb, J.P. Biberian, Surf. Sci. 38 (1976) 619.
[391] A. Klekamp, E. Umbach, Surf. Sci. 284 (1993) 291.
[392] H. Pfnür, C. Schwennicke, J. Schimmelpfennig, in: H.-J. Freund, E. Umbach (Eds.), Adsorption on Ordered Surfaces of Ionic Solids and Thin Films, Springer, Berlin, 1993, p. 24.
[393] A. Klekamp, R. Reissner, E. Umbach, in: H.-J. Freund, E. Umbach (Eds.), Adsorption on Ordered Surfaces of Ionic Solids and Thin Films, Springer, Berlin, 1993, p. 35.
[394] P. Zeppenfeld, M. Büchel, J. George, R. David, G. Comsa, C. Ramseyer, C. Girardet, Surf. Sci. 366 (1996) 1.
[395] C. Ramseyer, C. Girardet, P. Zeppenfeld, J. George, M. Büchel, G. Comsa, Surf. Sci. 313 (1994) 251.
[396] A. Glachant, M. Bienfait, M. Jaubert, Surf. Sci. 148 (1984) L665.
[397] J.T. Stuckless, N. Al-Sarraf, C. Wartnaby, D.A. King, J. Chem. Phys. 99 (1993) 2202.
[398] S. Schroeder, M.C. McMaster, J.A. Stinnett, R.J. Madix, Surf. Sci. 297 (1993) L148.
[399] H. You, S.C. Fain Jr., Surf. Sci. 151 (1985) 361.
[400] W.C. Fan, A. Ignatiev, Phys. Rev. B 38 (1988) 366.
[401] K. Grzelakowski, I. Lyuksyutov, E. Bauer, Surf. Sci 216 (1989) 3958.
[402] J. Kröger, S. Lehwald, H. Ibach, Phys. Rev. B 58 (1998) 1578.
[403] R.J. Gooding, B. Joos, B. Bergersen, Phys. Rev. B 27 (1983) 7669.
[404] J.M. Houlrik, D.P. Landau, Phys. Rev. B 44 (1991) 8962.
[405] A.C. Hillier, M.D. Ward, Phys. Rev. B 54 (1996) 14037.
[406] K.J. Strandburg (Ed.), Bond-Orientational Order in Condensed Matter Systems, Springer, Berlin, 1992.
[407] W. Janke, Int. J. Theor. Phys. 29 (1990) 1251.
[408] Y. Saito, Phys. Rev. Lett. 48 (1982) 1114.
[409] K. Vollmayr, J.D. Reger, M. Scheucher, K. Binder, Z. Phys. B 91 (1993) 113.
[410] J.M. Phillips, Phys. Rev. B 51 (1995) 7186.
[411] J.Z. Larese, M. Harada, L. Passell, J. Krim, S. Satija, Phys. Rev. B 37 (1988) 4735.
[412] E. Granato, J.M. Kosterlitz, S.C. Ying, Phys. Rev. B 39 (1989) 4444.

[413] G.H. Peters, Surf. Sci. 347 (1996) 169.
[414] A. Alavi, I.R. McDonald, Mol. Phys. 69 (1990) 703.
[415] H. You, S.C. Fain Jr., Faraday Discuss. Chem. Soc. 80 (1985) 159.
[416] M. Trabelsi, J.P. Coulomb, Surf. Sci. 272 (1992) 352.
[417] C. Minot, M.A. Van Hove, J.-P. Biberian, Surf. Sci. 346 (1996) 283.
[418] L.W. Bruch, J. Chem. Phys. 79 (1983) 3148.
[419] R.D. Diehl, M.F. Toney, S.C. Fain Jr., Phys. Rev. Lett. 48 (1982) 177.
[420] R.D. Diehl, S.C. Fain Jr., Surf. Sci. 125 (1983) 116.
[421] A.B. Harris, A.J. Berlinsky, Can. J. Phys. 57 (1979) 1852.
[422] A. Patrykiejew, Thin Solid Films 137 (1986) 363.
[423] A. Patrykiejew, Thin Solid Films 143 (1986) 97.
[424] A. Patrykiejew, Thin Solid Films 150 (1987) 89.
[425] F.Y. Hansen, J.W. Bruch, Phys. Rev. B 51 (1995) 2515.
[426] B. Kuchta, R.D. Etters, Phys. Rev. B 36 (1987) 3400.
[427] D. Marx, O. Opitz, P. Nielaba, K. Binder, Phys. Rev. Lett. 70 (1993) 2908.
[428] J. Talbot, D.J. Tildesley, W.A. Steele, Molec. Phys. 51 (1984) 1331.
[429] R. Wang, S.-K. Wang, H. Taub, J.C. Newton, J.R. Dennison, H. Schechter, Phys. Rev. B 35 (1987) 5841.
[430] S.-K. Wang, J.C. Newton, R. Wang, H. Taub, J.R. Dennison, H. Schechter, Phys. Rev. B 39 (1989) 10331.
[431] Y.P. Yoshi, D.J. Tildesley, Mol. Phys. 55 (1985) 999.
[432] M. Roth, R.D. Etters, Phys. Rev. B 44 (1991) 6581.
[433] G. Lange, D. Schmicker, J.P. Toennies, H. Weiss, J. Chem. Phys. 103 (1995) 2308.
[434] H.-J. Freund, Ber. Bunsenges. Phys. Chem. 99 (1995) 1261.
[435] S. Picaud, C. Girardet, A. Glebov, J.P. Toennies, J. Dohrmann, H. Weiss, J. Chem. Phys. 106 (1997) 5271.
[436] A.W. Meredith, A.J. Stone, J. Chem. Phys. 104 (1996) 3058.
[437] N.-T. Vu, A. Jaklian, D.B. Jack, J. Chem. Phys. 106 (1997) 2551.
[438] A. Vigiani, G. Cardini, V. Schettino, J. Chem. Phys. 106 (1997) 5693.
[439] W. Hu, M.-A. Saberi, A. Jakalian, D.B. Jack, J. Chem. Phys. 106 (1997) 2547.
[440] A. Patrykiejew, J. Penar, S. Sokołowski, Molec. Phys. 62 (1987) 785.
[441] A. Patrykiejew, S. Sokołowski, Adv. Colloid Interface Sci. 30 (1989) 203.
[442] J. Heidberg, E. Kampfshoff, R. Kühnemuth, O. Schönekäs, H. Stein, H. Weiss, Surf. Sci. Lett. 226 (1990) L43.
[443] J. Heidberg, E. Kampfshoff, R. Kühnemuth, O. Schönekäs, Surf. Sci. 272 (1992) 306.
[444] O. Berg, G.E. Ewing, Surf. Sci. 220 (1989) 207.
[445] J. Schimmelpfennig, S. Folsch, M. Henzel, Surf. Sci. 250 (1991) 198.
[446] G.Y. Liu, G.N. Robinson, G. Scoles, P.A. Heiney, Surf. Sci. 262 (1992) 409.
[447] J.S. Francisco, M.M. Maricq, Acc. Chem. Res. 29 (1996) 391.
[448] J.S. Francisco, J. Phys. Chem. 98 (1994) 5650.
[449] J.S. Fransisco, J. Chem. Phys. 105 (1996) 3338.
[450] T.S. Lee, C.M. Rohlfing, J.E. Rice, J. Chem. Phys. 6593 (1992) 6593.
[451] J. Suzanne, V. Panella, D. Ferry, M. Sidoumou, Surf. Sci. Lett. 293 (1993) L912.
[452] D. Alfe, S. Baroni, Surf. Sci. 382 (1997) L666.
[453] M. Weinelt, W. Huber, P. Zabisch, H.-P. Sterrück, P. Ulbricht, U. Birkenheouer, J.C. Boettger, N. Rösch, J. Chem. Phys. 102 (1995) 9709.
[454] L. Vattuone, Y.Y. Yeo, D.A. King, J. Chem. Phys. 104 (1996) 8096.
[455] A. Eichler, J. Hefner, Phys. Rev. B 57 (1998) 10110.
[456] C. Girardet, P.N.M. Hoang, A. Marmier, S. Picaud, Phys. Rev. B 57 (1998) 11931.
[457] J. Heidberg, B. Redlich, D. Wetter, Ber. Bunsenges. Phys. Chem. 99 (1995) 1333.
[458] D. Ferry, A. Glebov, V. Senz, J. Suzanne, J.P. Toennies, H. Weiss, J. Chem. Phys. 105 (1996) 1697.
[459] D. Ferry, A. Glebov, V. Senz, J. Suzanne, J.P. Toennies, H. Weiss, Surf. Sci. 377/379 (1997) 643.
[460] D. Marx, S. Sengupta, P. Nielaba, K. Binder, Surf. Sci. 321 (1994) 195.
[461] D. Marx, S. Sengupta, O. Opitz, P. Nielaba, K. Binder, Mol. Phys. 83 (1994) 31.
[462] A. Patrykiejew, S. Sokołowski, A. Soroka, T. Zientarski, K. Binder, in preparation.